Design Strategies for Optimizing High Burnup Fuel in Pressurized Water Reactors

by

Zhiwen Xu

B.E., Engineering Physics,
Tsinghua University, P.R.China (1998)

B.E., Computer Science,
Tsinghua Univerisity, P.R.China (1998)

Submitted to the Department of Nuclear Engineering
in partial fulfillment of the requirements for the degree of

DOCTOR OF PHILOSOPHY

at the

MASSACHUSETTS INSTITUTE OF TECHNOLOGY

January 2003

Copyright © 2003 Massachusetts Institute of Technology
All rights reserved

Signature of Author _____
Department of Nuclear Engineering
January 10, 2003

Certified by _____
Michael J. Driscoll (thesis supervisor)
Professor Emeritus of Nuclear Engineering

_____
Mujid S. Kazimi (thesis supervisor)
TEPCO Professor of Nuclear Engineering

Accepted by _____
Jeffrey A. Coderre
Chairman, Department Committee on Graduate Students

Design Strategies for Optimizing High Burnup Fuel in Pressurized Water Reactors

by

Zhiwen Xu

Submitted to the Department of Nuclear Engineering
on January 23, 2003, in partial fulfillment of
the requirements for the degree of
Doctor of Philosophy

Abstract

This work is focused on the strategy for utilizing high-burnup fuel in pressurized water reactors (PWR) with special emphasis on the full array of neutronic considerations. The historical increase in batch-averaged discharge fuel burnup, from ~30 MWd/kg in the 1970s to ~50 MWd/kg today, was achieved mainly by increasing the reload fuel enrichment to allow longer fuel cycles: from an average of 12 months to about 18 months. This also reduced operating costs by improving the plant capacity factor. Recently, because of limited spent fuel storage capacity, increased core power output and the search for increased proliferation resistance, achieving burnup in the 70 to 100 MWd/kg range has attracted considerable attention. However the implications of this initiative have not been fully explored; hence this work defines the practical issues for high-burnup PWR fuels based on neutronic, thermal hydraulic and economic considerations as well as spent fuel characteristics.

In order to evaluate the various high burnup fuel design options, an improved MCNP-ORIGEN depletion program called MCODE was developed. A standard burnup predictor-corrector algorithm is implemented, which distinguishes MCODE from other MCNP-ORIGEN linkage codes.

Using MCODE, the effect of lattice design (moderation effect) on core design and spent fuel characteristics is explored. Characterized by the hydrogen-to-heavy-metal ratio (H/HM), the neutron spectrum effect in UO_2/H_2O lattices is investigated for a wide range of moderation, from fast spectra to over-thermalized spectra. It is shown that either wetter or very dry lattices are preferable in terms of achievable burnup potential to those having an epithermal spectrum. Wet lattices are the preferred high burnup approach due to improved proliferation resistance. The constraint of negative moderator temperature coefficient (MTC) requires that H/HM values (now at 3.4) remain below ~6.0 for PWR lattices.

Alternative fuel choices, including the conventional solid pellets, central-voided annular pellets, Internally- & eXternally-cooled Annular Fuel (IXAF), and different fuel forms are analyzed to achieve a wetter lattice. Although a wetter lattice has higher burnup potential than the reference PWR lattice, the requirement of a fixed target cycle energy production necessitates higher initial fuel enrichments to compensate for the loss of fuel mass in a wetter lattice. Practical issues and constraints for the high burnup fuel include

neutronic reactivity control, heat transfer margin, and fission gas release. Overall the IXAF design appears to be the most promising approach to realization of high burnup fuel.

High-burnup spent fuel characteristics are compared to the reference spent fuel of 33 MWd/kg, representative of most of the spent fuel inventory. Although an increase of decay power and radioactivity per unit mass of initial heavy metal is immediately observed, the heat load (integration of decay power over time) per unit electricity generation decreases as the fuel discharge burnup increases. The magnitude of changes depends on the time after discharge. For the same electricity production, not only the mass and volume of the spent fuel are reduced, but also, to a lesser extent, the total heat load of the spent fuel. Since the heat load in the first several hundred years roughly determines the capital cost of the repository, a high burnup strategy coupled with adequate cooling time, may provide a cost-reduction approach to the repository.

High burnup is beneficial to enhancing the proliferation resistance. The plutonium vector in the high-burnup spent fuel is degraded, hence less attractive for weapons. For example, the ratio of Pu-238 to Pu-239 increases with burnup to the 2.5 power. However, the economic benefits are uncertain. Under the current economic conditions, the PWR fuel burnup appears to have a shallow optimum discharge burnup between 50 and 80 MWd/kg. The actual minimum is influenced by the financing costs as well as the cost of refueling shutdowns. Since the fuel cycle back-end benefits will accrue to the federal government, the current economic framework, such as the waste fee based on the electricity produced rather than volume or actinide content, does not create an incentive for utilities to increase burnup.

Different schemes exist for fuel management of high burnup PWR cores. For the conventional core design, a generalized enrichment-burnup correlation (applicable between 3 w/o and 20 w/o) was produced based on CASMO/SIMULATE PWR core calculations. Among retrofit cores, increasing the number of fuel batches is preferred over increasing the cycle length due to nuclear fuel cycle economic imperatives. For future core designs, a higher power-density core is a very attractive option to cut down the busbar cost. The IXAF concept possesses key design characteristics that provide the necessary thermal margins at high core power densities. In this regard, the IXAF fuel deserves further investigation to fully exploit its high burnup capability.

Thesis Supervisor: Michael J. Driscoll
Title: Professor Emeritus of Nuclear Engineering

Thesis Supervisor: Mujid S. Kazimi
Title: TEPCO Professor of Nuclear Engineering
Director, Center for Advanced Nuclear Energy Systems

Acknowledgements

The keen help, patient guidance and generous support of Professor Michael J. Driscoll and Professor Mujid S. Kazimi, my thesis supervisors, are greatly appreciated. Lots of inspiration throughout this work comes directly from them.

I am grateful to two members of the Advanced Fuel Cycle Group at the MIT Center for Advanced Nuclear Energy Systems (CANES): Dr. Edward E. Pilat for his contribution to conventional PWR core review and invaluable advice on burnable poison usage, Dr. Pavel Hejzlar for numerous discussions on MCODE development and the internally and externally cooled annular fuel concept. Special thanks are due to my colleagues Dr. Xianfeng Zhao, Dr. Yun Long, Mr. Dean Wang, Mr. Eugene Shwageraus, and Mr. Dandong Feng who provided help on various aspects of the work.

In terms of the MCODE benchmark problem (9.75 w/o UO_2 with a conventional PWR lattice under cold conditions), I wish to express my gratitude to Dr. Hyung-Kook Joo from KAERI for providing results of HELIOS and to Dr. Tamer Bahadir from Studsvik of America, Inc., for providing results of CASMO-4 (internal version). The corrected version of ORIGEN2.1 supplied by Dr. Allan G. Croff from Oak Ridge National Laboratory is also acknowledged.

This thesis could not have been completed without the endless love and support from my family. I would like to give special thanks to my wife, Kun Yu, for wading through past five years of difficulties and achievements with me at MIT. My dear son, Chen Y. Xu, three years old, is now able to speak words clearly and likes to jump and run. I thank my mother-in-law, Ying Ma, for helping us taking care of my son. The thesis is dedicated to them.

This work has been partially funded by the Idaho National Engineering & Environmental Laboratory (INEEL) through the Advanced Fuel Project, and by the DOE's support of the annular fuel project through a NERI grant.

Table of Contents

Abstract ..... **i**
Acknowledgement ..... **iii**
Table of Contents ..... **iv**
List of Figures ..... **x**
List of Tables ..... **xv**
Abbreviations for Organizations ..... **xvii**
Nomenclature ..... **xviii**
1. Introduction **1**
1.1 Background 1
1.2 High Burnup Review 3
1.2.1 UO_2 Fuel 3
1.2.2 Literature Review 4
1.3 Motivation 6
1.3.1 Incentives 6
1.3.2 High Burnup Implementation 8
1.4 Objectives 9
1.5 Analysis Tools 10
1.5.1 Studsvik Core Management System (CMS) Code Package 10
1.5.2 MCNP-4C 12
1.5.3 ORIGEN2 12
1.5.4 MCODE 13
1.5.5 VIPRE 13
1.5.6 FRAPCON-3 14
1.6 Thesis Organization 14
2. High Burnup Issues of Current PWR Designs **17**
2.1 Introduction 17
2.2 Conventional PWR Description 21
2.2.1 General Description 21

2.2.2 Reactivity Control 21
2.3 Licensing/Design/Operating Considerations 27
2.3.1 Licensing Issues 28
2.3.2 Design Considerations 28
2.3.3 Operational Issues 34
2.4 High Burnup Core Scoping Analysis 37
2.4.1 Core Modeling 37
2.4.2 Multi-Batch Burnup 40
2.4.3 Single-Batch Discharge Burnup (B_1) Correlation 41
2.4.4 Discharge Burnup vs. Cycle Length 44
2.4.5 Resource Utilization 46
2.4.6 Haling Power Distributions 50
2.5 Consideration on Retrofit, High Burnup Core Schemes 53
2.5.1 Longer Cycle Length 53
2.5.2 More Batches 55
2.5.3 Conclusions 55
2.6 Chapter Summary 56
3. MCODE Development 58
3.1 Introduction 58
3.2 Methodology 61
3.2.1 Overview 61
3.2.2 MCNP Tallies and One-Group Cross Section Preparations 64
3.2.3 Flux Normalization 67
3.2.4 ORIGEN Depletions 69
3.2.5 Coupling Between MCNP and ORIGEN 70
3.3 High Burnup UO_2 Lattice Benchmark 73
3.3.1 Pin Cell Model 73
3.3.2 Code Descriptions 75
3.3.3 Benchmark Results and Analysis 75
3.4 Sensitivity Calculations 82
3.4.1 Timestep Size 83

3.4.2 Energy Release per Fission 84
3.4.3 ORIGEN Libraries 86
3.4.4 Statistical Errors 87
3.5 General Remarks on MCNP/ORIGEN Linkage Codes 87
3.5.1 MCNP Issues 87
3.5.2 ORIGEN Issues 89
3.5.3 Future Trends 90
3.6 Chapter Summary 91
4. Neutron Spectrum Effects 93
4.1 Introduction 93
4.2 Lattice Geometry Effect 97
4.2.1 Unit Cell Model 97
4.2.2 Results & Discussions 98
4.3 Parametric Study of Moderation Effects 100
4.3.1 Introduction 100
4.3.2 Initial k_∞ 102
4.3.3 Reactivity-Limited Burnup 107
4.3.4 Neutron Spectrum 110
4.3.5 Discussion 113
4.4 Other Fuel Types 113
4.5 Cycle Length Constraints 115
4.6 Core Size, Power Density, and Neutron Leakage 118
4.6.1 Introduction 118
4.6.2 PWR Core Size and Leakage Reactivity Penalty 118
4.6.3 Leakage in Highly-Undermoderated Systems 120
4.6.4 Long-Cycle Cores 121
4.6.5 Summary 122
4.7 Chapter Summary 123
5. Alternative Fuel Choices 125
5.1 Introduction 125
5.2 Inert Matrix Fuel (IMF) 129

5.2.1 Introduction....129
5.2.2 Burnup Potential, Cycle Length, and MTC Considerations....129
5.2.3 Lattice Optimization....133
5.2.4 Conclusion....134
5.3 Center-Voided Annular Fuel Pellet....135
5.3.1 Introduction....135
5.3.2 Void-Filling Materials....136
5.3.3 Comparison to Solid Fuel Pin....137
5.4 Internally and Externally-Cooled Annular Fuel (IXAF)....138
5.4.1 Introduction....138
5.4.2 Four-Factor Formula Considerations....140
5.4.3 From Solid to Annular: A Step-by-Step Variation Approach....141
5.4.4 Results and Discussion....143
5.4.5 The Eigenvalue Ladder....148
5.4.6 RIM Effects....149
5.5 Chapter Summary....154
6. Practical Issues of High Burnup in Wetter Lattices....155
6.1 Introduction....155
6.2 Neutronic Reactivity Control....157
6.2.1 Introduction....157
6.2.2 Burnable-Poison-Free Core Analysis....159
6.2.3 Poisoning the Core....163
6.2.4 Design Considerations....177
6.3 Heat Transfer Considerations....181
6.3.1 Introduction....181
6.3.2 Hot Channel Analysis....182
6.3.3 Discussion....185
6.4 Fuel Performance Considerations....186
6.5 Chapter Summary....189
7. High Burnup Effects on Spent Fuel Characteristics....191
7.1 Introduction....191

7.2 Waste Disposal Characteristics 192
7.2.1 Characteristics of Today's Discharged Fuel 192
7.2.2 High Burnup via High-Enriched Uranium 194
7.2.3 Neutron Spectrum Effects (H/HM) 206
7.2.4 Power Density Effect 207
7.3 Proliferation Resistance 208
7.3.1 Introduction 208
7.3.2 Higher Discharge Burnup 211
7.3.3 Neutron Spectrum Effect (H/HM Variation) 212
7.4 Other Considerations 214
7.5 Chapter Summary 214
8. Economics Aspects of High Burnup 215
8.1 Introduction 215
8.2 Nuclear Fuel Cycle Economics 216
8.2.1 Introduction 216
8.2.2 The Fuel Cycle Cost Calculation 218
8.2.3 High Burnup for Conventional PWRs 222
8.2.3.1 Enrichment Increase 222
8.2.3.2 Effect of a Wetter Lattice 225
8.2.4 Operational Strategies 228
8.2.5 High Burnup in Different Neutron Spectra 231
8.3 Operation and Maintenance Considerations 234
8.3.1 Introduction 234
8.3.2 Refueling Outages 234
8.4 Case Study of Power Uprating 237
8.5 Chapter Summary & Recommendations 238
9. Summary, Conclusions, and Recommendations 240
9.1 Summary of Motivation 240
9.2 MCODE Development 240
9.3 Neutron Spectrum Effect by H/HM Variations 243
9.4 Neutronic Considerations of Alternative Fuel Choices 245

9.5 Practical Issues....246
9.5.1 Reactivity Control....246
9.5.2 Thermal Hydraulics Considerations....247
9.5.3 Fuel Performance....249
9.6 High-Burnup Spent Fuel & Proliferation Resistance....250
9.7 Economic Considerations....251
9.8 Recommendations for Future Work....252
9.8.1 MCODE Development....252
9.8.2 Detailed Core Design....252
9.8.3 High Burnup Fuel Performance Studies....253
9.8.4 Policy Studies....253
9.8.5 Proliferation Study....253
9.8.6 Recycling Issue....253
Reference....254
Appendix A. High Burnup Core Input Files for CMS Code Package....265
Appendix B. MCODE (Ver. 1.0, February 2002) User's Manual....275
Appendix C. Input Files for the High Burnup Benchmark Problem....296
Appendix D. Input Files for Axial Enrichment Zoning Calculations....300
Appendix E. VIPRE Input Files....303

List of Figures

Figure 1.1 Atmospheric CO_2 concentration over the last millennium....1
Figure 1.2 Historical discharge burnup trend over the 1980-2000 period (PWR)....3
Figure 1.3 Flow of calculations for the CMS code package....11
Figure 2.1 Uranium-235 enrichment over the 1876-2000 time period....20
Figure 2.2 Cross sectional view of control rod locations....23
Figure 2.3 Control bank insertion limits versus percent rated thermal power....24
Figure 2.4 Thermal design margin considerations....29
Figure 2.5 Margins of high burnup cores (right) compared to standard PWR (left) 35
Figure 2.6 Axial offset anomaly example....36
Figure 2.7 Quarter-core model of 193-assembly conventional PWR core....38
Figure 2.8 Core depletion calculations for various fuel enrichments 42
Figure 2.9 Burnup-enrichment relations for typical PWRs 43
Figure 2.10 Discharge burnup versus cycle length map for a typical PWR....44
Figure 2.11 Natural uranium utilization for typical PWRs....47
Figure 2.12 Separative work utilization for typical PWRs....47
Figure 2.13 Haling and poison-free BOC assembly power distributions 51
Figure 2.14 Axial core power distributions 52
Figure 2.15 Reactivity and critical boron for the single batch core....53
Figure 2.16 Boron worth for the single batch core 54
Figure 3.1 Illustration of MCODE architecture....60
Figure 3.2 Flow diagram of MCODE....63
Figure 3.3 Pin cell model (not to scale)....73
Figure 3.4 Eigenvalue comparison between MCODE, CASMO-4, and HELIOS 79
Figure 3.5 Eigenvalue difference from CASMO-4 as a function of burnup 79
Figure 3.6 Plutonium vector comparison with CASMO-4 as a function of burnup 82
Figure 3.7 Effect of time step size on the convergence 83
Figure 3.8 Burnup sensitivity to the macro burnup timestep size....84
Figure 3.9 Burnup calculation sensitivity to the energy release per fission 85

Figure 3.10 Burnup calculation sensitivity to ORIGEN libraries....86
Figure 4.1 Lattice unit cells....97
Figure 4.2 MCODE depletion histories for different lattice unit cells....99
Figure 4.3 Relative eigenvalue differences from the square lattice unit cell....99
Figure 4.4 Water density variation with pressure at 310°C....101
Figure 4.5 Initial k_∞ as a function of H/HM ratio....103
Figure 4.6 Soluble poison effects on 4.5 and 9.75 w/o UO_2 fuel....105
Figure 4.7 CASMO-4 prediction of reactivity-limited, single-batch burnup, B_1....108
Figure 4.8 Conversion ratio (initial) for 9.75 w/o U-235 case....109
Figure 4.9 MCODE/CASMO results for 9.75 w/o enrichment....110
Figure 4.10 Neutron spectrum for different enrichments at H/HM=3.4....111
Figure 4.11 Neutron spectrum for 9.75 w/o under different moderation conditions....112
Figure 4.12 Eight combinations of fissile and fertile materials....114
Figure 4.13 Burnup capability of various combinations of fissile and fertile materials....114
Figure 4.14 Reactivity-limited burnup capability using different methods of varying H/HM....116
Figure 4.15 Single-batch cycle length for different schemes of varying H/HM....117
Figure 4.16 Sensitivity of migration area and length to moderator-to-fuel ratio....120
Figure 5.1 Schematic showing fuel design options....128
Figure 5.2 Burnup histories of the IMF and reference cases....131
Figure 5.3 IMF depletion curves as a function of time (effective full power days)....131
Figure 5.4 MTC at BOL as a function of boron concentration....132
Figure 5.5 The initial k_∞ and burnup potential of CERMET fuel....133
Figure 5.6 The energy production (EFPD) as a function of H/HM....134
Figure 5.7 Single-batch burnup capabilities for various filling materials....136
Figure 5.8 Single-batch cycle length for various filling materials (9.75 w/o)....137
Figure 5.9 Single-batch cycle length comparison between annular fuel and solid fuel....138
Figure 5.10 Illustration of step-by-step changes (clean case approach)....145
Figure 5.11 Reactivity change versus burnup for solid and IXAF cases....147
Figure 5.12 Reactivity change versus time for solid and IXAF cases....147
Figure 5.13 The eigenvalue ladder for solid and annular IXAF fuels....148

Figure 5.14 Power distributions in IXAF and solid fuel.....150
Figure 5.15 Local burnup distribution in the fuel pellet.....151
Figure 5.16 Local conversion ratio at BOL for the solid and IXAF cases.....152
Figure 5.17 Plutonium distributions.....152
Figure 6.1 Schematic demonstration of various linear power limits.....156
Figure 6.2 Standard Westinghouse 17×17 assembly model.....158
Figure 6.3 Depletion histories of 18-month PWR fuel and high burnup fuel.....159
Figure 6.4 BOC reactivity and boron worth as a function of H/HM.....161
Figure 6.5 BOC core critical boron concentration as a function of H/HM.....161
Figure 6.6 Range of burnable poison control trajectories using LRM.....164
Figure 6.7 Cross sections of various nuclides in the thermal energy range.....167
Figure 6.8 Depletion curves for HB-REF case with 156 IFBA rods.....169
Figure 6.9 Depletion curves for HB-REF case with all IFBA rods.....169
Figure 6.10 Burnable-poison pin layouts.....171
Figure 6.11 $\rho(B)$ histories for burnable poison pins with 6 wt% Gd_2O_3.....172
Figure 6.12 $\rho(B)$ histories for burnable poison pins with 8 wt% Gd_2O_3.....172
Figure 6.13 $\rho(B)$ histories for burnable poison pins with 10 wt% Gd_2O_3.....173
Figure 6.14 $\rho(B)$ histories for all fuel (9.75 w/o UO_2) pins poisoned with erbia.....174
Figure 6.15 Comparison of burnable poisons in a conventional PWR assembly.....174
Figure 6.16 Comparison of burnable poisons in a high burnup, conventional PWR assembly (9.75 w/o).....175
Figure 6.17 Poisoning the high burnup assembly with a wet lattice.....176
Figure 6.18 Schematic of axial heterogeneous fuel loading.....178
Figure 6.19 The effect of axially heterogeneous fissile distribution on initial neutronic parameters.....179
Figure 6.20 Depletion curves for axial zoning cases.....180
Figure 6.21 MDNBR and pressure drop as a function of H/HM for solid fuel pin.....184
Figure 6.22 Maximum fuel temperature as H/HM increases (rod diameter).....184
Figure 6.23 MDNBR comparison in hot channel for the IXAF and reference solid pin.185
Figure 6.24 Fuel temperature distributions at BOC.....187
Figure 6.25 Fission gas release calculations for various fuel pins.....188

Figure 7.1 In-situ radioactivity for typical PWR spent fuel as a function of time.....193
Figure 7.2 Radioactivity per MTIHM versus time after discharge.....197
Figure 7.3 Radioactivity per GWyr(e) versus time after discharge.....198
Figure 7.4 Decay power per MTIHM after discharge.....199
Figure 7.5 Decay power per GWyr(e) after discharge.....200
Figure 7.6 Accumulated decay heat per MTIHM after discharge.....201
Figure 7.7 Accumulated decay heat per GWyr(e) after discharge.....202
Figure 7.8 Correlation between decay power and radioactivity.....203
Figure 7.9 Correlation between decay energy and radioactivity.....203
Figure 7.10 The WDV of nuclides in PWR spent fuel as a function of time.....206
Figure 7.11 Total plutonium and maximum Np-237 for spent fuel with 100 MWd/kg, 12% initial U-235 enrichment.....207
Figure 7.12 Power density effect on spent fuel characteristics.....208
Figure 7.13 Pu-238 fraction versus burnup for several initial U-235 enrichments.....211
Figure 7.14 CASMO-4 pin cell predictions of isotopic composition of Pu in spent fuel at 100 MWd/kg for lattices with initial enrichment of 12%.....212
Figure 7.15 Spontaneous neutron and heat generation rates vs. H/HM at 100 MWd/kg, 12w/o initial U-235 enrichment.....213
Figure 8.1 Nuclear electricity generation cost breakdown.....215
Figure 8.2 Flow chart of current once-through fuel cycle.....218
Figure 8.3 A schematic cash flow diagram for the current once-through fuel cycle.....219
Figure 8.4 Fuel cycle cost for 18-month conventional PWRs.....223
Figure 8.5 Sensitivity to SWU costs for 18-month-cycle PWRs.....224
Figure 8.6 Reload fuel enrichment requirement with H/HM.....226
Figure 8.7 Fuel cycle costs with discharge burnup (same core energy production).....227
Figure 8.8 Fuel cycle decomposition for the central-voided annual fuel.....228
Figure 8.9 Uranium utilization for different neutron spectra.....233
Figure 8.10 SWU utilization for different neutron spectra.....233
Figure 8.11 Refueling cost levelization.....235
Figure 8.12 Refueling cost as a function of cycle length.....236
Figure 9.1 Eigenvalue difference from CASMO-4 as a function of burnup.....242

Figure 9.2 Plutonium vector comparison with CASMO-4 as a function of burnup 242
Figure 9.3 MCODE/CASMO results for 9.75 w/o enrichment 244
Figure 9.4 MDNBR and pressure drop as a function of H/HM for solid fuel pin 248
Figure 9.5 MDNBR comparison in hot channel for the IXAF and reference solid pin...249
Figure 9.6 Fission gas release calculations for various fuel pins.....250
Figure 9.7 Relative decay power after discharge.....251

List of Tables

Table 1.1 Evolution of the Westinghouse PWR fuel assembly 5
Table 1.2 Pros and cons of high burnup fuel 7
Table 1.3 Conceptual evaluations of four principal high-burnup schemes 9
Table 2.1 The production cost reduction in going from 12 to 24 month cycles 18
Table 2.2 Operating parameters for a typical Westinghouse 4-loop PWR.....22
Table 2.3 Typical parameters in CASMO-4 runs 39
Table 2.4 Optimum parameters for uranium utilization at fixed cycle lengths 49
Table 2.5 Optimum parameters for SWU utilization at fixed cycle lengths.....49
Table 3.1 MCNP-tallied one-group cross sections 65
Table 3.2 Capture cross sections and branching ratios of Am-241 and Pm-147 67
Table 3.3 Numerical examples of various coupling schemes.....72
Table 3.4 MCODE comparison with MOCUP and MONTEBURNS.....73
Table 3.5 Pin cell model parameters (cold condition at 300 K) 74
Table 3.6 Initial compositions (cold condition at 300 K) 74
Table 3.7 Summary of benchmark codes.....75
Table 3.8 The chosen 39 actinides in MCODE 76
Table 3.9 The chosen 100 fission products in MCODE 77
Table 3.10 Fractional differences of nuclide concentration at 100 MWd/kg 81
Table 3.11 Recoverable energy per fission (MeV/fission) for important nuclides.....85
Table 4.1 Comparison of PWR lattices.....96
Table 4.2 Pin cell model parameters.....98
Table 4.3 Optimum Height-to-Diameter ratios, H/D, for cylindrical reactor cores 119
Table 4.4 Summary of alternative core design tradeoff scaling 122
Table 5.1 Material properties of supporting matrices.....130
Table 5.2 Neutronic parameter summary of supporting matrices.....132
Table 5.3 CASMO-4 and MCNP results for IXAF and reference solid fuel at BOL.....139
Table 5.4 Operating conditions and geometric parameters of solid and IXAF cases.....141

Table 5.5 Eigenvalues, contributing parameters, and reactivity feedback coefficients at BOL 146
Table 6.1 Poison-free, BOC core parameters for various designs (18-month cycle) 162
Table 6.2 Fuel cycle limiting criteria 163
Table 6.3 Properties of boron, gadolinium, and erbium 166
Table 6.4 Practically-considered ways of varying H/HM 181
Table 7.1 High burnup spent fuel under consideration 194
Table 7.2 Comparison of 100 and 50 MWd/kg spent fuel characteristics 204
Table 7.3 Actinide compositions (wt%) in high-burnup spent fuel 205
Table 7.4 Plutonium isotope properties important to proliferation resistance 209
Table 7.5 Plutonium category divisions 210
Table 7.6 Approximate isotopic composition correlations for current PWR lattices with H/HM=3.4 210
Table 8.1 The fuel cycle economics parameters 222
Table 8.2 Fuel cycle cost comparison of different high burnup strategies 229
Table 8.3 Revised fuel cycle cost comparison of different high burnup strategies 236
Table 9.1 MCODE comparison with MOCUP and MONTEBURNS 241
Table 9.2 Comparison of strategies to achieve high burnup in PWR cores 244
Table 9.3 Poison-free, BOC core parameters for various designs (18-month cycle) 246
Table 9.4 Practically-considered ways of varying H/HM 247

Abbreviations for Organizations

AEC	Atomic Energy Commission (US)
ANL	Argonne National Laboratory (US)
BNFL	British Nuclear Fuels, Ltd. (UK)
CANES	Center for Advanced Nuclear Energy Systems (MIT)
DOE	Department of Energy (US)
EPRI	Electric Power Research Institute (US)
ERDA	Energy Research and Development Administration (US)
IAEA	International Atomic Energy Agency
INEEL	Idaho National Engineering & Environmental Laboratory (US)
INER	Institute of Nuclear Energy Research (Taiwan)
INPO	Institute of Nuclear Power Operations (US)
JAERI	Japan Atomic Energy Research Institute (Japan)
KAERI	Korea Atomic Energy Research Institute (Republic of Korea)
LANL	Los Alamos National Laboratory (US)
NEA	Nuclear Energy Agency (OECD)
NRC	Nuclear Regulatory Commission (US)
OECD	Organisation for Economic Co-operation and Development
ORNL	Oak Ridge National Laboratory (US)
PNNL	Pacific Northwest National Laboratory (US)
TEPCO	Tokyo Electric Power Co., Inc. (Japan)

Nomenclature

ACT	actinides
AOA	Axial Offset Anomaly
AOO	Anticipated Operational Occurrence
AP	activation products
at%	atom percent
ATWS	Anticipated Transients without Scram
BOC	Beginning of Cycle
BOL	Beginning of Life
BOR	boron concentration
BP	Burnable Poison
BWR	Boiling Water Reactor
CERCER	ceramic fuel particle dispersed in a ceramic matrix
CERMET	ceramic fuel particle dispersed in a metallic matrix
CHF	Critical Heat Flux
CMS	Core Management System
CR	Conversion Ratio
CRD	control rod
CZP	Cold Zero Power
DNBR	Departure from Nucleate Boiling Ratio
DUPIC	direct use of PWR spent fuel in CANDU
EFPD	Effective Full Power Day
EFPM	Effective Full Power Month
EFPY	Effective Full Power Year
EOC	End of Cycle
EOL	End of Life
FBR	Fast Breeder Reactor
FP	fission product
FTC	Fuel Temperature Coefficient

H/HM	Hydrogen to Heavy Metal Atom Ratio
HBWR	Heavy Boiling Water Reactor
HFP	Hot Full Power
HLW	High-Level Waste
HTGR	High Temperature Gas-cooled Reactor
HZP	Hot Zero Power
IFBA	Integrated Fuel Burnable Absorber
IHM	Initial Heavy Metal
IMF	Inert Matrix Fuel
IXAF	Internally and eXternally-cooled Annular Fuel
LMFBR	Liquid Metal Fast Breeder Reactor
LOCA	Loss of Coolant Accident
LOFA	Loss of Flow Accident
LOHA	Loss of Heat-sink Accident
L^3P	Low Leakage Loading Pattern
LRM	Linear Reactivity Model
LWR	Light Water Reactor
MCNP	Monte Carlo N-Particle Transport Code
MCODE	MCNP-ORIGEN DEpletion Program
MDNBR	Minimum Departure from Nucleate Boiling Ratio
METMET	metallic fuel in metallic matrix
MOCUP	MCNP-ORIGEN Coupled Utility Program
MONTEBURNS	Monte Carlo Burnup code
MOX	mixed oxide (UO_2 and PuO_2) fuel
MSLB	Main Steam Line Break
MTC	Moderator Temperature Coefficient
MTIHM	Metric Ton Initial Heavy Metal
MWd/kgIHM	MWd per kg IHM, equivalent to GWD per MTIHM
NFC	Nuclear Fuel Cycle
O&M	Operation and Maintenance
ORIGEN	Oak Ridge Isotope GENeration and Depletion Code

PCI	Pellet-Cladding Interaction
PCMI	Pellet-Cladding Mechanical Interaction
ppm	part per million
PWR	Pressurized Water Reactor
RCCA	Rod Cluster Control Assembly
RGPu	Reactor Grade Plutonium
rms	Root Mean Square
SCWR	Super Critical Water cooled Reactor
SSP	solid solution pellet (homogeneous)
SWU	Separative Work Unit
TFU	fuel temperature
TMO	moderator temperature
VIPRE	Versatile Internals and Component Program for Reactors; EPRI
WGPu	Weapon Grade Plutonium
w/o	weight percent
wt%	weight percent

1. Introduction

"A journey of a 1000 miles begins with a single step"
— Chinese Proverb

1.1 Background

Energy demand in developing nations is increasing to support their growing populations and economies. In addition, as aging power plants in the United States and Europe are replaced, new electrical capacity is needed. Generally speaking the demand will be met by a combination of fossil, renewable, and nuclear energy sources. However, there are specific problems associated with currently existing energy sources.

Fossil-fueled energy leads to accumulation of greenhouse gases (global warming issue). It is shown in Figure 1.1 [1] that atmospheric carbon dioxide (CO_2) concentration has increased more than 30% since industrialization (about 1800) while the CO_2 level before 1800 is almost constant. Fossil resources, such as coal, oil, and natural gas, are also very rare in many areas.

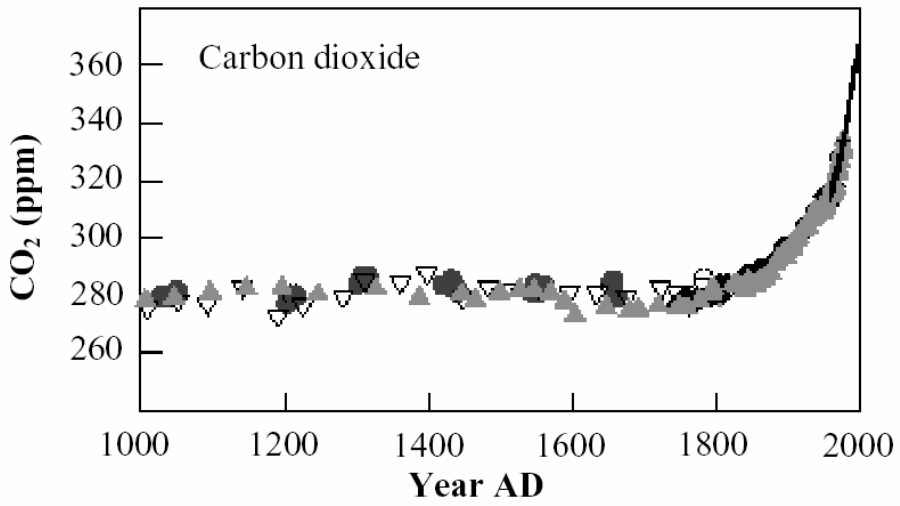

Figure 1.1 Atmospheric CO_2 concentration over the last millennium [1].

Some renewable energy resources, such as hydro, are in limited supply; and others, such as wind power, are of intermittent nature, while some are not technologically mature. Most renewable energy options, such as solar and wind power, are by nature very dilute (low power density), which significantly increases the cost. However, although not competitive under current market conditions, those options are well supported by governments and the public.

Nuclear power, as an economical, safe, and clean energy source, is one promising option (perhaps the only option) capable of large-scale and short-term deployment. In addition, nuclear power can be used for hydrogen production [2], which is able to both decrease the operation & maintenance (O&M) cost by adopting a mode of operations that is not as limited by regional and seasonal electricity requirements and produce a clean energy inventory in the form of hydrogen. By 2050, hydrogen, not electricity, may be the largest long-distance energy carrier [3]. However, there are several challenges facing future possible expansion of nuclear energy:

1. *economic viability* — Nuclear power has to be economically competitive with other energy sources. In particular, future nuclear power plant development should take into consideration the advances in technology of all other energy sources and the deregulated electricity market. Better engineering approaches need to be devised so that both the high capital cost and the long construction time can be reduced. This is a fundamental commercial constraint on nuclear energy.
2. *spent fuel & proliferation resistance* — The spent fuel issue needs to be actively studied and resolved. The cost of storage, handling, and disposition of spent fuel should be better defined and incorporated into current nuclear fuel cycle economics with less uncertainty. More practical guidelines for the back end of the nuclear fuel cycle need to be discussed and finalized. The proliferation potential of both the front end of the fuel cycle and of spent fuel needs to be minimized especially when nuclear power is more widely spread around the world in the future. This unique feature of nuclear power is the main focus of governments.
3. *public acceptance* — Nuclear power must improve public confidence by continuing to demonstrate a long history of safe operation. Also the safety issue in nuclear power is very closely related to its economic performance since reliability signifies reduced occurrence of precursor events which might lead to more severe consequences.

1.2 High Burnup Review

1.2.1 UO_2 Fuel

Almost all LWRs are using uranium dioxide (UO_2) as fuel except that some nuclear power plants are fueled partially with mixed oxide fuel (MOX), i.e., PuO_2 mixed with UO_2. Nevertheless, uranium is the major fuel in the form of UO_2. Compared to other fuel forms, such as the metallic U/Zr alloy, there are distinct advantages of UO_2 fuel, such as its high chemical/irradiational stability, high melting temperature, and the ease of fabrication (low cost) [4]. Hence, uranium dioxide fuel is the primary form considered for high burnup fuels.

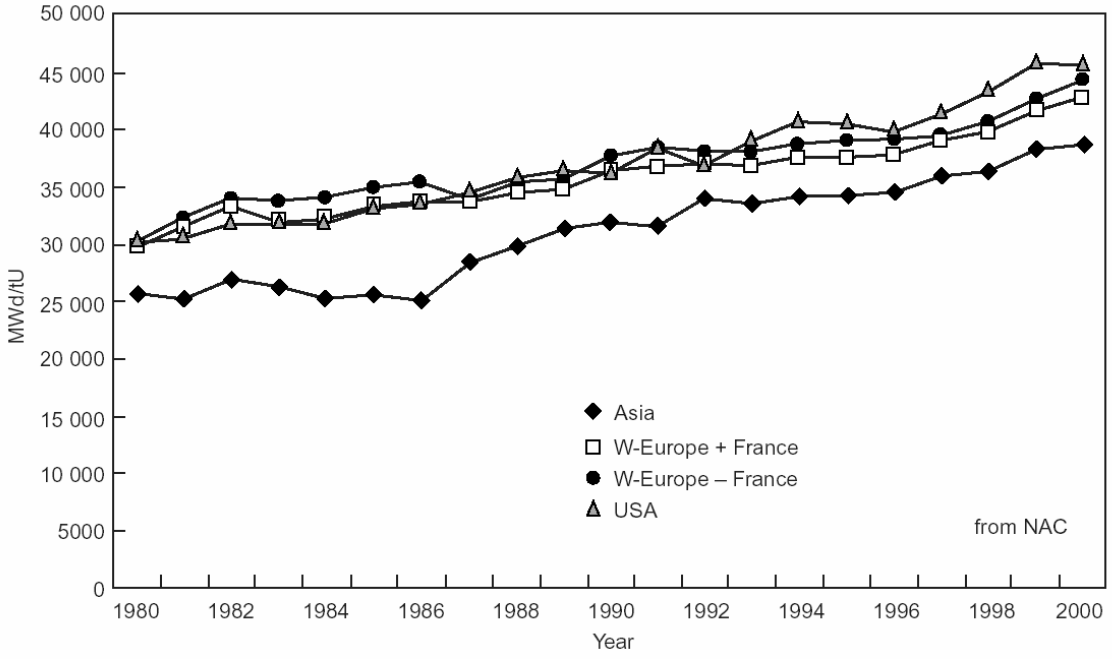

Figure 1.2 Historical discharge burnup trend over the 1980-2000 period (PWR) [5].

The basic issue of UO_2 fuel associated with its high burnup characteristics is its U-235 enrichment level, which is closely related to the total fuel cost. The historical trend has shown an increase in discharge burnup, e.g., the average increase of discharge burnup in the 1990s is about 1 MWd/kg per year for PWRs as shown in Fig. 1.2 [5]. The high

burnup was a strategy to respond to nuclear energy economics by improving fuel utilization. This was mainly achieved by increasing the average reload UO_2-fuel enrichment from ~2.5 w/o in the 1970s to ~4 w/o today. The UO_2 fuel licensing enrichment limit is, however, set by the US Nuclear Regulatory Commission (NRC) as 5 w/o for current fuel fabrication plants. Increasing this to enable higher burnup needs to be scrutinized because this will involve significant changes in the supporting front-end infrastructure of the nuclear fuel cycle. For example, enrichment facility operators need to re-examine their criticality precautions and enrichment (separative work unit, SWU) capability. However, this licensing limit is not a technical barrier but an arbitrarily-defined conservative enrichment limit for the front end of the LWR fuel cycle from a criticality safety perspective. Another consideration governing the fuel enrichment limit is proliferation resistance. It is obviously easier to divert higher enriched fresh UO_2 fuel to weapon usage. The U-235 enrichment deemed to be significant in this regard is 20 w/o, which sets the upper enrichment limit. In addition, the International Atomic Energy Agency (IAEA) has promulgated another enrichment limit, 10 w/o, as a technical barrier against proliferation potential [6]. Therefore, the typical enrichment level used in the present work is 9.75 w/o unless otherwise specified. This represents a conservative ceiling on the highest desirable enrichment under strict proliferation constraints.

1.2.2 Literature Review

As seen in Fig. 1.2, fuel burnup has been gradually increased over the past twenty years. In fact, this trend of pursuing higher discharge fuel burnup persists ever since the first large scale commercial PWR of Yankee Rowe in 1960. In the early 1970s the average burnup for a PWR in the US was about 20 MWd/kg. In the late 1970s discharge burnups in the 33 MWd/kg range were achieved. Table 1.1 summarizes the Westinghouse PWR fuel assembly evolution before 1985 under the influences of technological progress as well as the economic, political, and regulatory environment [7]. Few global assembly design changes have been made since then.

Table 1.1 Evolution of the Westinghouse PWR fuel assembly [7].

Date	Design Feature	Primary Impacts	Comment
1963	Grid Springs	Economics	Enable separate rod and assembly fabrication, eliminate brazing, reduce parasitic absorption
1965	Mixing Vanes	Licensing	Improve DNB margin
1967	Rod Cluster Control	Economics Reliability	Minimize water slot peaking; further reduce parasitic material
1967	Improved Grid	Licensing Reliability	Further improve DNB margin, provide better rod support; improve control of channel spacing; change to Inconel to improve spring characteristic
1968	Zircaloy Clad	Economics	Further reduce parasitic material
1968	Helium Prepressurization	Reliability	Minimize fuel clad interaction potential; preclude rod flattening
1971	Zircaloy Thimbles	Economics	Further reduce parasitic material
1975	17×17 Fuel Array	Licensing	Reduce peak kW/ft; reduce calculated LOCA temperature; reduce rod duty
1981	Reconstitutable Bottom Nozzle	Reliability	Simply assembly repair or rod replacement
1982	Optimized Fuel Assembly (Smaller diameter rods, Zircaloy grids, increased burnup)	Economics	Further reduce parasitic material; improve fuel cycle economics
1984-85	VANTAGE 5 (Axial blankets, IFBA, RTN, IFM, increased burnup)	Margin Flexibility Economics	Improved neutron economy, increased DNB and LOCA margin, facilitate repair/removal

At MIT, there have been efforts to design long operating cycle LWR cores in the 1990s in order to improve the economic performance by increasing the plant capacity factor. Reload core designs for a 38.8-effective-full-power-month (EFPM) PWR cycle and a 45-EFPM BWR cycle were developed by M. V. McMahon to offer nuclear utilities the opportunity for economic benefit by permitting higher plant capacity factors and by reducing the number of costly refueling operations that must be performed [8]. The designs use a single-batch loading strategy to stay within current fuel burnup licensing limits of 60 MWd/kg and contain fuel enrichment as high as 7.4 w/o. However, an economic analysis of these cores shows that extended-cycle cores do not offer a significant economic benefit over conventional practice.

In a later detailed economic study [9], it was recognized that the extra fuel costs that would be incurred from implementing an extended cycle would stem from the increased enrichment necessary to maintain criticality for the life of the core. Multi-batch refueling is more economical than single-batch fueling for cycle lengths not in the ultra-long range, i.e., 48 calendar months for the PWR. The current 3-batch fuel management, 18-month PWR is about the optimum. Unless quite substantial improvements in technol-

ogy are forthcoming or economic circumstances change significantly, departure from two- to four-batch management or longer than 2- to 3-yr cycles in LWRs is not economically attractive compared to current industry practice [10, 11].

Since parametric studies indicated that the economically optimum length for a PWR, single-batch core is about 36 calendar months, such a PWR core was then designed by L. Garcia-Delgado [12]. Fuel was enriched to 6.5 w/o and gadolinia selected as the burnable poison mixed with UO_2. This 36-month core is economically competitive with an 18-month reference core under certain operational conditions.

Besides the work done at MIT, there has been an EPRI study (so-called robust fuel program) on optimizing LWR cycle length and fuel burnup [13]. It was shown that for the 18-month cycle of a PWR core, fuel costs decline by about 4.2% as the batch average discharge burnup increases from about 49,900 to 53,800 MWD/MT.

In addition, some fuel testing activities on high burnup (> 50 MWd/kg) are in progress in the heavy boiling water reactor (HBWR) at Halden [14]. Both urania and MOX fuels are being studied regarding thermal behavior, conductivity degradation, and aspects of fission gas release. This activity demonstrates continued commercial interest in further improving fuel burnup.

1.3 Motivation

1.3.1 Incentives

After a brief review of the historical trend of increasing discharge burnup for PWRs via an enrichment increase, the motivation for pursuing high burnup and potential barriers to achieve this goal is clear and readily summarized in Table 1.2 (assuming a once-through fuel cycle). In summary high burnup holds the promise of reduced fuel cycle cost, smaller reload core fractions, longer cycle lengths, and decreased spent fuel storage requirements for the once-through fuel cycle [15]. High burnup is now a common design characteristic of Generation-IV reactors [16].

Table 1.2 Pros and cons of high burnup fuel.

UNIVERSAL BENEFITS	COMMON CHALLENGES
1. Reduced number or size of assemblies per MWe·yr, hence reduced fuel handling, storage, transportation, and disposal 2. Less Pu in spent fuel per unit energy derived and poorer weapon-usable isotopics 3. Better utilization of resources	1. Reactivity control due to excess fissile material in an extended cycle 2. Cladding corrosion for longer cycles 3. Fission gas release 4. Higher dose and heat rate per kg of spent fuel, hence longer on-site storage for decay (for current canisters) 5. Higher enrichment requires upgrade and relicensing of front end facilities

The reduction of spent fuel (both volume and mass) is a key advantage for high burnup strategy when considering its broad implications to the back-end fuel cycle, particularly under the once-through fuel cycle constraint. As mentioned in the previous section, nuclear waste has been one of the major challenges that limit the future potential of nuclear expansion. There is widespread public concern about spent fuel radiological hazards and its potential escape to the bio-sphere. In the US, the Yucca Mountain site in Nevada was designated by law to be the candidate geologic disposal site. However, the capacity of Yucca Mountain is limited. Therefore, a high burnup strategy is an important approach to effectively increasing the capacity of the repository by reducing the generation of spent nuclear fuel.

From a proliferation point of view, high burnup spent fuel possesses a higher radioactivity inventory and has better proliferation resistance. Generally speaking more fission products are accumulated in the high burnup spent fuel, which act as an additional technical barrier for diverting the spent fuel. The plutonium in the high burnup spent fuel (a sensitive nuclear material) is less desirable in terms of both the radiation barrier and its isotopic composition (more Pu-238 and Pu-240). In fact, if one could achieve full burnup (destroy all the heavy metal), proliferation would not be an issue.

On the other hand, high burnup fuel poses a challenge on the materials side, namely, more cladding corrosion (higher neutron fluence and/or longer in-core time) and increased fission gas release from the fuel pellet [17, 18]. The traditional Zircaloy, the current cladding material, has almost reached its technological limits. New cladding materials, such as the M5 solid-wall alloy developed at Framatome-ANP, have much better corrosion performance [5]. Other fuel vendors and laboratories also have advanced zirco-

nium-based alloys under development. The increased fission gas release also needs to be considered for appropriate fuel pin design. Overall, these material barriers constitute major technical difficulties in achieving higher burnup.

1.3.2 High-Burnup Implementation

It should also be realized that "high burnup" is not really a rigorous concept but a subjective one. For various groups, at different times, or in different regions, the term high burnup might have significantly different values. In particular, countries which reprocess and recycle LWR fuel might come to different conclusions than the US (which currently deploys only the once-through fuel cycle). In addition, the word "burnup" is imprecise. For example, in the fuel management field, the burnup usually refers to the batch-averaged discharge burnup. In contrast, the fuel analyst pays more attention to the so-called peak pin, which has the highest burnup among all fuel pins. Fundamentally, the definition of burnup is the energy production associated with a unit mass of initial heavy metal within specific regions. For example, the assembly has its average burnup and each pin in the assembly also has its individual burnup. Since the energy production is directly related to revenue for utilities, the burnup concept is an important measure of the value of the fuel. The essence of high burnup is to extract more energy from the same mass of initial heavy metal, i.e., more efficient usage of nuclear fuel, which results in more consumption of U-235 and better utilization of plutonium produced during operations.

There are four principal specific options, starting from conventional PWRs, by which to exploit high burnup capability (Table 1.3):

I. Increase cycle length at the same linear power, using the current 3-batch fuel management scheme;
II. Keep current cycle length and linear power, increase the number of batches;
III. Design a very long life core with single-batch refueling at reduced power density;
IV. Increase power density, burn faster, keep the same cycle length and refueling rate.

Each has its particular advantages and disadvantages. Options I and II are retrofitable into current LWR cores, and options III and IV are likely to be acceptable for new cores only.

Table 1.3 Conceptual evaluations of four principal high-burnup schemes.

	Option	UNIQUE BENEFITS	SPECIAL CHALLENGES
RETROFIT CORES	I. longer cycle	✓ Save on refueling expenses	✘ Harder to meet power peaking limits ✘ Need more control poison
	II. more batches	✓ Reduced ore and SWU per MWe·yr (relative to Option I, but not vs. current practice) ✓ More fuel shuffling options; reduced reactivity difference between assemblies and over the core	✘ Fewer than other options
NEW CORES	III. single batch	✓ Improved institutional safeguards ✓ Reduced on-site operations and staffing ✓ Large refueling saving	✘ More expensive fuel ✘ Need more control poison or higher conversion ratio (latter further increases fuel costs)
	IV. increase power density	✓ Save on carrying charges ✓ Possible to reduce core volume ✓ Shorter clad exposure in reactor compared to I,II,III	✘ Need new fuel pin and assembly design ✘ Harder to meet thermal hydraulic limits (DNBR, LOCA, fuel melt)

1.4 Objectives

The primary objectives of the work reported here are to determine the neutronically-achievable high burnup potential and to identify viable high burnup core designs taking into consideration the operational neutronic parameters (such as reactivity control and feedback), engineering constraints (such as thermal hydraulics and fuel performance) and other important aspects (such as spent fuel characteristics, proliferation resistance, nuclear fuel cycle economics, etc.). For a conventional PWR core and fuel design, i.e., existing plants, there is a very limited design space to increase burnup. The most effective way is to increase the average reload enrichment (higher initial reactivity), which needs detailed analysis/verification in order to satisfy NRC safety regulations. However, when taking a broader view, one should optimize the lattice design to achieve high burnup. In addition, various new fuel options, including annular fuel with or without internal cooling, and new fuel material compositions, such as CERCER, CERMET or METMET, need to be considered. The overall strategies for design and deployment of high burnup cores

need to be addressed and analyzed. The impact of high burnup fuels on the contemporary fuel cycle in a sustainable environment also needs to be assessed.

In summary, the effort is targeted at a full exploration of high burnup fuel characteristics and the strategies of developing and utilizing high burnup fuels in PWRs. Note that although various options are investigated, none of them is optimized. Therefore, the present strategic study is not intended to propose a detailed new design, but to identify the directions that have the best potential for providing a satisfactory design.

1.5 Analysis Tools

As a relatively mature subject, there are many modern computer codes available to perform various tasks in reactor design calculations. Although a purely analytic solution to the fundamental full-scope neutron transport equation with generalized boundary conditions is still unknown, computer simulation codes can provide sufficiently accurate numerical solutions for a given problem when measured against real plant operating data. For example, the maximum error of SIMULATE-3 predictions of a typical LWR core power distribution is within 5% of a nuclear power plant's measured data through the entire cycle [19]. Therefore, with these advanced tools, reactor core design and evaluation are feasible and conclusions/insights/findings can be based on those calculations reliably. In reality, nuclear utilities usually perform calculations beforehand and use the resulting output as guidance in operating reactors.

In the following, several state-of-the-art codes, which are utilized in the present work, are introduced:

1.5.1 Studsvik Core Management System (CMS) Code Package

The Studsvik (now called Studsvik Scandpower Inc. after merging with another reactor physics code developer) Core Management System (CMS) code package consists of CASMO-4 [20], TABLES-3 [21], and SIMULATE-3 [22]. Combined together, these licensing-level, commercial codes are capable of performing LWR core reload analysis and are being widely used by utilities to do routine fuel management calculations. Figure 1.3 shows the tandem way of running the CMS code package, i.e., CASMO-4 (lattice

code) generates two-group cross sections and other parameters (such as discontinuity factors) for each type of assembly, TABLES-3 then reads CASMO-4's card image files (`.cax`) and transfers them into a binary-format library; then SIMULATE-3 (advanced nodal code) can perform core reload analysis (different core loading patterns) based on the generated library. Each of the CMS codes is described in the following paragraphs.

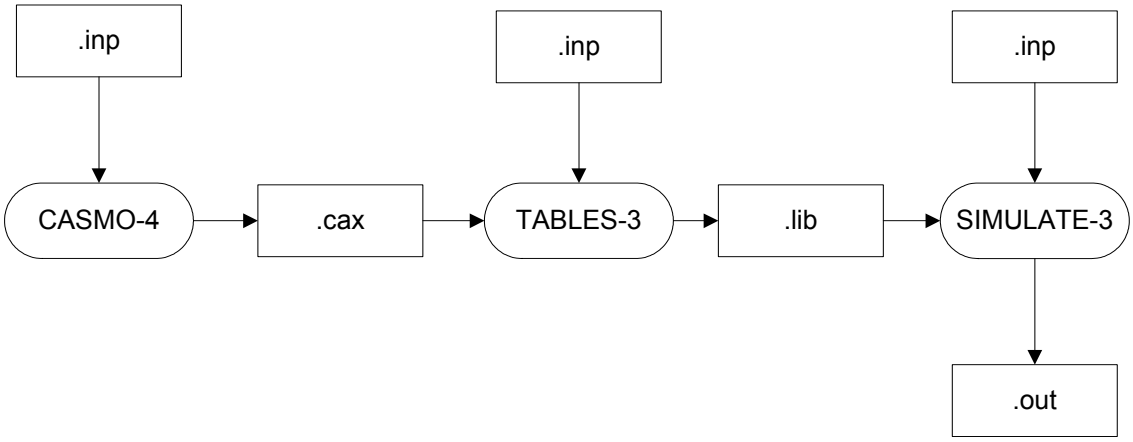

Figure 1.3 Flow of calculations for the CMS code package.

CASMO-4 is a multi-group two-dimensional transport code entirely written in FORTRAN 77. As a deterministic lattice physics code, it is used for burnup calculations of LWR assemblies or pin cells. The code can represent geometries consisting of cylindrical fuel rods of varying compositions in a square/hexagonal lattice. Version 4 of CASMO uses the iterative, 2-dimensional characteristic solution KRAM [23], which solves the 2-dimensional Boltzmann transport equation in the fully heterogeneous lattice to give the flux distribution. This represents a significant improvement from previous versions of CASMO, which are all based on entirely traditional collision probability methods.

TABLES-3 is a data processing code which links CASMO to SIMULATE. The code processes the following types of data from CASMO output card image files to generate a binary SIMULATE-readable library: two-group cross sections, discontinuity factors, fission product data, detector data, pin power reconstruction data, kinetic data, and isotopics data.

SIMULATE-3 is a two-group, three-dimensional (steady-state) modern nodal code, which can be used to perform in-core fuel management studies, core design calcu-

lations, and calculation of safety parameters. The code itself is an example of the success of advanced modern nodal methods, which are formulated consistently and without any adjustable parameters to match reference solutions. Detailed comparisons with critical assembly measurements have demonstrated that PWR pin-by-pin power distributions have root mean square (rms) differences of about 1.0% relative to measured data. Peak pin powers were predicted with rms differences of less than 0.5% relative to measured data [19].

1.5.2 MCNP-4C

MCNP [24] is a general purpose, generalized-geometry, continuous-energy, coupled neutron/photon/electron Monte Carlo N-Particle transport code developed at the Los Alamos National Laboratory (LANL). The stochastic model is pre-eminently realistic (a theoretical experiment) where the spatial and energy treatments are in principle exact. Therefore, given sufficient neutron histories and appropriate cross section libraries, MCNP solves the neutron transport equation exactly for any type of reactor. Unlike deterministic codes, such as CASMO-4, MCNP is, in principle, universally applicable to any transport calculation (for example not limited to LWRs). In this sense, it is the *best* transport code available today.

The only disadvantage of MCNP compared to deterministic codes is its demanding CPU requirements. For example, in order to obtain acceptable statistical variations, hours of MCNP calculations are usually needed whereas CASMO-4 takes only seconds.

1.5.3 ORIGEN2

ORIGEN2.1 [25] is a one-group, point depletion and radioactive decay code developed at the Oak Ridge National Laboratory (ORNL). Instead of solving the complicated neutron transport equation like CASMO-4 and MCNP, ORIGEN2.1 uses a relatively unsophisticated one-group neutronics calculation focusing on the detailed isotopic composition calculations. Typically a total of 1700 nuclides are considered including 130 actinides, 850 fission products, and 720 activation products. Therefore, in terms of isotopic representation, ORIGEN2.1 is complete. The code is ideal for calculating spent fuel characteristics (composition, thermal power, radioactivity, toxicity, etc.). However, for burnup

calculations, an advanced physics code is needed to adjust the effective one-group cross section library to represent correct neutron spectrum.

1.5.4 MCODE

The MCNP-ORIGEN DEpletion program (MCODE) is an MCNP-ORIGEN linkage code developed by the author, which combines the continuous-energy Monte Carlo code, MCNP-4C, and the one-group depletion code, ORIGEN2.1, to perform burnup calculations. MCNP is capable of providing the neutron flux and effective one-group cross sections for different MCNP-defined regions. ORIGEN, in turn, carries out multi-nuclide depletion calculations for each region and provides material compositions to update beginning-of-timestep MCNP input. This console program is entirely written in ANSI C. Chapter 3 will present in detail the development as well as the verification of the code.

1.5.5 VIPRE

VIPRE (Versatile Internals and Component Program for Reactors; EPRI) [26] was developed for nuclear power utility thermal-hydraulic analysis. The code was designed to help evaluate LWR core safety limits including minimum departure from nucleate boiling ratio (MDNBR), critical power ratio (CPR), fuel and clad temperatures, and coolant state in normal operation and assumed transient conditions by solving the set of finite-difference conservation equations for mass, energy and momentum of the coolant in interconnected subchannels, assuming incompressible thermally expandable homogeneous flow. Although the formulation is based on a homogeneous coolant for each finite volume, non-mechanistic models are included for sub-cooled boiling and vapor/liquid slip in two-phase flow.

VIPRE modeling structure is based on subchannel analysis. The core, fuel bundle or any other section of symmetry is defined as an array of parallel flow channels with lateral connections between adjacent channels. A channel may represent a small area between fuel rods or a larger area representing several assemblies. The shapes and sizes of these subchannels are arbitrary, depending on the expected level of detail in the analysis. In areas where the fuel design is expected to be critical, the fuel is analyzed in detail, while in the rest of the core average values are good enough. The code is tailored to the utilities' analytical requirements in fuel reload analysis, allowing for example the use of

several critical heat flux (CHF) correlations, and having the capability to iterate operating conditions to attain a given MDNBR (safety requirement), and to include thermal transport within fuel rods including a gap conductance model.

1.5.6 FRAPCON-3

FRAPCON-3 [27] is a fuel performance code for calculating steady-state fuel behavior at high burnup (up to 65 MWd/kg) developed jointly by Pacific Northwest National Laboratory (PNNL) and Idaho National Engineering & Environmental Laboratory (INEEL). Based on a single channel coolant enthalpy rise model, the code iteratively calculates the interrelated effects of fuel and cladding temperature, rod internal gas pressure, fuel and cladding deformation, fission gas release, fuel swelling and densification, cladding thermal expansion and irradiation-induced dimensional changes, cladding corrosion, and crud deposition as functions of time and fuel rod power.

1.6 Thesis Organization

This report is structured in nine chapters. This chapter (Chapter 1) begins with a rudimentary introduction of the background, high burnup review, motivation, objectives, and analysis tools used. The central idea in this effort is to investigate the strategy of high burnup fuels using a PWR as an example.

Chapter 2 then looks at current existing standard Westinghouse PWRs and investigates operational limitations, material challenges, and economic implications of the high burnup approach. This serves as a basic review of where PWR core features stand today and some practical limits that need to be considered. Conventional core neutronic calculations are also performed to scope out the operating regimes of various approaches. It is concluded that within the retrofit cores the high burnup approach of more batches is preferred.

Chapter 3 presents the development of MCODE in order to perform high burnup neutronic calculations for a wide range of options. High burnup, itself, is a challenge for the neutronic calculations due in part to the more complex fuel compositions at higher burnup. State-of-the-art reactor physics codes have been tuned to deal with conventional

burnups. It is thus necessary to have at least one or two reference calculations to verify results. Detailed benchmark calculations against CASMO-4 and HELIOS have been done, which show satisfactory agreement, i.e., when predicting the full-power operating time of the 18-month cycle the difference is only about 3 days.

Chapter 4 discusses the major parameter, moderator-to-fuel ratio, in UO_2/H_2O lattices. Since light water is used as both a coolant and a moderator, a useful parameter is the hydrogen-to-heavy-metal (H/HM) ratio. A virtual experiment, varying water density from its value in a standard Westinghouse PWR lattice, is performed and promising H/HM ranges are identified for high burnup applications. In addition to conventional uranium fuel, various fissile/fertile combinations, such as U-235/Th-232 and Pu-239/U-238, are briefly examined.

Chapter 5 turns to alternative advanced fuel options to achieve a wetter lattice, including annular fuel with or without internal cooling, CERCER, CERMET, and METMET fuel compositions. Although the wetter lattice has an increased burnup, a reduction of the energy production is observed for all these cases due to smaller core heavy metal loadings. Again the examination is still focused on neutronic characteristics.

Chapter 6 considers practical issues & constraints including the reactivity control and engineering constraints in lattice optimization. The reactivity control of high-burnup wetter cores poses a challenging problem. Burnable poison and soluble poison are investigated. Design changes, including axial heterogeneity and annular fuel, are discussed as a possible way to reduce the reactivity swing. Thermal margins and fuel aspects are addressed in engineering considerations for various approaches tried to effectively vary H/HM, such as internally cooled annular fuel and thinner rods.

Chapter 7 is devoted to the spent fuel issue for various H/HM lattices. The waste disposal characteristics are compared for various burnups. The effect of power uprate is discussed from the spent fuel perspective. The technical proliferation resistance barrier is also addressed in terms of plutonium vector. Finally wetter lattices are recommended for high burnup applications.

Chapter 8 is an overall assessment of the impact of high burnup on the contemporary nuclear fuel cycle. Various parts of the fuel cycle are discussed in regard to their response to higher fuel burnup, and an economics assessment is included.

Chapter 9 summarizes the work done, provides concluding remarks and makes recommendations for future work.

2. High Burnup Issues of Current PWR Designs

"Much effort, much prosperity"
— Euripides (485BC-406BC)

2.1 Introduction

The current fleet of commercial PWRs (69 operating reactors as of 2002 in the US, 212 units worldwide as of 2002 [28]), mostly built in the 1970s, has demonstrated excellent safety features and economic performance as large centralized power suppliers in today's electricity market. In the US, there has been only one major reactor accident leading to severe core damage: at Three Mile Island in 1979, which had essentially no environmental impact and no public injuries because of the preservation of the high-integrity reactor containment. Since then, a series of advanced reactors, such as the Westinghouse AP600/AP1000, have been designed and evaluated with emphasis on: (1) passive or inherent safety, (2) short construction time with simplified design, (3) one-step licensing, and (4) standardization. However, no advanced reactors have been built in the US to date and it is expected that many current PWRs can successfully extend their operating licenses from their original 40 years to 60 years or more. For instance, recently the operating licenses of Turkey Point-3 and -4 (two PWRs, each rated at 693 MWe), located in Florida City, FL, were renewed for an additional 20 years by the NRC [29]. Therefore, in this Chapter, the discussion of high burnup issues is focused on these conventional PWRs, which represent substantial assets and extensive industry practices.

Economic competitiveness is naturally of primary interest to utilities. Generally speaking the busbar electricity cost in the OECD countries can be decomposed into three components: capital cost (57%), operation & maintenance (O&M) cost excluding fuel (23%), and nuclear fuel cycle (NFC) cost (20%) [30]. Note that the given nuclear electricity cost breakdown is typical for current PWRs and will be different for a new plant. The capital cost accounts for more than half of the busbar cost, but it is a fixed sunk cost. The sum of the O&M cost and the nuclear fuel cycle cost is also called the production

cost, which is affected by fuel management strategy. The O&M cost, in principle, should increase with time due to plant aging. Meanwhile, there are other factors, such as accumulation of operating experience, advancing technological innovations, increasing operating cycle lengths, etc., which should more or less compensate for any increasing trend. The fuel cycle cost is primarily determined by the details of fuel management. In turn, there are many choices available to improve the production cost, which takes into account the lost revenue due to refueling downtime and the purchase of replacement energy[*]. High burnup, as a common factor, provides necessary operational flexibilities. Three major high burnup strategies have been realized in industry:

1. Increasing the cycle length by loading more fresh fuel and/or the same amount at higher enrichment, which leads to fewer refueling outages and gives rise to higher capacity factors. Historically the cycle length has increased from 12 months to nowadays 18 months or even 24 months. In fact, the longer cycle length increases the fuel cycle cost [31]. For example, the fuel cycle cost of an 18-month cycle is about 10% more expensive than a 12-month cycle. However, this can be compensated by the savings in O&M cost due to improved capacity factor (as shown in Table 2.1 [32]). In addition, the less frequent refueling outages also decrease the radiation exposure to workers, production of low-level waste and potential radiation release to the environment.

Table 2.1 The production cost reduction in going from 12 to 24 month cycles [32].

		Dollars Per Year
Increased fuel cycle costs:		$ 4.7 million
Savings due to:		
Replacement power	$ 8.5 million	
Refueling labor	$ 1.5 million	
Cycle design/licensing	$ 0.2 million	$ 10.2 million
Net gain		$ 5.5 million

[a]For a 950 MWe PWR plant.

2. Increasing the discharge burnup by increasing reload fuel enrichment for fixed cycle length (say 18 months). This strategy implies constant O&M cost. The savings come from the nuclear fuel cycle cost due to the reduction in fuel assemblies required and

[*] Under a deregulated electricity market, there is generally no obligation for nuclear utilities to purchase replacement energy from elsewhere. The only effect of shutdown refueling is losing revenues. However, under long-term contracts the utilities may have to purchase replacement energy.

more efficient fuel utilization (more batches). It is shown later in this chapter that there is an optimum reload fuel enrichment (around 5 w/o) with minimum fuel cycle cost (actually best utilization of uranium resources) under the once-through fuel cycle constraint. The industry practice is now close to the optimum point. As pointed out in Chapter 1, this approach is the main way of achieving high burnup when limited by the 5 w/o enrichment limit. In this way, spent fuel storage requirements are also alleviated due to the reduction in the number of discharged assemblies.

3. Increasing the rated power to sell more electricity (hence accrue more revenue) with acceptable costs, i.e., affordable changes to the plant itself. For the same cycle length and number of reload assemblies, a power upgrade can also save carrying charges by burning fuel faster (again higher fuel enrichment is needed). Uprating is currently an attractive approach with utilities, particularly under the current deregulated electricity market environment. Nuclear plant upratings result in plant power increases of up to 10 to 20 percent, which reinforces the economic viability of nuclear power (the market value of added energy) [33].

In reality, all three options can be adopted simultaneously in the same reactor. A common feature is that the increased fuel enrichment is the driving engine to achieve a higher burnup by increasing the initial reactivity. In responding to these strategies, new fuel assembly designs have been introduced by increasing the number of fuel rods in an assembly. The PWR fuel assembly lattice has increased from 14×14/15×15 to 16×16/17×17 and even 18×18/19×19 in European countries. The larger number of fuel rods increases the total heat transfer area although fuel rod diameters are slightly reduced, which results in a lower linear heat rate (lower fuel temperature) and a lower surface heat flux (more margin to DNBR) for a fixed core power output. The low fuel temperature is beneficial in reducing both the stored energy in fuel pellets (lower clad temperature following a LOCA accident) and the thermal expansion of pellets (less pellet-cladding interaction, PCI) [34].

In a core reload analysis, an important focus is the minimization of power peaking. In this regard, loading more fresh fuel assemblies with lower fuel enrichment is helpful although it will increase the fuel cycle cost. There is a trade-off between managing core power peaking and choosing the number of reload assemblies. Typically for each reload, several types of fuel assemblies are used (so-called split batches) while the maximum uranium enrichment is limited by 5 w/o. The split batch technique can both alleviate the

core peaking control and accommodate different core residence time within the same reload fuel assemblies. Hence, there is not much option space under the current enrichment limit (5 w/o) as shown in Fig. 2.1 [5] since the maximum U-235 enrichment is already very close to 5 w/o. The discussions in this chapter, therefore, will not be restricted by the NRC limit but will stay within the 20 w/o proliferation limit.

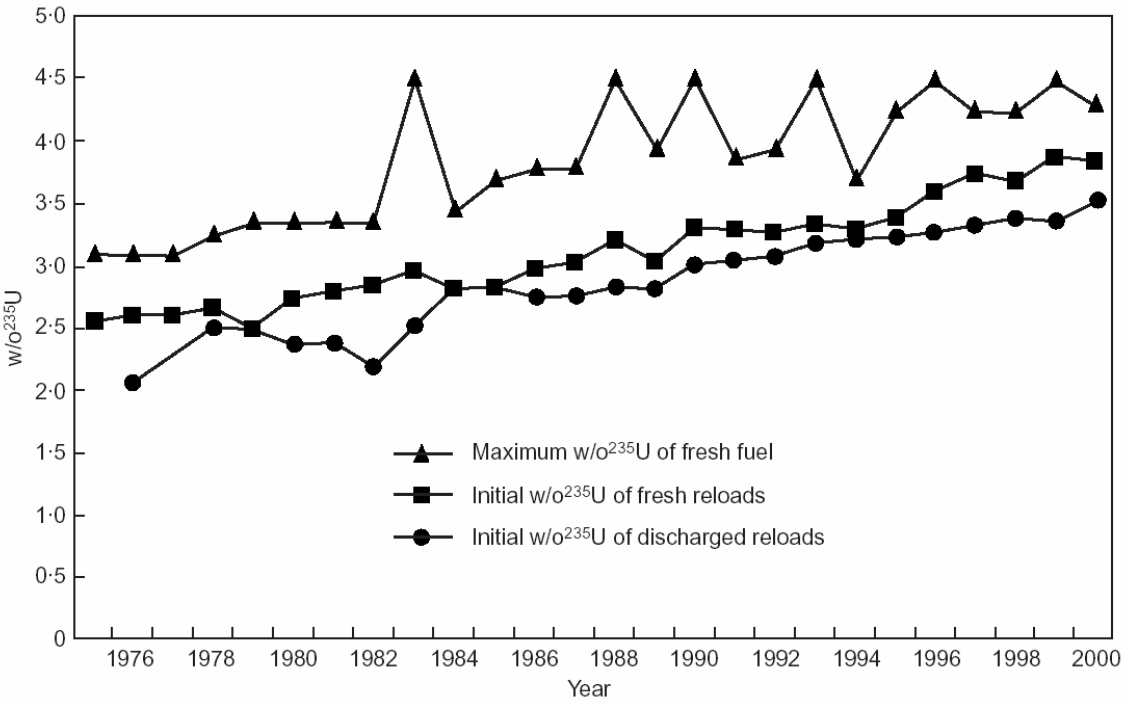

Figure 2.1 Uranium-235 enrichment over the 1976-2000 time period [5].

In this Chapter, a typical Westinghouse 4-loop PWR (the dominant type in the PWR category) will be taken as the reference case. A full range of scoping calculations for fuel between 3 and 20 w/o enrichments are performed for this reference case. The operating/design/licensing limits and safety features related to high burnup are then discussed. Various challenges and opportunities, such as materials limitations, economic penalties/gains, are addressed as high burnup issues for conventional PWRs.

2.2 Conventional PWR Description

2.2.1 General Description

As a pioneer in PWR technology, Westinghouse (now part of the Nuclear Utilities Business Group of British Nuclear Fuels, BNFL) had the largest number of PWRs in commercial operation including licensing to Framatome of France and Mitsubishi of Japan (technology transfer) [34]. A standard four-loop PWR (3411 MWth), the most common Westinghouse plant, is used here to represent conventional PWRs. The important core parameters are summarized in Table 2.2.

2.2.2 Reactivity Control

Reactivity control is necessary to suppress the excess reactivity needed to achieve desired cycle energy. There are three means of neutronic reactivity control: control rods, soluble poison (also known as chemical shim), and burnable poison. The basic objectives of reactivity control are to allow for power maneuverability, to ensure acceptable power distributions (and power peaking), and to provide shutdown margin (since reactivity increases at lower temperatures).

Control Rods

Figure 2.2 shows the locations of the control rods (also called rod cluster control assemblies, RCCA) and the spare reactor vessel head penetrations, which are positioned symmetrically in the core [35]. These spare locations can be used to install additional control rods if needed, so that no dramatic change is required to add more shutdown margin. In fact the number of penetrations on the reactor head depends on each specific reactor. The more-recently-built reactors have fewer penetrations since each penetration through the head might introduce potential problems, such as stress concentrations and material corrosion.

Table 2.2 Operating parameters for a typical Westinghouse 4-loop PWR.

Operating Parameter	Value
1. Plant	
Number of primary loops	4
Total heat output of the core (MWth)	3411
Total plant thermal efficiency (%)	34
Electrical output of plant (MWe)	1150
Energy deposited in the fuel (%)	97.4
Energy deposited in the moderator (%)	2.6
2. Core	
Core barrel inside diameter/outer diameter (m)	3.76/3.87
Mass of fuel UO_2 (MT)	101.0
Mass of fuel as U (MTU)	88.2
Mass of cladding material (MT)	23.1
Rated power density (kW/liter-core)	104.5
Specific power (kW/kgU)	38.7
Average linear heat generation rate (kW/ft)	5.6
Core volume (m^3)	32.6
3. Primary coolant	
System pressure (MPa)	15.51
Total core flow rate (Mg/sec)	18.63
Effective core flow rate for heat removal (Mg/sec)	17.7
Rated coolant mass flux ($kg/m^2 \cdot sec$)	2087.6
Core inlet temperature (°C)	292.7
4. Fuel rods	
Total number	50,952
Fuel density (% of theoretical)	94
Pellet diameter (mm)	8.19
Pellet height (mm)	13.4
Fuel-clad radial gap width (μm)	82
Cladding material	Zircaloy-4
Cladding thickness (mm)	0.57
Clad outer diameter (mm)	9.5
Active fuel height (m)	3.66
5. Fuel assemblies (17×17 square lattice)	
Number of assemblies	193
Number of fuel rods per assembly	264
Number of grids per assembly	7
Pin-to-pin pitch (mm)	12.6
Assembly pitch (mm)	214
6. Rod cluster control assemblies (RCCA)	
Neutron absorbing material	Ag(80)-In(15)-Cd(5)
Cladding material	Stainless Steel (SS) 304
Cladding thickness (mm)	0.46
Number of RCCA clusters	53

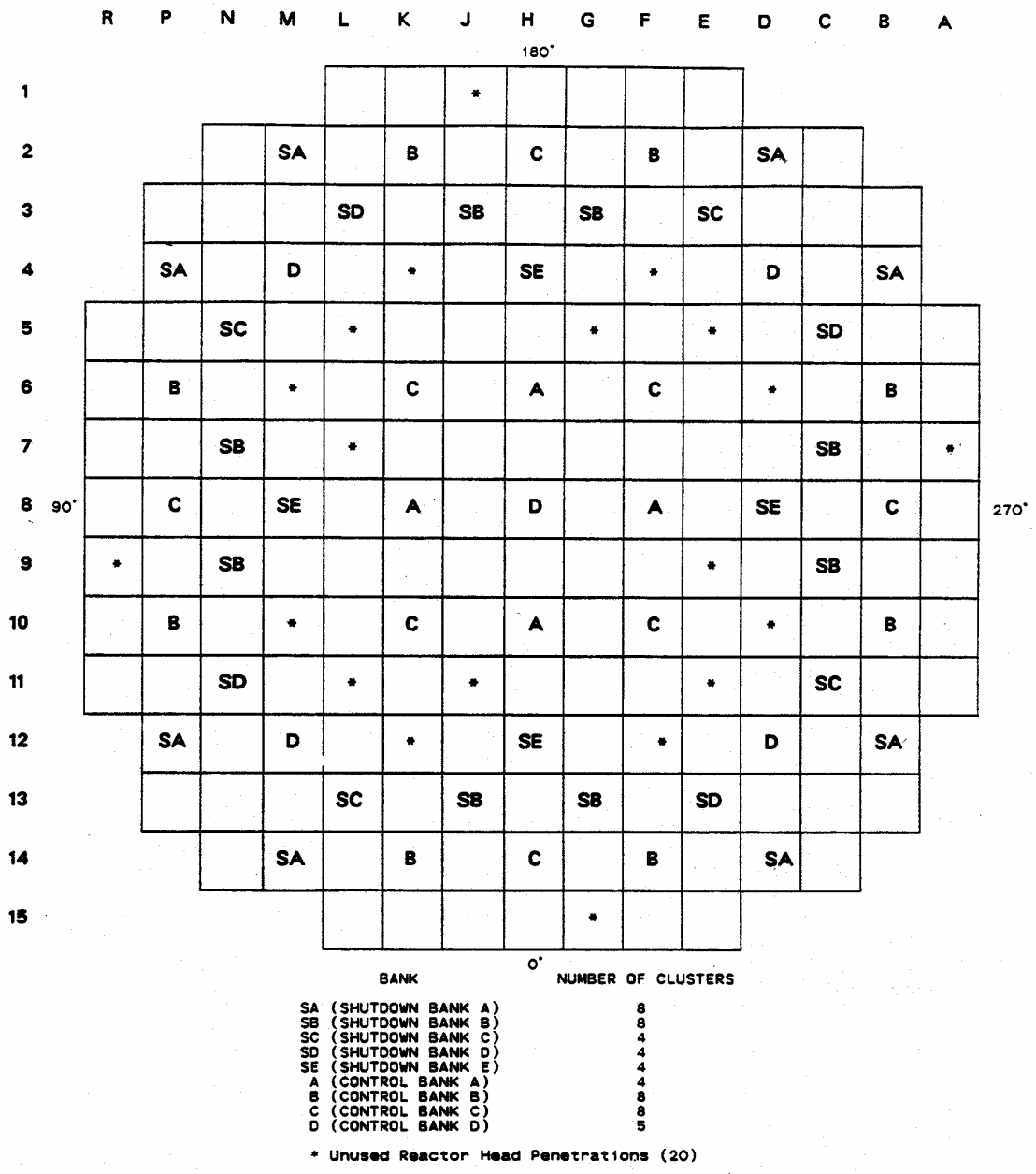

Figure 2.2 Cross sectional view of control rod locations [35].

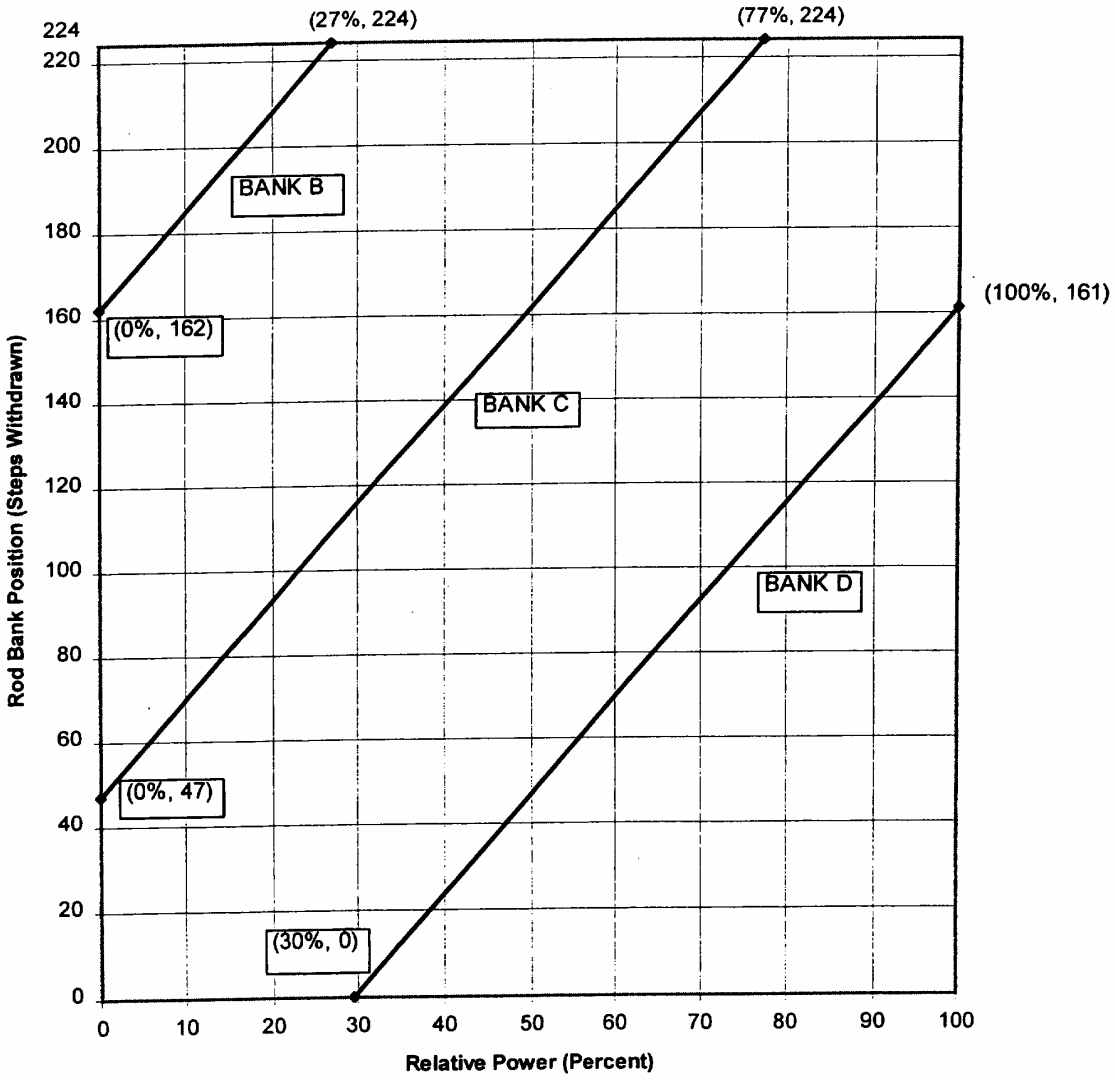

Figure 2.3 Control bank insertion limits versus percent rated thermal power [36].

As shown in Table 2.2, a silver-indium-cadmium (Ag-In-Cd) alloy is used as the control rod poison traditionally. If more reactivity control is required, there are other strong-absorption material options available such as boron carbide with enriched B-10. The RCCA's are classified into two groups (Fig. 2.2): the control banks and the shutdown banks. Since the control rods create large localized flux depressions, they are not the principal means to change power level in base-loaded PWRs, i.e., plants that are not designed for load-following. The major function of the RCCA's is to ensure the shutdown margin.

However, there exist other designs of control rods specifically for PWR power maneuvering. For example, Framatome has designed so-called "gray" rods with lower neutron absorption compared to normal control rods which are referred to as "black" rods. These gray rods create smaller flux perturbations and can thus be used for power adjustments, which are faster than using soluble boron adjustments. Therefore, gray control rods make load-following operation possible over a wide range of powers. Westinghouse has used fewer control rods in some RCCA's, which yields similar effects as the gray rods.

As an example, the control rod insertion limits for a typical PWR [36] include:

- All shutdown banks should be fully withdrawn during normal operation.
- The control banks shall be limited in physical insertion as shown in Figure 2.3.

Under steady-state operation only one bank is allowed and only partial insertion at full power. For our purposes, all control rods are assumed fully out during normal core operation, which provides the maximum scram reactivity capability at all times.

Soluble Poison

Soluble poison, also known as chemical shim, involves using boric acid (H_2BO_3) dissolved in the primary loop water. Reactivity control by soluble poison is very uniform across the whole core. Soluble boron is used to compensate for long-term fuel burnup effects. Since this form of reactivity control can be precisely programmed and introduces no local neutronic perturbations and residues, it is a useful option. However, its usage in PWRs is restricted by two other considerations: (1) primary-loop water chemistry, (2) moderator temperature coefficient (MTC).

In the form of boric acid (H_2BO_3), the soluble poison reduces the pH value in the primary coolant. LiOH is used to increase the pH value, but an upper limit applies. The net result is that roughly speaking the boron concentration should be below 2000 ppm to avoid material corrosion problems. Note here the unit ppm, i.e., part per million, refers to the mass ratio between the boron in H_2BO_3 and water (H_2O). For example, 1 ppm boron means 1 gram of boron in boric acid diluted into 10^6 grams of water. More precisely, the term boron here means natural boron, which consists of 18.3 wt% B-10 and 81.7 wt% B-11 (or 19.9 at% B-10 and 80.1 at% B-11). Only B-10 has a significant absorption cross section, primarily via (n,α) reaction:

$$^{10}\mathrm{B} + n \rightarrow {}^{7}\mathrm{Li} + {}^{4}\mathrm{He}\,.$$

Another constraint comes from consideration of the moderator temperature coefficient (MTC), since negative temperature coefficients make the reactor self-regulating and stable against many perturbations (thus desirable from the safety point of view). Adding boron to the water introduces additional positive reactivity when the water temperature rises (and its density decreases). Therefore, to ensure a negative MTC, the plant operator limits the concentration of soluble boron.

In summary, the rough upper limit of boron concentration based on these two considerations is about 2000 ppm. The effectiveness of soluble boron (ppm) heavily depends on coolant conditions (e.g., hot full power versus cold shutdown) and the blackness of the core due to high U-235 or plutonium content (spectrum hardening).

Burnable Poison

Contemporary core designs employ low-leakage loading patterns, which can effectively reduce both the pressure vessel fluence and the fuel cycle cost (better neutron economy) due to decreased neutron leakage. This necessitates usage of burnable poisons because the low-leakage loading pattern puts fresh fuel assemblies in the core interior and only burned assemblies at the periphery of the core. The beginning-of-cycle peaking would be severe without burnable poisons. The significant initial reactivity of a long-cycle-length core must be controlled. Since soluble poison is limited to about 2000 ppm, burnable poison is introduced to compensate for the excess reactivity of fresh fuel assemblies at the beginning-of-life. In addition, since the local assembly power is directly related to its re-

activity relative to the reactivity of its adjacent assemblies, the peaking can be controlled by designing appropriate burnable poison loading patterns.

The typical burnable poison loadings include IFBA (integrated fuel burnable absorber, a thin ZrB_2 coating on fuel pellet surfaces), Gd_2O_3, or Er_2O_3. Ideally the burnable absorber should be fully depleted at the end-of-cycle. However, there is a burnable poison residual penalty at the end of cycle depending on the specific type and amount of burnable poison loading. Several detrimental effects are associated with burnable poison usage: (1) the residual burnable poison penalty, which reduces the cycle length, (2) the displacement of a volume of fuel, which reduces the fuel loading, (3) the additional helium gas from IFBA and reduced fuel thermal conductivity from gadolinia and erbia. The free-of-poison calculation of a high burnup core would typically overestimate the cycle length. In fact, the core-wide burnable poison loading design is a major task to satisfy power peaking & reactivity control limits in the core reload design. We will address these considerations in Chapter 6.

2.3 Licensing/Design/Operating Considerations

Safety issues need to be paid sufficient attention, especially for new operating strategies lacking operating experience. The fundamental goal of nuclear safety is to ensure the normal operation of power plants and to prevent radionuclide releases to the environment. In general, there are three barriers against potential radionuclide releases: nuclear fuel cladding, primary loop pressure boundary, and containment. The actinides mostly are constrained within the fuel pellet and certain fission products in gaseous form can be released from the solid fuel pellet into the free volume inside the fuel rod. The cladding serves as the first barrier to confine these radionuclides. The pressure boundary of the primary loop and the containment building are the second and the third barrier, respectively. In the following discussions, the nuclear fuel safety (first barrier) is examined.

As with increased burnup, current fuel safety criteria, mostly established before the 1980s and targeted for low burnup, need revision, which requires more accurate models based on appropriate experimental results. There have been recent attempts to reconsider the safety criteria under current situations, i.e., increased fuel discharge burnup and

core power density [37]. Historically, fuel safety margins are conservative. However, taking advantage of conservative margins is difficult since (1) precise margins vary from plant to plant; (2) more advanced computational tools based on scientific understandings are needed for fuel designs.

Regulatory considerations include all aspects of fuel safety, giving rise to guidelines to prevent radiological hazards to the public from commercial reactor operations. Therefore, the fuel design must address regulatory considerations and stay within certain limits to ensure safety. Given a specific fuel design, there still exist certain operational flexibilities depending on the individual plant.

2.3.1 Licensing Issues

Current NRC guidelines provide for a safety review of the materials, thermal, and mechanical fuel design [38], which implements Appendix A of 10 CFR, Part 50 [39]. Four generic licensing requirements include:

- No fuel rod failure, i.e., the fuel cladding remains intact, under normal operation and anticipated operational occurrences (such as core startup, shutdown);
- Guaranteed control rod insertability for the fuel system;
- Limiting the number of failed fuel rods for postulated accidents;
- Guaranteed coolability of the fuel system.

2.3.2 Design Considerations

The design bases address the above four regulatory requirements. The acceptance criteria are then provided to satisfy those objectives under normal operation and anticipated operational occurrences. Note that fuel rod defects during manufacturing are not considered.

Minimum Departure from Nucleate Boiling Ratio (MDNBR)

The most limiting constraint on the thermal power output of a PWR is the minimum DNBR (ratio of the calculated critical heat flux, CHF, to the actual local heat flux) among all fuel rods in the core. There are many CHF correlations developed by fuel vendors, such as the W-3 correlation by Westinghouse. These CHF correlations, produced by fitting to data from full-scale tests, relate the CHF to the operational parameters such as coolant flow rate, quality, actual heat flux, etc. A DNBR limit is required to ensure that

the heat transfer mechanism on the fuel rod surface remains as nucleate boiling heat transfer with a 95% probability at the 95% confidence level. Figure 2.4 [40] illustrates the thermal margin considerations from the heat transfer perspective.

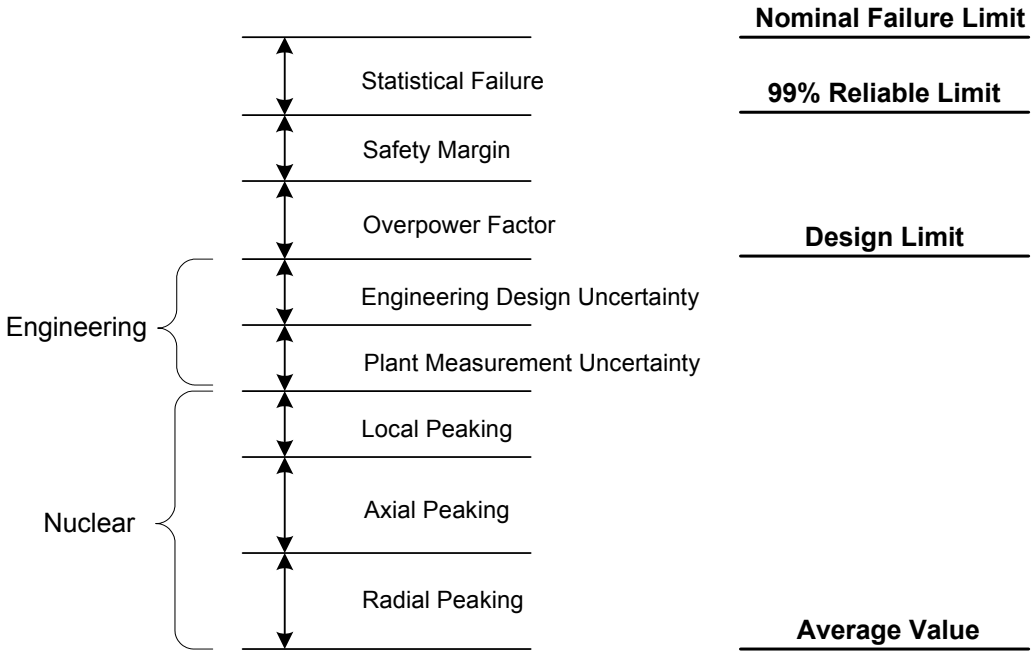

Figure 2.4 Thermal design margin considerations [40].

In order to avoid detailed analysis of anticipated operational occurrences (AOO), one usual design practice is to maintain the MDNBR above 1.3 under the worst operating scenario, i.e., 112% overpower for a worst axial power distribution pin accompanied by an elevated inlet core coolant temperature of 4°F and a pressure swing of 30 psi [41]. It is obvious that such a "worst" operating condition is highly conservative because these adverse inputs can hardly happen simultaneously. Therefore, this conservative calculation is generally deemed as strong evidence that the core has sufficient thermal hydraulic margin to withstand the full spectrum of transients/accidents. Consequently the lengthy process of analyzing those transients, such as rod cluster control assembly (RCCA) ejection, main steam line break (MSLB), loss of flow accident (LOFA), loss of coolant accident (LOCA), loss of heat sink accident (LOHA), reactivity insertion (power excursion), anticipated transients without scram (ATWS), etc., can be deferred in initial scoping studies.

Under high burnup circumstances with more crud deposition and oxidation on the fuel cladding surface, the MDNBR would be affected by the accuracy of the CHF corre-

lations which were mostly based on fresh cladding experiments. During a longer cycle, the worst axial power profile in a core could possibly be more severe compared to a conventional 18 month cycle.

Peaking Factors

The core peaking factors are primary indices of the power distribution. In order to improve core performance, there is strong incentive to keep the core power as flat as possible by reducing the power peaking factors to a minimum. Specifically two commonly-used peaking factors are discussed: the total peaking factor and the maximum enthalpy rise factor.

The total peaking (hot spot) factor is defined as

$$F_q = \frac{\text{the core-maximum local linear power}}{\text{the core-average linear power}}, \tag{2.1}$$

which characterizes the total peaking including both the axial and the radial contributions. The limiting value is 2.50 for a typical Westinghouse 4-loop PWR (also depending on the type of fuel) [35]. Furthermore the hot spot factor can be decomposed into a nuclear factor and an engineering factor. The nuclear factor usually comes from neutronic core analysis, for example, using the CMS package by Studsvik. The engineering factor typically includes a 4% margin for analysis uncertainties and 4% for manufacturing tolerances. Therefore, the typical design limit for the nuclear total peaking factor is 2.31.

The maximum enthalpy rise (hot channel) factor is defined as

$$F_{\Delta h} = \frac{\text{the maximum fuel rod power}}{\text{the average fuel rod power}}, \tag{2.2}$$

which is needed for DNBR hot channel analysis. The typical limit is 1.65 for a Westinghouse PWR [35]. Applying the same 1.08 engineering factor yields 1.53 for the nuclear hot channel factor limit.

As noted above, one should be aware that these peaking limits are for specific fuel assembly designs. For example, increasing the number of grids and/or better mechanical design of the grids in the fuel assembly would improve the thermal hydraulic margins (and would increase peaking limits). Therefore, the design limits of peaking factors are supplied by the individual fuel vendors. Flexibility in these limits has provided large de-

sign space in core design and facilitated the implementation of low-leakage fuel management with high burnup and long cycles.

Reactivity Feedback Coefficients

From the neutronics point of view, the essence of core design is to maintain a critical neutronic condition as well as the ability to stabilize it within certain ranges. The reactivity (or the eigenvalue) of the core characterizes the criticality of the nuclear fission reactions. Under steady-state operating conditions, the core effective reactivity is zero (and the core effective eigenvalue is 1.0). The reactivity feedback effects are major concerns since they determine the transient response. In general negative reactivity feedback coefficients are required for stabilization.

The moderator temperature coefficient (MTC) is defined as the change of reactivity per unit change in temperature of moderator. For a typical PWR, it is required to be non-positive under hot full power conditions and may be slightly positive below certain power level, e.g., $\leq$12.6 pcm/K up to 70% power [35]. The basic physics reason for a negative MTC is the decreased water density (less moderation) at higher temperatures whereas the temperature change of water itself (change in Maxwellian spectrum temperatures) has negligible contribution to the MTC. The MTC is sensitive to soluble boron concentration, control rod positions and the burnup (or time) in a cycle. Although negative values of the MTC are desired, too strong a negative MTC could lead to large reactivity insertion problems under the cold water injection scenario.

The fuel temperature coefficient (FTC) is defined as the reactivity change per unit change in temperature of fuel. For UO_2 fuel pellets, the thermal expansion ($\alpha \sim 10^{-5}$/K) is very small and can be ignored. The negative FTC is largely from the Doppler broadening of the U-238 absorption, thus the FTC is usually also called the Doppler coefficient. Typically its magnitude is about one order of magnitude smaller than the MTC. Under normal (steady-state) operating conditions, the fuel temperature variations are small. Therefore the FTC is not important in routine operations except at initial heatup and upon shutdown. However, the Doppler reactivity feedback occurs on a very short time scale because fission energy is deposited in situ (no need for heat transfer to occur). This unique benign feature makes the FTC much more valuable to safety than any other feedback coefficient [42].

The overall power coefficient is of practical interest, which is specified in terms of reactivity change per percentage power level change. This feedback coefficient includes all the temperature changes in the core. However, the xenon effect is excluded in the definition because the power coefficient refers to short term effects only.

With more fissile loaded in the high burnup core (long cycle length), the hardened neutron spectrum leads to a less negative FTC (less Doppler absorption) and a more negative MTC (moderation more important). However, further consideration of soluble/burnable poisons will also affect these coefficients. In general, it is expected that the feedback coefficients of the high burnup core should fall within the range spanned by current designs.

Shutdown Margin

The reactor has to have the ability to reach sub-criticality under any circumstances during the entire operating cycle. The soluble poison and the control rods are then required to provide sufficient negative reactivity (neutron absorption) to provide a certain percentage of subcriticality.

The shutdown margin is the reactivity margin after all control rods are fully inserted (with the largest worth control rod stuck out) at a minimum boron concentration under various operational scenarios. Typically, the shutdown margin is $\Delta\rho \geq 0.0130$ for a Westinghouse PWR [35], which is about twice the U-235 delayed neutron fraction (2β).

For harder spectrum (blacker) cores, the control rod worth is reduced. However, the initial reactivity required in a blacker core is also smaller. Therefore, satisfying the shutdown margin might not be an issue. In fact, there exist better control rod options, such as boron carbide (B_4C) with enriched B-10. Akin to the feedback coefficients, the current safety criteria still apply for high burnup cores. One should be again aware that control rod worth should be within the proper range considering the control rod withdrawal and ejection accidents.

Fuel Performance Issues

High burnup has a significant impact on fuel performance requirements. Roughly speaking, the allowable burnup is limited by steady-state fission gas release from the fuel pellet,

cladding performance (such as oxide layer thickness), and the fuel reactivity initiated accident (RIA) performance [34].

The fission gases, mainly noble gases (xenon and krypton), accumulate with increasing burnup. They are released from the solid fuel pellet to the free volume (such as the fuel-cladding gap, the central void, and the porosity) within the fuel pin, which depend on the fuel temperature, temperature gradient, power history, and the fuel burnup [43]. At low fuel temperatures, the fission gas release occurs only on the external surface of the fuel pellet by either a direct flight from the fuel (recoil) or a knockout due to a fission fragment, a collision cascade or a fission spike. This so-called athermal fission gas release is quite small at low burnup since it affects only the outer-most layer of fuel (~10μm). Beyond a certain burnup threshold (~40 MWd/kg), the athermal fission gas release starts to increase substantially due to microstructure changes of the fuel pellet. At high fuel temperatures (~1200°C at low burnup, but probably drops with burnup [44]), the fission gas motion becomes important and the thermally-activated diffusion of fission gas migration plays a role. In addition, fuel material changes take place, such as gas bubble germination, fuel swelling, grain boundary interconnection, etc. In summary the high fuel temperature case is much more challenging than the athermal case (it is even worse at high burnup). Hence, fast reactor fuel (high temperature and high burnup) has a much larger gas plenum to accommodate the much larger amount of released fission gases [44].

A direct consequence of increased release of fission gases is higher fuel rod internal pressure, which is desired to remain smaller (or at least not much larger) than the core coolant pressure to prevent outward cladding creep. The typical fission gas release percentage for a PWR is less than 5% [44]. For IFBA loaded fuel pins, helium gas is generated from B-10 which sets a limit on the IFBA loadings. The increased rod internal pressure is particularly important under transient conditions. For example, the pressure difference across the cladding might become large due to loss of system pressure during a LOCA [37]. The degraded fuel thermal conductivity due to fission gas is also of concern. The pellet thermal expansion leads to pellet-cladding mechanical interactions (PCMI), especially important during a transient. The current limit to preclude PCMI failures is that the plastic strain in the cladding should not exceed 1% [38]. Future designs might have different values depending on R&D progress in studies of nuclear fuel and cladding. An-

other common criterion is that fuel centerline melting should be avoided because of the large volume expansion upon melting.

The eventual goal is to maintain the cladding intact. Therefore, the cladding performance is a key factor in reducing fuel rod failures. It has been traditionally assumed that cladding overheating will not occur if the thermal hydraulic limit (DNBR for PWR) is satisfied, which has been proved by industry practice. In addition the cladding has certain limits on oxidation, hydriding, embrittlement, and corrosion products buildup (crud). For example, the embrittlement criterion of 10 CFR Part 50 requires that the peak cladding temperature be below 2200°F (1204°C) and the maximum oxidation thickness under 17% of cladding thickness before oxidation. Instead of the traditional Zircaloy-4, new cladding material options exist with better corrosion/oxidation resistance, such as ZIRLO^{TM} by Westinghouse and M5 by Framatome.

In summary high burnup poses a challenge for fuel performance primarily due to increased fission gas release and reduced effective cladding thickness. The peak fuel rod discharge burnup limit is set by NRC as 62 MWd/kg (also depending on specific fuel). Active research is under way in this area to identify different mechanisms of fuel behavior and to design/manufacture high burnup fuels [17, 18].

2.3.3 Operational Issues

Figure 2.5 [45] illustrates the operational constraints and safety margins for high burnup cores requiring higher-enriched fuel. Defined as the allowed variation of core parameters that would occur under normal operating conditions without requiring unanticipated operator action, the operating margin is set by the specified margin to the safety limit (normally unchanged). Reductions in operating margins often occur in high burnup cores due to their larger range of burnup. For example, the nuclear enthalpy rise hot channel factor is closer to the design limit of 1.53 for a longer cycle core. This requires more operator action to stay within the design limit. There are also some operational issues common for high burnup cores, such as incomplete rod insertion and axial offset anomaly.

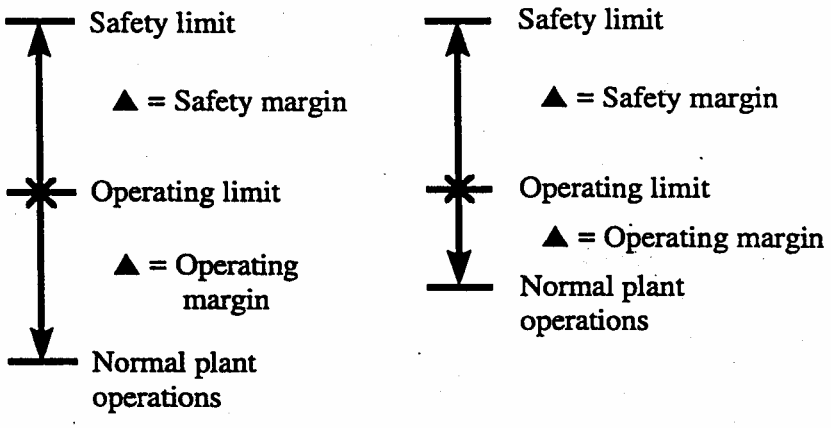

Figure 2.5 Margins of high burnup cores (right) compared to standard PWR (left) [45].

Incomplete Control Rod Insertion

Incomplete control rod insertion has been observed in several reactors in the US and Europe, which was an important safety issue (the shutdown margin might be affected). For example, on January 30, 1996, five control rods did not fully insert after the reactor was manually scrammed at Wolf Creek Generating Station [45]. All of the affected control rods were in the same model of fuel assemblies on their third operating cycle with assembly burnup over 49 MWd/kg. It was found out that this was due to the guide thimble distortion resulting from excessive compressive loading. Later, ZIRLO™ was used to replace Zr-4 so that reduced corrosion and better dimensional stability are achieved. Based on the experience from these events, the incomplete control rod insertion problem has been solved, i.e., there have been no further occurrences of incomplete control insertion since then [46].

Axial Offset Anomaly (AOA)

The core axial offset is defined as the difference in neutron flux level between the top half of the core and bottom half of the core. Significant differences have been observed between the measured and predicted core axial offset (typically more negative than predicted) mainly in high burnup cores. Figure 2.6 shows an example of axial offset anomaly over one fuel cycle. Several concerns arise from the axial offset anomaly:

- Shutdown margin is reduced due to the deviation of flux shape. Power derating is therefore needed for some period of time in the case of severe axial offset anomaly.

- The control rod differential worth and the xenon distribution are affected, which would eventually invalidate the core design predictions. The calculated peaking factors may not be appropriate for use under axial offset anomaly conditions.
- Operational flexibilities are reduced under certain core operating axial offset limits.

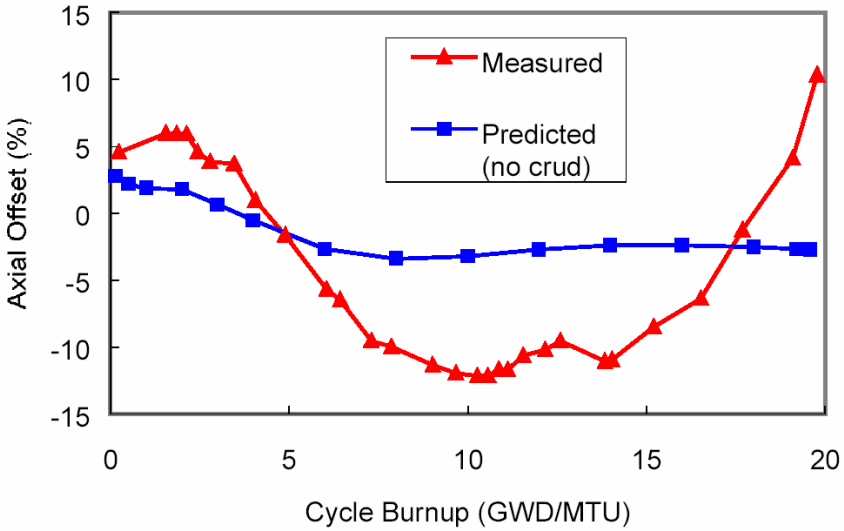

Figure 2.6 Axial offset anomaly example [46].

It was concluded that the axial offset anomaly was caused by boron deposition on the crud layer of the fuel rod surface [46]. Common operating characteristics of the axial offset anomaly include high radial power peaking, high heat fluxes, high core outlet temperatures, high fuel burnup (longer core endurance), and high boron concentrations with extended fuel cycles. However, modeling the phenomenon has been unsuccessful to date in terms of accurately predicting the axial offset anomaly occurrence for a given core design. This behavior might appear in one cycle and disappear in the next subsequent cycle. In order to reduce axial offset, one can reduce the heat flux and peaking factors, reduce the assembly bypass flow, or move the beginning-of-cycle power peak towards the bottom of the core [45].

Power History Envelope

The thermal/mechanical burnup-dependent limits can be avoided by defining a limiting rod power history envelope curve for PWRs, which represents a ceiling for the maximum

allowable fuel rod operating power. At high burnup the fuel rods are limited to low power levels [47], which requires the high-burnup assemblies to be placed in low-power regions of the core. However, high-burnup assemblies are needed in core management to reduce power peaking, i.e., placed in high-flux regions of the core. Therefore, this dilemma leads to problems if too many high-burnup assemblies need to be especially constrained in the core [48].

2.4 High Burnup Core Scoping Analysis

Based on the given plant description of a typical PWR, a wide range of high burnup core scoping analyses were performed where the enrichment spans from 3 w/o to 20 w/o. The licensing-level core simulation code package (includes CASMO-4 [20], TABLES-3 [21], and SIMULATE-3 [22]) from Studsvik is used to model the reference PWR core. Although only the burnable-poison-free, single-batch core loading pattern is calculated, results are then generalized for multi-batch fuel management using the linear reactivity model (LRM) [49]. The optimum cycle length and discharge burnup are discussed from an economics perspective. In addition, the Haling power distribution (the best achievable power shape) is presented to illustrate the increasing demands for burnable poison for longer cycles (higher fuel enrichment). This study differs from previous work on discharge burnup optimization [50] and EPRI's current robust fuel program [13] in that our scoping analysis investigates a much broader range. Detailed core design efforts are needed in the future for further investigation of practical considerations. It should also be noted that the preliminary results here are not fully optimized, for example with respect to the optimization of axial/radial blankets and burnable poison loading considerations.

2.4.1 Core Modeling

The quarter core (lower right hand quadrant, Figure 2.7) is modeled in 3 dimensions with 24 axial nodes. There are four radial nodes for each assembly (2×2). A moderate complexity core model is adopted [51] which includes:

- Base burnup case with instantaneous fuel temperature (TFU), moderator temperature (TMO), soluble boron concentration (BOR), and control rod (CRD) branches;
- Burnup calculations at low and high TFU, TMO, and BOR histories;
- Data produced for 2-D tables with TABLES-3.

The core is simulated under steady-state hot full power (HFP) conditions with all control rods fully withdrawn. The typical parameters are shown in Table 2.3. Appendix A lists input files for the typical 5 w/o case.

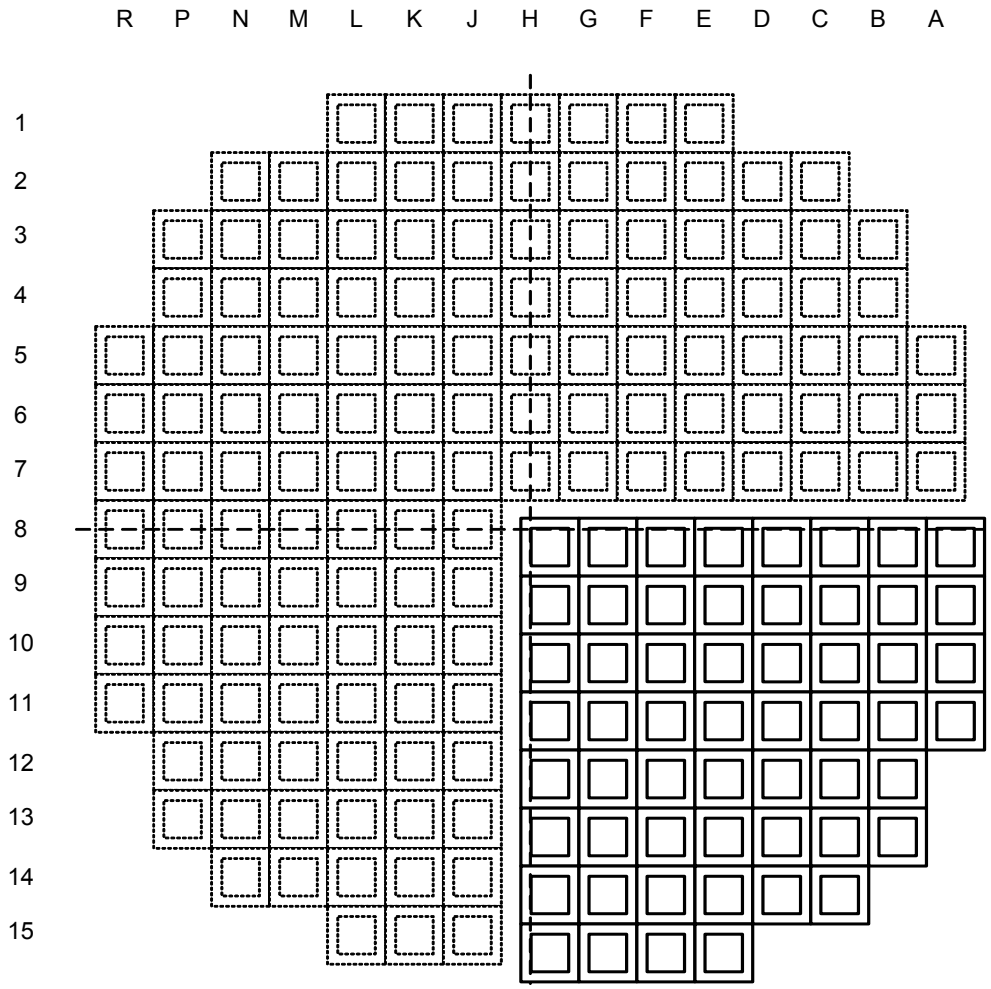

Figure 2.7 Quarter-core model of 193-assembly conventional PWR core.

Table 2.3 Typical parameters in CASMO-4 runs.

Parameters	Base Case	Instantaneous Branches
Base Case		
Fuel temperature (K)	900	565.8, 1200
Moderator temperature (K)	583.1	565.8, 600, 615
Boron concentration (ppm)	450	0, 900, 2000
Control rod position	Fully withdrawn	Fully inserted
Fuel temperature histories		
Fuel temperature (K)	565.8, 1200	—
Moderator temperature (K)	583.1	—
Boron concentration (ppm)	450	—
Control rod position	Fully withdrawn	—
Moderator temperature histories		
Fuel temperature (K)	900	—
Moderator temperature (K)	565.8, 600	—
Boron concentration (ppm)	450	—
Control rod position	Fully withdrawn	—
Boron concentration histories		
Fuel temperature (K)	900	—
Moderator temperature (K)	583.1	—
Boron concentration (ppm)	0, 900, 2000	—
Control rod position	Fully withdrawn	—

The PWR hydraulics feedback iterations are enabled via a simple heat balance model, which assumes that (1) the core inlet flow is known; (2) coolant channels are isolated, i.e., cross-flow ignored, and the core exit water remains sub-cooled; (3) pressure drop across the core is ignored, i.e., the water everywhere in the core is under the same pressure; (4) the energy generated by the node is deposited in the coolant in situ [19].

There are several core neutronic iteration control options available. Practical plant simulation would use a soluble boron criticality search, i.e., where soluble boron concentration is varied in iterative calculations to reach criticality. However, for these scoping study cases, the enrichment is very high compared to normal plants, which makes boron criticality search difficult to converge especially at the beginning of cycle. The eigenvalue criticality search is adopted instead. For the 9.75 w/o enriched fuel, the single batch discharge burnup values for the eigenvalue criticality search and the critical boron search are 70.8 MWd/kg and 75.1 MWd/kg, respectively. In general, the boron-criticality-search gives slightly higher burnup due to spectrum shift effects (an initial high boron concentration increases conversion ratio and the low boron concentration later in cycle increases eigenvalue). In this sense, these single-batch discharge burnup

eigenvalue). In this sense, these single-batch discharge burnup estimations based on the eigenvalue criticality search are therefore conservative.

The reflector calculations are taken from typical PWR analyses, which compute cross sections and discontinuity factors for a steel baffle surrounded by water. The top/bottom/radial reflector calculations set up boundary conditions for the PWR core. It was found that reflector calculation results are not sensitive to the fuel material. For example, using 5 w/o or 20 w/o UO_2 fuel in the reflector calculations gives almost identical core burnup. In reality the reflector models are specific for each plant because the thickness of the water baffle and the configurations of the core periphery vary.

2.4.2 Multi-Batch Burnup

Besides the fresh fuel enrichment, the discharge burnup is also affected by the fuel management scheme. Using the linear reactivity model [49], one finds the discharge burnup, B_d, for a steady-state core having n-batch fuel management (1/n-th of the core refueled each cycle):

$$B_d = nB_c = \frac{2n}{n+1} B_1 , \tag{2.3}$$

where B_1 is the single-batch $(n=1)$ loaded core burnup,

B_c is the cycle burnup.

Note that for non-integer value of n, the prescription is slightly more complex (see Ref. [49], page 33 about the discussion of unequal batch size). The key quantity in the above equation is the single-batch core burnup, which is directly related to the fuel discharge burnup given a specific number of batches, n. It can be approximated by taking the burnup value from a reactivity vs. burnup curve (depletion history) where the infinite medium eigenvalue, k_∞, decreases to 1.03 or the infinite medium reactivity, ρ_∞, falls to 0.03 (a 3% leakage effect is assumed for PWRs). Here our approach is to simulate the single-batch reactor core directly using uniform fuel loading, which is carried out using the typical Westinghouse 4-loop PWR core model. By varying the number of batches for the core reloading, one can change discharge burnup between B_1 ($n=1$) and $2B_1$ ($n=\infty$). The more batches, the higher the discharge burnup.

Meanwhile, as n and the discharge burnup increases at a fixed B_1, the cycle burnup decreases; this means that more frequent reloading of the core is needed. Assuming

equal power sharing under steady state conditions, the cycle burnup, B_c (MWd/kgIHM), is proportional to the cycle length as follows:

$$B_c = 30.44\times10^{-3} q_{SP} T_c L = 30.44\times10^{-3} \frac{q_P}{\rho_{IHM}} T_c L, \tag{2.4}$$

where q_{SP} is the specific power (W/gIHM ≡ kW/kgIHM),

q_P is the core average power density (kW/liter-core),

ρ_{IHM} is the initial heavy metal density averaged over the core volume (g/cm^3-core),

T_c is the calendar cycle length (months, defined as 30.44 days per month),

L is the capacity factor (fraction of full power days averaged over the entire cycle).

Under steady-state operating conditions, the specific power and the power density are kept constant (for instance, typical specific power and power density values for UO_2-fueled PWRs are 38.7 kW/kg and 104.5 kW/liter, respectively). In reality the fresh fuel is typically operating at higher than average specific power, and at below average specific power during subsequent cycles. Considering the seasonal pattern of electricity demand, it is usually desired to make the cycle length as a multiple of 6 months (half of one year). Nowadays, the dominant cycle length is 18 months. The corresponding typical PWR cycle burnup at a capacity factor of 87% is then 18.45 MWd/kg using Eq.(2.4).

2.4.3 Single-Batch Discharge Burnup (B_1) Correlation

The primary responsibility of a fuel cycle management team is to choose an appropriate fuel enrichment to satisfy specific cycle length requirements economically. The single-batch discharge burnup plays an important role in the estimate of average reload fuel enrichment. An equivalent form to Eq. (2.3) can be written as

$$B_1 = \frac{n+1}{2} B_c. \tag{2.5}$$

One can then compute the single-batch discharge burnup from the cycle burnup (determined by the operating conditions) and the number of batches. Obviously the B_1 will depend on many variables, such as the reactor design, average fuel enrichment, etc. However, for conventional PWRs, it is mainly a function of fuel enrichment. It was found in Ref. [52] that a quadratic fit (applicable up to 7 w/o) can be employed to relate core-average reload fuel enrichment, X_P, and B_1:

$$X_{\mathrm{P}} = 1.348 + 0.04884 B_{\mathrm{I}} + 0.001275 B_{\mathrm{I}}^{2}, \tag{2.6}$$

where X_{P} is the average fuel reload enrichment (w/o),

B_{I} is the single-batch discharge burnup (MWd/kg).

And the reversion of Eq. (2.6) takes the form:

$$B_{\mathrm{I}} = 28\sqrt{X_{\mathrm{P}} - 0.88} - 19.2\,. \tag{2.7}$$

Note that this correlation was derived for enrichment up to 7 w/o and was validated against spent fuel data and results from the Studsvik Core Management System (CMS) codes (CASMO-4, TABLES-3, and SIMULATE-3). This applicable range is rather narrow for high burnup considerations. A broader range correlation was, therefore, prepared based on SIMULATE-3 PWR core predictions. Although burnable poison usage, such as gadolinium and erbium, is not considered in this parametric calculation (i.e., no residual reactivity penalties), the licensing-level CMS code package is adequate to produce convincing first-order estimates based on a 3-dimensional PWR core model. For detailed designs, further refinements are definitely needed.

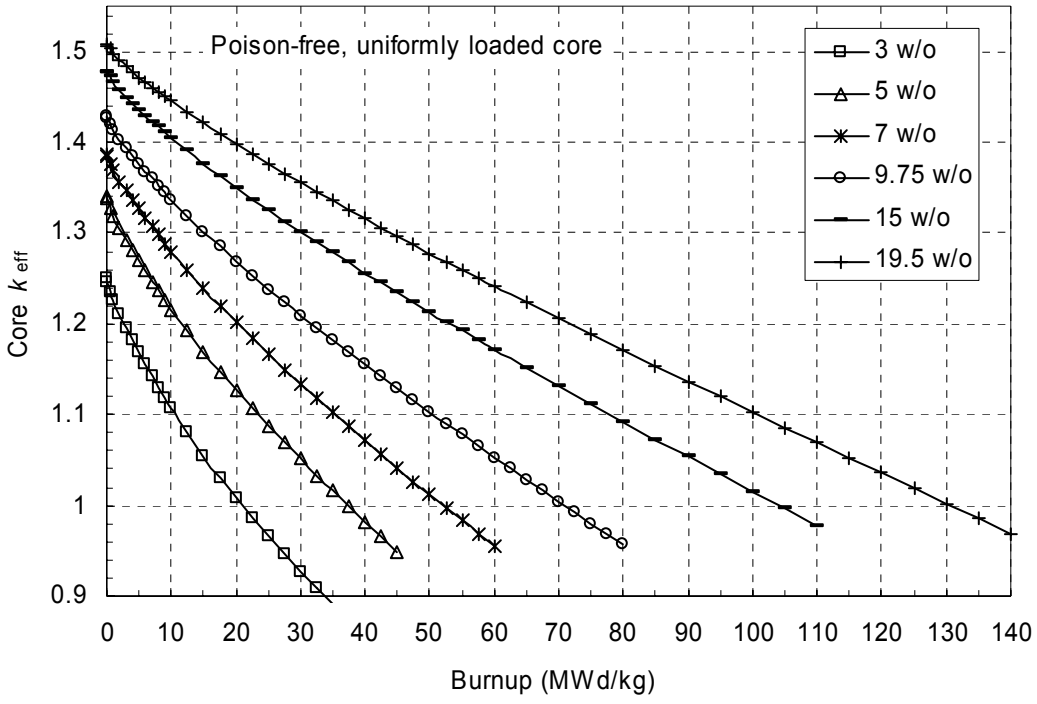

Figure 2.8 Core depletion calculations for various fuel enrichments.

Fig. 2.8 shows the core burnup calculation results for a series of reload fuel enrichments. The range of single batch burnup values using 3 w/o to 20 w/o enriched fuel is between 20 MWd/kg and 130 MWd/kg. Based on these SIMULATE-3 results, a new correlation extending the applicable range up to 20 w/o (proliferation resistance upper limit) is obtained:

$$\begin{aligned} X_P &= 0.41201 + 0.11508 B_1 + 0.00023937 B_1^2 \\ &= 0.41201 + \frac{B_1}{8.6896} + \left(\frac{B_1}{64.635} \right)^2 \end{aligned} \quad , \tag{2.8}$$

and its reversion,

$$B_1 = 64.6 \sqrt{X_P + 13.4} - 240.4 \tag{2.9}$$

As shown in Fig. 2.9, below 7 w/o enrichment, these two correlations, Eqs. (2.7) and (2.9), agree well, but the discrepancy increases as enrichment increases above 7 w/o. The old correlation (2.7) underestimates the burnup capability of high enrichments. Overall the new correlation (2.9) is more linear over the entire enrichment range (≤ 20 w/o) than the old one: within ±3% for enrichments between 5 w/o and 20 w/o,

$$B_1 = 6.549 X_P + 5.186 \tag{2.9a}$$

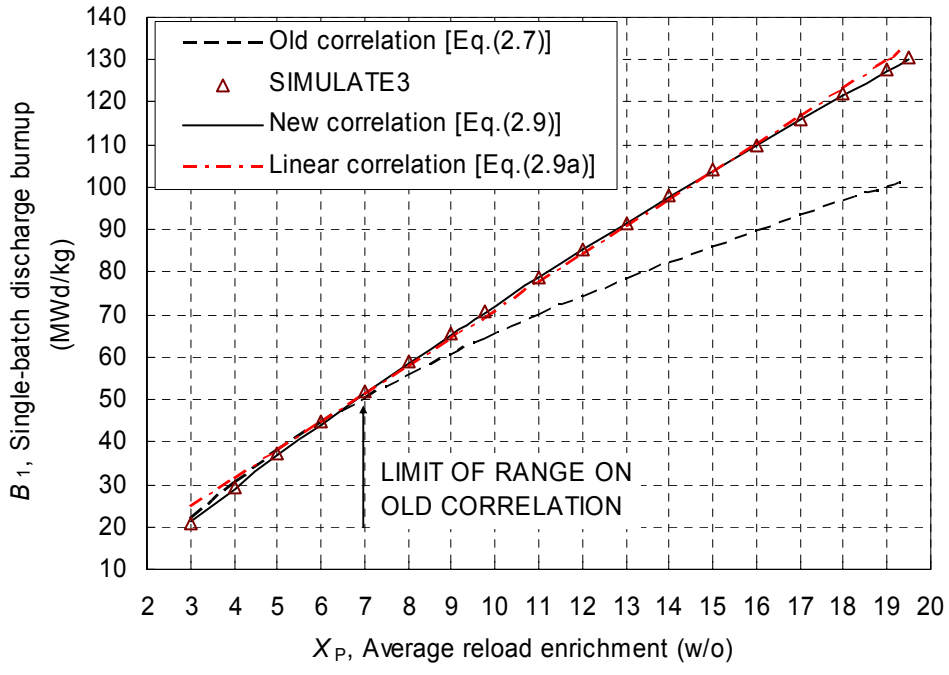

Figure 2.9 Burnup-enrichment relations for typical PWRs.

2.4.4 Discharge Burnup vs. Cycle Length

Using the single-batch discharge burnup correlation (2.9) from the last section, one is ready to explore the best operational strategy (in the sense of economics) under certain operational constraints of PWRs. First, four important parameters of interest are identified as follows:

1. n, number of staggered batches;
2. T_c, cycle length in units of calendar months;
3. B_d, discharge burnup $\left(B_d = nB_c\right)$;
4. X_P, average reload enrichment.

Since the cycle burnup, B_c, is proportional to the cycle length, T_c, as given in Eq. (2.4), we don't distinguish these two variables in the following discussions.

The above variables are not independent of each other but subject to the two relations given by Eqs. (2.3) and (2.9). Therefore, given any two variables, the other two can be determined. Figure 2.10 shows the relationship among those four variables (the specific power is 38.7 kW/kgIHM and the capacity factor is 87%).

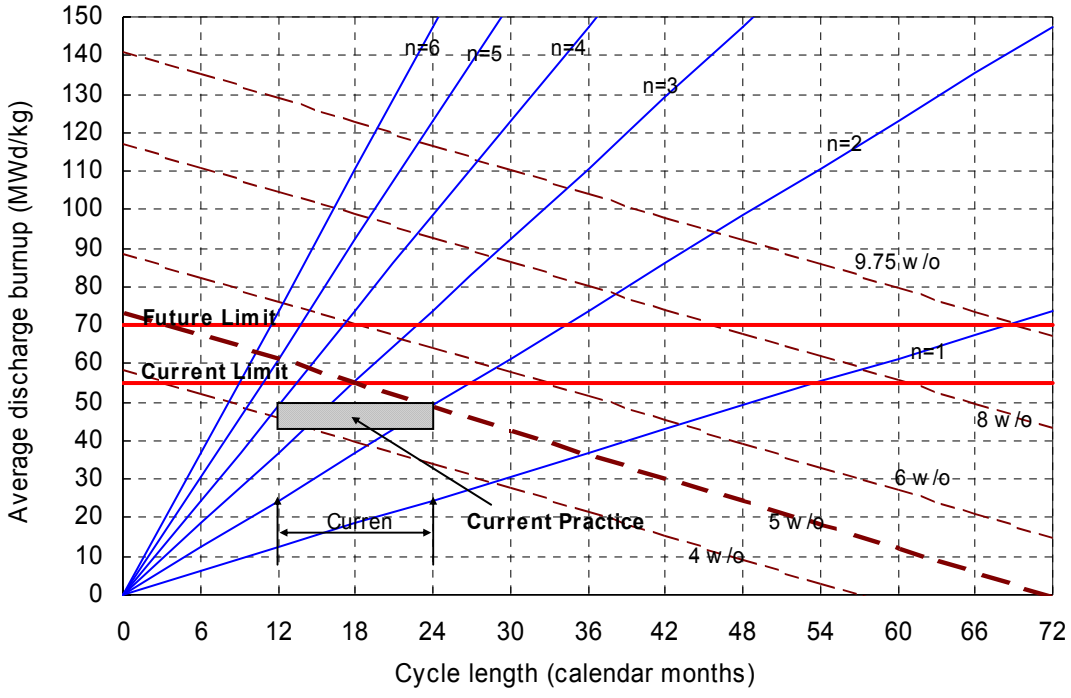

Figure 2.10 Discharge burnup versus cycle length map for a typical PWR.

Several interesting observations can be made from Fig. 2.10:

(1) To achieve as long a cycle length as possible (to reduce the refueling outage cost and to significantly improve the capacity factor), one strategy is to use single batch fuel management [53]. As can be seen in Fig. 2.10, under fixed reload enrichment, a larger n leads to a higher discharge burnup at the expense of shortening the cycle length. In addition, if considering the discharge burnup licensing limit, the single batch strategy is beneficial to confine the fuel discharge burnup within the limit. There are currently proposed special applications of this single batch, very long cycle fuel loading scheme, for example, the so-called STAR (Secure, Transportable, Autonomous Reactor) system (50-150 MWe) whose major goal is to make a nuclear reactor small enough to be transportable and serve in remote areas (such as islands) as a nuclear battery [54]. Another example is the IRIS (International Reactor Innovative and Secure) program [55], a leading candidate for the LWR options in Generation IV studies, which focus on a super long life (about 8 years) core to greatly simplify reactor operating & maintenance and spent fuel storage. However, for all those long life core designs, the fuel cycle cost is more expensive compared to conventional PWRs since a larger fraction of the fissile in the fuel remains unburned. It is disadvantageous in terms of resource utilization. The gains from other savings have to compensate for the more expensive fuel cycle cost to make this option attractive.

(2) If one stays within the current refueling window, i.e., between 12 months and 24 months, Higher discharge burnup requires a larger number of batches and/or higher enrichment. The actual limits on discharge burnup need to be studied carefully from the engineering feasibility point of view. In this multi-batch approach, the fuel is utilized more completely and the resource utilization might be potentially superior to conventional PWRs due to the larger n. The shuffling scheme is very complicated since there are many types of fuel having different burnup (large n).

It should be noted that the above discussions are based on conventional PWR configurations. For new reactors of unconventional design and/or different power density the single batch burnup correlation as well as all the other operating parameters might be quite different. However, the fundamental logic remains the same. In reality, other factors also come into play, such as the frequency of unplanned outages and the efficiencies of online maintenance, which makes it difficult, if not impossible, to precisely forecast the dis-

charge burnup. The analysis here only serves as an illustration of the principle of core fuel management.

2.4.5 Resource Utilization

The indices of fuel utilization are important indicators of nuclear fuel cycle economics. They also reflect the efficiency of resource usage, which is particularly important considering long-term resource supply, cost and availability. Specifically, two utilization factors are discussed here, natural uranium utilization (U_U) and separative work unit (SWU) utilization (U_{SWU}).

The uranium utilization, U_U, is defined as the energy production during fuel burnup per unit mass of natural uranium required:

$$U_U \equiv \frac{B_d}{F/P}, \text{ (MWd/kgU}_{NAT}\text{)} \tag{2.10}$$

where B_d is the discharge burnup (MWd/kgIHM),

F is the natural uranium feed to the enrichment plant (kg),

P is the enriched uranium fuel, i.e., the initial heavy metal (kg).

Note that the tails enrichment is taken as 0.3 w/o in F/P in the present analysis. The uranium utilization characterizes the burnup efficiency in terms of natural uranium.

Similarly one can define the separative work utilization as the energy production during burnup per unit SWU:

$$U_{SWU} \equiv \frac{B_d}{S/P}, \text{ (MWd/kgSWU)} \tag{2.11}$$

where the separative work S (kgSWU) is defined as

$$S \equiv P \cdot V(X_P) + (F - P)V(X_W) - F \cdot V(X_F), \tag{2.12}$$

with $V(X_i) \equiv (1 - 2X_i)\ln\frac{1 - X_i}{X_i}$ for X_i expressed as weight fractions. The subscript i represents P (product), F (natural uranium feed), or W (waste tails). The separative work utilization measure represents the usage efficiency of the SWU.

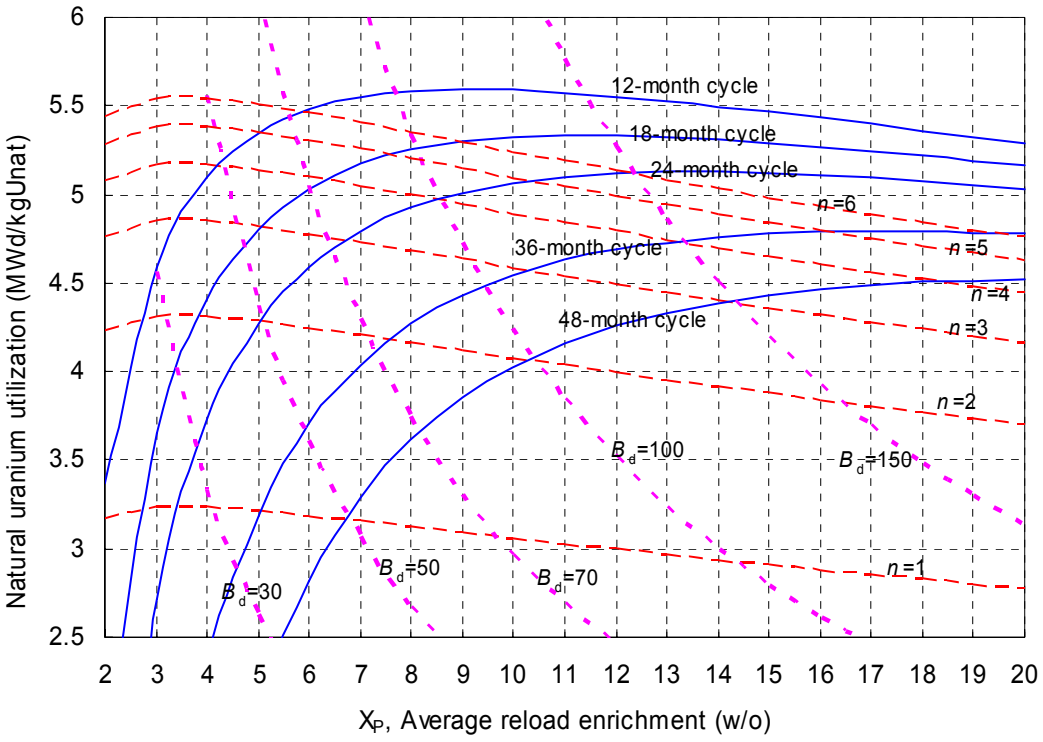

Figure 2.11 Natural uranium utilization for typical PWRs.

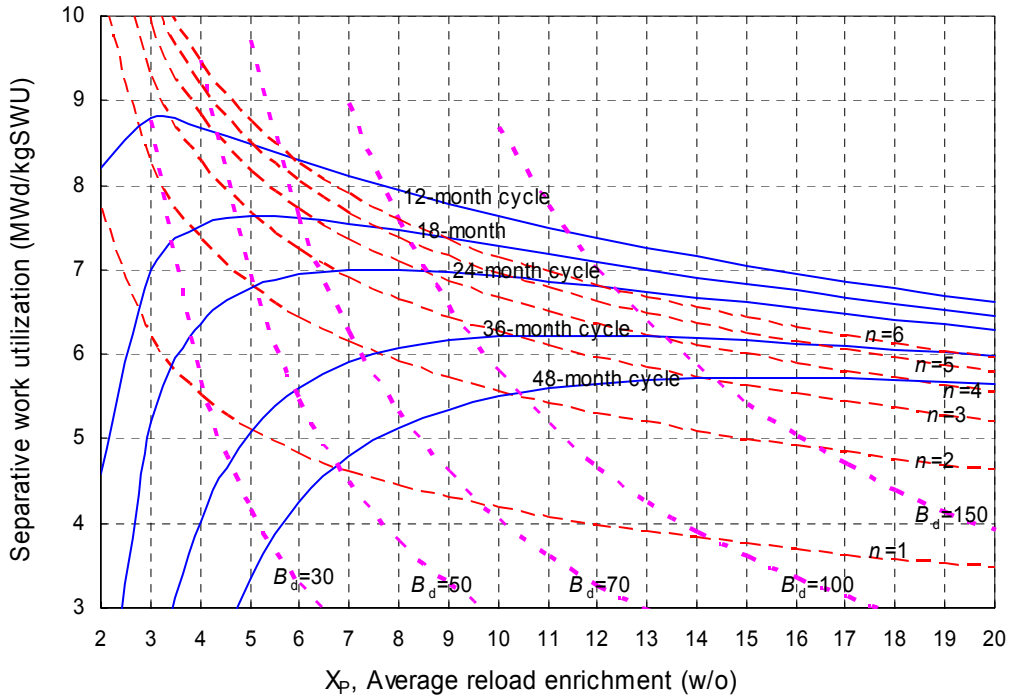

Figure 2.12 Separative work utilization for typical PWRs.

The natural uranium utilization and SWU utilization were computed based on the correlation (2.9). Three series of data including fixed cycle length, fixed number of batches, and fixed discharge burnup are plotted in Figs. 2.11 and 2.12 respectively. Again, the specific power and capacity factor are assumed the same as in the preceding section.

It is interesting that both utilization indices exhibit similar behavior except that U_{SWU} does not display an optimum value for a fixed number of batches whereas a previous study [52, 56] shows an optimum. The potential reasons include: (1) the difference in the tails enrichment (0.25% in [52, 56] and 0.3% here); (2) the difference between single-batch burnup correlations at low burnup (enrichment).

For a fixed discharge burnup, the utilization indices show a sharp monotonic decrease as enrichment increases. Since the discharge burnup is a product of the number of batches and the cycle burnup, increasing the enrichment will lead to a smaller n but concurrently higher cycle burnup (hence cycle length) in order to keep the discharge burnup as a constant. Consequently the fuel utilizations are penalized (under-burn).

For a fixed number of batches, there exists a weak maximum for the natural uranium utilization between 3 w/o and 4 w/o. The SWU utilization shows a monotonic decrease with enrichment. A long life batch-loaded core (corresponding to $n=1$) will suffer from less efficient usage of resources compared to multi-batch approaches. The decrease of natural uranium utilization appears almost linear whereas the decrease of SWU utilization exhibits exponential behavior, i.e., there is a steeper decrease at lower enrichment values.

Perhaps the most interesting case is to fix the cycle length. Five lines representing cycle lengths from 12 months to 48 months are shown. For each individual cycle length there is an enrichment, which maximizes uranium or SWU utlization. For example, the optimum enrichment of an 18-month cycle is ~11 w/o from Fig. 2.11 (U_U) and ~5 w/o from Fig. 2.12 (U_{SWU}). As a matter of fact, the optimum enrichment, $\hat{X}_P$, can be found analytically for U_U and U_{SWU} by substituting the analytic B_1 correlation into these utilizations and setting the derivatives to be zero. Using Eqs. (2.3) and (2.5), the discharge burnup can be expressed as:

$$\begin{aligned} B_d &= 2B_l - B_c \\ &= 129.2\sqrt{X_P + 13.4} - 480.8 - B_c , \end{aligned} \tag{2.13}$$

and the utilization can be then written as:

$$U = \frac{129.2\sqrt{X_P + 13.4} - 480.8 - B_c}{aX_P + b}, \tag{2.14}$$

where a, b are constants characterizing either F/P for uranium utilization or S/P for SWU utilization (linearized approximation). Setting the derivatives to zero will give the optimum enrichment for a fixed cycle length (cycle burnup). Once the optimum enrichment is obtained, one can further compute the associated parameters such as B_d and n. Tables 2.4 and 2.5 show optimum values under various fixed cycle lengths for uranium utilization and SWU utilization respectively.

Table 2.4 Optimum parameters for uranium utilization at fixed cycle lengths.

T_c (months)	B_c (MWd/kg)	$\hat{X}_P$ (w/o)	$\hat{n}$	$\hat{B}_d$ (MWd/kg)	$\hat{U}_U$ (MWd/kgU_{NAT})
12	12.30	9.14	9.8	120	5.59
18	18.45	11.3	7.8	143	5.34
24	24.60	13.4	6.6	163	5.13
36	36.90	17.3	5.4	198	4.79
48	49.19	19.9	4.4	216	4.52

Table 2.5 Optimum parameters for SWU utilization at fixed cycle lengths.

T_c (months)	B_c (MWd/kg)	$\hat{X}_P$ (w/o)	$\hat{n}$	$\hat{B}_d$ (MWd/kg)	$\hat{U}_{SWU}$ (MWd/kgSWU)
12	12.30	3.07	2.5	31.2	8.80
18	18.45	5.26	3.2	58.8	7.64
24	24.60	7.42	3.4	84.1	7.00
36	36.90	11.5	3.4	127	6.23
48	49.19	15.3	3.3	162	5.72

Table 2.4 shows that higher burnup via increasing reload enrichment is favored for 18-month cycle conventional PWR cores from the natural uranium utilization point of view. Short cycle length necessitates a larger number of batches. The increase of uranium utilization is rapid at low enrichments whereas the decrease is rather small after exceeding the optimum value (Fig. 2.11). Comparing curves of different cycle lengths, one finds that increasing cycle length is rather detrimental to the utilization. At 5 w/o enrichment, the transition from a 12-month cycle to an 18-month cycle will reduce both utilizations ~10%. This impact is smaller with increasing enrichments, which therefore provides an-

other push to longer cycle length and higher burnup via higher enrichments as a way to increase utilization (hence improve nuclear fuel cycle economics).

Compared to the uranium utilization, the optimized SWU utilization leads to lower enrichment for a fixed cycle length. For the current 18-month cycle, the SWU utilization is already about the optimum value (~ 5 w/o). Further increased cycle length supports higher enrichment fuel. However, three-batch fuel management appears best even with various fixed cycle lengths as seen from Table 2.5.

Since the natural uranium ore purchase and the SWU cost consist of more than 70% of the total fuel cycle cost, the realistic optimized enrichment for the fuel cycle cost will lie within the enrichment ranges spanned by Table 2.4 and 2.5. Although going beyond 5 w/o enrichment is not economic for a constant number of batches (consistent witn Ref. [10]), there is still room for improving fuel cycle economics for a constant cycle length. It should also be recognized that assembly manufacturing and post-irradiation storage costs will favor longer cycle lengths. The eventual fuel cycle cost will depend on the market conditions, e.g., the SWU and uranium ore cost. Therefore, although the core physics is the same, different conclusions might be drawn at different time periods. Note that the effect of additional enrichment required to offset the residual reactivity of burnable poison is not included here.

2.4.6 Haling Power Distributions

In order to minimize power peaking during the cycle, Haling proposed a strategy of operating reactors in the 1960s [57]. Although this operating strategy was originally for BWRs, it can analogously be applied to PWRs. In the 1990s, there were extensive studies based on the Haling principle to minimize PWR power peaking and to generate optimal core reload patterns [58]. In fact, the industry PWR core reload practice also confirms the Haling principle although sometimes designers themselves are not aware of that [59].

The Haling principle states that: *For any given set of end-of-cycle conditions, the power peaking factor is maintained at the minimum value when the power shape does not change during the operating cycle. End-of-cycle conditions may be considered to consist of such parameters as exposure of the fuel and the amount of residual poison or control blade (if any) remaining in the core at the conclusion of each operating cycle. It is assumed that at the end of each cycle the reactivity of the fuel is a decreasing function of*

exposure. This is usually the case in power reactors, although there may be a short period at the start of the cycle when fuel reactivity increases due to the effect of burnable poison or a high initial conversion ratio. One should be aware that under extreme conditions, i.e., heavily-poisoned core, the Haling principle might not hold [60].

The Haling power distribution is the best available power shape although the Haling principle itself does not give an explicit method of obtaining this power distribution in reality (non-constructive). The difference between this ideal Haling power shape and the real BOC power shape reflects the burnable poison requirements. Therefore, given a specific core loading pattern, it is more precise to say "approaching minimal power peaking" instead of "minimizing power peaking" because the minimal power shape already exists. In addition, it is not surprising that the burnup using Haling power shape, so-called Haling exposure, is typically larger than real core burnup. To some extent, this reflects the maximum core utilization from a power profile perspective.

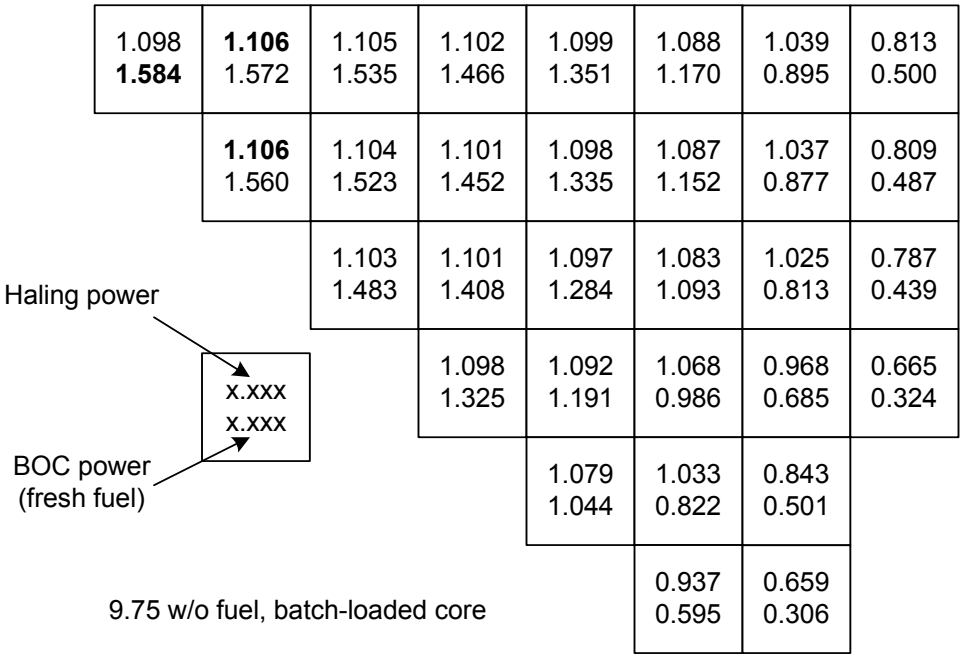

Figure 2.13 Haling and poison-free BOC assembly power distributions.

Fortunately, SIMULATE-3 endows one with the capability of computing the Haling power shape. As an illustration of reactivity control requirements for a high burnup core, a uniformly loaded core with 9.75 w/o enriched fuel was evaluated for its Haling power distribution with Haling exposure of 70.8 MWd/kg. Figure 2.13 shows the Haling

assembly power distributions (radial) and Figure 2.14 shows the core axial power distributions. In Figure 2.13, there are significant differences in the central core region which suggests considerable burnable poison requirements in that region. Peripheral assemblies have significantly lower power generation due to leakage. As indicated by Haling calculations, the smallest-achievable assembly power peaking for the 70.8 MWd/kg cycle is 1.106.

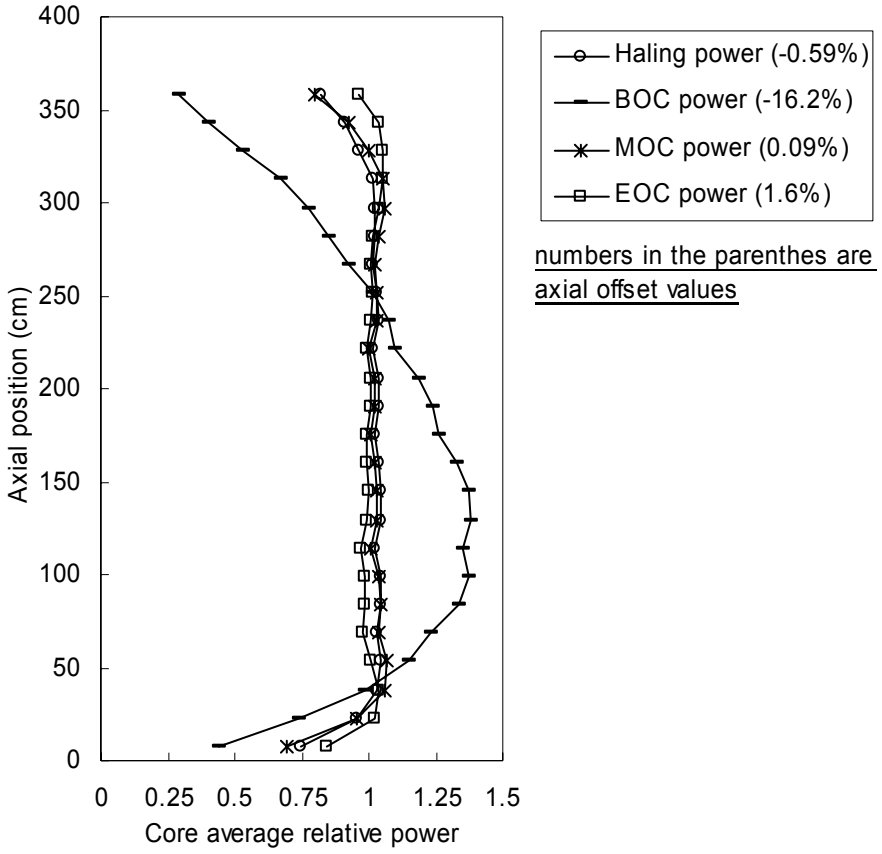

Figure 2.14 Axial core power distributions.

Figure 2.14 shows the large axial power peaking for the poison-free, fresh core. In addition to the Haling power distribution, the BOC (0 MWd/kg), MOC (35 MWd/kg), and EOC (70 MWd/kg) axial distributions are also given. With increasing burnup, the fuel automatically burns to a more uniform axial profile. Therefore, in typical PWR burnable poison loading designs, there are no special considerations for zoning axial burnable poisons. The Haling power shape agrees best with the middle-of-cycle (MOC) power

shape. Although the BOC axial offset is large, it still falls within operating axial offset limits.

2.5 Considerations on Retrofit, High Burnup Core Schemes

As summarized in Table 1.2, one has essentially two directions to go in order to realize high burnup in the world of retrofit cores: either (1) longer cycle length or (2) more batches.

2.5.1 Longer Cycle Length

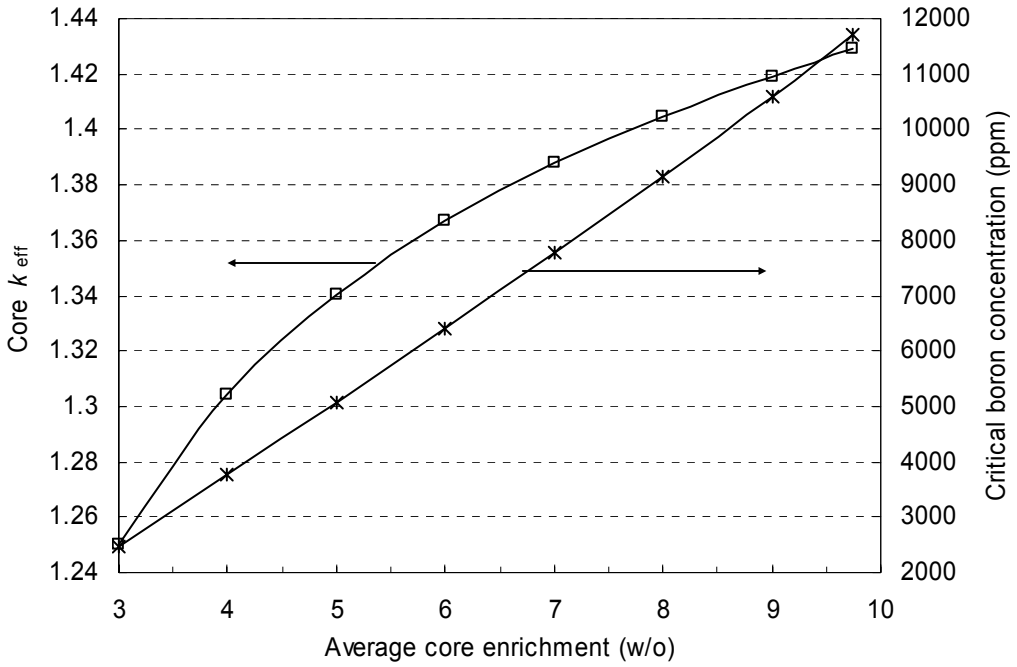

Figure 2.15 Reactivity and critical boron for the single batch core.

Since the cycle burnup is roughly determined by the amount of fissile material present at BOC, a longer cycle requires more fissile material, which in turn hardens the neutron spectrum. Excess reactivity control is an issue because of higher initial core reactivity (more fissile) and reduced control material worth (hardened neutron spectrum). Figure 2.15 shows the initial core multiplication factor and the critical boron concentration re-

quirement as a function of the fuel enrichment. Although the increasing k_{eff} with average core enrichment is less than linear, the critical boron concentration is roughly a linear function of core enrichment. This indicates a harder neutron spectrum (smaller boron worth as shown in Figure 2.16) at higher core enrichment.

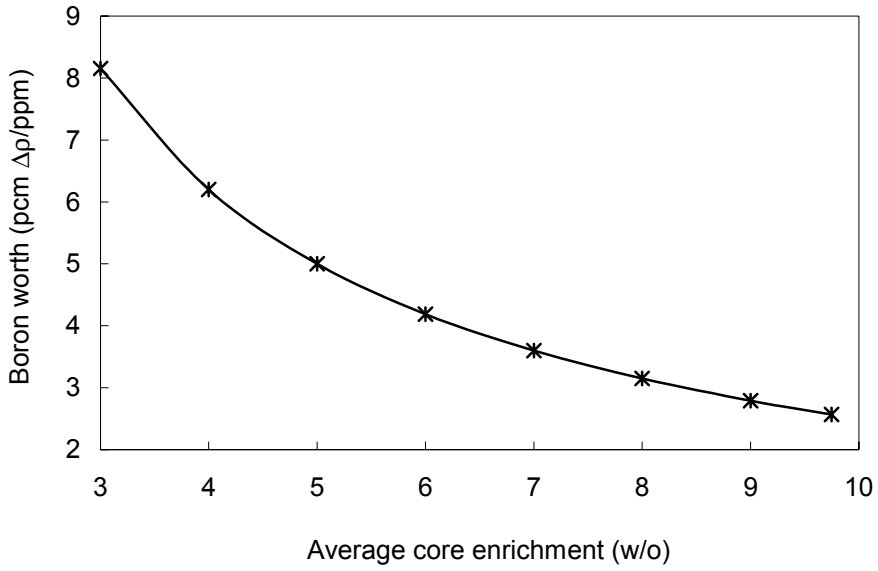

Figure 2.16 Boron worth for the single batch core.

Therefore better control rods design is often needed for a longer cycle core, which might require more control rods and/or stronger absorbers. Under steady state operation, the major concern is the shutdown margin requirement. The soluble poison usage roughly is limited to ≤ 2000 ppm due to MTC and primary-loop water chemistry considerations. There are also limits on the burnable poison loadings. In addition, the low leakage loading pattern (L^3P) is preferred in the extended fuel burnup cycle since larger leakage savings can be achieved [61]. This requires the fresh reload assembly to be located in the center of the core, which further increases the poison requirement. Practically speaking it is a challenge to design a 3-batch core with ≥ 48-month cycle length while satisfying all the thermal, mechanical, neutronic, and materials design limits [8, 12].

2.5.2 More Batches

If one increases the number of batches while keeping the current cycle length, there will be lower technical barriers from the reactivity control point of view. The amount of the reload fissile material will be roughly the same as the current level. The control requirement will then be similar to a current core. The only difference from current cores is that there are fewer assemblies loaded at each refueling, but at a higher enrichment. The burnable poison will be loaded in fewer assemblies with more in each of them so that the overall burnable poison loadings are roughly the same as the current requirement. For the same fuel enrichment, this approach (more batches) will give a bonus burnup due to increased n according to Eq. (2.3). For example, using 9.75 w/o fuel (B_1=70.8MWd/kg), the 3-batch discharge burnup gives 106 MWd/kg while the 18-month cycle with n=6.7 gives 123 MWd/kg. The additional burnup of 17 MWd/kg comes from the larger number of batches (6.7), which is almost one additional free cycle. It is therefore economically more attractive than the longer cycle approach.

As a matter of fact, under the constraint of constant cycle length, it was found in previous core scoping study that there is still room for improving fuel cycle economics compared to current practice by using higher enriched UO_2 fuel and more batches. Tables 2.4 and 2.5 show that for the 18 month cycle the optimum enrichment is 11.3 w/o for natural uranium utilization and is 5.26 w/o for SWU utilization. Actual optimum enrichment for the fuel cycle will then lie within the range of ~5 to ~10 w/o. This points out a promising direction for implementing high burnup in an economic manner.

2.5.3 Conclusions

Based on the above discussion, the approach of more batches while keeping the current cycle length is favored over the longer cycle approach due to economic and technical considerations.

- *economic imperative* In fact, the trend of increased operational effectiveness (fewer forced outages, shorter refueling time) to increase capacity factor has reduced the option space for further improvement via a cycle length extension. It is clear that a large increase in cycle length leads to a more expensive nuclear fuel cycle. On the contrary increasing the number of batches increases fuel discharge burnup, which provides immediate savings from the nuclear fuel cycle cost as shown in Tables 2.4 and 2.5.

- *technical considerations* The long cycle core often requires high fissile contents at BOC (and more burnable poison as well). The hardened spectrum reduces control material worth. Hence the current control rods are usually found to be inadequate to provide shutdown margins [8, 12]. In a core design with more batches, however, it is easier to control the BOC reactivity. Complex fuel shuffling codes exist which can automate the reload analysis. For example, for the 9.75 w/o reload fuel, only ~29 assemblies are refueled in the outage and there are 7 batches of assemblies in the core with a full range of burnup up to nearly 123 MWd/kg. The shuffling optimization space is much larger compared to current practice.

One uncertainty with the use of more batches is the burnup constraint imposed by other considerations. With more batches in the core, the fuel achieves a much higher burnup compared to a long cycle core. For the 9.75 w/o UO_2, 18-month-cycle core, the discharge burnup can be as high as 123 MWd/kg, which is well beyond the current burnup licensing limit of 62 MWd/kg. Therefore, although neutronically and economically favored, the high burnup approach via more batches must await technical progress in advanced fuel studies for high burnup applications.

2.6 Chapter Summary

A typical Westinghouse 4-Loop PWR (3411 MWth) has been described to define a base case as the reference plant condition. Three currently-available means of reactivity control, i.e., control rods, soluble poison, and burnable poison, are reviewed. Various issues, including licensing, design, and operational considerations, are then addressed and how they might be affected by high fuel burnup. Practical core designs are required to meet these limits in order to have adequate margins to operate the core.

The reference PWR core is then modeled to perform a scoping study on high burnup capabilities/feasibilities within the 20 w/o proliferation enrichment limit. Burnup calculations of single-batch-loaded cores with a series of enrichments are made, from which an extended version of the single-batch burnup correlation vs. reload fuel enrichment is obtained. Note that lattice parameters from the reference PWR remain the same for all calculations. Future re-optimization of lattices is therefore expected to better exploit the

higher enrichment fuel. Various operational options are made evident based on the scoping studies. To achieve a certain discharge burnup, the lower the fuel enrichment, the better the fuel cycle economics (conservation of U-235 resources). From the fuel utilization map, one concludes that under the constraint of a fixed cycle length, the fuel cycle cost (utilization) can be improved for enrichments above the current reload 4.5 w/o enrichment up to 8 or 9 w/o, but will decrease as enrichment further increases at a relatively slow rate. Results also show that controlling power peaking and maintaining control margins are more demanding for high burnup approaches involving longer cycles.

For retrofit cores, the high burnup approach of using more batches is preferred based on fuel cycle economic and neutronic considerations. The economic consideration is mainly from a fuel cycle perspective while the O&M cost is not addressed such as the refueling shutdown cost. For a fixed cycle length, the refueling shutdown cost however is also constant. Therefore, under the constraint of fixed cycle length, the refueling shutdown cost has essentially no effect on economic optimization.

3. MCODE Development

"The sages do not consider making no mistakes as a blessing. They believe, rather, that the great virtue of man lies in his ability to correct his mistakes and to continually make a new man of himself"
— Wang Yang-Ming (1472-1529)

The ability to carry out validated high-burnup physics calculations for various fuel options and moderator conditions as well as innovative heterogeneous designs is essential to achieving the goal of the present work. In this chapter, the development work of MCODE (MCNP-ORIGEN DEpletion program), which extends MCNP to incorporate burnup calculations, is presented. This presentation is sufficiently complete to explain how the code satisfies present research goals. The description here reflects the work completed by April 2002 [62]. An updated code manual will be issued later as a separate report which includes more recent progress and the source code listing.

3.1 Introduction

Due to the steady advances of computer power in recent decades, the continuous-energy Monte Carlo based codes are becoming more widely used in routine reactor design calculations. Although they are generally much more computationally-demanding than deterministic methods such as collision probability methods, they provide exact solutions to neutron transport equations given a sufficient number of neutron histories and appropriate neutron cross section libraries. Since the Monte Carlo method is, in principle, a virtual analog to the real world, the capabilities to solve transport problems are unlimited as long as one can model the desired system. As a matter of fact, the powerful geometric modeling capability of MCNP enables extreme flexibilities in reactor designs.

MCNP-4C [24], a recent MCNP version, is a general purpose, generalized geometry, continuous energy, time-dependent, Monte Carlo transport code for neutrons/photons

/electrons developed at Los Alamos National Laboratory (LANL). But it only provides a snapshot of the reactor and is unable to perform burnup calculations. Therefore, a one-group depletion code, ORIGEN2.1 [25], which also performs radioactive decay calculations, is used to carry out burnup calculations. This computer code uses the matrix exponential method to solve a large system of coupled, linear, first-order ordinary differential equations with constant coefficients. A linkage program, MCODE (MCNP-ORIGEN DEpletion program), has been developed at MIT to manage data transfer and to couple and run these two codes in a repetitive sequence.

The idea of combining MCNP and ORIGEN dates back to the late 1980s. In the beginning, users coupled the two codes in a manual way, i.e., ran MCNP first, copied the output from MCNP and organized it into ORIGEN input format, then ran ORIGEN to update the initial MCNP input and re-ran MCNP, and so on (e.g. [63]). This approach is only practical for a few timesteps and several nuclides. For routine burnup calculations, however, this approach is not acceptable in terms of user time requirements and the propensity to introduce errors. A console program is needed to automate running of MCNP and ORIGEN. In the late 1990s, the Idaho National Engineering and Environmental Laboratory (INEEL) distributed the first MCNP/ORIGEN linkage program, MOCUP (MCNP-ORIGEN Coupling Utility Program) [64]. Shortly thereafter, the Los Alamos National Laboratory (LANL) released their version of an MCNP/ORIGEN coupler, MONTEBURNS [65]. Since then, other coupling programs have appeared in the literature [66, 67]. Compared to deterministic codes, the Monte Carlo-based depletion code has broader applications, and sometimes plays a unique role in research. As a practical example, in the early 1990s, the Institute of Nuclear Energy Research (INER) in Taiwan built a research reactor which would require certain tools to perform depletion prediction calculations. MCNP, being the ideal tool of modeling the research reactor, cannot do depletion calculations. Therefore, they purchased a linkage code (similar to MCODE) from Germany at the price of about $200,000 [68].

MCODE is entirely written in ANSI C (about 3000 lines of source code) and is fully portable under Windows and UNIX environments. Users interact with MCODE only, which manages MCNP/ORIGEN runs and their coupling internally. Figure 3.1 illustrates the MCODE architecture.

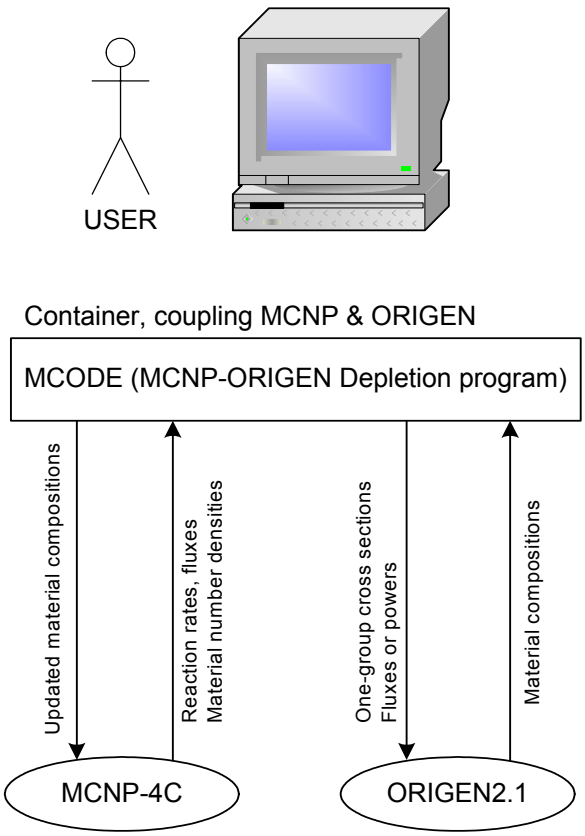

Figure 3.1 Illustration of MCODE architecture.

As a console program, MCODE distinguishes itself in two categories:

1. *Friendly user interface and easy usability* The input files are substantially categorized and simplified, reducing several inputs to only two input files (MCNP and MCODE input files). Succinct summaries are appended at the end of the log file and detailed output data can be found in a separate output file. Automatic generation of MCNP tally specifications and ORIGEN input files at each burnup point greatly ease the users' burden of code running so that much more attention can be paid to the problem itself. A user's manual is included in Appendix B, which clearly states the specific input format as well as some practical guidelines and recommendations for running MCODE on various platforms (ranging from a single workstation to a cluster machine). The built-in usability reduces the training time for a novice and improves confidence in results.
2. *Improved functionality* The way of coupling MCNP and ORIGEN in MCODE is unique. A standard burnup predictor-corrector algorithm is implemented in the

code, which permits larger timesteps. Two ORIGEN normalization options, constant flux or constant power, are available, which preserves the flexibility of running ORIGEN. Precise burnup state points can now be achieved using power normalization, which was once a concern [69]. The EOL neutron absorption importance summary for each active cell is computed and attached in the end of the output file, which gives a guideline for choosing an appropriate representation of nuclides in MCNP.

As with any code, a verification process is necessary for MCODE. In this chapter one benchmark calculation is presented for a high burnup pin cell problem. High burnup is a challenge for MCODE because one needs to track an increased number of important fission products and actinides in MCNP calculations. This benchmark is a standard PWR lattice with 9.75 w/o enriched UO_2 fuel under cold conditions. The isotopic compositions from CASMO-4 and HELIOS at 100 MWd/kg are compared with MCODE results. The eigenvalues are also compared as a function of burnup. Both show satisfactory agreement compared to the relevant literature [70]. When predicting the full power operating time of an 18-month cycle, the difference between MCODE and CASMO-4/HELIOS is only about 3 days. A series of additional sensitivity calculations for the high burnup unit cell problem are then made in order to demonstrate the robustness of the code and further identify the potential benchmark differences against CASMO-4 and HELIOS. General discussions, remarks, and summaries on MCNP/ORIGEN linkage codes are given at the end.

3.2 Methodology

3.2.1 Overview

In routine reactor design burnup calculations, a key objective is to determine the time-dependent fuel material compositions as well as the eigenvalues as a function of burnup. Two basic mechanisms of fuel depletion are under consideration: 1) various nuclear reactions such as nuclear fissions, neutron captures, etc., and 2) the decay of radioactive isotopes. Once material compositions are known eigenvalues can then be calculated efficiently using MCNP for the specified geometry.

Mathematically, the burnup problem can be formulated as follows. For a given nuclear energy system (such as a lattice pin cell, or an assembly, or even the whole core), the entire space can be divided into many zones, such as fuel/gap/cladding/water for a pin cell model, with appropriate boundaries. In MCNP-4C each zone is called a cell and is defined by its bounding surfaces. Some of the zones containing actinide isotopes (those with atomic number greater than or equal to 90) and/or neutron absorbers (such as gadolinium and hafnium) are called active cells, in which the compositions are assumed uniform and known at the beginning (t=0). Denote a material vector $\mathbf{X}_i(t)$ as the atom number density for active cell i. Suppose there are n active cells altogether. The objective of the burnup calculation is to obtain a material vector $\mathbf{X}_i$, i = 1, 2, …, n, at a specified time T given the operating history of the nuclear system. The material balance process can be described at any time t by the following depletion equation [71]:

$$\frac{dX_{ij}}{dt} = \sum_{k=1}^{N_i} l_{k\to j}\lambda_k X_{ik} + \sum_{k=1}^{N_i} f_{k\to j} X_{ik}\int \sigma_k(E)\phi_i(E)dE - \lambda_j X_{ij} - X_{ij}\int \sigma_j(E)\phi_i(E)dE \qquad (3.1)$$

$$i = 1, 2, \cdots, n; \quad j = 1, 2, \cdots, N_i$$

where X_{ij} = atom number density of nuclide j in cell i,

N_i = number of nuclides in cell i,

$l_{k\to j}$ = fraction of radioactive disintegrations by k that lead to formation of j,

λ_k = radioactive decay constant of nuclide k,

$f_{k\to j}$ = fraction of neutron absorptions by k that lead to formation of nuclide j,

$\phi_i(E)$ = spatial-average neutron energy spectrum in cell i,

$\sigma_k(E)$ = neutron absorption cross section of nuclide k.

In the framework of MCODE burnup calculations, one-group cross sections and one-group flux in each active cell are computed by MCNP, with which ORIGEN libraries are updated, i.e., preparation of the coefficients in Eq. (3.1). Note that it is not practical to calculate one group cross sections in MCNP for all nuclides in ORIGEN due to the excessive CPU time demanded, and the unavailability of many MCNP cross sections. Only a finite set of important ones (e.g., strong neutron absorption contributors), typically ~20 actinides and ~50 fission products, is considered in MCNP calculations.

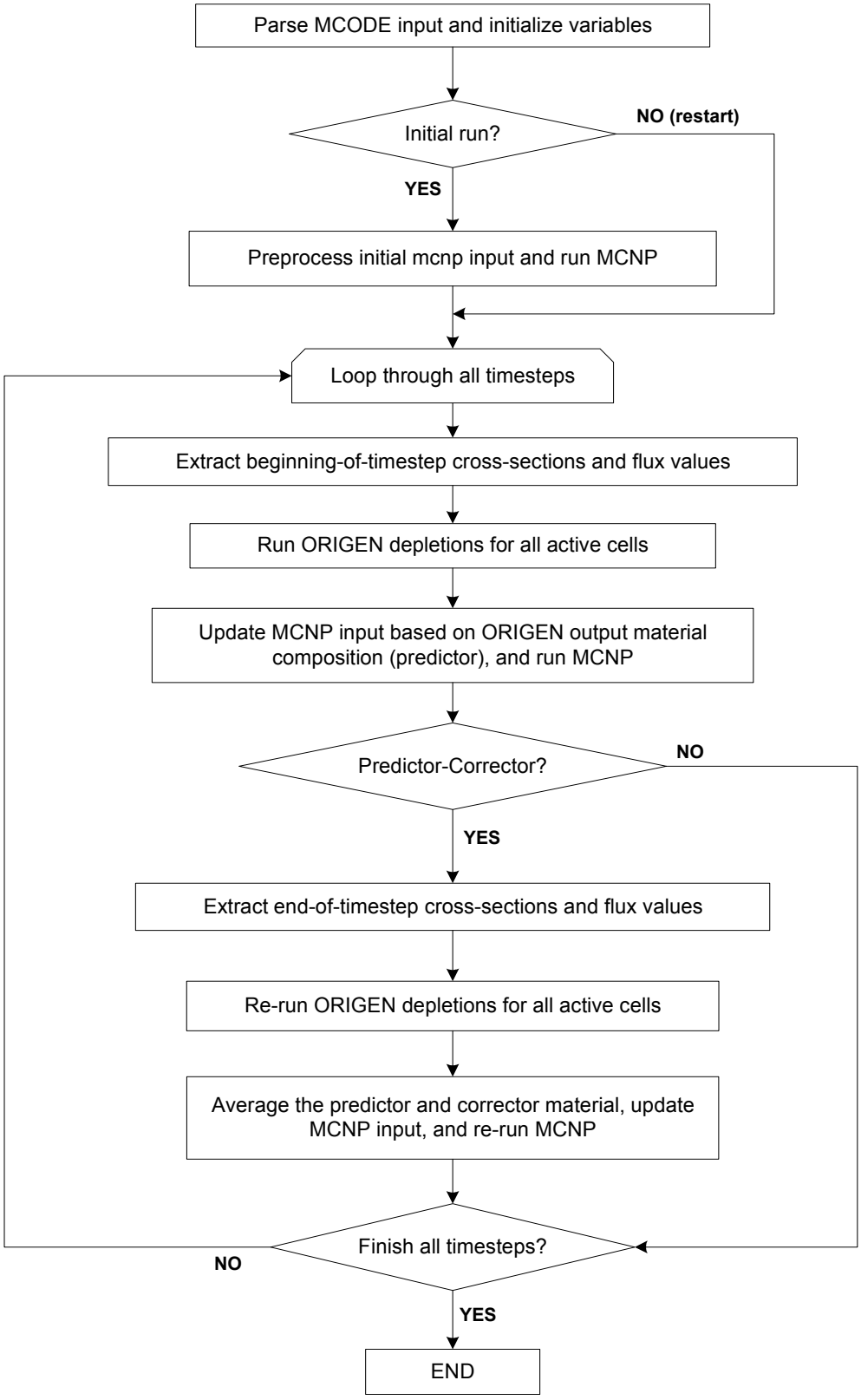

Figure 3.2 Flow diagram of MCODE.

The coefficients in Eq. (3.1), such as one-group cross sections, are obviously not constant over the entire cycle. Therefore, in order to solve this equation, the time T needs to be divided into a number of small time intervals, during which the coefficients are assumed to be constant. Particularly at the beginning of irradiation, a small timestep size is usually needed to account for the buildup of steady state xenon/samarium concentrations in light water reactors. After ~20 MWd/kg, a larger size timestep is acceptable, for example, 5 MWd/kg. Assuming constant cross section and flux within each time interval, one can then use the matrix exponential method to solve these small time intervals in a tandem way. Since MCNP only accounts for important isotopes, all other cross sections not provided must use values from ORIGEN one-group cross section libraries, which are fairly good for specific types of reactors and fuels. In this way, ORIGEN maintains the material reservoir typically including about 1300 unique nuclides (essentially all currently-identified isotopes).

The flow of calculations of MCODE is shown in a simplified diagram illustrated in Figure 3.2. As can be seen, it alternately executes MCNP and ORIGEN to do burnup calculations.

3.2.2 MCNP Tallies and One-Group Cross Section Preparations

Various reaction rates (different reaction types and different isotopes within the cell) and the one-group flux in each individual active cell are provided by MCNP flux tallies as:

$$\begin{cases} \Phi_i = \int \phi_i(E)\,dE \\ R_{ijk} = \int \sigma_k^j(E)\,\phi_i(E)\,dE \end{cases}, \tag{3.2}$$

where $\sigma_k^j(E)$ = microscopic cross section of isotope j with type k,

Φ_i = the region averaged one group flux in cell i,

R_{ijk} = reaction rates of type k with nuclide j in cell i.

These tallies in MCNP come from track length estimates of cell flux and reaction rates (tally type F4 in MCNP). Generally speaking track length estimates are quite reliable because there are frequently many tracks in a cell compared to the number of collisions, leading to many contributions to this tally. The adequacy of each of these tallies is indicated by a so-called relative error, defined as the ratio between the standard deviation and the mean value of that quantity. For a well-behaved tally, increasing number of neutron

histories, N, reduces the relative error according to $\sim 1/\sqrt{N}$. It is recommended in the MCNP manual that the quality of the tally is deemed as generally reliable when its relative error is below 0.10 [24]. Often relative errors also depend on quantities to be calculated. For example, it is relatively easy to achieve a small relative error for the eigenvalue of the system while it is difficult to obtain low relative error values for a region-averaged flux tally calculation in a small volume.

The desired microscopic one group cross section of type k with nuclide j in cell i is then

$$\sigma_{ijk} = \frac{R_{ijk}}{\Phi_i}. \tag{3.3}$$

There has been no attempt to judge the statistical quality of results from MCNP in MCODE. All values of one group flux and one-group cross sections are accepted and used directly.

In the current version of MCODE, two groups of nuclides under consideration are:

- actinides (ACT) that contains heavy metal nuclides with atomic number $Z \geq 90$ and their decay daughters;
- fission products (FP) produced by fissions and their decay/capture products.

Specifically, the effective one-group cross sections of fission products and actinides are shown in Table 3.1. Only the neutron capture cross section is considered for fission products since the neutron absorption of fission products is primarily via (n, γ) reaction. For actinides, four types of cross sections are considered including capture, fission, $(n, 2n)$, and $(n, 3n)$ reactions because actinides are important in terms of generating fission source neutrons and evolving into higher-mass actinides.

Table 3.1 MCNP-tallied one-group cross sections.

	Reaction type	MCNP reaction number
Actinides	(n, γ)	102
	(n, f)	–6
	$(n, 2n)$	16
	$(n, 3n)$	17
Fission products	(n, γ)	102

Since there is a limited amount of actinides, it is relatively straightforward to identify representative nuclei. The identification of fission products representation is, however, an ad hoc process especially for high burnup applications, because numerous fission products are being generated [72]. The fractional neutron importance (absorption) of most individual fission products is small and one needs to consider at least 40 in the usual discharge burnup range (40-60 MWd/kg) for LWRs. For high burnup (say 100MWd/kg), more fission products are needed to account for a reasonably complete neutron absorption fraction, e.g., 100 fission products (and 39 actinides) are chosen in the high burnup pin cell benchmark calculation to account for 99.99% of neutron absorptions and 99.58% of material mass at EOL.

With one-group cross sections from MCNP available, one can readily update the ORIGEN one-group cross section library. However, there are refined requirements of one-group cross sections in ORIGEN, i.e., for the capture or $(n,2n)$ reaction, not only the total one group cross section but also the fraction of reactions leading to ground state nuclei are needed. Thus, the MCNP-tallied total one-group cross section needs to be decomposed to two parts to feed into ORIGEN libraries:

$$\sigma^{\mathrm{MCNP}} = \sigma^{\dagger} + \sigma^{*}, \tag{3.4}$$

where σ^{MCNP} = MCNP-tallied one-group cross section,

$\sigma^{\dagger}$ = nuclear reaction that leads to formation of ground state nuclei,

σ^{*} = nuclear reaction that leads to formation of excited state nuclei.

Here, the branching ratio (BR) is defined as the fraction of reactions leading to excited nuclei formation:

$$\mathrm{BR} = \frac{\sigma^{*}}{\sigma^{\dagger} + \sigma^{*}}. \tag{3.5}$$

In general, nuclear measurements are needed to determine the branching ratio for certain types of nuclear reactions [73]. Therefore, the current implementation of MCODE simply uses the same branching ratios as in the original ORIGEN cross section libraries.

Fortunately there are very few important excited nuclides in LWR calculations. Two important excited isotopes are Am-242m and Pm-148m [74]. Table 3.2 gives effective one-group capture cross sections of Am-241 and Pm-147 (precursors of Am-242m and Pm-148m) from ORIGEN2.1 one-group cross section libraries `PWRUE.LIB` (3-cycle

PWR library, thermal spectrum) and FFTFC.LIB (fast flux test facility core library, fast spectrum). These two nuclides show significant formation of excited nuclei in capture reactions. It is also seen from Pm-147 that in general the branching ratio depends on the neutron spectrum.

Table 3.2 Capture cross sections and branching ratios of Am-241 and Pm-147.

		Am-241	Pm-147
Thermal (PWRUE.LIB)	$\sigma^{\dagger}$ (barn)	83.03	59.62
	σ^{*} (barn)	20.76	28.09
	BR (%)	20.0	32.0
Fast (FFTFC.LIB)	$\sigma^{\dagger}$ (barn)	1.133	0.9675
	σ^{*} (barn)	0.2831	1.334
	BR (%)	20.0	58.0

3.2.3 Flux Normalization

MCNP generates various one-group cross sections and one-group flux values, using track length estimates, for ORIGEN. The one-group cross section values are in units of barns and ready to use. Since all tallies in MCNP are normalized as per fission source neutron, the flux values are in units of (number-of-neutrons) per (fission-source-neutron·cm^2), which needs to be multiplied by a constant factor to convert into (number-of-neutrons) per (cm^2·second). The typical way of calculating this flux multiplication factor (FMF) as recommended in the MCNP manual [24] and Ref. [75] is

$$\text{FMF} = \frac{P \cdot \bar{\nu}}{Q \cdot k_{\text{eff}}} \tag{3.6}$$

where P = total power of the entire system (watts),

$\bar{\nu}$ = average fission neutrons per fission event,

Q = average recoverable energy (excludes neutrinos) per fission event (J/fission),

k_{eff} = eigenvalue of the system.

There have been extensive discussions on the correct interpretation of variables in Eq. (3.6) and procedures for their evaluation were suggested [69, 76]. The ambiguity lies within the value of Q. It takes some effort to calculate this average value over an entire system having different actinides among the active cells. As burnup proceeds, the acti-

nide species vary correspondingly. ORIGEN employs the following relation to calculate recoverable energy per fission for each actinide including the energy of non-fission capture and decay energy [71]:

$$Q(Z,A)\ \text{(MeV/fission)} = 1.29927\times10^{-3}\left(Z^2A^{0.5}\right)+33.12, \tag{3.7}$$

where Z and A are the atomic number and atomic mass, respectively. Therefore, the average recoverable energy also changes with burnup. In addition, both k_{eff} and $\bar{\nu}$ are needed. As discussed in Ref. [69], scaling by k_{eff} for non-critical systems (mostly the case in burnup calculations) also carries uncertainties, because while fission rates scale well with k_{eff}, one-group fluxes may not.

A more rigorous and conceptually-transparent way is to obtain the flux multiplication factor based on an energy balance as follows:

$$\text{FMF} = \frac{P}{\sum_{i=1}^{n}\sum_{j=1}^{m_i} N_{ij}\left[\int \sigma_{ij,f}(E)\phi_i(E)\,dE\right]V_iQ_j} \tag{3.8}$$

where P = total power of the system,

N_{ij} = the number density of actinide j in active cell i,

$\sigma_{ij,f}(E)$ = fission cross section of actinide j in active cell i,

$\phi_i(E)$ = spatial-average neutron spectrum in active cell i,

V_i = volume of active cell i,

Q_j = recoverable energy for actinide j,

m_i = total number of actinides in active cell i.

Eq. (3.8) appears more complex than Eq. (3.6). However, all quantities involved are transparent and readily available during the computational process and evaluation of Eq. (3.8) takes a negligible fraction of CPU time in comparison to MCNP runs. Moreover, Eq. (3.8) together with Eq. (3.7) is fully compatible with the ORIGEN2 depletion scheme. Thus, Eq. (3.8) was implemented in MCODE. Meanwhile, the flux multiplication factor is also calculated using Eq. (3.6) and reported in the detailed output file. Equation (3.6) is implemented in MONTEBURNS [65]. MOCUP reads the normalization factor from a separate input file and its supply is left to the user's responsibility [64]. Fundamentally there is no conceptual difference between these two equations; both give the instantaneous flux multiplication factor. For example, for the high burnup pin cell problem, typical

values of flux multiplication factor using Eqs. (3.6) and (3.8) are 3.20115×10^{13} and 3.19679×10^{13} respectively (only 0.1% difference).

3.2.4 ORIGEN Depletions

ORIGEN is the depletion module incorporating MCNP-calculated one-group cross sections and flux values for each active cell. There are two modes of depletion, either constant power (IRP in ORIGEN) or constant flux (IRF in ORIGEN), which implies that either power or flux will be constant for each active cell within the timestep. In reality the overall power of the system is usually maintained at a certain level under steady state operations. The constant-power depletion mode can ensure a certain energy production for a given timestep. On the contrary, the constant-flux depletion mode can not guarantee the desired energy production because the beginning-of-timestep flux can only ensure the beginning-of-timestep power level.

Under constant flux depletion, the average flux through the timestep is needed. Strictly speaking a so-called internal burnup corrector in ORIGEN, as proposed in [69], should be used according to the following procedure:

1. Extract one-group cross sections and flux values from MCNP output
2. Calculate the flux multiplication factor and obtain beginning-of-timestep flux values
3. Execute a trial ORIGEN run with constant beginning-of-timestep flux values
4. Compute the ratio of energy production between rated power and the trial ORIGEN run (average to beginning-of-timestep ratio)
5. Use the average to beginning-of-timestep ratio to correct beginning-of-timestep flux values
6. Re-run ORIGEN with adjusted constant timestep-average flux and obtain final results.

This internal burnup corrector technique in ORIGEN ensures validity of constant-flux-mode depletion. The expense to be paid is running ORIGEN twice per timestep, which is unimportant since the fraction of CPU time of ORIGEN runs is negligible compared to MCNP running time. However, this internal burnup corrector is not implemented in the current version of MCODE because (1) the predictor-corrector algorithm in the burnup calculation provides a correction of the constant flux approach (fluxes based on beginning-of-timestep and end-of-timestep); (2) the following constant power depletion can completely avoid this problem.

Under constant power depletion, the power is guaranteed as the rated power. Power fractions for each active cell are calculated as follows:

$$f_i = \frac{\sum_{j=1}^{m_i} N_{ij} \left[\int \sigma_{ij,f}(E) \phi_i(E) dE \right] V_i Q_j}{\sum_{k=1}^{n} \sum_{j=1}^{m_k} N_{kj} \left[\int \sigma_{kj,f}(E) \phi_k(E) dE \right] V_k Q_j} \tag{3.9}$$

where symbols have the same meaning as in Eq. (3.8). Then, the power of each active cell is determined by multiplying the given total power with the fraction factor.

For a well-defined problem, one should expect to have almost identical results between these two ways of normalization (with predictor-corrector option turned on). This provides a degree of self-validation, hence increased confidence in one's results.

3.2.5 Coupling between MCNP and ORIGEN

The coupling between MCNP and ORIGEN needs to be given special attention. It is a key issue for the linkage codes which ultimately determines the quality of the results. Because the cross sections, flux values and power fractions in active cells undergo continuous changes with time throughout reactor operation, beginning-of-timestep values are not fully representative of the entire timestep, unless the timestep is exceedingly small. Better estimates of timestep-average values are needed.

In our formulation, denote the timestep as $[t_{n-1}, t_n]$. The material vectors $\mathbf{X}_i,\ i = 1, 2, \cdots, n$ are known at t_{n-1}. The question is then how to solve Eq. (3.1) to obtain end-of-timestep values. One thing to note is that Eq. (3.1) can also be written in a compact vector form:

$$\frac{d\mathbf{X}_i(t)}{dt} = \mathbf{A}_i(t)\mathbf{X}_i(t), \qquad i = 1, 2, \cdots, n \tag{3.10}$$

where the matrix **A** is called the transition matrix.

Previous sections have discussed preparation of this transition matrix (one group fluxes and one group cross sections). Here a peer-to-peer conceptual comparison of coupling is made among three existing linkage codes, MCODE, MOCUP, and MONTEBURNS.

In MOCUP, beginning-of-timestep cross sections and flux values in active cells are assumed constant over the entire timestep. Then, the analytic solution at the end of the timestep is

$$\mathbf{X}_i(t_n) = \left[\exp\left(\mathbf{A}_i(t_{n-1})\Delta t\right)\right]\mathbf{X}_i(t_{n-1}) \tag{3.11}$$

In MONTEBURNS, the so-called middle timestep approach is deployed, i.e., the estimated middle-of-timestep values are extracted to build the transition matrices to represent the entire timestep, namely

$$\mathbf{X}_i(t_n) = \exp\left(\mathbf{A}_i\left(\frac{t_{n-1}+t_n}{2}\right)\Delta t\right)\mathbf{X}_i(t_{n-1}) \tag{3.12}$$

In MCODE, a standard predictor-corrector approach is implemented [77]. The burnup depletion is calculated twice, first using the spectra corresponding to the isotope vector at the start of the step and then, after a new spectrum calculation, using the spectra at the end of step. Average number densities from these two calculations are taken as the end-of-timestep material compositions.

$$\begin{aligned}
\mathbf{X}_i^{\mathrm{P}}(t_n) &= \left[\exp\left(\mathbf{A}_i(t_{n-1})\Delta t\right)\right]\mathbf{X}_i(t_{n-1}) \\
\mathbf{X}_i^{\mathrm{C}}(t_n) &= \left[\exp\left(\mathbf{A}_i^{\mathrm{P}}(t_n)\Delta t\right)\right]\mathbf{X}_i(t_{n-1}) \\
\mathbf{X}_i(t_n) &= \frac{\mathbf{X}_i^{\mathrm{P}}(t_n)+\mathbf{X}_i^{\mathrm{C}}(t_n)}{2}
\end{aligned} \tag{3.13}$$

In order to illustrate the accurateness of each coupling approach, numerical examples are first examined. Instead of a vector equation (3.10), one considers its corresponding scalar equation:

$$\frac{dx(t)}{dt} = a(x)x(t), \qquad (0 < t < 0.1), \tag{3.14}$$

with $x(t=0)=1$. Various forms of $a(x)$ (corresponding to a transition matrix) are considered as shown in Table 3.3. Using the formulations (3.11), (3.12), and (3.13), one can compute various results and the relative errors versus the true solution. It is clear that the simple and computationally straight-forward approach adopted in MOCUP is the least accurate approximation of the three (about one order of magnitude error higher than that of MONTEBURNS and MCODE from Table 3.3). Further comparisons between MONTEBURNS and MCODE show that the error of MONTEBURNS roughly doubles

the error of MCODE. In other words, for fixed timestep sizes, MCODE is expected to be twice as precise as MONTEBURNS. It is concluded that the predictor-corrector approach in MCODE better accounts for the non-linear behavior of transition matrices. Large time step sizes are therefore allowed in MCODE. In fact the standard predictor-corrector algorithm is the proven algorithm for burnup calculations for all licensing-level reactor physics codes, such as CASMO-4 [23] and HELIOS. It is conceptually simpler and numerically more accurate than the middle-timestep approach in MONTEBURNS.

Table 3.3 Numerical examples of various coupling schemes.

$a(x)$	Exact solution		MOCUP		MONTEBURNS		MCODE	
	$x(t)$	$x(t=0.1)$	$x(t=0.1)$	Error	$x(t=0.1)$	Error	$x(t=0.1)$	Error
C (const)	e^{Ct}	$e^{0.1C}$	$e^{0.1C}$	0	$e^{0.1C}$	0	$e^{0.1C}$	0
$1/x$	$1+t$	1.1	1.1052	0.47%	1.0998	–0.02%	1.0999	–0.01%
$\sqrt{x}$	$\left(\frac{2}{2-t}\right)^2$	1.1080	1.1052	–0.28%	1.1080	0	1.1080	0
x	$\frac{1}{1-t}$	1.1111	1.1052	–0.53%	1.1109	–0.02%	1.1110	–0.01%
x^2	$\frac{1}{\sqrt{1-2t}}$	1.1180	1.1052	–1.3%	1.1169	–0.1%	1.1175	–0.04%
x^5	$(1-5t)^{-\frac{1}{5}}$	1.1487	1.1052	–3.8%	1.1370	–1.0%	1.1422	–0.7%

One should be aware of the fact that the middle-time-step approach in MONTEBURNS is both an advantage and a disadvantage. Two MCNP runs are needed for MCODE while typically only one MCNP run at middle-timestep is needed for MONTEBURNS. This roughly doubles the running time of MCODE. However, one disadvantage of the middle-timestep approach is the effect on iteration procedures because eigenvalues will be calculated at the middle of the timestep, not at the end of the timestep. If eigenvalues at the end of timestep are needed, additional MCNP runs are required (same computation time required as MCODE then). With advances in computation power, the impact of doubling the running time of MCNP will be less significant for burnup calculations. For example, the recently-built 30-CPU cluster machine at MIT has significantly reduced MCNP running time by a factor of ~20 [78].

Comparisons of MCODE with MOCUP and MONTEBURNS are summarized in Table 3.4.

Table 3.4 MCODE comparisons with MOCUP and MONTEBURNS.

	MCODE	MOCUP	MONTEBURNS
Developer	MIT	INEEL	LANL
Year	2001	1995	1999
Language	ANSI C	ANSI C	FORTRAN, PERL
Portability	Excellent	Good	Good
User involvement	Small	Extensive	Small
Running flexibility	Excellent	Excellent	Good
Normalization	Power or flux	Flux	Flux
Coupling manner	Standard predictor-corrector algorithm	Beginning-of-timestep representation	Middle of timestep representation

3.3 High Burnup UO_2 Lattice Benchmark

3.3.1 Pin Cell Model

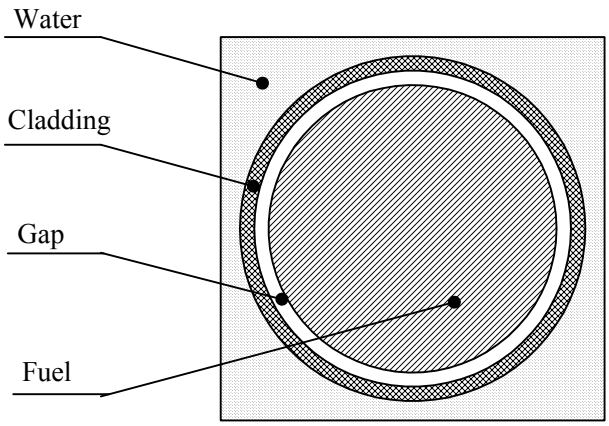

Figure 3.3 Pin cell model (not to scale).

A single pin cell model (Fig. 3.3) of a standard Westinghouse 17×17 PWR assembly has been employed to benchmark MCODE. Boundaries of the unit cell are set to be reflecting. This model represents the cross section (two-D) of the fuel pin while ignoring axial de-

pendence (in MCNP the pin cell is 4 cm in height with top and bottom reflecting boundaries). In order to use the ENDF/B-VI MCNP libraries provided with the code, isothermal cold conditions (room temperature, 300K) are used. The fuel is uranium dioxide with 9.75 w/o U-235 enrichment which results in high burnup (~100MWd/kg). It is, therefore, a challenge to MCODE since large numbers of actinides and fission products are needed. Since this is well above the current burnup licensing limit of 60 MWd/kg, it is also a challenge to CASMO-4 and HELIOS (two available deterministic codes). Note that all the codes treat the entire fuel region as one lumped block. Actual calculations show that refinement of the fuel representation (dividing the fuel pellet into several concentric regions) gives almost the same results. Detailed pin cell model parameters are shown in Table 3.5 and the initial compositions are shown in Table 3.6.

Table 3.5 Pin cell model parameters (cold conditions at 300 K).

Parameters	Values
Fuel pellet radius (cm)	0.4096
Cladding inner radius (cm)	0.4178
Cladding outer radius (cm)	0.4750
Pin pitch (cm)	1.26
Fuel density (g/cm^3)	10.3
Cladding density (g/cm^3)	6.550
Coolant density (g/cm^3)	0.997
Power density (kW/liter core)	104.5
Specific power (W/gU)	34.6679

Table 3.6 Initial compositions (cold conditions at 300 K).

	Nuclide	Weight percent (w/o)	Number density (1/cm^3)
Fuel (9.75 w/o UO_2)	U-234	0.0688	1.82239E+19
	U-235	8.5946	2.26826E+21
	U-238	79.4866	2.07128E+22
	O-16	11.8500	4.59686E+22
Cladding (Zircaloy-4)	O	0.125	3.08281E+20
	Cr	0.10	7.58663E+19
	Fe	0.21	1.48338E+20
	Zr	98.115	4.24275E+22
	Sn	1.45	4.81835E+20
Coolant (H_2O)	H-1	11.19	6.66295E+22
	O-16	88.81	3.33339E+22

3.3.2 Code Descriptions

Results of MCODE were benchmarked against CASMO-4 [20] and HELIOS [79]. Those two codes are licensing-level, industry standard burnup calculation tools, which solve the transport equation based on deterministic methods. The input files of benchmark calculation are included in Appendix C for CASMO-4 and MCODE. One thing to note is that CASMO-4 uses neutron cross section libraries processed from JEF-2.2 and ENDF/B-6; while MCODE is entirely based on ENDF/B-6 library data. However, we still use CASMO-4 as the reference and use HELIOS results to double check its validity. The main features of each code are summarized in Table 3.7:

Table 3.7 Summary of benchmarking codes [69].

	MCODE	CASMO-4	HELIOS
Cross section libraries	ENDF/B-6	ENDF/B-6, JEF2.2	ENDF
Code developer	MIT	Studsvik	Scandpower
Transport treatment	Monte Carlo	KRAM characteristics	CPM+CCPM
Resonance treatment	Monte Carlo	collision probability	subgroup method
Number of energy groups	continuous	70	45
Burnup algorithm	predictor-corrector	predictor-corrector	predictor-corrector
Leakage	No	No	No
Actinide representation	39	Th231 thru Cf252	Th230 thru Cm246
Fission products	100	~200	115

3.3.3 Benchmark Results and Analysis

Forty-nine burnup steps are chosen between 0 and 100 MWd/kg for the benchmarking calculations. The running options for MCODE are power normalization with burnup predictor-corrector algorithm on. There are 39 actinides (ACT) and 100 fission products (FP) considered in the burnup calculations, which accounts for ≥ 99.95% total mass and neutron absorptions at 100 MWd/kg. Table 3.8 and 3.9 shows the chosen 39 actinides and 100 fission products in MCODE, respectively. Most data files are standard MCNP libraries [80]. The UTXS data library was prepared at the University of Texas at Austin [81]. And other libraries were evaluated at LANL, INEEL, or ORNL which came through INEEL. Mass conservation is preserved. Each MCNP run takes about 1 hour with 225,000 neutron histories and the entire run takes about 4 days with MCODE using a DEC alpha workstation.

Table 3.8 The chosen 39 actinides in MCODE.

Actinide	Absorption fraction at 100 MWd/kg	ZAID	Library name	Source	Temperature (K)
TH232	1.942E-09	90232.60c	endf60	ENDF/B-VI.0	294
PA231	4.185E-08	91231.60c	endf60	ENDF/B-VI.0	294
PA233	4.038E-10	91233.50c	endf5u	ENDF/B-V.0	294
U232	2.294E-08	92232.60c	endf60	ENDF/B-VI.0	294
U233	1.469E-07	92233.60c	endf60	ENDF/B-VI.0	294
U234	2.004E-03	92234.60c	endf60	ENDF/B-VI.0	294
U235	1.979E-01	92235.60c	endf60	ENDF-VI.2	294
U236	2.009E-02	92236.60c	endf60	ENDF-VI.0	294
U237	1.945E-04	92237.50c	endf5p	ENDF/B-V.0	294
U238	2.888E-01	92238.60c	endf60	ENDF-VI.2	294
NP236	1.373E-07	93236.35c	endl85	LLNL	0
NP237	1.509E-02	93237.60c	endf60	ENDF-VI.1	294
NP238	2.138E-04	93238.35c	endl85	LLNL	0
NP239	3.988E-04	93239.60c	endf60	ENDF-VI.0	294
PU238	9.642E-03	94238.60c	endf60	ENDF-VI.0	294
PU239	2.759E-01	94239.60c	endf60	ENDF-VI.2	294
PU240	8.745E-02	94240.60c	endf60	ENDF-VI.1	294
PU241	8.136E-02	94241.60c	endf60	ENDF-VI.1	294
PU242	9.741E-03	94242.60c	endf60	ENDF-VI.0	294
PU243	2.831E-06	94243.60c	endf60	ENDF-VI.2	294
AM241	3.338E-03	95241.60c	endf60	LANL/T-2	294
AM242	4.484E-05	95242.50c	endf5u	ENDF/B-V.0	294
AM242M	6.645E-04	95242.51c	rmccs	ENDF/B-V.0	294
AM243	5.272E-03	95243.60c	endf60	ENDF-VI.0	294
AM244	9.812E-07	95244.96c	hfirxs1	JENDL-3.2	300
CM242	5.717E-05	96242.60c	endf60	ENDF-VI.0	294
CM243	3.820E-05	96243.60c	endf60	ENDF-VI.0	294
CM244	1.108E-03	96244.60c	endf60	ENDF-VI.0	294
CM245	7.549E-04	96245.60c	endf60	ENDF-VI.2	294
CM246	3.253E-06	96246.60c	endf60	ENDF-VI.2	294
CM247	6.533E-07	96247.60c	endf60	ENDF-VI.2	294
CM248	1.337E-08	96248.60c	endf60	ENDF-VI.0	294
CM249	1.000E-12	96249.96c	hfirxsa1	JENDL-3.2	300
BK249	5.463E-09	97249.60c	endf60	ENDF-VI.0	294
BK250	1.000E-12	97250.96c	hfirxsa1	JENDL-3.2	300
CF249	1.330E-09	98249.60c	endf60	ENDF-VI.0	294
CF250	4.001E-09	98250.60c	endf60	ENDF-VI.2	294
CF251	3.229E-09	98251.60c	endf60	ENDF-VI.2	294
CF252	1.000E-12	98252.60c	endf60	ENDF-VI.2	294
Sum	1.000				

Table 3.9 The chosen 100 fission products in MCODE.

Fission products	Absorption fraction at 100 MWd/kg	ZAID	Library name	Source	Temperature (K)
BR 81	5.465E-04	35081.55c	misc5xs	LANL/T-2	294
KR 82	1.164E-04	36082.50c	rmccsa	ENDF/B-V.0	294
KR 83	7.975E-03	36083.50c	rmccsa	ENDF/B-V.0	294
KR 84	1.272E-04	36084.50c	rmccsa	ENDF/B-V.0	294
RB 85	3.337E-04	37085.55c	misc5xs	LANL/T-2	294
RB 87	2.105E-04	37087.55c	misc5xs	LANL/T-2	294
SR 90	4.451E-04	38090.96c	ornlxsa1	ENDF/B-VI	300
Y 89	6.030E-04	39089.60c	endf60	ENDF/B-VI.0	294
ZR 91	1.437E-03	40091.96c	ornlxsb1	ENDF/B-VI	300
ZR 92	3.014E-04	40092.62c	zr92.300	UTXS	300
ZR 93	8.540E-03	40093.50c	kidman	ENDF/B-V.0	294
ZR 94	1.455E-04	40094.62c	zr94.300	UTXS	300
ZR 96	1.395E-03	40096.62c	zr96.300	UTXS	300
NB 95	1.178E-04	41095.96c	ornlxsb1	ENDF/B-VI	300
MO 95	2.601E-02	42095.50c	kidman	ENDF/B-V.0	294
MO 96	5.520E-04	42096.96c	ornlxs1	ENDF/B-VI	300
MO 97	5.885E-03	42097.60c	mason1	ENDF/B-VI	294
MO 98	2.050E-03	42098.50c	mason1	ENDF/B-V	294
MO100	1.441E-03	42100.50c	mason1	ENDF/B-V	294
TC 99	4.983E-02	43099.50c	kidman	ENDF/B-V.0	294
RU100	1.049E-03	44100.96c	ornlxsb1	ENDF/B-VI	300
RU101	2.161E-02	44101.50c	kidman	ENDF/B-V.0	294
RU102	1.761E-03	44102.60c	mason1	ENDF/B-VI	294
RU103	3.953E-04	44103.50c	mason1	ENDF/B-V.0	294
RU104	1.200E-03	44104.96c	ornlxsb1	ENDF/B-VI	300
RH103	9.109E-02	45103.50c	rmccsa	ENDF/B-V.0	294
RH105	4.846E-03	45105.50c	rmccsa	ENDF/B-V.0	294
PD104	2.227E-03	46104.96c	ornlxs1	ENDF/B-VI	300
PD105	1.155E-02	46105.50c	kidman	ENDF/B-V.0	294
PD106	8.134E-04	46106.96c	ornlxs1	ENDF/B-VI	300
PD107	5.402E-03	46107.96c	ornlxs1	ENDF/B-VI	300
PD108	7.543E-03	46108.50c	kidman	ENDF/B-V.0	294
PD110	1.043E-04	46110.96c	ornlxs1	ENDF/B-VI	300
AG109	1.656E-02	47109.60c	endf60	ENDF-VI.0	294
CD110	7.849E-04	48110.62c	cd110.300	UTXS	300
CD111	6.547E-04	48111.62c	cd111.300	UTXS	300
CD112	7.195E-05	48112.62c	cd112.300	UTXS	300
CD113	1.931E-03	48113.60c	mason1	ENDF/B-VI	294
CD114	7.773E-05	48114.62c	cd114.300	UTXS	300
IN115	1.332E-03	49115.60c	mason1	ENDF/B-VI	294
SB121	2.773E-04	51121.96c	ornlxsb1	ENDF/B-VI	300
SB123	2.000E-04	51123.96c	ornlxsb1	ENDF/B-VI	300
TE128	9.441E-05	52128.96c	ornlxsa1	ENDF/B-VI	300
I127	1.698E-03	53127.60c	endf60	LANL/T-2	294
I129	3.611E-03	53129.60c	endf60	ENDF-VI.0	294
XE131	6.015E-02	54131.50c	kidman	ENDF/B-V.0	294
XE132	8.545E-04	54132.62c	xe132.300	UTXS	300
XE133	5.488E-04	54133.60c	mason1	ENDF/B-VI	294
XE134	5.381E-04	54134.62c	xe134.300	UTXS	300
XE135	9.652E-02	54135.50c	endf5mt	ENDF/B-V	294
XE136	2.331E-04	54136.62c	xe136.300	UTXS	300
CS133	6.973E-02	55133.60c	endf60	ENDF-VI.0	294

Table 3.9 The chosen 100 fission products in MCODE (continued).					
CS134	1.127E-02	55134.60c	endf60	ENDF-VI.0	294
CS135	9.690E-03	55135.60c	endf60	ENDF-VI.0	294
CS137	2.031E-04	55137.60c	endf60	ENDF-VI.0	294
BA134	9.040E-04	56134.62c	ba134.300	UTXS	300
BA137	3.427E-04	56137.62c	ba137.300	UTXS	300
BA138	3.044E-04	56138.60c	endf60	ENDF-VI.0	294
LA139	8.063E-03	57139.60c	mason1	ENDF/B-VI	294
CE140	4.870E-04	58140.96c	ornlxsb1	ENDF/B-VI	300
CE141	3.210E-04	58141.60c	mason1	ENDF/B-VI	294
CE142	7.485E-04	58142.96c	ornlxsb1	ENDF/B-VI	300
CE144	1.282E-04	58144.96c	ornlxsb1	ENDF/B-VI	300
PR141	1.026E-02	59141.50c	kidman	ENDF/B-V.0	294
PR143	5.287E-04	59143.60c	mason1	ENDF/B-VI	294
ND142	3.843E-04	60142.96c	ornlxsb1	ENDF/B-VI	300
ND143	1.078E-01	60143.50c	kidman	ENDF/B-V.0	294
ND144	3.878E-03	60144.96c	ornlxsb1	ENDF/B-VI	300
ND145	3.565E-02	60145.50c	kidman	ENDF/B-V.0	294
ND146	1.121E-03	60146.96c	ornlxsb1	ENDF/B-VI	300
ND147	3.368E-04	60147.50c	kidman	ENDF/B-V.0	294
ND148	1.966E-03	60148.50c	kidman	ENDF/B-V.0	294
ND150	6.844E-04	60150.96c	ornlxsb1	ENDF/B-VI	300
PM147	2.884E-02	61147.50c	kidman	ENDF/B-V.0	294
PM148	3.553E-03	61148.50c	kidman	ENDF/B-V.0	294
PM148M	6.715E-03	61148.60c	mason1	ENDF/B-VI	294
PM149	3.269E-04	61149.50c	kidman	ENDF/B-V.0	294
SM147	1.652E-02	62147.50c	kidman	ENDF/B-V.0	294
SM148	1.694E-03	62148.96c	ornlxsa1	ENDF/B-VI	300
SM149	3.700E-02	62149.50c	endf5u	ENDF/B-V.0	294
SM150	1.727E-02	62150.50c	kidman	ENDF/B-V.0	294
SM151	3.048E-02	62151.50c	kidman	ENDF/B-V.0	294
SM152	3.699E-02	62152.50c	kidman	ENDF/B-V.0	294
SM153	2.515E-04	62153.60c	mason1	ENDF/B-VI	294
SM154	3.053E-04	62154.96c	ornlxsa1	ENDF/B-VI	300
EU151	3.505E-05	63151.60c	endf60	ENDF-VI.0	294
EU153	3.655E-02	63153.60c	endf60	ENDF-VI.0	294
EU154	3.111E-02	63154.50c	endf5u	ENDF/B-V.0	294
EU155	3.112E-02	63155.50c	kidman	ENDF/B-V.0	294
EU156	1.178E-03	63156.60c	mason1	ENDF/B-VI	294
GD154	6.484E-04	64154.60c	endf60	ENDF-VI.0	294
GD155	2.134E-03	64155.60c	endf60	ENDF-VI.0	294
GD156	2.305E-03	64156.60c	endf60	ENDF-VI.0	294
GD157	4.577E-03	64157.60c	endf60	ENDF-VI.0	294
GD158	2.424E-04	64158.60c	endf60	ENDF-VI.0	294
TB159	2.237E-04	65159.96c	ornlxsb1	ENDF/B-VI	300
DY160	9.107E-05	66160.96c	ornlxsb1	ENDF/B-VI	300
DY161	1.437E-04	66161.96c	ornlxsa1	ENDF/B-VI	300
DY162	1.116E-04	66162.96c	ornlxsa1	ENDF/B-VI	300
DY163	7.231E-05	66163.96c	ornlxsa1	ENDF/B-VI	300
Sum	0.9991				

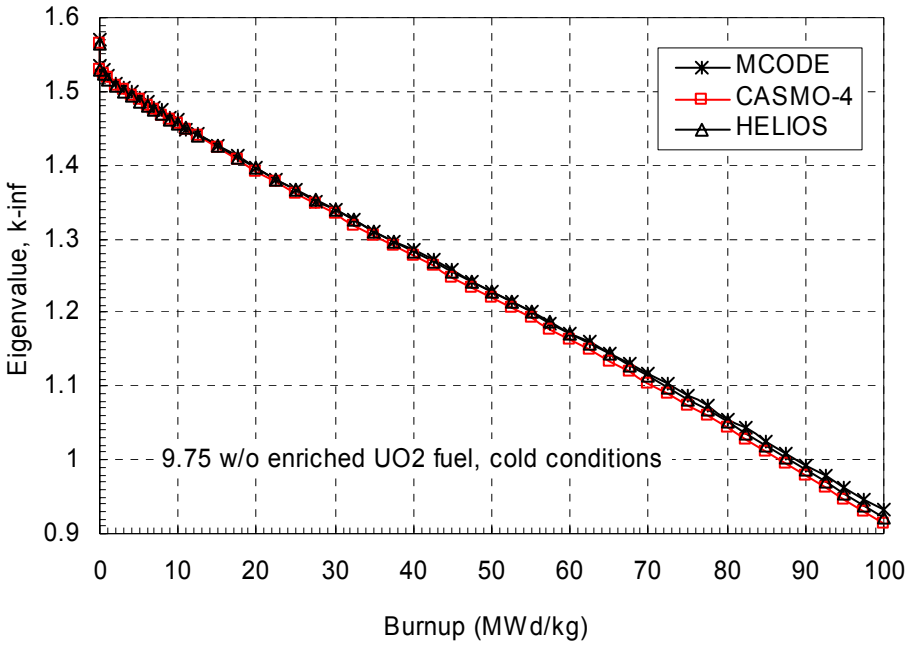

Figure 3.4 Eigenvalue comparison between MCODE, CASMO-4, and HELIOS.

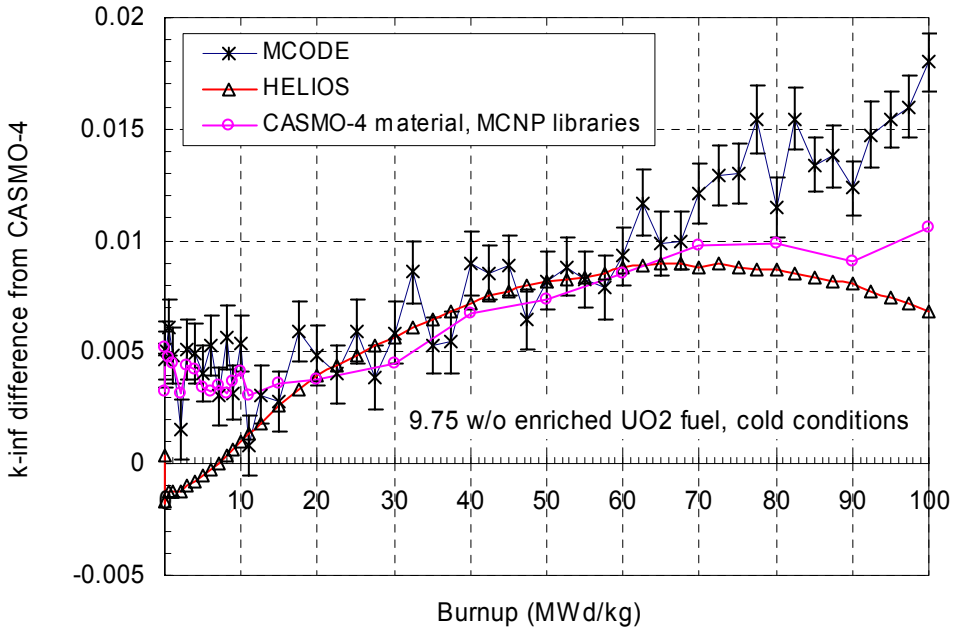

Figure 3.5 Eigenvalue difference from CASMO-4 as a function of burnup.

Figure 3.4 shows the comparison of eigenvalue history among MCODE, CASMO4, and HELIOS, and Figure 3.5 shows the difference from CASMO-4. It can be seen from Figure 3.4 that before 60 MWd/kg there is a nearly a constant Δk between MCODE and CASMO-4. Then it grows almost in a linear way. HELIOS agrees with CASMO-4 better than MCODE. At 100 MWd/kg burnup, the eigenvalue difference is about 0.015. This result is better compared to previous benchmark efforts [69] where the eigenvalue difference reaches 0.01 at 60 MWd/kg. For example, if one projects the burnup difference over one LWR 18-month cycle, the predicted cycle length difference has decreased from the previous 1 week to a current 3 days. Circled points indicate MCNP criticality calculations using the CASMO-4 output material vectors and MCNP ENDF-VI libraries. This isolates the static library difference and shows that the constant Δk before 80 MWd/kg is mainly due to the library difference. This observation is consistent with other benchmark efforts using JEF and ENDF libraries [82]. Generally speaking the eigenvalue using ENDF libraries is slightly higher than that using the JEF library. Even at 100 MWd/kg, the static library difference still accounts for about two thirds of the eigenvalue discrepancy between MCODE and CASMO-4. In addition, the dynamic library difference should also be taken into consideration, i.e., the burnup effect caused by library differences. From the author's experience, it appears that there are more fertile isotopes converted to fissile in MCODE than in CASMO-4 which phenomenologically explains the eventual linear increase in eigenvalue difference. Several other causes might also contribute, such as statistical error propagation, or empirical treatments in CASMO-4 or HELIOS. From an engineering point of view, MCODE is sufficiently accurate and gives consistent results.

In addition to the eigenvalue comparison, an isotope composition comparison at 100 MWd/kg is presented in Table 3.10 along with uncertainties for uranium fuel from [70]. Note that these uncertainties are given as the spread of isotope concentrations from dozens of calculations. The referenced numbers are results for 44.34 MWd/kg burnup UO_2 fuel while our comparison is at a more challenging 100MWd/kg. Most of the material compositions agree with CASMO-4 within typical uncertainties. Taking into consideration the high burnup the differences are acceptable. Table 3.10 also confirms that overall there are more fissile species present for MCODE. It is clear from Table 3.10 that

the fissile excess can be attributed to higher consumption of U-238, which results in more Pu-239 and less U-235 consumption.

The Am-242m concentration difference between CASMO-4 and MCODE is significant, which needs further attention.

Table 3.10 Fractional difference from CASMO-4 in nuclide concentration at 100MWd/kg.

Isotopes	CASMO-4 (#/cm^3)	HELIOS	MCODE	Max typical uncertainties [70]
Mo-95	1.22281E+20	NA	–0.17%	1.85%
Tc-99	1.16862E+20	NA	4.54%	4.21%
Ru-101	1.19274E+20	NA	–0.30%	1.76%
Rh-103	4.60151E+19	NA	3.30%	5.40%
Ag-109	6.99101E+18	NA	14.62%	10.21%
Cs-133	1.14516E+20	NA	8.15%	5.60%
Cs-135	6.98202E+19	NA	0.35%	3.63%
Nd-143	7.42463E+19	NA	0.34%	4.51%
Nd-145	7.10908E+19	NA	–0.08%	1.46%
Sm-147	9.57151E+18	NA	14.09%	9.12%
Sm-149	1.24554E+17	NA	–5.83%	15.61%
Sm-150	2.67571E+19	NA	8.08%	8.50%
Sm-151	7.68167E+17	NA	–10.27%	22.31%
Sm-152	9.39450E+18	NA	–16.19%	9.68%
Eu-153	1.18378E+19	NA	–11.36%	8.52%
U-234	6.71252E+18	0.86%	1.20%	8.99%
U-235	2.59522E+20	–1.24%	2.10%	8.12%
U-238	1.96718E+22	–0.11%	–0.17%	2.60%
Np-237	3.42341E+19	0.98%	–8.90%	9.42%
Pu-238	1.96654E+19	–0.08%	–8.26%	13.86%
Pu-239	1.47667E+20	2.05%	5.61%	7.12%
Pu-240	6.31059E+19	6.49%	8.77%	5.27%
Pu-241	4.28013E+19	1.21%	5.13%	6.86%
Pu-242	2.62275E+19	–3.92%	–3.05%	8.39%
Am-241	2.35052E+18	–4.40%	9.96%	5.29%
Am-242m	3.38273E+16	NA	103%	NA
Am-243	6.23202E+18	19.86%	23.22%	10.40%
Total actinides	2.02803E+22	–0.08%	–0.07%	NA
Total fissile	4.92807E+20	0.37%	2.96%	NA
Total fertile	1.97875E+22	–0.09%	–0.15%	NA

The plutonium vectors are also compared graphically as a function of burnup as shown in Fig. 3.6, which indicates satisfactory agreement.

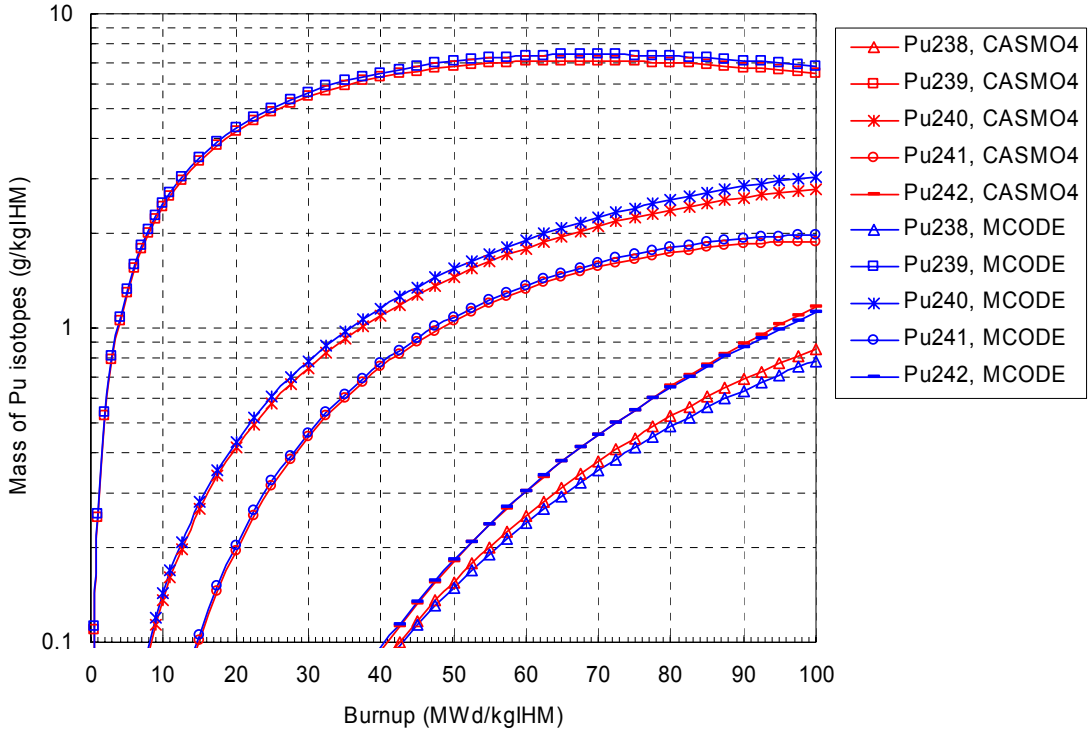

Figure 3.6 Plutonium vector comparison with CASMO-4 as a function of burnup.

From the code-vs-code benchmarking of the high burnup UO_2 lattice under cold conditions, it is concluded that MCODE is suitable and ready to be used in burnup calculations. Even for high burnup cases, the eigenvalue comparisons are still within ~0.02 of CASMO-4, and even closer to HELIOS. The material composition predictions are also acceptable compared to the comprehensive uranium benchmark reported by OECD in Ref. [70].

3.4 Sensitivity Calculations

In addition to the benchmark calculation, a series of sensitivity calculations were performed in order to investigate the most efficient way of running MCODE, to further verify the code itself (robustness), and to extract guidelines for running MCODE. We still use the high burnup lattice with 9.75 w/o enrichment as in the last section.

3.4.1 Timestep Size

There are two types of burnup timestep size: (1) macro burnup timestep size; (2) micro burnup timestep size. The macro burnup timestep is the time step between two MCNP calculations which refresh the one-group cross section libraries (spectrum effect). And the micro burnup timestep size refers to the ORIGEN burnup time steps between two MCNP calculations. Here the macro burnup timestep size is studied. One can first calculate a reference solution with fine timesteps. Then, gradually enlarging the timesteps will yield divergence of the results.

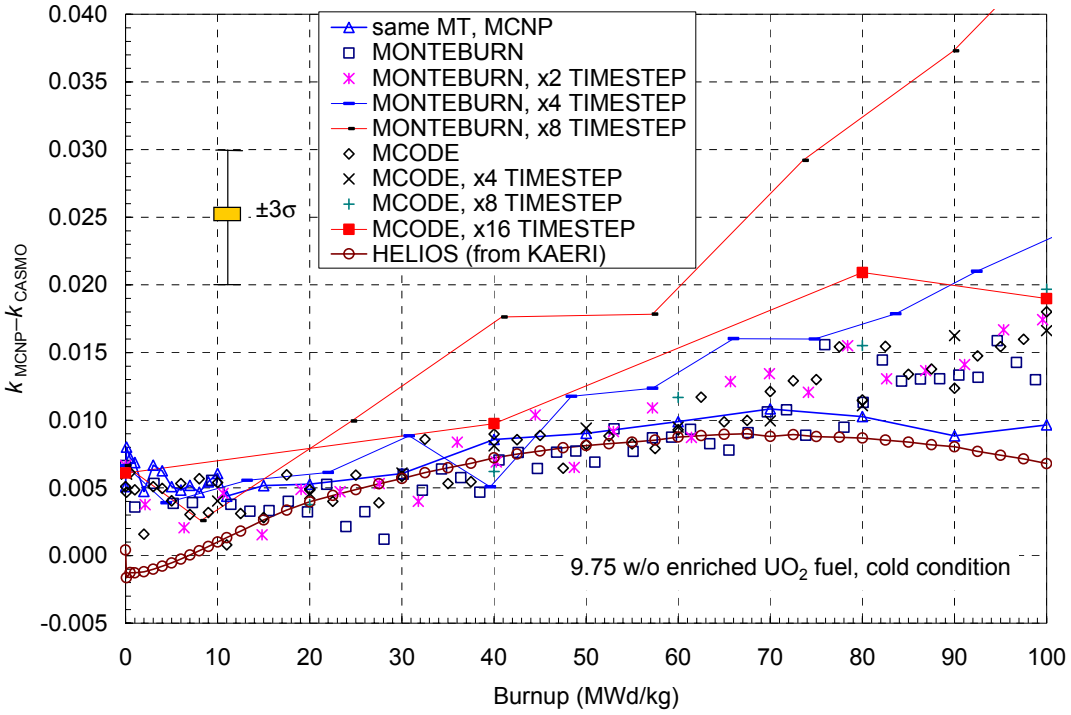

Figure 3.7 Effect of time step size on the convergence.

The curve "same MT, MCNP" was obtained by using number densities generated by CASMO-4 as an input for MCNP runs along the burnup curve to eliminate dependency of the results on library usage. Thus all the results should be compared against this curve. The convergence for cases with various time step sizes is shown in this figure. Results from MCODE and MONTEBURNS are given which shows that even with doubling of the time step sizes MCODE still converges faster than MONTEBURNS, i.e., the case

of MCODE ×16 TIMESTEP is agrees better with reference results than the case of MONTEBURN ×8 TIMESTEP. This behavior confirms the analytical results in Table 3.3 that MCODE is twice as accurate as MONTEBURNS.

In addition, the eigenvalue at 100 MWd/kg is computed and compared in MCODE with predictor-corrector option on as time step size is increased (Figure 3.8). It suggests that the macro burnup timestep should not exceed 10 MWd/kg for LWR applications.

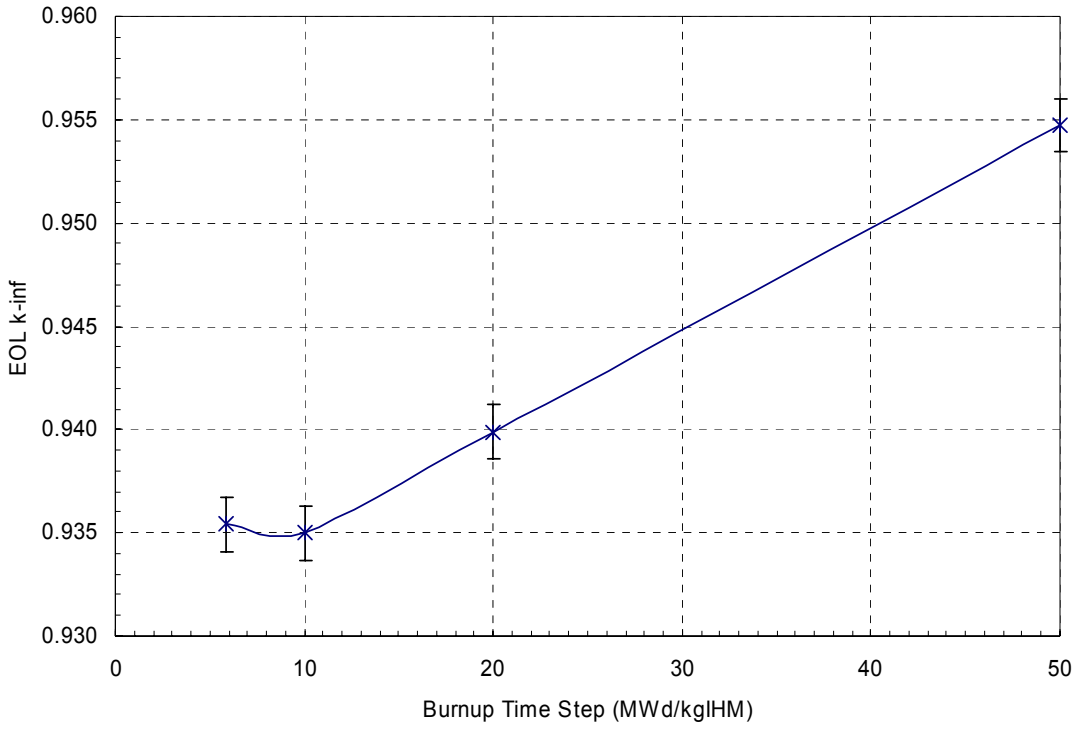

Figure 3.8 Burnup sensitivity to the macro burnup timestep size.

3.4.2 Energy Release per Fission

The recoverable energy release per fission (defined as all the usable energy associated with each fission event, including subsequent capture) is an important quantity which determines the fission reaction rate given a certain power level. Unfortunately there always exists a certain degree of uncertainty in the recoverable energy per fission since the neutron capture contribution depends on specific fuel/structural materials and neutron spectrum. Table 3.11 shows recoverable energy per fission for several important nuclides. In general these values agree well between CASMO-4 and ORIGEN. A run was made

where CASMO-4 energy release values were substituted into ORIGEN2, but that made essentially negligible changes in results when running MCODE. Therefore it is concluded that energy release per fission doesn't account for the differences between MCODE and CASMO-4.

Table 3.11 Recoverable energy per fission (MeV/fission) for important nuclides.

Nuclides	Experiment [83]	CASMO-4	ORIGEN2
U-235	202.64±0.86 (thermal) 203.41±0.89 (fast)	202.23	201.70
U-238	208.96±1.05 (fast)	199.73	202.77
Pu-239	211.44±1.06 (thermal) 212.26±1.09 (fast)	209.09	210.60
Am-242m	214.91±1.67 (thermal)	210.96	215.53

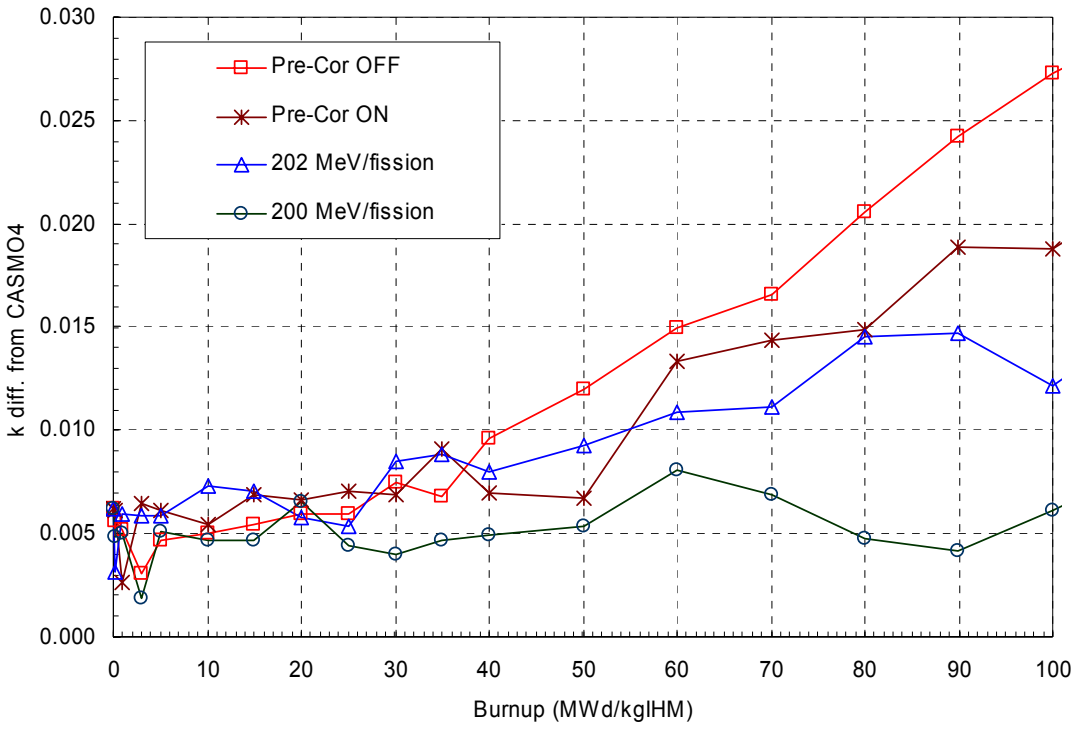

Figure 3.9 Burnup calculation sensitivity to the energy release per fission.

However, this quantity is very important. After modifying the ORIGEN code to use various constant recoverable energy release values per fission, several MCODE runs were made. Fig. 3.9 shows the MCODE results. Note that the ORIGEN code is recompiled for each run. It is not surprising to see that as energy release per fission decreases

the eigenvalue difference also decreases. The underlying physics reason is that for smaller energy release per fission, more actinides need to be burned to reach the same burnup; therefore the eigenvalue is lowered in MCODE which leads to better agreement with CASMO-4.

3.4.3 ORIGEN Libraries

One should use appropriate libraries in the burnup calculation in order to take care of non-MCNP-tallied materials. However, for a sufficient representation of nuclides, the MCODE runs should be robust and the dependence on ORIGEN libraries should be weak in terms of neutronic parameters. Only fission product yields are affected by different ORIGEN libraries whereas one-group cross sections of all important nuclides are updated at each timestep. As an exercise, four ORIGEN libraries were tried:

- `PWRUE.LIB` — 3-cycle PWR extended burnup (50 MWd/kg) library
- `BWRUE.LIB` — 4-cycle BWR extended burnup (40 MWd/kg) library
- `CANDUNAU.LIB` — natural uranium fueled CANDU library
- `FFTFC.LIB` — fast flux test facility core library.

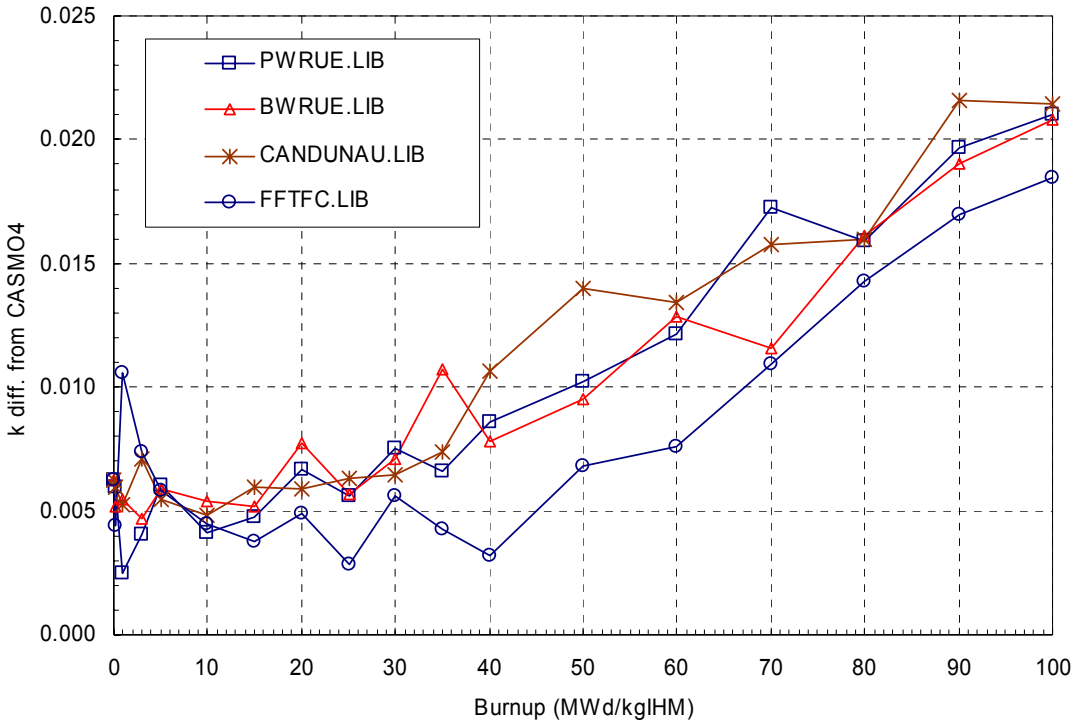

Figure 3.10 Burnup calculation sensitivity to ORIGEN libraries.

Figure 3.10 shows that results are fairly close to each other and not sensitive to specific one-group ORIGEN libraries. In terms of reactivity, dependence on ORIGEN libraries is weak since most important isotopes are regularly updated from MCNP runs to do burnup calculations.

3.4.4 Statistical Errors

The MCNP results are always associated with certain statistical variations. The question of the necessary statistical quality of MCNP runs is naturally raised for burnup calculations. It was found earlier that MCNP has a certain kind of ability to self-adjust the statistical error [64]; the present author's experience is consistent. Typically the tallied one-group cross sections will have ≤ 5% relative error (excluding (n,2n), (n,3n) reactions). Ref. [84] also confirms that it is not necessary to consider the propagation/buildup of the statistical error for burnup calculations. Due to the nature of the statistical error, the effect on material compositions tends to be canceled after many time steps in burnup calculations. Numerically a burnup curve with fewer neutron histories has a larger oscillation around the smoothed trend than a burnup curve with more neutron histories.

3.5 General Remarks on MCNP/ORIGEN Linkage Codes

3.5.1 MCNP Issues

Efficient Computation

The major application of MCNP in the present work has been for criticality calculations (kcode calculations). Although MCNP has been used for more than 40 years, no effective methods for variance reduction in the problems of our interest have been found. Many researchers have tried using adjoints from deterministic calculations, fission matrices, etc., to reduce variance for criticality calculations, but have not succeeded in demonstrating that such methods are generally worthwhile.

Part of the cause for this situation has to do with the nature of reactors: in a well-designed reactor, the importance of a neutron in causing fissions varies by only a modest

factor for any part of the reactor. This is in contrast to shielding problems, where the importance may vary by many orders of magnitude. Hence, there is very little to be gained from favoring important neutrons at the expense of unimportant ones.

A practical trick is that one can re-use the same equilibrium source file to reduce CPU time for multiple MCNP calculations with identical geometric configurations. It is often used in MCODE burnup calculations. Since, in general, a criticality calculation (kcode) has two stages, the inactive cycles (the initial iteration serves to distribute neutrons closer to the fundamental mode) and the active cycles (effective accumulation of neutron histories/tallies), the generated source file reduces the time spent in inactive cycles. However, this does not reduce variance because the variance is only associated with the active cycles.

Neutron Cross Section Libraries

Another issue is the availability of continuous-energy cross section libraries for MCNP usage. Currently there are three libraries under use at MIT:

1. that originally shipped with MCNP-4C [80];
2. the UTXS library, which expands the temperature range [81];
3. INEEL-supplied libraries, including minor actinides and some fission products.

Two concerns are (1) the availability of temperature dependence in the libraries and (2) the availability of fission product (rare or artificial isotopes) libraries.

Usually MCNP cross section libraries are evaluated at a certain temperature. A free gas thermal treatment will be performed by sampling the thermal motion of the nuclei when using that library under a different temperature. However, the cross section resonance broadening, a key issue in computing the Doppler coefficient, is not considered. One needs to use a multi-temperature neutron cross section library to evaluate the reactivity at different temperatures in order to calculate the Doppler coefficient. In addition, the cross section evaluation at different temperatures should be consistent. A multi-temperature library will therefore be convenient for users, particularly for reactivity feedback calculations.

The second concern is about the availability of some fission product libraries. All important fission products need to be tracked in MCNP and some rare or artificial isotopes appear in the fission process. The current list of missing fission products includes:

Ge-77, As-77, Se-81, Se-83, Br-82, Br-83, Kr-85, Kr-85m, , Kr-87, Sr-91, Zr-97, Nb-96, Nb-97, Mo-101, Tc-100, Tc-101, Rh-104, Rh-106, Pd-109, Pd-111, Ag-110, Ag-110m, Cd-117, In-116, In-117, Sn-121, Sb-122, Te-131, I-128, Xe-137, Cs-138, Ba-139, Pr-144, Nd-149, Nd-151, Pm-150, Sm-155, Eu-158, Gd-159.

3.5.2 ORIGEN Issues

ORIGEN2.1 was released in the early 1980s and has not been significantly reviewed for nearly twenty years except for some small fixes of bugs and the update of its one-group cross section libraries [85].

Recently a mass deficiency was found at MIT [85] illustrating a logic error in the ORIGEN2.1 code, which was related to the generation of fission products from fissions. The current fission yields only include fissions in Th-232, U-233, U-235, U-238, Pu-239, Pu-241, Cm-245, and Cf-249. Actually yield values for Cm-245 and Cf-249 are the same as those for Pu-241 to facilitate special types of calculations because those yield data are not available in ENDF/B-IV [71]. For one of these actinides with given fission yield, it is rather straightforward to calculate the fission product generation. However, for actinides without known yields (unconnected actinides), ORIGEN 2.1 uses the following procedures to generate fission products:

- The total fission rate is calculated for all unconnected actinides.
- The largest contributor (nuclide) to the total fission rate is identified.
- The nearest actinide with explicit yields is found for the largest contributor.
- The fission products are generated according to the nearest actinide with explicit yield.

However sometimes among the unconnected actinides, there can be a uniform distribution of fission rates, which might invalidate the maximum-fission-contributor approach. The main bug identified in ORIGEN2.1 is this logic error in `SUBROUTINE FLUXO` to properly accumulate the total fission rate for all unconnected actinides. A better approach is to find nearest neighbors with explicit yields for each unconnected actinide. This has been implemented to update ORIGEN2.1 by A. G. Croff [85].

Besides source code maintenance, the ORIGEN data also needs to be updated. Fission yield data need to be revised according to recent ENDF/B-VI data. Other data, such as half lives and the branching ratios, also need to be reviewed.

Based on Ref. [86], the importance of library data can be prioritized as follows:

1. One-group cross section values for specific types of reactors (key factor, but has been taken care of by MCODE or similar linkage code)
2. The decay data (including half-lives, probabilities of each decay mode, recoverable energy in decay) has a much smaller impact on isotopic compositions compared to cross sections (40% versus 2% [86])
3. Fission product yield data; generally this will increase several percent for some FP, and the fission Q also affects the U-235 concentration by several percent. (systematic change)

However, these conclusions are all based on current burnup, ~30MWd/kg. Tasks 2 and 3 under the high burnup situation will be more demanding.

One should be aware of the fact that for burnup calculations using any MCNP/ORIGEN linkage-type code, ORIGEN plays a key role.

3.5.3 Future Trends

The linkage code is an external program that combines MCNP and ORIGEN. However, there is an alternative way of doing burnup calculations with MCNP. This other approach is to modify MCNP directly, adding a few more subroutines to MCNP itself. This approach, compared to linkage codes, has some advantages as well as disadvantages. The good things are that they integrate with MCNP more tightly, i.e., more efficient usage of MCNP: for example, no need to read cross section libraries at each burnup step. However, this might also be a disadvantage. Since MCNP is continuously evolving (as improved and maintained by LANL), it is difficult to keep pace with the revisions. On the other hand, the linkage code only involves using the output from MCNP which is fairly stable over a longer period of time. It is easy to maintain the code separately. Therefore, in the author's perspective the future trend of Monte Carlo based burnup codes will be:

- In the short/medium term, the linkage code will suffice;
- In the long term, MCNP will incorporate the burnup calculation capability if really necessary.

There is also some interest in applying MCNP to substitute for deterministic lattice physics code, such as CASMO-4, to work with nodal codes (e.g., SIMULATE) since Monte Carlo codes are general-purpose and exact. However, this effort has not been quite satisfying primarily due to two practical difficulties: (1) the group scattering cross sec-

tions are not directly available in the current version of MCNP; (2) all quantities from MCNP have some degree of statistical error which adds fluctuations to nodal parameters. There has been some work on modifying MCNP to calculate the scattering cross section [87]. However, burnup dependence of multi-group cross section generation is not considered in Ref. [87]. One of the puzzling results in Ref. [88] is the fact that when homogenized, two-group cross sections and discontinuity factor ratios are generated by MCNP, and then used in the nodal code, the MCNP results are not reproduced. Previous nodal calculations with discrete ordinates method show that approximations corrected by discontinuity factors reproduce the reference results to within round off errors. It was later found out that statistical fluctuations in the Monte Carlo results prevent a precise evaluation of the accuracy of nodal results based on interpolated parameters [88]. Further investigations on this subject are needed.

3.6 Chapter Summary

In this Chapter, MCODE (Ver. 1.0, February 2002) is described and benchmarked against deterministic codes with satisfactory agreement. All major nuclide differences between CASMO-4 and MCODE fall within the range of typical uncertainties for international IAEA/NEA PWR benchmarks of UOX and MOX. When predicting the full-power operating time of an 18-month cycle the difference is only about 3 days, which is essentially due to the library difference (ENDF vs. JEF). Compared to other linkage codes, MCODE excels in its unique way of coupling MCNP and ORIGEN based on the predictor-corrector approach.

MCODE is a fairly versatile linkage code, which extends MCNP's ability to do burnup calculations. In addition, MCODE shows great portability across various platforms (from Windows to UNIX, Linux, even to clusters). Although developed for high burnup applications in LWRs, MCODE has been extensively used at MIT by other research projects dealing with HTGR and FBR core designs as well.

The current version of MCODE is limited to do depletion calculations in which only actinides and fission products are considered. In the future activation products

should also be included, especially B-10. Correspondingly the (n, α) reaction needs to be tallied.

4. Neutron Spectrum Effects

"Real knowledge is to know the extent of one's ignorance"
— Confucius (551-479 BC)

4.1 Introduction

The neutron spectrum in a reactor is largely determined by the moderator that slows down the fission neutrons. Light water reactors (LWRs) use water as the moderator and the coolant. Neutron moderation by hydrogen atoms in LWRs is essential to reducing the energy of fission neutrons (~2 MeV) to thermal neutrons (~0.05 eV at 310°C) so that the large thermal fission cross section of U-235 (and of other fissionable isotopes as well) can most easily sustain a neutron chain reaction. The thermal Maxwellian spectrum is a typical feature of such reactors. In contrast, the neutrons in a reactor that uses liquid metal (such as sodium or lead) as the coolant are poorly moderated. Fission neutrons will induce their next fission events at a much higher energy than thermal. Such a spectrum is often referred to as a fast spectrum. Between the two extreme cases, the neutron spectrum is generally designated as "epithermal" or $1/E$ since $\phi(E)$ takes on this shape in simple slowing down theory. The precise boundaries of the distinct regions are, of course, somewhat arbitrary, but the distinction is nevertheless a useful guide [92].

There have been extensive studies of neutron moderation for LWRs over a narrow range about current practice because the moderator temperature coefficient (MTC) has to be maintained negative during normal operation for safety reasons. Recently the concept of a Super Critical Water cooled Reactor (SCWR) was selected as one of the six promising Generation-IV reactor designs [93]. Current SCWR design effort is focusing on a thermal spectrum reactor. At the other extreme, steam-cooled lattices have been studied dating back to the 1960s [94] motivated primarily by better utilization of uranium resources due to higher values of conversion ratio. However, there has been no systematic study of the moderation effects in water lattices over the entire range, from fast to thermal, on fuel utilization in a once-through (no reprocessing) fuel cycle appropriate for ad-

vanced reactors. This Chapter, therefore, presents a generic scoping study of moderation effects so that their impact on overall strategic goals is made evident in a more explicit manner.

Our strategy for the study of moderation effects was to vary the hydrogen-to-heavy-metal (H/HM) ratio and carry out depletion calculations for various initial enrichments, focusing on the initial reactivity, $k_\infty(t=0)$, and on the reactivity-limited burnup. While recent work has investigated water-cooled systems with both higher and lower coolant densities than conventional PWRs [95], most such work has been for a fuel cycle with recycling and plutonium fueling. It is, therefore, not evident that lattices optimized for such service will also prove best for non-recycle application using U-235 enriched reload fuel. Considerable commonality should exist, however, at high burnup since bred plutonium will then dominate the neutronics.

Five schemes of varying H/HM are investigated in the present work: varying water density, varying fuel rod pitch, varying fuel rod diameter, varying fuel density, and employing center-voided annular fuel pellets. When varying water density, no thermal hydraulic constraints are taken into account: the water density is arbitrarily varied over a wide range without considering the practicality of physical implementation. The purpose of this parametric study is to understand the basic neutronic behavior under different degrees of moderation. On the other hand, the other four variations are more realistic in that they satisfy certain constraints. For example, the fuel rod diameter cannot exceed the pin pitch due to geometric constraints. In all cases the operating conditions are assumed to be the same as current PWR conditions. It is important to note that the infinite cell calculations ignore neutron leakage and thus will significantly exaggerate the achievable burnup value in the fast region.

A standard 4-loop Westinghouse PWR lattice is modeled and single unit cell analysis is employed. For square pitch lattices (all PWR designs except VVER), the volume ratios of interest include (see Table 4.1 for symbol definitions):

$$V_M / V_{PIN} = \frac{P^2 - \frac{\pi}{4} D^2}{\frac{\pi}{4} D^2} = \frac{4}{\pi}\left(\frac{P}{D}\right)^2 - 1, \tag{4.1}$$

$$V_{\mathrm{M}}/V_{\mathrm{F}} = \left(\frac{V_{\mathrm{M}}}{V_{\mathrm{PIN}}}\right)\left(\frac{V_{\mathrm{PIN}}}{V_{\mathrm{F}}}\right) = \left(V_{\mathrm{M}}/V_{\mathrm{PIN}}\right)\left(\frac{D}{d}\right)^2, \tag{4.2}$$

and the hydrogen to heavy metal atom (H/HM) ratio is then given by:

$$\mathrm{H/HM} = \frac{2\cdot\left(\rho_{\mathrm{H_2O}}\cdot\frac{N_{\mathrm{A}}}{M_{\mathrm{H_2O}}}\right)\cdot V_{\mathrm{M}}}{\left(\rho_{\mathrm{UO_2}}\cdot\frac{N_{\mathrm{A}}}{M_{\mathrm{UO_2}}}\right)\cdot V_{\mathrm{F}}} = 2\cdot\left(\frac{M_{\mathrm{UO_2}}}{M_{\mathrm{H_2O}}}\right)\left(\frac{\rho_{\mathrm{H_2O}}}{\rho_{\mathrm{UO_2}}}\right)\left(V_{\mathrm{M}}/V_{\mathrm{F}}\right) \approx 30\left(\frac{\rho_{\mathrm{H_2O}}}{\rho_{\mathrm{UO_2}}}\right)\left(V_{\mathrm{M}}/V_{\mathrm{F}}\right). \tag{4.3}$$

For a triangular pitch (VVER), the moderator-to-fuel ratio is

$$V_{\mathrm{M}}/V_{\mathrm{PIN}} = \frac{\frac{\sqrt{3}}{2}P^2 - \frac{\pi}{4}D^2}{\frac{\pi}{4}D^2} = \frac{2\sqrt{3}}{\pi}\left(\frac{P}{D}\right)^2 - 1, \tag{4.4}$$

and the formulas for $V_{\mathrm{M}}/V_{\mathrm{F}}$, H/HM are again Eqs. (4.2) and (4.3).

A survey of current PWR lattices in Table 4.1 shows the moderation ratio for different fuel product lines. Since the lattice pitch is not given explicitly in the reference, it is computed from the assembly width divided by the number of pins along one side of the assembly. In this way the extra peripheral layer of the assembly due to intra-assembly clearance is included in the lattice pin pitch. However, this only leads to < 1% increase in unit cell volume; therefore, the inaccuracy associated with this calculation can be ignored. On average the H/HM value for a PWR is approximately 3.5. The H/HM value for the traditional Westinghouse PWR (17×17 lattice) is ~3.4; the lattice type in Table 4.1 from BNFL/Westinghouse is their new fuel design called Performance+, which has a larger H/HM value of 3.89. In particular, the data for VVER-1000 comes from Ref. [97], and annular fuel pellets with ~10% void are used in that reactor so that the H/HM value reaches 3.80. Overall, there is a trend to pursue increased moderation in PWRs.

At the end of this chapter, the core size, power density and neutron leakage issues are also discussed. The goal is to clarify some of these interacting considerations, rather than to prescribe definitive optimized designs. A significant increase in lattice migration length as H/HM decreases is observed, which leads to much more neutrons lost by leakage.

Table 4.1 Comparison of PWR lattices [96, 97].

Designer	Pitch P (cm)	Rod Dia. D (cm)	Pellet Dia. d (cm)	Pellet Den. ρ (g/cm^3)	V_M/V_{PIN}	V_M/V_F	H/HM†
ABB Atom							
16×16	1.435	1.075	0.911	10.50	1.27	1.77	3.56
17×17	1.26	0.95	0.819	10.50	1.24	1.67	3.36
18×18	1.275	0.95	0.805	10.50	1.29	1.80	3.63
ABB CENP							
14×14	1.47	1.118	0.968	10.5	1.20	1.60	3.23
16×16	1.29	0.970	0.826	10.5	1.25	1.73	3.48
BNFL/Westinghouse							
17×17	1.26	0.914	0.784	10.5	1.42	1.93	3.89
European Fuel Group (EFG)							
14×14	1.407	1.072	0.929	10.47	1.19	1.59	3.21
15×15	1.43	1.072	0.929	10.5	1.27	1.69	3.39
17×17	1.26	0.95	0.819	10.47	1.24	1.67	3.37
Framatome Cogema Fuels (FCF)							
15×15	1.434	1.06	0.918	10.52	1.33	1.77	3.57
17×17	1.26	0.95	0.819	10.52	1.24	1.67	3.35
Fragema							
14×14	1.408	1.072	0.929	10.5	1.20	1.59	3.21
15×15	1.43	1.072	0.929	10.5	1.27	1.69	3.39
16×16	1.434	1.075	0.912	10.5	1.27	1.76	3.54
17×17	1.26	0.95	0.819	10.5	1.24	1.67	3.36
18×18	1.275	0.95	0.806	10.5	1.29	1.80	3.62
Korea Nuclear Fuels							
14×14	1.407	1.016	0.8748	10.43	1.44	1.94	3.94
16×16	1.29	0.97	0.826	10.46	1.25	1.73	3.49
17×17	1.26	0.95	0.8192	10.43	1.24	1.67	3.38
Mitsubishi							
14×14	1.407	1.072	0.929	10.41	1.19	1.59	3.23
15×15	1.43	1.072	0.929	10.41	1.27	1.69	3.42
17×17	1.26	0.95	0.819	10.41	1.24	1.67	3.39
VVER-1000							
Hex	1.275	0.91	0.755*	10.5	1.16	1.89	3.80

† H/HM uses the estimated value of the H atom concentration at 300°C for a water density of 0.705 g/cm^3.

* annular pellet, 0.24 cm diameter central hole.

** All dimensions are cold (room temperature): pitch increases by ~ 0.2% when hot.

*** After considering the presence of water-filled guide tubes and the gap between assemblies, the whole core H/HM value can be obtained through multiplying unit cell H/HM by ~ 1.16.

4.2 Lattice Geometry Effect

4.2.1 Unit Cell Model

The unit cell is a central concept of reactor physics, which represents a basic unit of repeating structures in the core. As introduced in the previous section, the H/HM parameter characterizes the main neutronic characteristics for LWR lattices. Unit cell analysis on various lattice geometries is then made to verify this conclusion.

There are currently two types of lattice geometries being used in industry: square lattices (the dominant type in Western designs) and hexagonal lattices (mainly in Russia). In addition there exists another possible arrangement: the triangular lattice. Figure 4.1 shows the geometries of these lattices. In addition, the cylindrical pin cell is also illustrated since it is of theoretical interest and represents a common modeling approximation. In fact, there exist only these three types of regular lattices: triangular, square, and hexagonal.

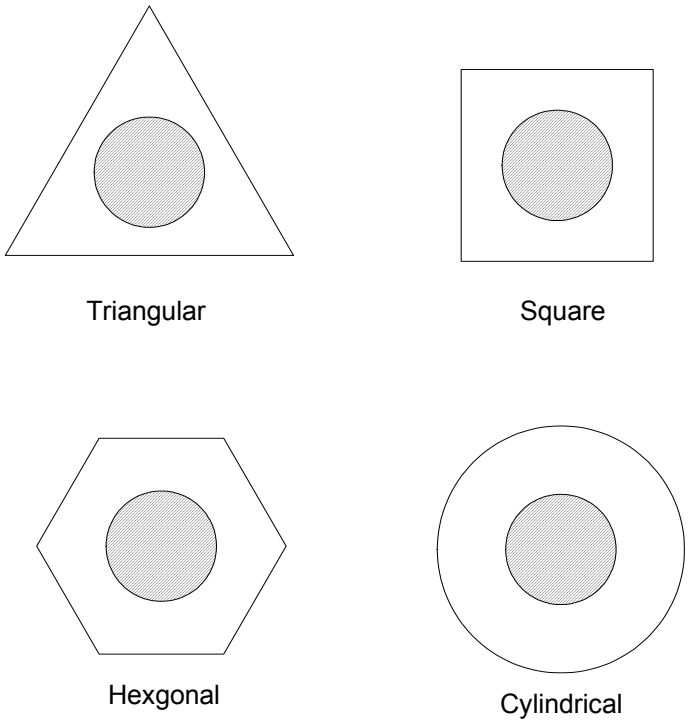

Figure 4.1 Lattice unit cells.

The square unit cell model (hot conditions) of a standard four-loop Westinghouse 17×17-lattice assembly is adopted as the reference case. For the other three unit cells, the flow (coolant) area and the fuel rod design with 9.75 w/o enriched UO_2 are kept the same as the square lattice. Therefore, H/HM values are the same for all four lattices. Operating conditions, such as fuel/clad/moderator temperatures and the power density, are assumed to be the same for all cases. Table 4.2 summarizes pin cell model parameters.

Table 4.2 Pin cell model parameters.

Parameters	Values
Fuel temperature (K)	900
Fuel percent of theoretical density (%)	94
Cladding temperature (K)	621
Moderator temperature (K)*	583.1
Power density (kW/kg HM)	38.13
Fuel pellet diameter (cm)**	0.8192
Fuel density (g/cm^3)	10.3
Fuel pellet to cladding gap (cm)	0.0082
Cladding inner radius (cm)	0.4178
Cladding outer radius (cm)	0.4750
Cladding density (g/cm^3)	6.550
Square lattice pin pitch (cm)	1.26
∗ Nominal temperature used for moderator.	
∗∗ All the dimensions are cold dimensions at room temperature.	

4.2.2 Results & Discussions

As a validation of the importance of moderation effects in thermal-spectrum dominated cores, burnup calculations based on the above four types of lattice models have been carried out with MCODE, all for 9.75 w/o enriched UO_2 fuel and nominal operating conditions for conventional Westinghouse PWRs (Table 4.2). H/HM values are kept the same for all unit cells. Figure 4.2 shows the burnup histories for each individual case. Figure 4.3 plots relative differences for other cases vs. the square lattice unit cell.

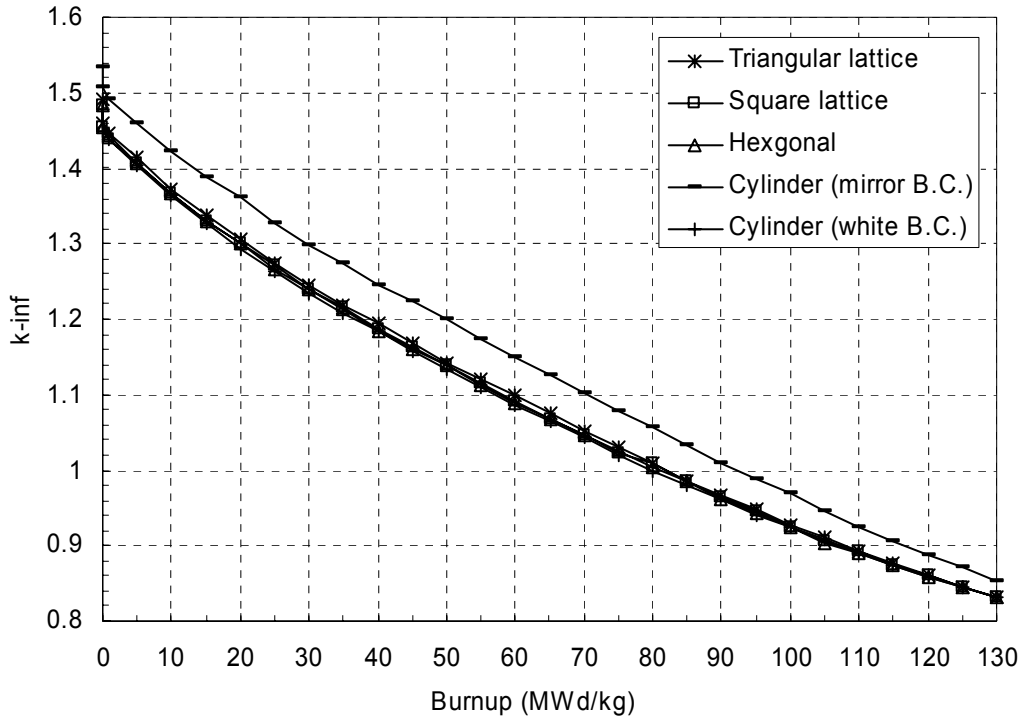

Figure 4.2 MCODE depletion histories for different lattice unit cells.

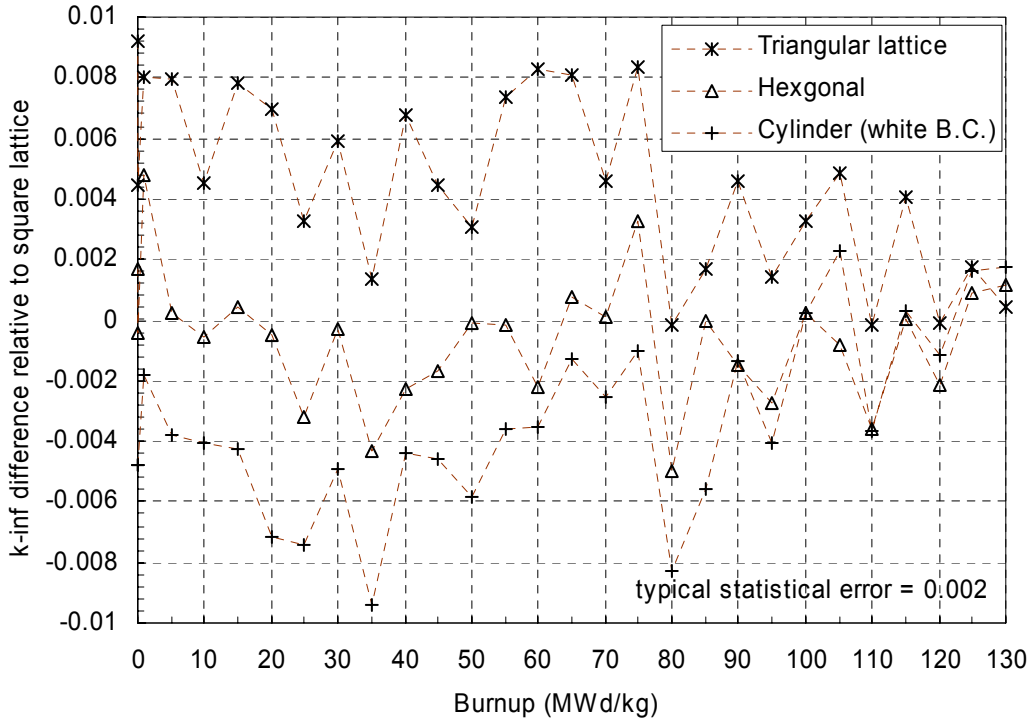

Figure 4.3 Relative eigenvalue differences from the square lattice unit cell.

Note that reflective boundary conditions are applied for all lattices if not specified. However, for a cylindrical pin cell the reflective boundary condition significantly overestimates the eigenvalue, which is a known problem due to the inappropriate scattering treatment on the boundary. The neutrons are trapped in the reflecting trajectory, circulating around the outer peripheral circular mirror virtually indefinitely. Using a "white" boundary condition for the cylindrical pin cell, in which neutrons hitting the periphery are reflected isotropically back into the pin cell, corrects this problem and gives reasonable results.

Except for the cylindrical unit cell with the mirror boundary condition, burnup curves agree satisfactorily for all cases. Fig. 4.3 further shows relative differences from the reference square lattice unit cell for other cases. The agreement improves as burnup increases. According to this calculation, the hexagonal lattice gives closest results to the reference square lattice cell. Although the lattice geometry affects the Dancoff factors, the H/HM ratio (for a given fuel rod design), as a primary physics consideration, is concluded to be sufficient to characterize neutronic behavior as shown in Figs. 4.2 & 4.3.

4.3 Parametric Study of Moderation Effects

4.3.1 Introduction

Based on the square lattice unit cell model (Table 4.2) and CASMO-4, a range of reload U-235 enrichments (4.5, 9.75, 12, 15, 19.5 w/o) has been calculated, and the lattice design implications have been calculated for a range of H/HM by varying the water density. These enrichments span from current practice up to the limit (< 20 w/o U-235) imposed by anti-proliferation requirements. The burnup of only one U-235 enrichment case (9.75 w/o) has also been computed for different moderation conditions using MCODE due to demanding CPU requirements for Monte Carlo calculations. However, the initial reactivity for all cases has been computed using MCNP. The purpose of using two codes is to verify the results and draw consistent conclusions, not to benchmark the accuracy of the results. Throughout our MCODE calculations, 16 actinides and 56 fission products are tracked in MCNP to provide burnup-dependent one-group cross sections and neutron flux for the ORIGEN2.1 depletion calculations.

The water density is arbitrarily varied over a wide range and all other conditions, such as geometry, fuel density, temperatures, etc., are kept constant for the square unit cell. The results then show clearly the tradeoffs in approaching the goal of designing high burnup cores.

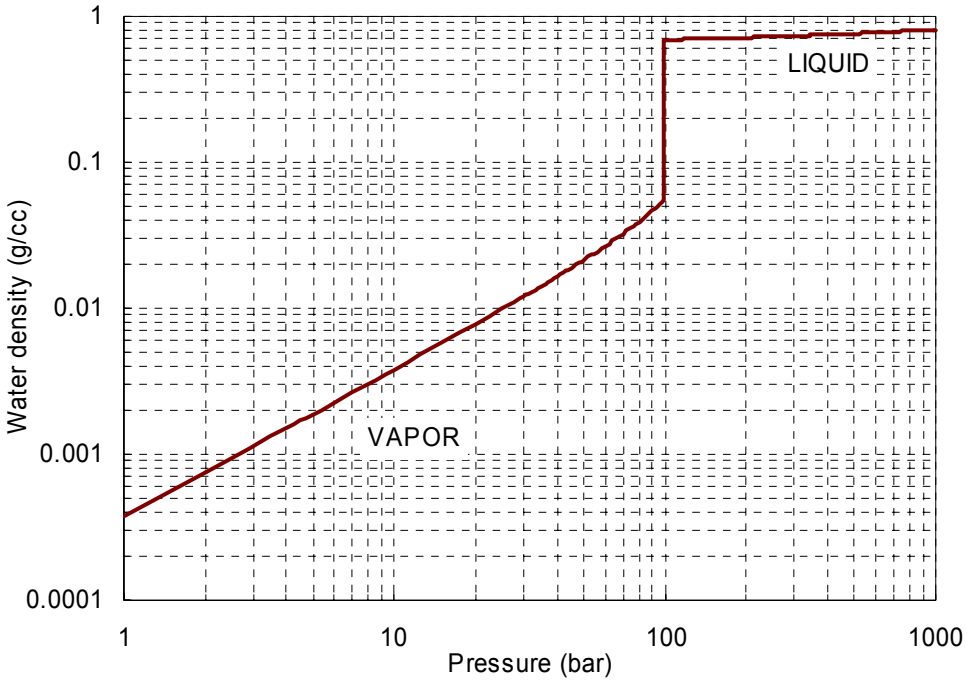

Figure 4.4 Water density variation with pressure at 310°C.

Although this approach (arbitrarily varying water density) is fictitious, there exist various practical ways to implement different moderation regimes, such as the implementation of cooling by steam, boiling water or superheated water. For a current Westinghouse PWR the core pressure is 155.1 bars, and the average water temperature in the core is 310°C. The corresponding water density is then 0.706 g/cm^3 [98]. (Note that liquid water is slightly compressible, hence this is not exactly the density at saturation pressure.) Figure 4.4 shows the wide range of changes in the assumed density (from 10^{-3} g/cm^3 to 10^0 g/cm^3, about 3 orders of magnitude). It can be seen that, especially at low pressure, the water vapor density can be varied widely. Thus theoretically steam cooling can be used at the lower water density values (less than 0.7 g/cm^3), and thereby the desired H/HM value can be achieved. In our geometry the corresponding range of H/HM of

interest is approximately from 0.005 to 5. As discussed in Ref. [94], several decades ago steam-cooled fast breeder reactor (FBR) designs were evaluated. There are also other ways to adjust the H/HM value as mentioned in the introduction of this chapter. For example it can be reduced a factor of roughly 3 by reducing the lattice pin pitch.

Based on current operating conditions (the system pressure), rough borders among fast, epithermal, and thermal regimes can be set. The saturation liquid and vapor densities at 155.1 bars are 0.594 g/cm^3 and 0.102 g/cm^3 respectively; and the corresponding H/HM values are 2.88 and 0.50, i.e., the fast region has an H/HM <0.50, the epithermal region has an H/HM between 0.50 and 2.88, and the thermal region has H/HM >2.88.

4.3.2 Initial k_∞

The focus here is on k_∞ of fresh UO_2/H_2O lattices: specifically the hot full power (HFP), xenon-free condition. Fuel pin size and lattice pitch were kept the same; while water density was varied over a wide range. The results from CASMO-4 and MCNP-4b are shown in Figures 4.5a through 4.5e. Satisfactory agreement between CASMO-4 and MCNP-4b is observed. The difference between the two codes shows that the initial reactivity of CASMO-4 falls within the statistical errors ($\pm 3\sigma$) of MCNP-4b in the thermal range near current PWR conditions, but not in the epithermal and fast regions, which is reasonable since CASMO-4 is designed to represent the physics of present day LWRs.

These plots provide information on several points of interest. The requirements for control are determined by the initial reactivity. Wetter or more highly enriched lattices need more control. For lattices in the subcritical region, it is obviously unnecessary to do depletion calculations, and current enrichment-level (4.5 w/o) UO_2 fuel cannot be used in fast reactors. The sign of the initial moderator temperature coefficient can also be immediately inferred from the figure by looking at the slope of the curve.

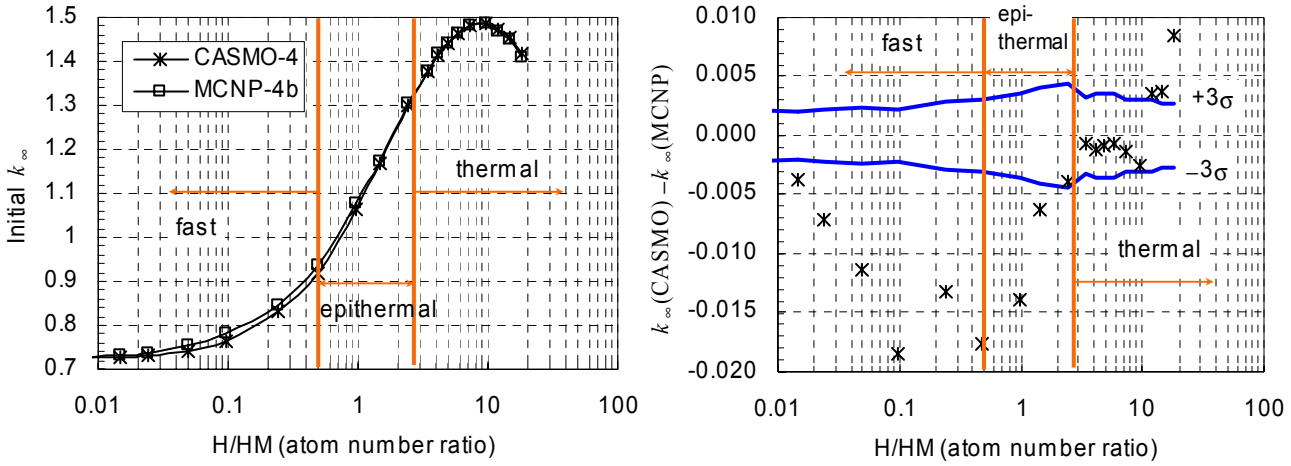

Figure 4.5a Initial k_∞ as a function of H/HM ratio, 4.5% U-235 enrichment.

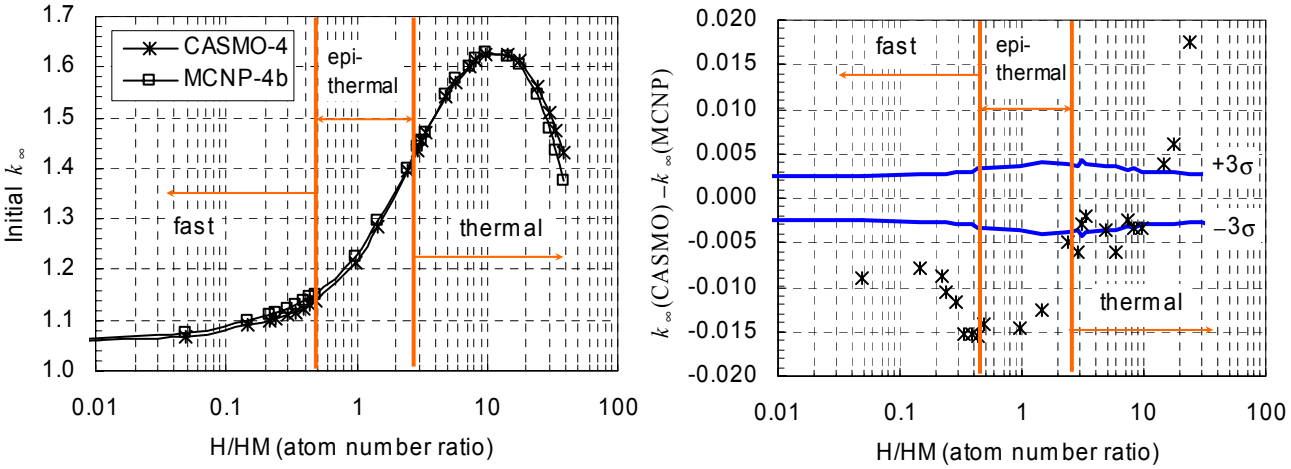

Figure 4.5b Initial k_∞ as a function of H/HM ratio, 9.75% U-235 enrichment.

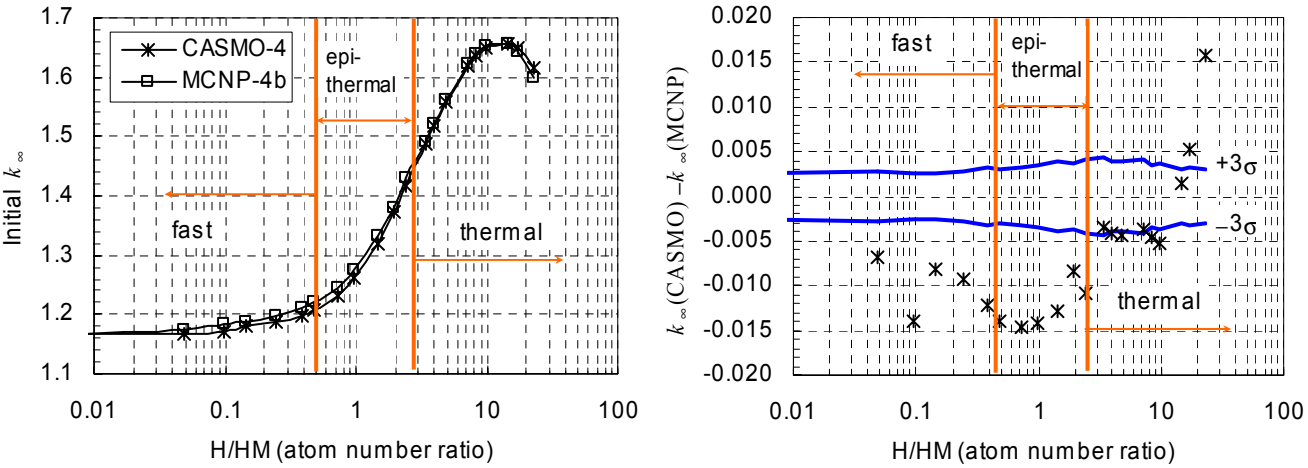

Figure 4.5c Initial k_∞ as a function of H/HM ratio, 12% U-235 enrichment.

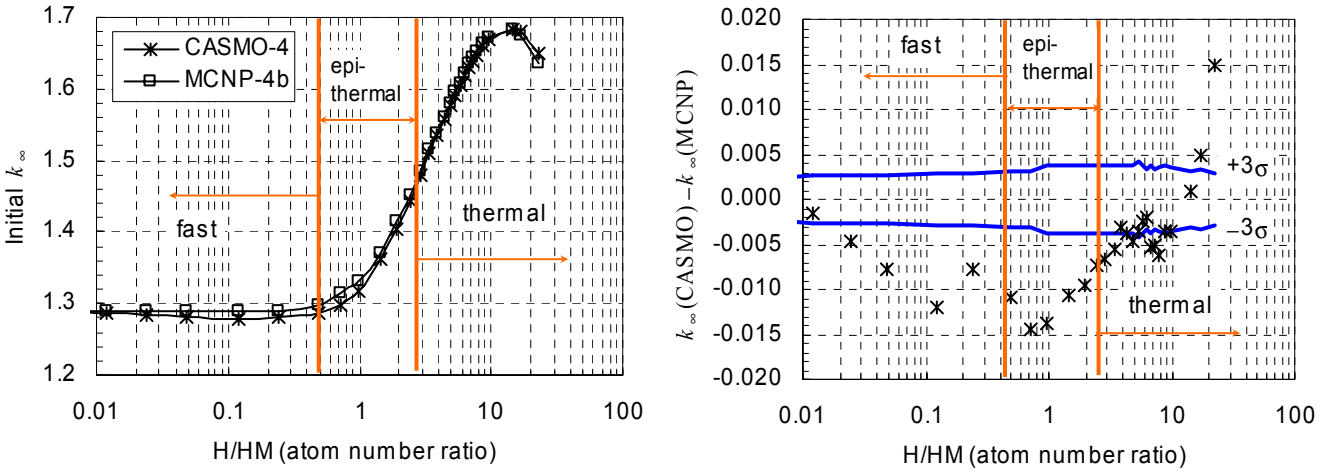

Figure 4.5d Initial k_∞ as a function of H/HM ratio, 15% U-235 enrichment.

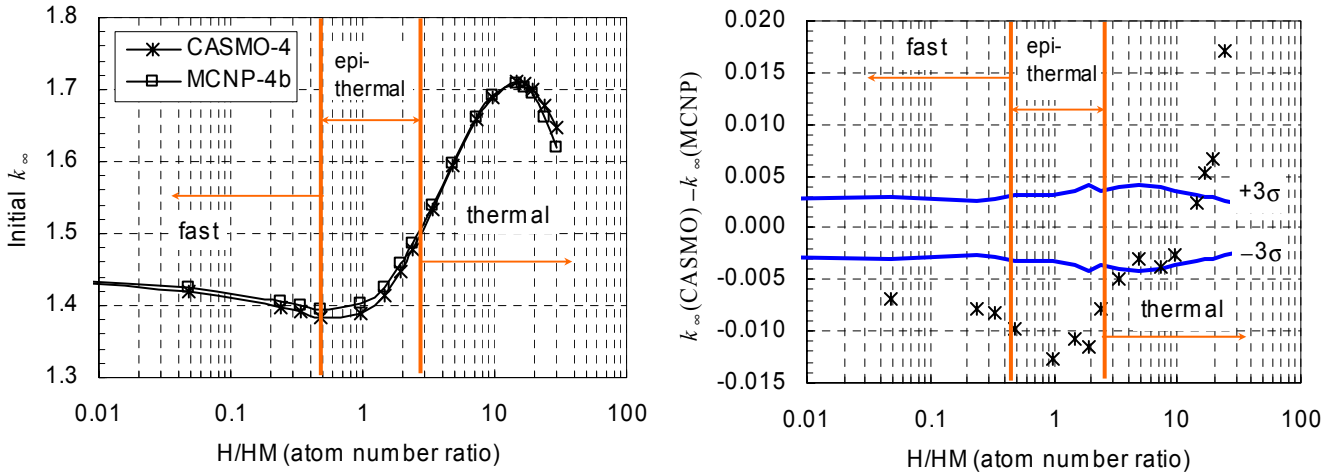

Figure 4.5e Initial k_∞ as a function of H/HM ratio, 19.5% U-235 enrichment.

In the thermal range, the k_∞ peaks at some point where the H/HM is close to 10, greater than the conventional PWR's H/HM value, 3.4. As H/HM increases, neutrons will be better thermalized due to the increased presence of hydrogen atoms. Up to some point, the thermalization will dominate; beyond that absorption of water begins to play a role so that the thermal neutron utilization degrades substantially and the k_∞ decreases. With increasing enrichment the peak k_∞ shifts to even higher values of H/HM. The slope of the curves roughly reflects the soluble-poison-free moderator temperature coefficient (MTC) defined as the change of reactivity per unit temperature of moderator (H_2O). Negative MTC is required for safety, which will exclude operating in the over-thermalized region

to the right of the peak in k_∞. In reality the change of moderator temperature means also a change in the moderator density. Higher moderator temperature and lower density both make the spectrum harder, hence reduce k_∞. In LWRs, the dominant effect is the density change which affects the slowing down rate, i.e.,

$$\mathrm{MTC} = \frac{\partial k_\infty}{\partial T_\mathrm{M}} \approx \frac{\partial k_\infty}{\partial N_\mathrm{H}} \frac{dN_\mathrm{H}}{dT_\mathrm{M}} = \frac{\partial k_\infty}{\partial (\mathrm{H/HM})} \frac{d(\mathrm{H/HM})}{dT_\mathrm{M}} \propto \frac{\partial k_\infty}{\partial (\mathrm{H/HM})} (-\alpha), \tag{4.5}$$

where T_M is the moderator temperature and α is the thermal expansion coefficient. Higher burnup will necessitate higher fuel enrichments, which will exacerbate the reactivity control requirements. This will affect the management of control poison distributions through the soluble and burnable portions. Figure 4.6 shows the effect of soluble poison on 9.75 w/o and 4.5 w/o UO_2 fuel. It can be seen that while the H/HM ratio of current LWRs is near the peak reactivity of the 4.5% enriched fuel, it is smaller than the ratio for the peak reactivity of the 9.75% enriched fuel.

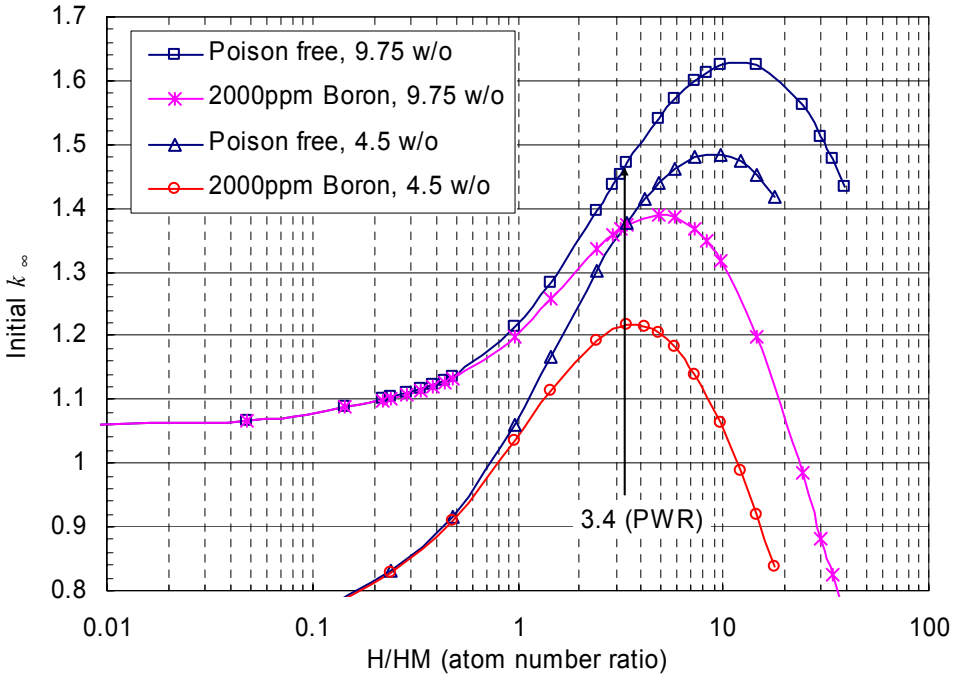

Figure 4.6 Soluble poison effects on 4.5 and 9.75 w/o UO_2 fuel.

In the epithermal region, the k_∞ decreases monotonically when reducing H/HM except for the 19.5 w/o case. As H/HM decreases, the migration length of neutrons in-

creases so that the lattice becomes more and more homogenized from the neutrons' viewpoint. The lumping effect decreases, and hardening of the neutron spectrum increases the resonance absorption of U-238 relative to U-235. Thus a monotonic decrease in k_∞ with decreasing H/HM is observed. For the 19.5 w/o case, the high enrichment further hardens the neutron spectrum so that the resonance absorption is reduced relative to fissile absorption because a higher fraction of neutrons is above the resonance region. Moreover the k_∞ in the epithermal region is smaller than in the other two regions, which therefore poses a serious neutronics problem: either voiding or flooding will cause positive reactivity feedback.

In the fast region, k_∞ is relatively flat especially for high enrichments (15 w/o, 19.5 w/o). The k_∞ is eventually set by the neutron utilization factor. However, from the 19.5 w/o case, it is clear that a positive MTC exists in this regime.

A brief explanation can also be shown as follows:

Consider a three-group (fast, epithermal, and thermal) model with the assumption that

1) fission can occur in all three groups;
2) fission neutrons are born in the fast group (group 1);
3) up-scattering is neglected;
4) neutrons can be scattered down into the neighboring group at most, i.e., the neutron cannot be scattered from the fast group to the thermal group directly.

For the fast group (group 1)

$$\frac{1}{k}\left(\nu\Sigma_{f1}\phi_1+\nu\Sigma_{f2}\phi_2+\nu\Sigma_{f3}\phi_3\right)-\Sigma_{a1}\phi_1-\Sigma_{21}\phi_1=0 \tag{4.6}$$

For the epithermal group (group 2)

$$-\Sigma_{a2}\phi_2-\Sigma_{32}\phi_2+\Sigma_{21}\phi_1=0 \tag{4.7}$$

For the thermal group (group 3)

$$-\Sigma_{a3}\phi_3+\Sigma_{32}\phi_2=0 \tag{4.8}$$

From the above equations, one can show that

$$k=\left(\frac{\Sigma_{a1}}{\Sigma_{a1}+\Sigma_{21}}\right)\left\{k_1+\left(\frac{\Sigma_{21}}{\Sigma_{a1}}\right)\left(\frac{\Sigma_{a2}}{\Sigma_{a2}+\Sigma_{32}}\right)\left[k_2+k_3\left(\frac{\Sigma_{32}}{\Sigma_{a2}}\right)\right]\right\} \tag{4.9}$$

where $k_1=\dfrac{\nu\Sigma_{f1}}{\Sigma_{a1}}$, (multiplication factor for the fast group)

$$k_2 = \frac{\nu\Sigma_{f2}}{\Sigma_{a2}}, \text{ (multiplication factor for the epithermal group)}$$

$$k_3 = \frac{\nu\Sigma_{f3}}{\Sigma_{a3}}. \text{ (multiplication factor for the thermal group)}$$

Both k_1 and k_3 are larger than k_2, in part since the eta value is smallest in the epithermal range. Furthermore, k_3 is much larger than k_1 and k_2 because the microscopic absorption cross section of fissile species is two orders of magnitude larger than that of U-238 in this group. Then we can discuss the asymptotic behavior of k for cores dominated by different energy spectra.

1) fast spectrum, $\Sigma_{21} \to 0$

$$k \to k_1$$

2) epithermal spectrum, $\Sigma_{21} >> \Sigma_{a1}$ and $\Sigma_{32} << \Sigma_{a2}$

$$k \to k_2$$

3) thermal spectrum, $\Sigma_{21} >> \Sigma_{a1}$ and $\Sigma_{32} >> \Sigma_{a2}$

$$k \to k_3$$

The removal cross section from group g' to g ($\Sigma_{gg'}$) is mainly due to the scattering by hydrogen atoms in water while the absorption cross section in group g' ($\Sigma_{ag'}$) is governed by the heavy metal. Thus, $\Sigma_{gg'}/\Sigma_{ag'}$ is proportional to H/HM in Eq. (4.9). This simplified way of inferring the behavior of reactivity versus H/HM explains the characteristic shapes of the plots in Fig. 4.5.

4.3.3 Reactivity-Limited Burnup

Let us examine here the reactivity-limited single-batch burnup, B_1 (for n-batch management multiply B_1 by $2n/(n+1)$ [49]) as a function of H/HM. B_1 is defined from the depletion curve k_∞ vs. B where $k_\infty = 1$. Thus, this is the ideal upper limit for single-batch management since leakage is not considered. Fig. 4.7 shows the CASMO-4 predictions of B_1 vs. H/HM for various initial enrichments. Several observations can be made:

1. A higher reactivity-limited burnup is achievable in either a wetter than normal or much dryer than normal lattice, while epithermal lattices are distinctly inferior performers.
2. Increasing the enrichment always leads to increased burnup limit for any lattice.

3. Within the 20% enrichment limit (due to proliferation concerns) the maximum attainable single-batch burnup in the thermal region is about 160 MWd/kg.
4. Increasing H/HM from that in current PWR lattices is more beneficial at higher enrichments. This suggests increasing H/HM for high burnup (high enrichment) applications.
5. The peak k_∞ in the thermal region moves to higher values of H/HM as the enrichment increases. Therefore, more water is needed to moderate the higher-enriched lattices.

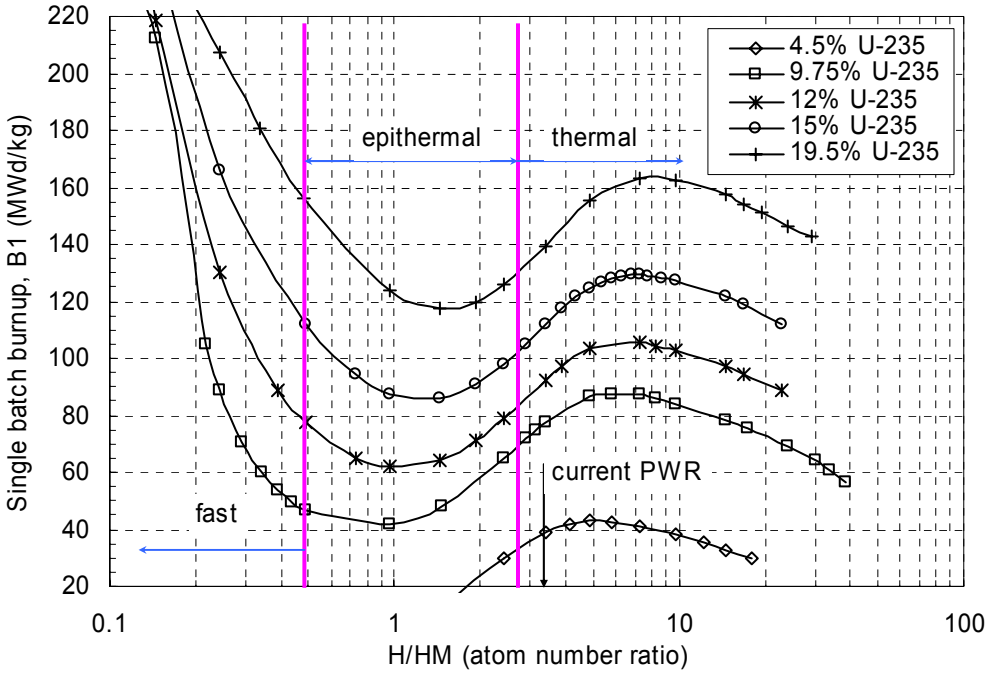

Figure 4.7 CASMO-4 prediction of reactivity-limited, single-batch burnup, B_1.

The behavior of Figure 4.7 can be well understood using the linear reactivity model. The single-batch discharge burnup, B_1, can then be determined by the initial reactivity and the slope of burnup, which is proportional to (1−CR). (CR is the conversion ratio, defined as the ratio of the fissile production rate to the fissile consumption rate.) As an illustration, the initial conversion ratio for the 9.75% U-235 case is shown in Figure 4.8. Overall the conversion ratio decreases monotonically as H/HM increases, i.e., the net fissile content will decline faster in a wetter lattice. By looking at Figure 4.5 and Figure 4.8, one can understand the behavior of Figure 4.7. In the thermal range, there is a peak in B_1, whose

location is to the right of the peak of k_∞. In the epithermal range, B_1 shows a minimum due to tradeoff between reduced initial reactivity and improved conversion ratio. For water-cooled lattices, it is not worthwhile to operate in the epithermal range under the constraints of the once-through fuel cycle. In the fast range, the effect of conversion ratio is dominant since the initial reactivity is nearly constant.

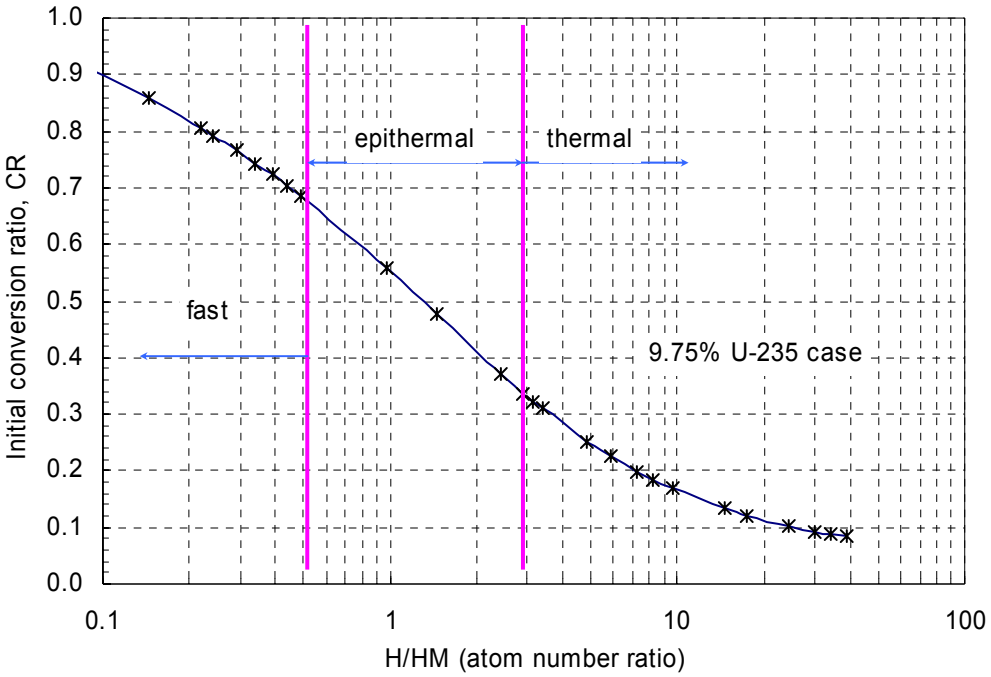

Figure 4.8 Conversion ratio (initial) for 9.75 w/o U-235 case.

One set of single-batch burnup B_1 for the 9.75% enrichment fuel unit cell case is shown in Figure 4.9 using MCODE. Two single-batch burnup B_1 curves are shown, one is without leakage (k_∞ = 1), and the other is with 3% leakage (k_∞ = 1.03). The typical trend through fast, epithermal, and thermal ranges is nevertheless the same. As can be seen MCODE overestimates the burnup compared to CASMO-4. Also it can be seen that the fast region is more sensitive to neutron leakage than the thermal region due to its much larger conversion ratio (smaller reactivity swing during burnup).

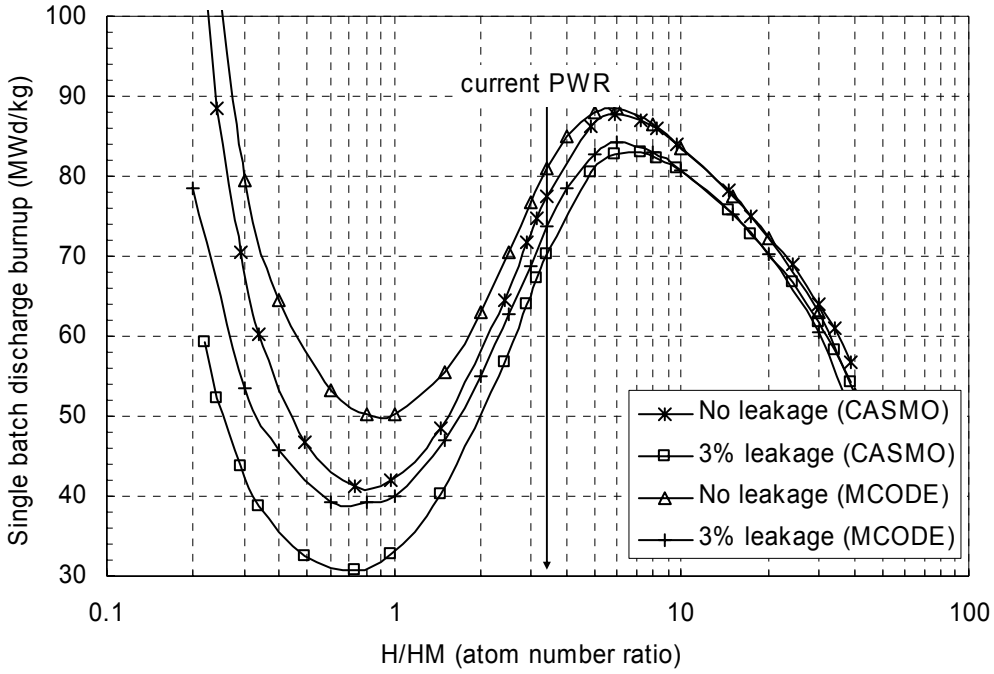

Figure 4.9 MCODE/CASMO results for 9.75 w/o enrichment.

In particular, it is observed that the single batch discharge burnup at a fixed enrichment is proportional to the natural uranium utilization and separative work utilization. Thus, the epithermal lattice is expected to have the lowest uranium and separative work utilization.

4.3.4 Neutron Spectrum

Neutron spectrum (the energy distribution of neutron populations) is a key neutronic characteristic. In LWRs, the neutron spectrum is determined by the neutron slowing down, thermalization, and neutron absorption (especially resonance absorption).

MCNP-4B was employed to calculate neutron energy spectra. Two sets of calculations are reported using the pin cell configuration described in Table 4.2: one set to study the spectrum effect as a function of enrichment and the other to study the spectrum effect as a function of moderation (H/HM) ratio by changing the water density. In both cases, constant pin power is assumed.

The MCNP-4B results are for a 244 energy group structure starting at 20 MeV, with a constant lethargy width of 0.1; all the energy spectra shown refer to the average flux in the fuel region of the pin cell.

Enrichment Variation

Three enrichment cases were investigated: 4.5 w/o, 9.75 w/o, and 15 w/o (all UO_2 fuel). The operating conditions are kept the same as a typical PWR, thus the H/HM ratio for these cases is the same. The thermal flux peak decreases as the enrichment increases due to the conservation of power level ($\Sigma_f\phi$) and the increase in Σ_f. The thermal peak of the 9.75 w/o case is roughly twice that of the 4.5 w/o case (Fig. 4.10). The fluctuations between 1 eV and 1000 eV are mainly due to the resonances in the cross section data. In the epithermal region the $\phi(E)$ is approximately $1/E$ ($\phi(u) \sim$ constant).

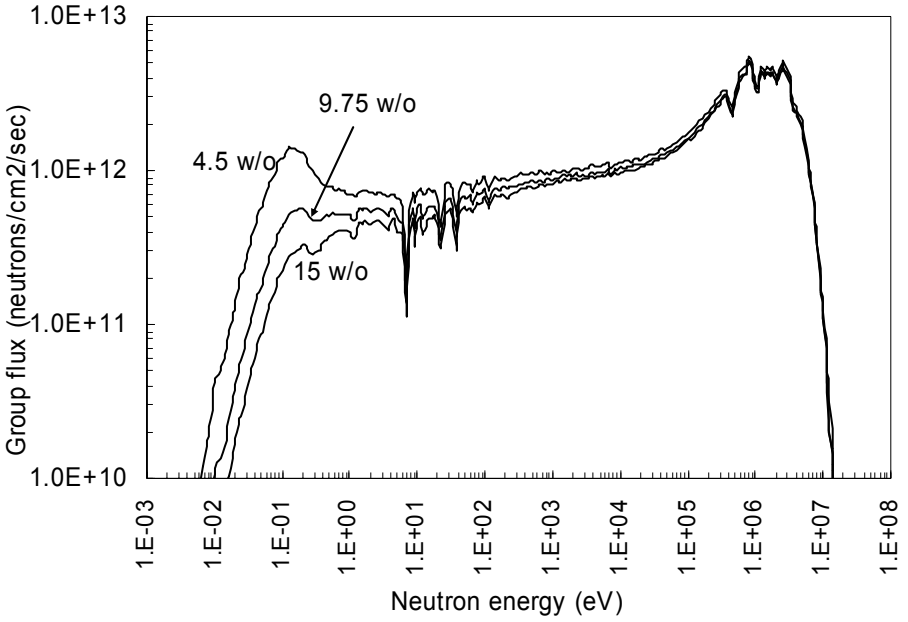

Figure 4.10 Neutron spectrum for different enrichments at H/HM = 3.4

Moderation Conditions

Based on the given PWR unit cell configuration (Table 4.2), the water density was set at different values to simulate different moderation conditions. The H/HM values employed were 14.6, 3.40 (normal PWR condition), and 0.146. Results are shown in Fig. 4.11.

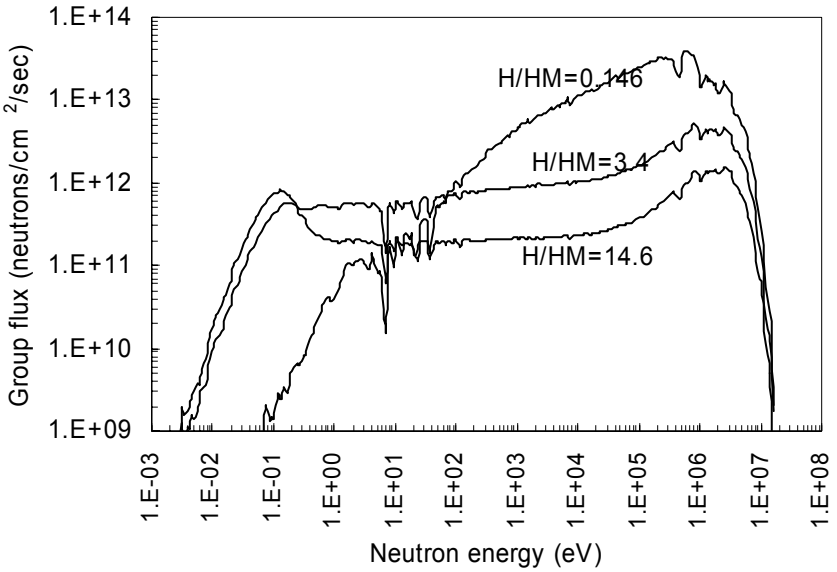

Figure 4.11 Neutron spectrum for 9.75 w/o under different moderation conditions.

Generally speaking the results can be explained using two-group theory (fast group ϕ_1 and thermal group ϕ_2):

$$\Sigma_{a2}\phi_2 = \Sigma_{21}\phi_1, \tag{4.10}$$

thus,

$$\frac{\phi_2}{\phi_1} = \frac{\Sigma_{21}}{\Sigma_{a2}} \sim \frac{\mathrm{H}}{X \cdot \mathrm{HM}}, \tag{4.11}$$

where X denotes enrichment. Therefore, either increasing the enrichment or reducing H/HM can harden the neutron spectrum.

Comparing Fig. 4.10 and Fig. 4.11, the effect on the neutron spectra from the variation of the moderation is greater than that for changing the enrichment since H/HM varies nearly two orders of magnitude.

The neutron energy spectrum is an import characteristic of a given reactor design. Generally, hardening the neutron spectrum leads to higher conversion ratio, thus better utilization of the uranium resource, especially if the spent fuel is reprocessed. High conversion ratio also gives a flatter $k(B)$ curve, which simplifies reactor control. However, since all control material worth under a hardened neutron spectrum is reduced, controlling the same amount of excess reactivity is more challenging.

4.3.5 Discussion

The behavior of single-batch burnup can be explained by considering the conversion ratio and the initial reactivity. The peak of B_1 is always at lower H/HM than the peak of k_∞. Thus the soluble-poison-free moderator temperature coefficient at beginning of cycle is always negative in the range of interest. The peak of B_1 shifts to the right as the enrichment increases, and the neutron spectrum hardens (Fig. 4.10). More water is then needed to thermalize the spectrum. The same holds for initial reactivity.

In general, wetter lattices than normal are recommended for generating maximum burnup for a given reload enrichment, as long as liquid water is the coolant. In particular, for high burnup (high enrichment) applications, wetter lattices are favored in PWRs. Thermal hydraulic constraints might be easier to meet. However, control of the large excess initial reactivity of wetter lattices must be accommodated. There is another constraint of note: core endurance (cycle length), which is proportional to the product of burnup and core fuel inventory. For constant core volume, the fuel inventory is less for wetter lattices. This will limit re-optimization of fuel assemblies for retrofit into current reactors.

4.4 Other Fuel Types

Up to now only uranium fuel has been discussed. However, other types of fuel are also of interest, in particular thorium and plutonium. Thorium is a potentially superior fertile material due to its ability to breed U-233 in reactors. Use of thorium would effectively increase the sustainability of nuclear power (enlarge the mineral reserve). Also, thorium would make the nuclear fuel cycle more proliferation resistant in view of significant reduction of plutonium generation per unit energy.

On the other hand, there has been continuous interest in burning plutonium (both reactor-grade and weapon-grade) in existing LWRs. As a sensitive material, plutonium poses serious proliferation concerns. Higher burnup would improve the proliferation resistance of plutonium by both reducing its amount per unit energy and degrading the isotopic mixture.

As a basic constraint on utilizing thorium and plutonium, the reactivity-limited single batch burnup has been computed for eight combinations of fissile and fertile fuels all in dioxide form (Fig. 4.12). It is desired for both cases to have a high burnup potential. Uranium dioxide fuel is also included as a reference case. All cases use 9.75 w/o initial fissile in the heavy metal.

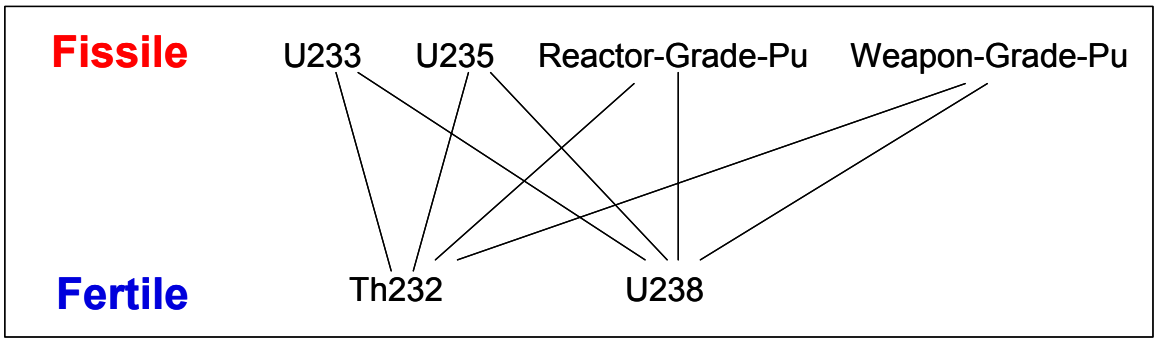

Figure 4.12 Eight combinations of fissile and fertile materials.

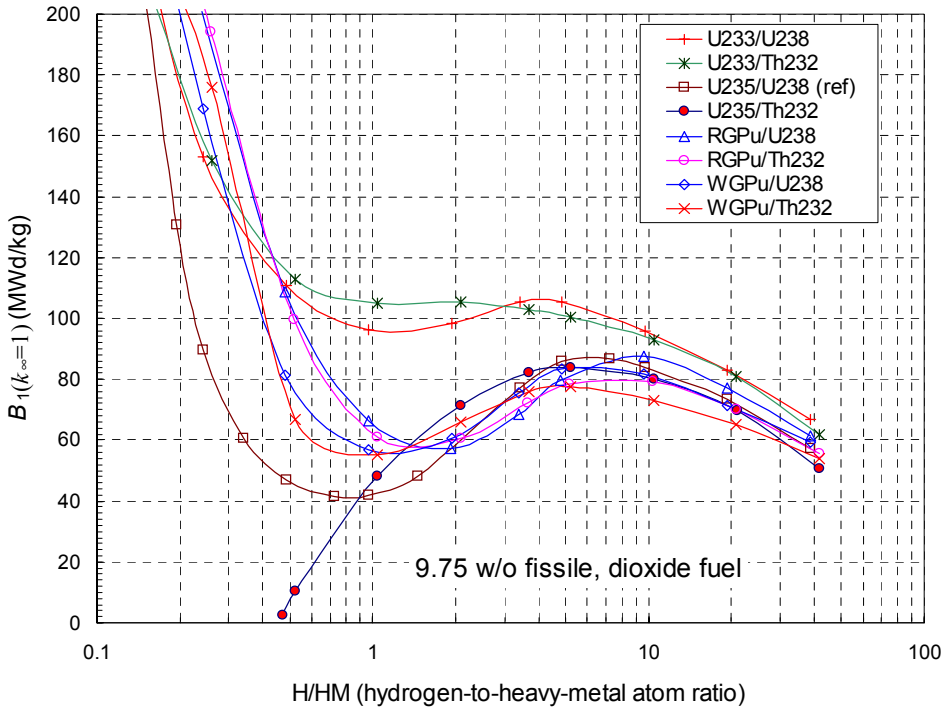

Figure 4.13 Burnup capability of various combinations of fissile and fertile materials.

The burnup capability of those eight fuel options are shown in Figure 4.13. The fuels are all in the form of di-oxide. It is shown that U-233 is a superior fissile material, which has higher burnup compared to other fissile materials. The epithermal region decrease in burnup is negligible for the U-233 case. Th-232, however, is a poor performer in terms of fertile materials, especially in the fast spectrum (low H/HM regime). Using thorium for Pu disposition leads to lower burnup compared to Pu mixture with uranium fuel. The U235/Th232 combination notably cannot achieve criticality in a fast spectrum (low H/HM regimes). At the same fissile weight percentage, the WGPu mixture achieves higher burnup in the thermal region, but lower burnup in the fast region compared to the RGPu mixture.

4.5 Cycle Length Constraints

In Section 4.3, a purely neutronics study was carried out on moderator-to-fuel ratio effects. In reality several schemes can be employed to adjust H/HM. In addition, the reactivity-limited B_1 is not sufficient to measure the core life. Another useful quantity is the energy production or the effective full power time (for the single batch case, the cycle length is B_1 times the initial heavy metal inventory). Therefore, in this section, four schemes of varying H/HM are considered: varying water density, varying pin pitch, varying fuel rod diameter, and varying fuel density. The single-batch core life (namely, T_1), defined in Eq (4.12), is computed for each scheme.

$$\mathrm{T}_1 = \left(\frac{1000}{365}\right) \cdot \frac{B_1 \times \text{Initial Heavy Metal Loading}}{\text{Power Density}}, \tag{4.12}$$

where T_1 is the single-batch core life, in units of effective full power years (EFPY);

B_1 is the reactivity-limited single-batch burnup, in units of MWd/kgHM;

IHM loading is in units of kg heavy metal (HM) per liter of core volume;

Power density is in units of kW per liter of core volume.

In order to consistently compare the cycle length, it is assumed that:

- the core volume is fixed;
- the total core power level is also fixed.

Under these two constraints, the core power density for all cases is the same; we take that value to be its present value in a typical PWR, 105 kW/liter. Note that fuel specific power, kW/kgHM, varies; however we did not change the average fuel temperature to reflect this, even for annular fuel pellets. The fuel enrichment used here is 9.75 wt%.

All five schemes start with the current PWR lattice configuration. When considering H/HM variations each method will have its own constraints. For example, when varying the rod diameter, the maximum value will be equal to the pin pitch.

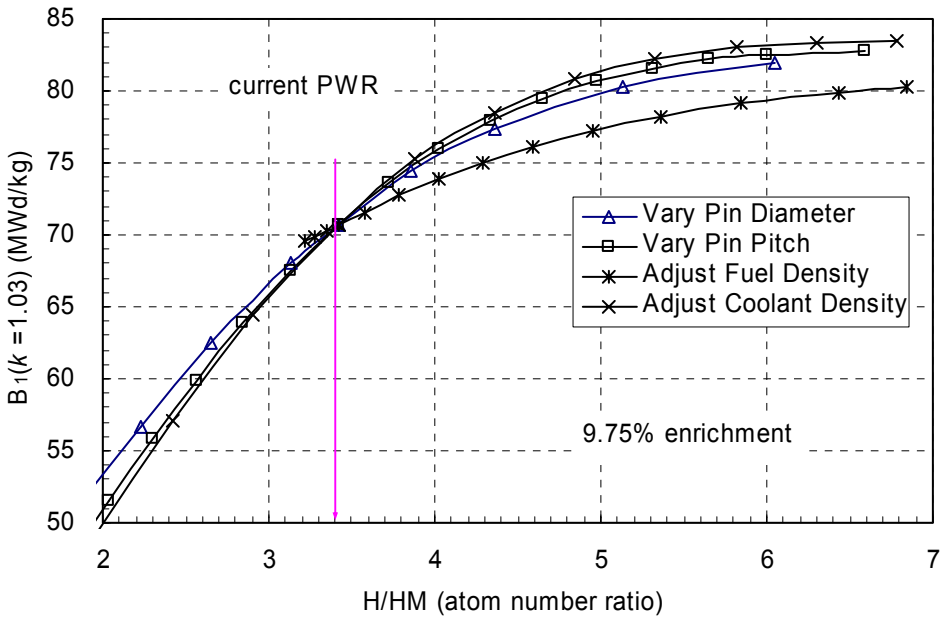

Figure 4.14 Reactivity-limited burnup capability
using different methods of varying H/HM.

Fig. 4.14 confirms the previous finding that increasing H/HM will improve the reactivity-limited burnup. Among three realistic implementations, increasing pin pitch gives maximum burnup potential for a fixed wetter lattice (same H/HM). The burnup approaches a plateau with H/HM increasing and the maximum discharge burnup is reached where H/HM = ~6.

Next the corresponding cycle length is examined (Fig. 4.15). Near the base case value, H/HM = 3.4, the burnup increases with increasing H/HM. However, the cycle length exhibits a complex behavior which reflects the tradeoffs between the initial core inventory and the burnup.

Employing annular fuel pellets, as a practical way to reduce fuel density, will also lead to a decrease in cycle length (similar to reducing the fuel density). Note that due to the high enrichment the cycle length is nevertheless very long. For this normal PWR lattice configuration the cycle length can be as long as 6.2 years. For annular fuel, the reduction in fuel inventory dominates over the burnup increase. But for high enrichment, this might not be a practical problem.

The current pitch is close to the optimum position, and the optimum pin diameter is also about the same. Changes in both to reduce the moderation will reduce burnup but increase total fuel loading, hence increase the EFPY slightly.

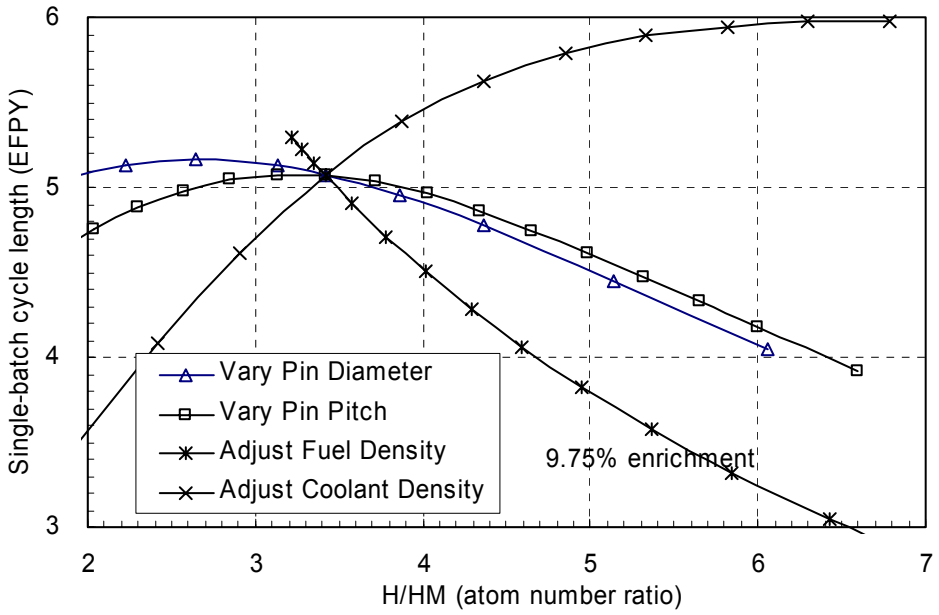

Figure 4.15 Single-batch cycle length for different schemes of varying H/HM.

The fuel density cycle length is sharply reduced (roughly equivalent to the heterogeneous smear density reduction of annular fuel pellets) by increasing H/HM, which implies that we should not dilute the fuel. In reality we cannot increase the fuel density beyond 100% theoretical density, unless a new material is used.

The coolant density is the only curve that shows an obvious increase in cycle length with increase in water density, but there is no physical way to implement this strategy.

Generally, we conclude that of all practical ways, the increase of H/HM from that of a normal PWR will lead to a decrease in cycle length even though the burnup is increased. Thus, it will be difficult to increase the burnup and cycle length simultaneously.

4.6 Core Size, Power Density, and Neutron Leakage

4.6.1 Introduction

Reactor physics and fuel cycle considerations are only one category of several which must be reconciled in an overall optimization of the reactor design tradeoff. Minimizing total cost of electricity requires attention to plant capital and operating and maintenance costs, since fuel cycle costs typically represent only about 20% of the total busbar cost. Hence factors such as refueling frequency, which impacts plant capacity factor, play a strong role in the compromise among conflicting goals.

More recently, ultra-long life, batch-loaded cores (8-15 years) in small reactors have been suggested as an added anti-proliferation safeguard for the world-wide LWR market. This favors reduced power density, which in turn introduces perturbations that propagate through the entire design process. Furthermore, material limits are always to be respected. For example, today it is primarily the durability of zirconium alloys which constrains the length of tolerable in-core service of LWR fuel.

In this section, the goal is to clarify some of these interacting considerations, rather than to prescribe definitive optimized designs.

4.6.2 PWR Core Size and Leakage Reactivity Penalty

Elementary reactor physics considerations [49, 99] and current design practice support core configurations having a height-to-diameter ratio, H/D, of approximately unity (see Table 4.3). Thus, the single variable of core diameter will suffice to characterize core physical size in what follows.

For realistic cases (more or less uniform core power density, reflected cores), the leakage reactivity penalty can be shown to be a constant times the product of migration length, M (M^2, the migration area is the mean square distance for a neutron from birth to absorption) times core surface-to-volume ratio, S/V [49]. One interpretation is that a

fraction (~25%) of all neutrons born within one M of the surface — about 7.5 cm in a PWR — leak out of the core. This linear S/V dependence is confirmed by CE studies of cores having 133, 177, 241 and 293 assemblies. (Ref. [100], Fig. 3-14)

Table 4.3 Optimum Height-to-Diameter ratios, H/D, for cylindrical reactor cores [49, 99].

Conditions	Criterion	$(H/D)_{OPT}$
(1) Bare homogeneous (uniform composition)	(a) minimum volume	$\frac{\pi}{\sqrt{2}\nu_0} = 0.924$ *
	(b) minimum leakage at constant volume	$\sqrt{\frac{\nu_0}{8}} = 0.548$
(2) Uniform power (Reflector has the same M as core.)	Minimum leakage (equivalent to minimum surface area) at constant volume	1.0
(3) Actual large PWR units		
Westinghouse 4-Loop		1.09
Combustion Engineering		1.10
B&W		1.12
(4) Variation with plant rating (Westinghouse)		
MWth	No. Of Assemblies	
1520	121	1.48
2652	157	1.21
3411	193	1.09
* ν_0 is the first root of the Bessel function J_0 (2.405).		

For commercial PWR lattices, the migration length is rather insensitive to small changes in the water-to-fuel ratio (or H/HM). M increases as H/HM decreases, but even for very tight pitch liquid H_2O cooled lattices, remains within about 10% of today's standard designs. Thus S/V, and more explicitly the (inverse of the) core diameter is the size variable which best determines leakage; or, alternatively, core volume to the minus one-third power. For constant power density, a 500 MWth core will have twice the leakage of a 4000 MWth core. If the latter loses 4% of the neutrons to leakage (leakage reactivity penalty, $\rho_L = 0.04$), then the smaller core loses 8%. Achievable reactivity-limited burnup varies as $(\rho_0 - \rho_L)$, where ρ_0 is the fresh-fuel, poison-free infinite medium reactivity [99] (0.24 is a representative value for current PWRs). Thus the above small core, using the same fuel as the larger one, will have a lower burnup capability by the factor:

$$\frac{0.24 - 0.08}{0.24 - 0.04} = 0.8;$$

or twenty percent less burnup and a corresponding 20% higher fuel cycle cost in mills/kWhre.

4.6.3 Leakage in Highly-Undermoderated Systems

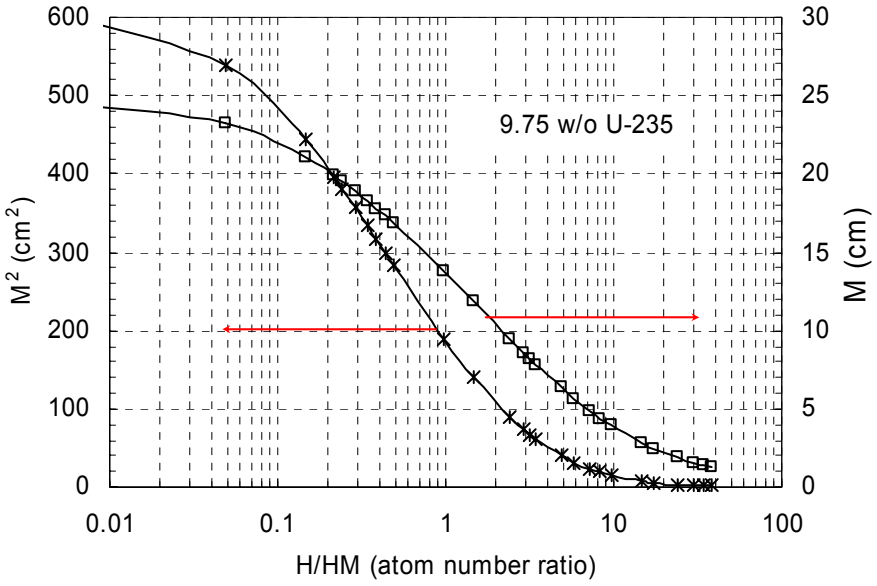

Figure 4.16 Sensitivity of migration area and length to moderator-to-fuel ratio.

With progressively reduced moderation, M increases monotonically. CASMO-4 was used to calculate M^2 (hence the more relevant M), for a constant fresh fuel enrichment. As can be seen in Fig. 4.16, for very hard spectrum systems, M, hence leakage, can be several times that of thermal spectrum cores of the same physical size. Exploiting this regime would require using supercritical water, steam, liquid metals, helium or other weak moderators as the coolant. This leakiness of fast cores is well known. Sodium (or lead-bismuth) cooled FBRs typically leak a third or so of their core neutrons into a surrounding breeding blanket. For a once-through fuel cycle, where the fertile blanket would be omitted to avoid production of chemically separable weapon-grade fissile material, the leakage losses are, therefore, quite substantial. Near the current PWR H/HM value of 3.4, it is possible to use a linear approximation to describe the dependence of M on H/HM:

$$M \approx 13.5 - 4.4 \ln(\text{H/HM}), \tag{4.13}$$

where $0.2 < \text{H/HM} < 10$.

Since liquid metal cooled cores have power densities almost three times higher than PWRs, their core size is proportionally smaller (for a given total power rating), which also aggravates the leakage problem. This is further motivation for focusing on thermal spectrum cores for economic, long-life, once-through applications.

4.6.4 Long-Cycle Cores

Indeed there are alternative approaches to long cycle core design. An intuitively different approach, which can be used in conjunction with changing the H/HM ratio, is to reduce power density, thereby increasing the calendar time to reach a given burnup. Small additional incremental improvements are also realized by the reactivity gains associated with reduced xenon poisoning and Doppler absorption in fertile resonances. There is, however, a penalty to be paid in terms of increased costs for the fuel since the same power output will require a larger core.

For cylindrical fuel rods of specified material, e.g. UO_2, the maximum allowable temperature rise, surface to centerline, is directly proportional to linear power, q' (kW/cm). Thus tight pitch cores, if limited only by this criterion, can deliver more power in a given volume, or occupy less volume at a given power. Conversely, at fixed volume and total power, the tight pitch core will have a lower linear power, and thus a slower burnup rate, with correspondingly longer endurance.

Several scaling relations embodying these considerations are summarized in Table 4.4. For example, comparing a tight pitch core to a conventional lattice of the same fuel composition and total inventory, and having the same linear and total powers, one has for the tight (T) and reference (R) core volumes (first row entry in Table 4.4):

$$\frac{V_{\mathrm{T}}}{V_{\mathrm{R}}} = \frac{1+\theta_{\mathrm{T}}+R_{\mathrm{T}}}{1+\theta_{\mathrm{R}}+R_{\mathrm{R}}}$$

where θ is the clad-to-fuel ratio and R is the moderator-to-fuel ratio.

For representative numerical values, the volume ratio is

$$\frac{V_{\mathrm{T}}}{V_{\mathrm{R}}} = \frac{1+0.35+0.5}{1+0.35+1.67} = 0.61$$

Thus, the core diameter ratio is

$$\frac{D_T}{D_R} = \left(\frac{V_T}{V_R}\right)^{1/3} = 0.85$$

Hence the tight pitch core has a 39% smaller volume and a 15% smaller diameter and height. For the same core volume the tight pitch lattice has a higher fuel inventory by a factor of 1/0.61 = 1.6 in which case it could operate at a 39% lower linear power and for 39% more effective full power days.

Table 4.4 Summary of alternative core design tradeoff scaling.

	CONDITION	RELATION
(1)	Constant total power Q, constant linear power q', and constant height-to-diameter ratio	$\left(\frac{D_2}{D_1}\right)^3 = \left(\frac{V_2}{V_1}\right) = \left(\frac{P_2}{P_1}\right)^2$
	And, for the same fuel diameter	$\left(\frac{P_2}{P_1}\right)^2 = \frac{1+\theta_2+R_2}{1+\theta_1+R_1}$
(2)	Constant core volume V, constant linear power q', and constant height-to-diameter ratio	$\frac{Q_2}{Q_1} = \left(\frac{P_1}{P_2}\right)^2$
	And, for same fuel diameter	$\left(\frac{P_2}{P_1}\right)^2 = \frac{1+\theta_2+R_2}{1+\theta_1+R_1}$
(3)	Constant core volume V, constant unit cell pitch And, for same moderator-to-fuel ratio R, linear power is also proportional to power density	$\frac{Q_2}{Q_1} = \frac{q'_2}{q'_1}$
(4)	Constant migration length M, constant height to diameter, same power profile. The leakage reactivity loss ρ_L scales as:	$\left(\frac{\rho_{L2}}{\rho_{L1}}\right) = \left(\frac{D_1}{D_2}\right) = \left(\frac{V_1}{V_2}\right)^{1/3}$
where θ = clad (plus gap) volume ÷ fuel volume R = moderator-to-fuel ratio D = core diameter P = power density		

4.6.5 Summary

It has been shown that a significant increase in lattice migration length, hence loss of neutrons by leakage, takes place as moderator-to-fuel ratio decreases. Hence the (infinite medium) value of k and reactivity-limited burnup of previous sections will be reduced by progressively larger fractions as H/HM decreases when one considers the more realistic

case of a finite core size. Lower burnup at fixed reload enrichment or increasing reload enrichment to restore burnup both increase fuel cost.

The above observations and the way in which core size scales with fuel enrichment and specific power suggest that hard spectrum cores (fueled with U-235 on a once-through cycle) are attractive only for specific applications where their compactness or suitability for ultra-long cycles can override their higher fuel cycle costs.

4.7 Chapter Summary

In the present work a systematic analysis has been made to scope out the characteristics of reactor cores fueled with uranium dioxide fuel, for high burnup service in a once-through fuel cycle. This has been done by varying the hydrogen-to-heavy-metal ratio and uranium enrichment in UO_2-fueled PWR lattices of otherwise conventional design. H/HM ratios range from that corresponding to "superdense" liquid water to highly dilute steam; and U-235 enrichments up to 20 w/o, the upper safeguards limit, are considered. This assures that cores having neutron spectra ranging from highly thermalized through epithermal, and into ultra-hard-spectra are included.

The CASMO-4 code was used throughout this investigation. But since it is being exercised far beyond its intended scope of proven applicability, extensive confirmatory calibrations were carried out with the Monte Carlo code MCODE (MCNP + ORIGEN).

From this chapter it is seen that somewhat wetter than normal UO_2-fueled lattices are optimal in terms of generating maximum energy (burnup) for a given reload enrichment, as long as one relies upon liquid water as the coolant. There is another constraint of note: core endurance (cycle length) in EFPY is proportional to the product of burnup and core fuel inventory. Thus EFPY decreases when H/HM is increased at a fixed total core volume. This will limit re-optimization of fuel assemblies by changing H/HM for retrofit into current reactors.

The single most important future task is to devise an approach for control of the excess reactivity in fresh wet lattice fuel and to quantify the reductions in attainable reactivity-limited burnup due to the neutron losses to poison during an operating cycle and to the end-of-cycle residual of burnable poisons such as Gd and Er. A 10 w/o en-

riched wet fuel will have an initial (poison-free) reactivity as much as twice that of todays PWR assemblies (at ~4.5w/o enrichment). One possibility is the use of annular fuel pellets containing a central zone of burnable poison, as suggested in Ref. [101]. This would have the dual advantages of increasing the H/HM ratio and avoiding the reduction in fuel thermal conductivity when rare earth oxide burnable poisons are mixed with UO_2. Annular pellets also operate at lower peak and average temperatures than solid pellets, which makes higher burnups more attainable from a fuel performance viewpoint. Another way of reducing BOC reactivity might be keeping the same cycle length but increasing the number of in-core batches (i.e., refueling smaller core fractions, $1/n$). Chapter 6 will discuss the BOC reactivity control in detail. Once this fundamental drawback is over-come, a routine full core design analysis is feasible for wetter lattices.

5. Alternative Fuel Choices

"Only those who will risk going too far can possibly find out how far one can go"
— T. S. Eliot (1888-1965)

5.1 Introduction

The nuclear fuel is the active part in a reactor where fission occurs and most of the liberated energy is deposited. Since commercial reactors require refueling every 12 or 18 months, nuclear fuel characteristics are open to evolutionary changes over the life of a power station. Moreover, the fuel behavior plays an important role in determining the practicality of high burnup extension as well as impacting plant operational modes.

The UO_2 pellet-type fuel, used almost exclusively in all current LWRs, has an extensive operational/industrial experience. Therefore, the previous chapter is devoted entirely to the oxide fuel and for H/HM neutronic studies. The oxide pellet fuel is likely to continue being a dominant fuel type in the foreseeable future. However, for higher power densities and for actinide reduction, some advanced fuel options have attracted considerable interest, such as the annular fuel pellet with or without internal cooling [102, 103], inert matrix fuel (IMF) element options (CERCER, CERMET, and METMET) [104], and renewed interest in thorium utilization [105, 106] and plutonium burning [107] in LWRs. Some of these fuel options significantly expand the H/HM option space. For example, the annular fuel and the IMF fuel can easily reach high H/HM values of ≥ 10. High fuel burnup is a common characteristic for all these fuels.

The first fundamental consideration of a fuel is its heavy metal isotopic composition. There exist several fissile and fertile material options: thorium, uranium, plutonium, and other higher actinides (such as neptunium). Almost all current commercial reactors are fueled with slightly-enriched uranium fuel (below 5 w/o) except that some of them are fueled partially with MOX (mixed plutonium and uranium) fuel. Uranium-235 is the only naturally occurring fissile isotope capable of fissioning upon absorbing a thermal neutron. The utilization of uranium fuel consists of both burning U-235 directly and burn-

ing the bred Pu-239 from U-238. Since the natural enrichment of uranium is very low (0.711 w/o), an enrichment process is needed to increase the U-235 concentration for application as LWR fuel (natural uranium can be used in the heavy water moderated reactors). Higher enrichment can be also pursued, but has a significant penalty on the fuel cost.

Although thorium is a naturally occurring actinide composed of the non-fissile Th-232, its value as nuclear fuel depends on converting it into U-233 by neutron capture. In this aspect, the thorium can be deemed as a substitute of U-238. Under the once-though fuel cycle constraint, it is a challenge to propose a practical and economic core design for thorium utilization in PWRs [108]. There are of course other considerations with thorium, one of which is the weapons proliferation concern. Since the thorium has a smaller atomic number than uranium, plutonium production can be significantly minimized (a reduction by a factor of 5 can theoretically be achieved [109]). The thorium fuel also has better ability to withstand higher burnup (reduced fission gas release) [18]. This might not be an issue for heterogeneous seed-blanket concepts because the limiting case is the seed uranium pin rather than the blanket thorium pin [101].

Plutonium, a byproduct of irradiation in uranium-fueled LWRs, is also a fuel material candidate. Such plutonium has a mixture of isotopes, some of which are not fissile in a thermal spectrum. In addition, there is some weapons grade plutonium from discarded weapons stockpiles that have become disposable in recent years as a result of negotiations between the US and Russia. Plutonium can be burned in LWRs not only to generate electricity, but also to lower proliferation risks, and even to reduce the long-term radiotoxicity of conventional nuclear spent fuel. The nuclear industry practice in Europe has demonstrated the technical feasibility of using mixed-oxide fuel (MOX) in LWRs. In countries that allow reprocessing of nuclear spent fuel (such as Britain, Japan and France), recycled actinides, other than uranium and plutonium, can also be useful as fuel material. For example, the U-Np-Pu fuel concept was proposed in order to achieve very high burnup in small water cooled reactors [110]. One should be aware of the fact that plutonium as well as minor actinides generally have small delayed neutron yields which complicates reactor control.

In this Chapter, the focus is on uranium-based fuel but in different fuel forms. Traditionally there are at least four investigated chemical compounds: uranium dioxide,

uranium carbide, uranium nitride, and U/Zr alloy. UO_2 is the basic (and the only) fuel material for commercial power reactors which has accumulated extensive usage experience. The selection of UO_2 over other candidates is based upon its excellent chemical/irradiation stability (especially in water coolant), high melting point, compatibility with cladding materials (Zircaloy or stainless steel), and ease of fabrication [4]. There is now essentially no industrial interest in departing from UO_2 fuel since the technology of UO_2 fuel is satisfactory and well established. Even for high burnup applications, the first candidate for LWRs will still be UO_2. Although uranium nitride is better in fuel thermal behavior, the practical consideration of its chemical reactivity with water and waste issues eliminate that option (isotopic separation of enriched N-15 may be needed) [111]. There is some interest in metallic fuel forms, namely a U/Zr alloy (pure uranium metal is not considered due to its poor dimensional stability under irradiation). It is conceivable that metallic fuel can have a lower centerline temperature because of better thermal conductivity, which leads to less stored thermal energy in fuel elements (a significant safety advantage during LOCAs but the chemical energy potential under severe accidents is a negative feature) [112].

Recently dispersion-type fuel, also called inert-matrix fuel (IMF), has become of strong interest, particularly for plutonium disposition (for which very high burnup is desired) [104]. The essential idea is to dilute the relatively weak fuel matrix with a much stronger supporting matrix to withstand the fuel fissions and thereby improve fuel performance from a materials point of view. The fuel loading in such a fuel is greatly reduced to accommodate an additional support matrix, which leads to a large H/HM value (wetter lattices). Typically much higher fissile contents have to be loaded to maintain cycle length as discussed in the next section. Depending on the type of fuel and the matrix, there are several variants of IMF including:

- CERCER, ceramic fuel particle dispersed in a ceramic matrix, such as UO_2/CeO_2;
- CERMET, ceramic fuel particle dispersed in a metallic matrix such as UO_2/Zircaloy;
- SSP, solid solution pellet (homogeneous), such as PuO_2 in CeO_2;
- METMET, metallic fuel in metallic matrix, such as U/Zr in Zircaloy.

In addition, the fuel geometrical form is open to evaluation. Annular fuel pellets with a central void are not uncommon. For example, Russian VVERs use this type of fuel with about 10% void fraction. Westinghouse PWR fuel designs also use this type of fuel

in the top/bottom blanket regions of a fuel assembly to reduce effective fuel loadings. Neutronically speaking, this is similar to the IMF concept, both of which can increase H/HM by reducing the fuel loading. The neutronic consequences are thus similar. Research on internally and externally-cooled annular fuel is in progress at MIT. This fuel concept is at an early stage of development offering a significant reduction in fuel temperature. Some of this fuel's neutronic characteristics will be addressed in this Chapter.

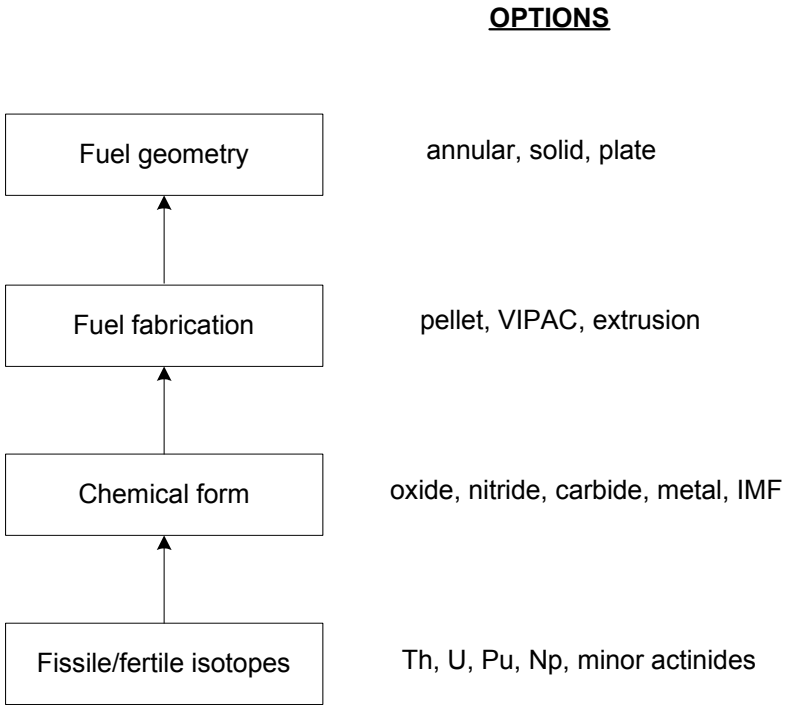

Figure 5.1 Schematic showing fuel design options.

It should be noted that these alternative fuel options are closely associated with different initiatives. They can also be used in a combined way. French researchers have proposed an advanced plutonium fuel assembly concept which uses a mix of annular and solid fuel rods in one assembly [113]. Figure 5.1 shows a hierarchical diagram of various fuel design options. For example, for the purpose of plutonium and minor actinide transmutation, the fertile-free inert matrix fuel concept is an attractive option. It is guaranteed to be a burner since there is no new generation of Pu or minor actinides. In this Chapter the main focus, however, is on the ability of these fuels to change a main lattice parameter, namely the H/HM.

5.2 Inert Matrix Fuel (IMF)

5.2.1 Introduction

The IMF concept is mainly of interest for the purpose of plutonium and minor actinides transmutation, which inevitably favors high burnup to burn more plutonium and minor actinides. However, it is investigated here solely from the high burnup potential perspective using uranium fuel. As discussed in the last Chapter, the neutronic consequence of reduced fuel loading is a wetter lattice (higher H/HM), i.e., a softer neutron spectrum. For the same uranium fuel enrichment, a higher reactivity-limited burnup is obtained for wetter lattices. However, the cycle length is usually shortened due to the reduced fuel loading. Therefore, in order to satisfy the cycle length requirements under rated power, higher-enriched uranium is needed. The principal issue is that the core must deliver a certain amount of total energy each intra-refueling interval (e.g., 18-24 months).

Cycle energy is proportional to the product of burnup and heavy metal inventory. For n-batch fuel management,

$$E_c = B_c M = \frac{B_d}{n} M, \qquad \text{MWd(thermal)}, \tag{5.1}$$

where B_c = whole-core cycle burnup increment, MWd/kg

M = total core heavy metal inventory, kg

B_d = steady-state core discharge burnup, MWd/kg

$1/n$ = fraction of core replaced per refueling.

5.2.2 Burnup Potential, Cycle Length and MTC Considerations

Several dispersion fuels are investigated and then compared to the reference UO_2 case. The IMF fuel here consists of 40% volume fraction of UO_2 (12.5 w/o enrichment) and 60% volume fraction of supporting matrix materials in order to completely encapsulate the individual fuel particles and form a continuous web of supporting matrices. The metallic matrix candidates considered include Zr, Cr, V, and W. Two ceramic matrix candidates are considered: ZrO_2 and CeO_2. The material properties of these supporting matrices are listed in Table 5.1. Among the four metal candidates, tungsten has very high melting temperature and excellent thermal conductivity. However, as shown in the following

calculations, it suffers from a very high neutron absorption cross section which makes it unsuitable as a matrix material. The ceramic matrices typically have lower thermal conductivity than the metals, but have higher melting temperatures.

Table 5.1 Material properties of supporting matrices [114, 115].

Matrix type	Matrices	Density (g/cc)	T_{melt} (K)	c_p (J/mol/K)	k (W/m/K))
Metal	Zr	6.511	2128	25.4	23
	Cr	7.140	2180	23.3	94
	V	6.110	2183	24.9	31
	W	19.25	3695	24.3	170
Ceramic	ZrO_2	5.68	2983	56.2	2.0
	CeO_2	7.65	2673	61.6	1.3

The reference case is a conventional 5 w/o-enriched UO_2 fuel. This way, the total amount of U-235 loading is conserved which roughly gives the same natural uranium resource requirement. In addition, a rule of thumb based on previous work is that comparable cycle energy will be generated if the U-235 mass is conserved in the core.

Given the same power density as the UO_2 fuel, the IMF fuel will exhibit:

1. higher specific power, kW/kgIHM, by a factor of 2.5;
2. higher burnup rate, also increased by 2.5;
3. if not otherwise offset, a shorter cycle by a factor of 2.5.

CASMO-4 runs of these cases are shown in Figs. 5.2 and 5.3 based on a conventional PWR unit cell. Fig. 5.2 compares k_∞ vs. burnup and Fig. 5.3 k_∞ vs. effective full power days. The latter confirms that the reactivity-limited cycle lengths are about equal (but not for V or Cr): a one-batch loaded core EFPD of ~1150; for n-batch management then, a cycle length of about 1150*2/(n+1), or 575 EFPD for n=3. Fig. 5.2 shows the large increase in burnup required for the CERMET, and the much larger excess reactivity required in fresh fuel as well. From a fuel cycle economics perspective, savings in the IMF fuel from carrying charges can be achieved due to an increased burnup rate (specific power). (see Chapter 8).

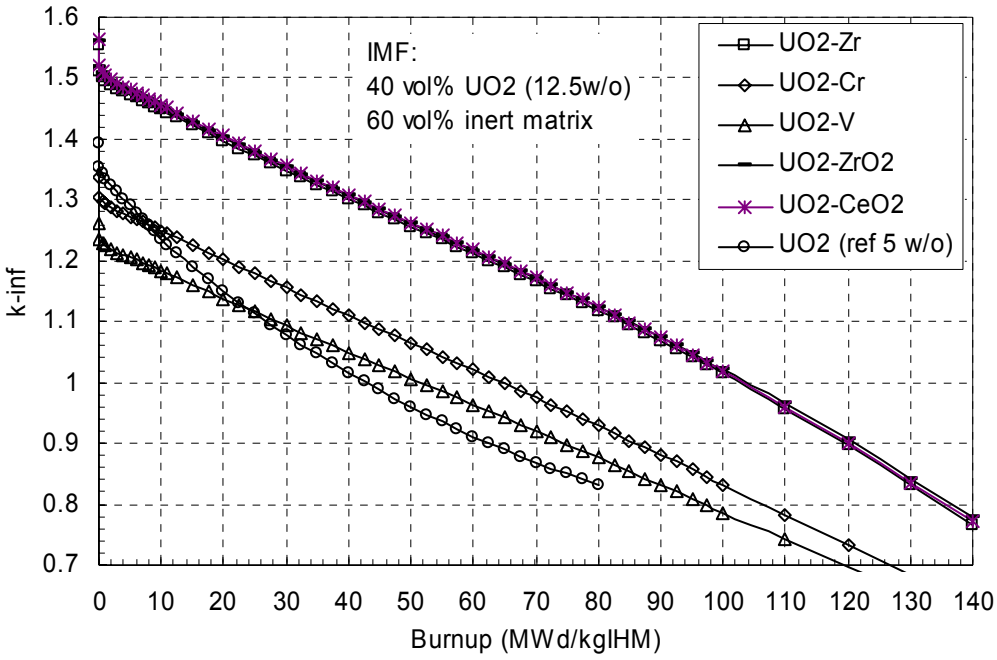

Figure 5.2 Burnup histories of the IMF and reference cases.

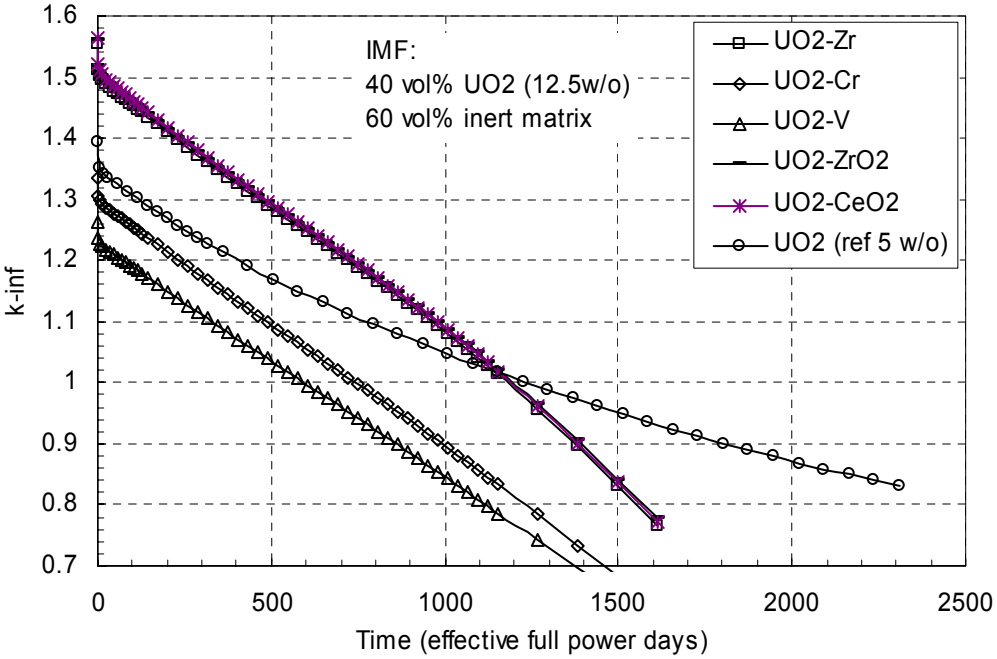

Figure 5.3 IMF depletion curves as a function of time (effective full power days).

Note that the CERMET case of UO_2 with W is not shown in Figs. 5.2 and 5.3 because that case has very low eigenvalues (subcritical). Tungsten has large neutron absorption cross sections and high number density. It is therefore not suited to be a matrix material from a neutronic point of view. Comparisons between the IMF fuels show that UO_2-Zr, UO_2-ZrO_2, and UO_2-CeO_2 all have roughly the same burnup capability. UO_2-Zr, though is worse than UO_2-ZrO_2, but is better than UO_2-V. Table 5.2 gives the neutronic parameters for these cases.

Table 5.2 Neutronic parameter summary of supporting matrices.

	Fuel	$k_\infty(t=0)$	CR(t=0)	$B_1(k_\infty=1.03)$ (MWd/kg)	$T_1(k_\infty=1.03)$ (EFPD)
Reference	UO_2	1.39409	0.408	37.7	1087
CERMET	UO_2-Zr	1.55512	0.207	97.1	1121
	UO_2-Cr	1.33601	0.230	57.9	668
	UO_2-V	1.26203	0.235	44.6	514
	UO_2-W	0.35561	0.326	0	0
CERCER	UO_2-ZrO_2	1.56050	0.209	98.4	1136
	UO_2-CeO_2	1.56366	0.207	98.0	1131

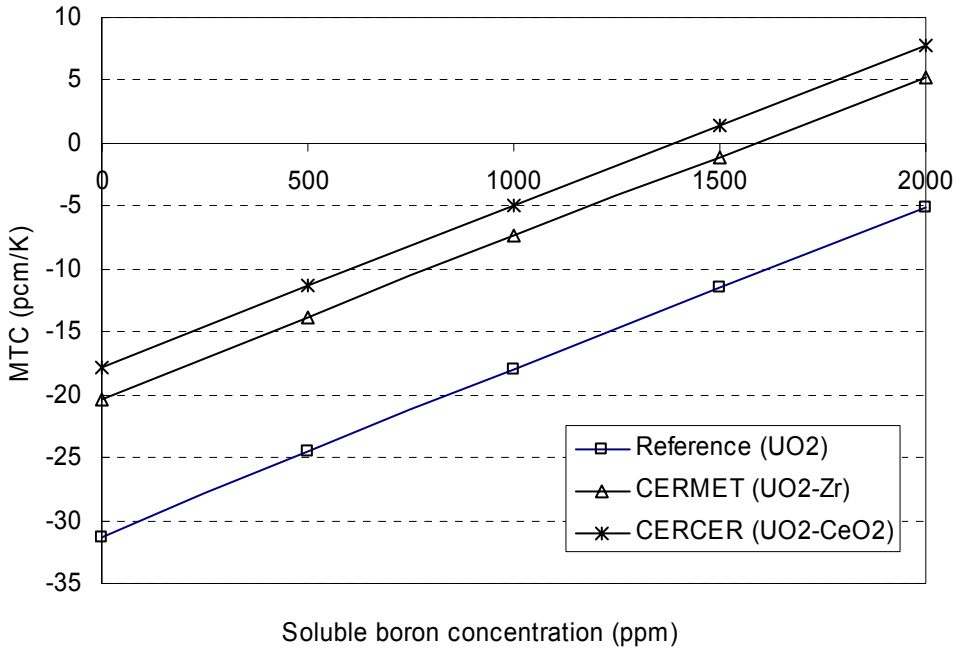

Figure 5.4 MTC at BOL as a function of boron concentration.

The H/HM value of the reference UO_2 case is 3.42 whereas the H/HM values for all the IMF cases are 8.53. Naturally one would worry about the MTC for such a wet lattice. Figure 5.4 shows the MTC at BOL as a function of soluble boron concentration. Although the IMF fuel demonstrates negative MTC under 0 ppm boron concentration at BOL, the magnitude of MTC is smaller for the IMF fuel compared to the reference UO_2 case due to a wetter lattice. Therefore the limiting boron concentration from the MTC constraint will be more demanding for the IMF fuel. Reactivity control of the IMF fuel will depend more on the usage of burnable poison.

5.2.3 Lattice Optimization

It was shown in Chapter 4 that the current PWR lattice is the (weak) optimum in terms of maximum energy production. A practical approach of varying fuel rod diameter is implemented here to search for the maximum energy production for the IMF fuel, using the 12.5w/o-enriched-UO_2(40 vol%)-Zr(60 vol%) CERMET as an example. Note that for the current lattice (rod diameter), the reference H/HM value for the UO_2/Zr CERMET fuel is 8.53. Throughout the rod diameter variation, the core power density is kept the same.

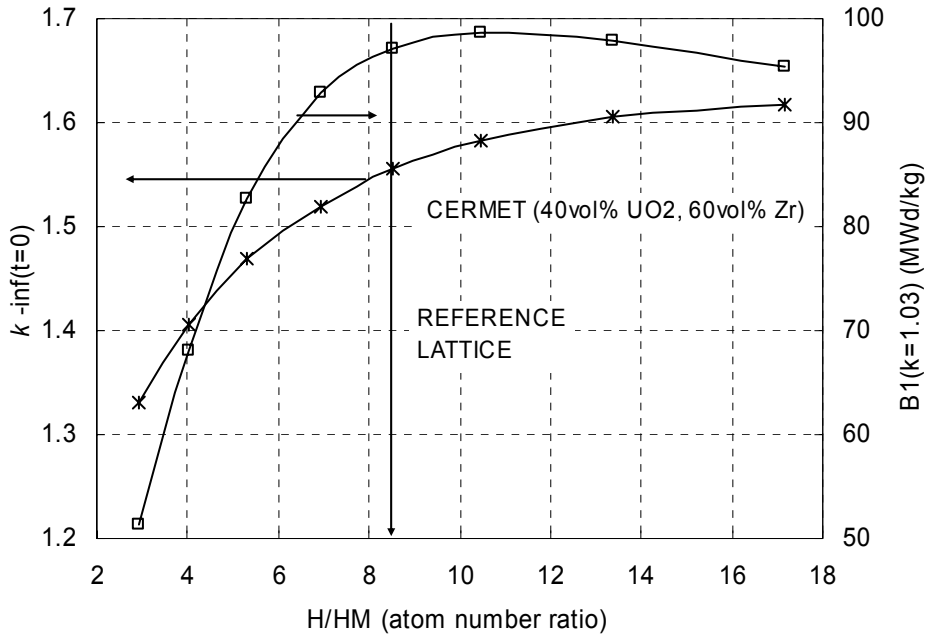

Figure 5.5 The initial k_∞ and burnup potential of CERMET fuel.

Figure 5.5 shows the results of varying H/HM via rod diameter changes for the CERMET fuel. The negative MTC can be seen for the reference lattice (H/HM = 8.53). The single batch burnup potential is close to maximum for the current lattice.

Since the power density is kept constant, the energy production can be expressed as effective full power days (EFPD). Figure 5.6 shows the single-batch cycle length has a maximum at a drier lattice. Therefore, for the IMF concept the optimum lattice in terms of maximum energy production might lead to use of larger-diameter pins. The larger pin would increase hydraulic resistance and require more pressure drop across the core (more powerful pumps needed).

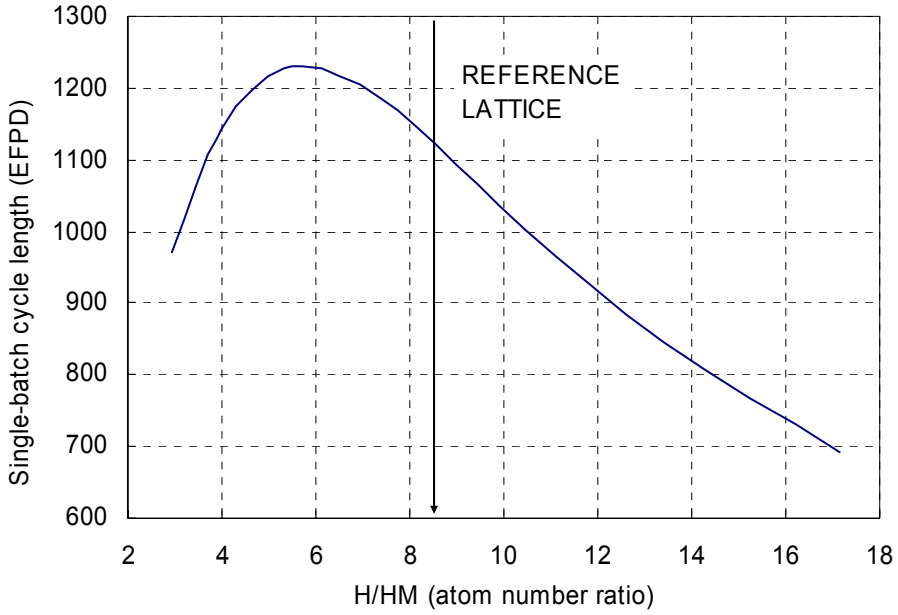

Figure 5.6 The energy production (EFPD) as a function of H/HM.

5.2.4 Conclusion

In summary the neutronic differences between the IMF and the reference solid UO_2 fuel include:

1. a different moderator-to-fuel ratio (H/HM);
2. a different thermal flux, hence xenon reactivity penalty;
3. additional parasitic absorptions in the IMF's supporting matrix material;
4. cooler fuel, hence reduced fraction of Doppler-related U-238 and Pu-240 captures;

5. more control poisons needed to hold down the much higher BOL reactivity for UO_2-Zr, UO_2-ZrO_2, and UO_2-CeO_2 (and depending more on burnable poison).

Taken together these considerations would motivate the use of a drier lattice by increasing the fuel pin diameter as shown in Fig. 5.6, but with of course thermal-hydraulic consequences.

5.3 Center-Voided Annular Fuel Pellet

5.3.1 Introduction

The center-voided annular fuel pellet is another approach to creation of a wetter lattice. Although like the IMF fuel it reduces fuel loading, this concept is neutronically superior due to the elimination of parasitic absorption by matrix materials. The discussion here will provide a comparison between the solid and annular fuel pellets.

The central void fraction of the annular fuel pellet is an important parameter. Typically it is ~10% for Russian VVER fuels. For larger void fractions, a supporting central plug is needed [116] to prevent relocation of fuel fragments from the inner surface of each fuel pellet. The central void also provides additional fission gas plenum volume. Furthermore, the central void provides room for burnable poison to suppress the initial excessive reactivity as implemented in a thorium seed-blanket core design [101].

A reduction of fuel temperature is also realized for the center-voided pellet. Hence the Doppler absorption is reduced compared to the solid fuel. The ratio of fuel temperature rise of annular to solid fuel pellets operating at the same linear power can be expressed as:

$$\frac{\Delta T_{\text{annular}}}{\Delta T_{\text{solid}}} = 1 - \frac{\ln\left(\frac{R_{\text{fo}}}{R_{\text{v}}}\right)^2}{\left(\frac{R_{\text{fo}}}{R_{\text{v}}}\right)^2 - 1}, \tag{5.2}$$

where R_{fo} is the outer radius of annular fuel and R_{v} is the void radius. A 10% void leads to a reduction of temperature rise by about 25% compared to a solid fuel pin generating the same linear power [117].

5.3.2 Void-Filling Materials

One concern about center-voided annular fuel pellets with large void fraction is the collapse of the thin annulus at high burnup. Plug materials are, therefore, usually recommended to keep the pellet geometry. The ideal material should have zero absorption. Here 3 plug options are examined: void, graphite, and zircaloy. Void represents an ideal case that sets up the up ceiling for the other materials. Graphite-filled annular fuel has been studied for MOX fuel designs to help soften the spectrum to increase the control rod worth and enhance reactivity feedback coefficients [118]. Zircaloy was also tried since zirconium has a very low absorption cross section. More realistic filling material is probably ZrO_2 since Zircaloy has a low melting point. However, the neutronic behavior of the two is similar as demonstrated in the discussion of the IMF fuel, UO_2-Zr versus UO_2-ZrO_2.

Figs. 5.7 and 5.8 show the single-batch burnup and cycle length respectively for UO_2 at an enrichment of 9.75 w/o.

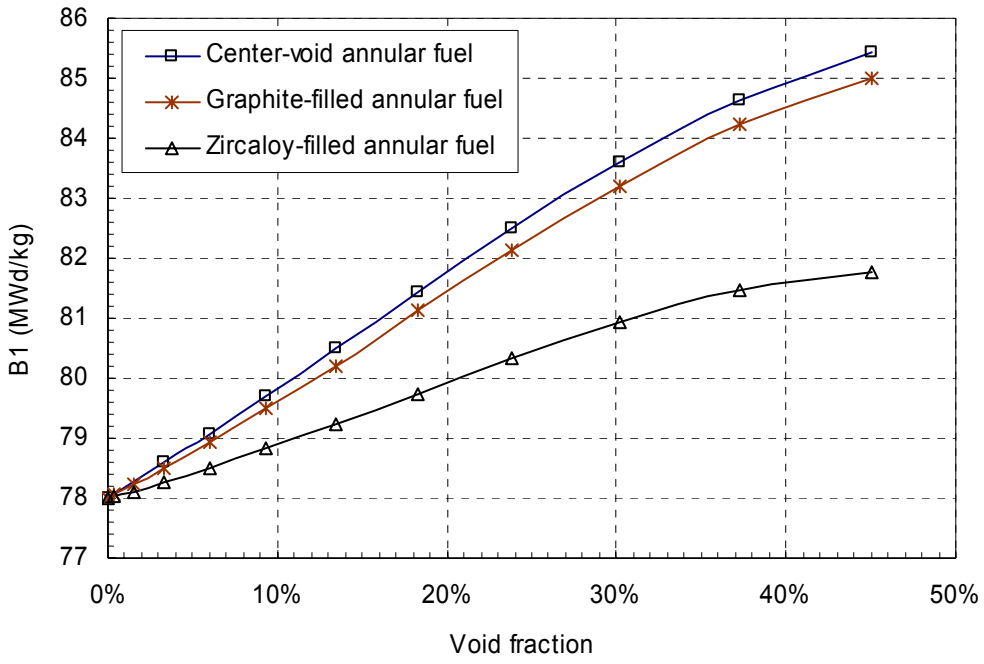

Figure 5.7 Single-batch burnup capabilities for various filling materials for annular fuel.

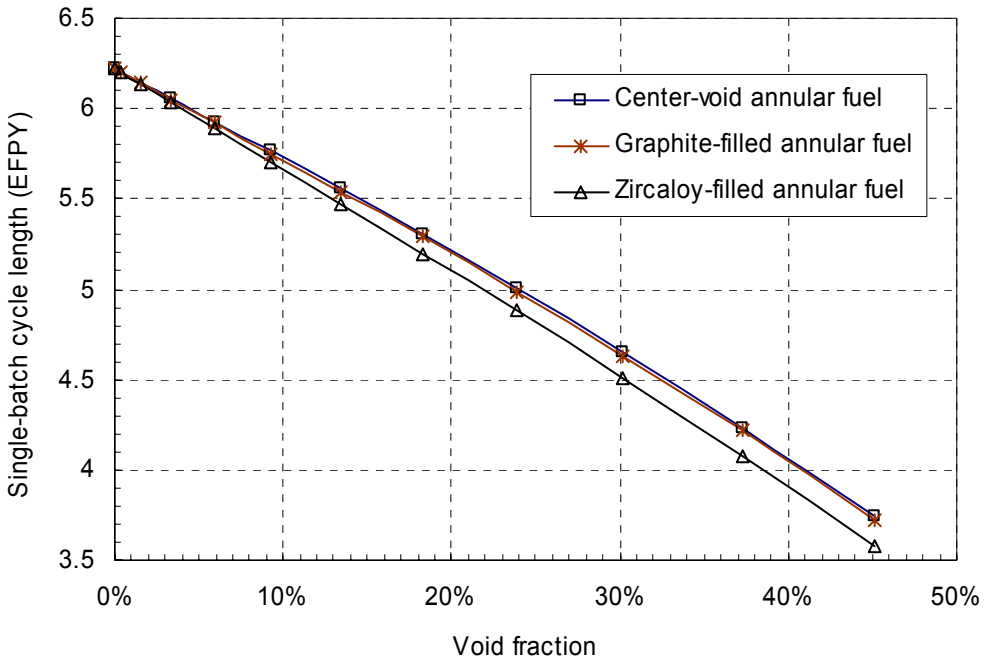

Figure 5.8 Single-batch cycle length for various filling materials (9.75 w/o enrichment).

The center-voided annular fuel has the highest burnup. This confirms that a fill material should have as low an absorption cross section as possible. Graphite-filled annular fuel is closer to the central-void annular fuel compared to the Zircaloy-filled annular fuel. Therefore, graphite is a better material for filling the central annular void if needed. The porous plug containing low density ceramic fiber is also a candidate since it provides fission product gas release space [116].

5.3.3 Comparison to Solid Fuel Pin

The solid fuel pin can also be adjusted to achieve various H/HM values by changing the rod diameter. The center-voided annular fuel (better performer according to last section than an inert material) is compared to the solid fuel pin. In Fig. 5.9, which shows the single-batch cycle length, it is seen that the energy production of a core of annular fuel is less than that achieved by the rod diameter reduction to reach the same H/HM value.

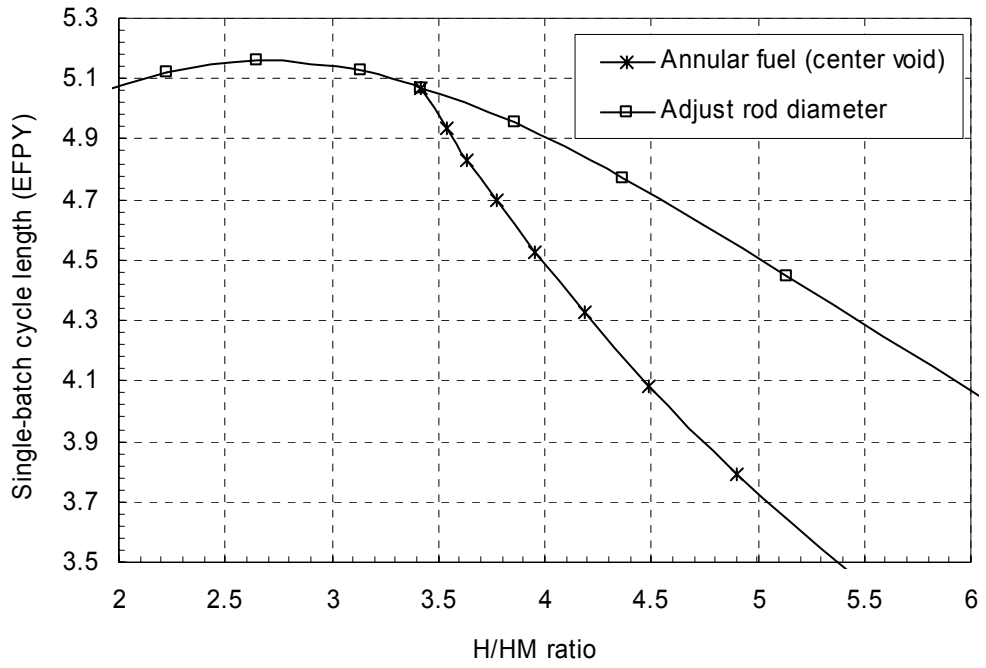

Figure 5.9 Single-batch cycle length comparison between annular fuel and solid rod.

Upon evaluation, it is concluded that the most desirable way of achieving wetter lattices is by optimizing the solid pellet diameter [119]. Thus we will not consider the annular pellet option further in this review. However, a very useful approach from thermal and safety perspectives is the internally and externally cooled annular fuel (IXAF). This is the subject of the next section.

5.4 Internally and Externally-Cooled Annular Fuel (IXAF)

5.4.1 Introduction

The concept of Internally and eXternally cooled Annular Fuel (IXAF) for PWRs was recently proposed at MIT [102], which has significant thermal hydraulic advantages, such as better DNBR (larger heat transfer area, thus lower surface heat flux) and lower fuel temperature, compared to conventional solid fuel pins. The much lower fuel temperature reduces the stored energy in fuel pellets (reducing the cladding temperature after LOCA) and the fuel pellet expansion (less PCI, thus higher burnup allowed) [34]. A 50% core

power density uprate for a Westinghouse 4-loop PWR may be achieved based on the IXAF concept with comparable or better thermal margins than conventional solid fuel pins [120]. Although the IXAF concept may be thought of as a neutronically inferior option due to increased U-238 resonance absorption and doubling of cladding parasitic absorption, there are other differences from the solid pins such as lower fuel temperature (hence a Doppler reactivity gain) that may be beneficial. Therefore, a detailed, step-by-step study (with a unit cell model) has been performed to assess the individual neutronic changes of the IXAF concept using MCNP-4C. The reactivity feedback coefficients, including the Doppler coefficient and the moderator temperature coefficient (MTC), were also computed.

One thing to remember is that although still under a thermal spectrum the IXAF design poses a challenge for the deterministic lattice code, CASMO-4. A default radial distribution of U-238 resonance integral is assumed in CASMO-4 [20]:

$$f(r) = 1 + 3e^{-9.7\sqrt{R-r}}, \tag{5.3}$$

where r is the radius and R is the fuel pellet outer radius. Furthermore the epithermal U-238 capture on the inner fuel surface is not accounted for, which leads to a lower neutron absorption (hence overestimates the eigenvalue). It was concluded that for the IXAF fuel the approximations of CASMO-4 for calculating the resonance integrals are not as accurate as for the other fuel types (e.g., solid fuel pin, annular fuel pin with central void or gadolinium inside) [121]. Table 5.3 compares the ratio of U-238 capture rate to U-235 fission rate, C^*, calculated by CASMO-4 and MCNP-4B for the IXAF design and the reference solid pin (both with 9.75 w/o UO_2 fuel). It was found that (1) for the case of reference solid pins, CASMO-4 agrees with MCNP-4B satisfactorily (within statistical error), (2) for the IXAF fuel, a confirmed overestimation of k_∞ and lower estimation of C^* is provided by CASMO-4. Hence, the depletion calculations for the IXAF will be based on MCODE.

Table 5.3 CASMO-4 and MCNP results for IXAF and reference solid fuel (at BOL).

	C^*		k_∞	
	CASMO-4	MCNP-4B	CASMO-4	MCNP-4B
Reference solid pin (17×17)	0.383	0.382±0.005	1.471	1.472±0.001
IXAF design (13×13)	0.390	0.433±0.005	1.461	1.427±0.001

5.4.2 Four-Factor Formula Considerations

In the early era of reactor design, the four-factor formula was widely used as an effective way to estimate the multiplication factor, k_∞, in order to circumvent the need for detailed cross-sectional values at all energies [122]. However, in our study the four factors are computed to identify individual contributions to the eigenvalue. Values for the solid fuel pin and IXAF fuel pin are compared to show the changes in neutronic characteristics.

The definition of the four-factor formula for a unit cell is first introduced as follows:

$$k_\infty \equiv \frac{\int_{\text{CELL}} dV \int_0^{+\infty} dE\ \nu\Sigma_{\text{f}}(\mathbf{r},E)\Phi(\mathbf{r},E)}{\int_{\text{CELL}} dV \int_0^{+\infty} dE\ \Sigma_{\text{a}}(\mathbf{r},E)\Phi(\mathbf{r},E)} = \varepsilon\eta fp\ . \tag{5.4}$$

The fast fission factor, ε, represents the ratio of the total rate of production of fission neutrons to the rate of production due to fissions in the thermal energy range*:

$$\varepsilon \equiv \frac{\int_{\text{FUEL}} dV \int_0^{+\infty} dE\ \nu\Sigma_{\text{f}}(\mathbf{r},E)\Phi(\mathbf{r},E)}{\int_{\text{FUEL}} dV \int_0^{E_2} dE\ \nu\Sigma_{\text{f}}(\mathbf{r},E)\Phi(\mathbf{r},E)}, \tag{5.5}$$

where E_2 is a cutoff energy separating the thermal region (where up-scattering is important) and the fast region. In the following calculations, the cutoff energy is taken as 0.5 eV (cadmium cutoff).

The Eta factor, η, is the ratio of the rate of fission neutrons created by thermal fissions to the rate of thermal neutron absorption in the fuel:

$$\eta \equiv \frac{\int_{\text{FUEL}} dV \int_0^{E_2} dE\ \nu\Sigma_{\text{f}}(\mathbf{r},E)\Phi(\mathbf{r},E)}{\int_{\text{FUEL}} dV \int_0^{E_2} dE\ \Sigma_{\text{a}}^{\text{FUEL}}(\mathbf{r},E)\Phi(\mathbf{r},E)}. \tag{5.6}$$

Note that the fuel refers to the mixture of heavy metal and its associated chemical components, for example, the UO_2 fuel will include both uranium and oxygen. Upon depletion, the fission products from actinides should also be considered.

The thermal utilization, f, is the ratio of the rate of the thermal neutron absorption in the fuel to the rate of overall thermal neutron absorption.

---

* Note that some definitions consider as fast neutrons only those with energies above U-238 fission threshold. Here the definition consistent with Henry will be followed, which also includes epithermal contributions.

$$f \equiv \frac{\int_{\text{FUEL}} dV \int_0^{E_2} dE\ \Sigma_{\text{a}}^{\text{FUEL}}(\mathbf{r},E)\Phi(\mathbf{r},E)}{\int_{\text{CELL}} dV \int_0^{E_2} dE\ \Sigma_{\text{a}}(\mathbf{r},E)\Phi(\mathbf{r},E)}. \tag{5.7}$$

The resonance-escape probability, p, is the ratio of thermal neutron absorption in the cell to the overall (thermal plus fast) neutron absorption in the cell.

$$p \equiv \frac{\int_{\text{CELL}} dV \int_0^{E_2} dE\ \Sigma_{\text{a}}(\mathbf{r},E)\Phi(\mathbf{r},E)}{\int_{\text{CELL}} dV \int_0^{+\infty} dE\ \Sigma_{\text{a}}(\mathbf{r},E)\Phi(\mathbf{r},E)} \tag{5.8}$$

It is the probability that a neutron will escape capture at energies above thermal.

The above four factors can be readily calculated with MCNP-4C using appropriate reaction rate tallies.

5.4.3 From Solid to Annular: A Step-by-Step Variation Approach

The reference solid fuel pin (Case 0) is taken from a standard Westinghouse PWR 17×17-lattice assembly to serve as the starting point. The end point is the newest IXAF design with a 13×13-lattice (Case 6) [120]. The operating conditions and geometric parameters for these two cases are summarized in Table 5.4.

Table 5.4 Operating conditions and geometric parameters of solid and IXAF cases.

Cases	Solid fuel pin (REF)	IXAF fuel pin
Lattice	17×17	13×13
Fuel rods per assembly	264	160
Guide tubes per assembly	25	9
Fuel density (g/cm^3)	10.4	
H_2O Temperature (K)	583.1	
Enrichment (w/o)	4.95	
Power density (kW/liter-core)	104.5	
Pin pitch (cm)	1.26	1.651
Fuel Temperature (K)	900	600
Rod inner r_{i} (cm)	—	0.4315
Inner clad outer r_{ico} (cm)	—	0.4890
Fuel inner r_{fi} (cm)	—	0.4950
Fuel outer r_{fo} (cm)	0.4096	0.7050
Outer clad inner r_{oci} (cm)	0.4178	0.7110
Rod outer r_{o} (cm)	0.4750	0.7685
$V_{\text{m}}/V_{\text{f}}^*$	1.667	1.838
$(S/V)_{\text{Fuel}}$ (cm^{-1})	4.883	9.524

∗ defined as the volume ratio between the moderator (H_2O) and the fuel (UO_2 only)

When comparing the reference solid fuel pin to the IXAF case, one can readily observe five differences:

- fewer number of pins, 17×17 vs. 13×13

  Keeping the same overall assembly dimensions, the IXAF necessitates larger pin size compared to a solid pin to accommodate inner flow. One needs to balance the inner and outer flow channels of the IXAF in terms of both the heat transfer split and flow split so that overall thermal hydraulic constraints are roughly the same for the two channels. Therefore, the reference assembly is a 17×17 lattice while the IXAF assembly is a 13×13 lattice.

- geometric configuration, solid vs. annular (surface-to-volume ratio difference)

  The IXAF pin has fuel surfaces cooled from both sides, which approximately doubles the surface-to-volume ratio in comparison with a solid pin.

- average fuel temperature, 900 K vs. 600 K

  Due to more efficient cooling of the IXAF (much smaller thermal resistance), the average fuel temperature has been shown to be much lower than the reference solid pin. Under normal operating conditions, the average fuel temperature is about 900 K for typical solid pins in PWR lattices while it is ~600 K for IXAF pins. This will increase the eigenvalue by about 0.03 due to a smaller cold-hot Doppler penalty.

- amount of cladding, one layer vs. two layers

  Since the IXAF fuel is cooled from both sides, two layers of cladding are required. Roughly speaking, the amount of Zircaloy is doubled (hence doubled parasitic neutron absorption).

- moderator-to-fuel volume ratio, 1.667 vs. 1.838.

Thus, in order to understand the fundamental neutronic differences between solid and annular fuel, five intermediate hypothetical cases (step-by-step variations) were created as a logical connection between the reference solid pin (Case 0) and the IXAF fuel (Case 6) as shown in Figure 5.10. Note that except for the difference specified, all other parameters are kept the same. For example, when transforming the enlarged solid fuel pin (Case 1) to the clean IXAF (Case 2), only the geometrical transformation from solid fuel

to annular fuel with water inside is carried out whereas all other conditions, such as the fuel temperature and water volume, are maintained. In particular, the clean IXAF case (Case 2) deserves special interest as a branching point with only geometric information included.

5.4.4 Results and Discussion

The eigenvalues as well as the reactivity feedback coefficients (the Doppler coefficient and MTC) for these cases were calculated at the beginning-of-life (BOL) with MCNP-4C (10^6 neutron histories for each case, thus statistical errors are small and ignored) as shown in Table 5.5. For better understanding of relative contributions from each of the five individual differences between solid and annular fuels, the eigenvalue is decomposed into the traditional four factors [122]: the fast fission factor ε, the neutron yield factor η, the thermal utilization f, and the resonance-escape probability p. Additional neutronic spectrum indices, such as C^*, ρ_{28}, δ_{25}, are also computed.

A major underlying neutronic effect is the resonance absorption behavior. The resonance integral, RI, which correlates as a linear function of square root of the surface to volume ratio, $\left(\sqrt{S/V}\right)_{\text{fuel}}$, explains the lattice size and the annular fuel geometric effects. The significant change of fuel shape has the largest contribution to the eigenvalue. The fuel temperature change and the double cladding effect roughly cancel each other. Increasing H/HM reflects this design change and follows a historical trend in industry and recent studies of high burnup. Comparing the reference solid and the final IXAF design, one finds the IXAF design still has a lower initial reactivity, but the burnup capability is almost the same as the reference solid case since the conversion ratio is larger for the IXAF design (Figure 5.11). The cycle length in units of effective full power days (EFPD), however, is about 10% smaller for the IXAF design due to about 10% less initial heavy metal loading in its wetter lattice (Figure 5.12). The beginning-of-life FTC and MTC of the IXAF design are comparable to those of the reference solid pins.

It is concluded that although the intrinsic changes of the IXAF design (annular geometry and doubling of cladding) lower the initial reactivity, it is possible (as demonstrated here) to recover most of the loss by taking into account other effects, such as larger pin size (fewer pins per assembly) and higher H/HM ratio. This points to a direction

of future IXAF fuel design, using fewer fuel pins with wetter lattices, whereas the traditional solid fuel design is moving to more fuel pins with wetter lattices.

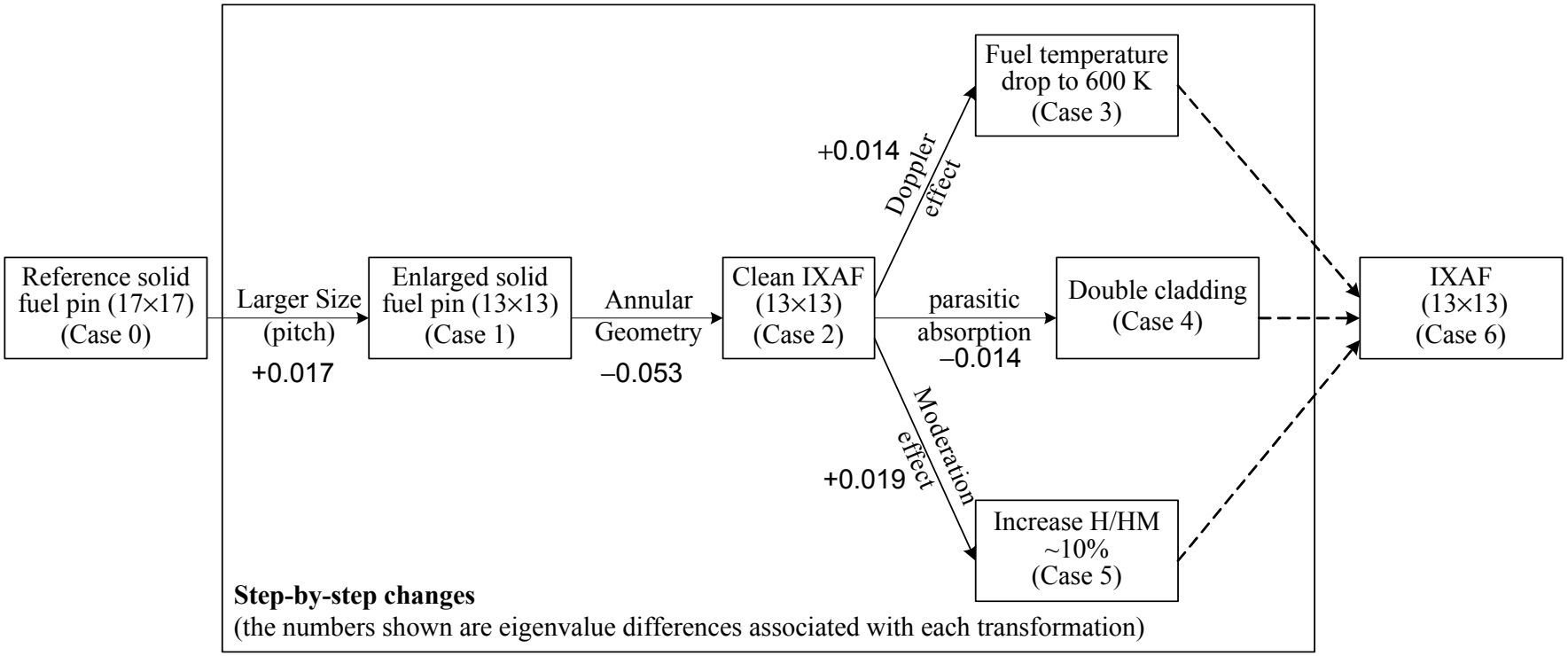

Figure 5.10 Illustration of step-by-step changes (clean case approach).

Table 5.5 Eigenvalues, contributing parameters, and reactivity feedback coefficients at BOL.

Cases	Case 0: Ref. solid pin (17×17)	Case 1: Larger pin (13×13)	Case 2: Clean IXAF (13×13)	Case 3: Clean IXAF lower T_{Fuel}	Case 4: Clean IXAF double clad	Case 5: Clean IXAF wetter lattice	Case 6: IXAF (13×13)
ε	1.410	1.404	1.423	1.420	1.419	1.381	1.376
η	1.910	1.910	1.910	1.910	1.910	1.910	1.911
f	0.9576	0.9549	0.9599	0.9599	0.9565	0.9563	0.9539
p	0.5417	0.5522	0.5218	0.5281	0.5196	0.5472	0.5502
k_∞	1.397	1.414	1.361	1.375	1.347	1.380	1.380
ICR	0.403	0.384	0.442	0.427	0.445	0.420	0.410
C^*	0.496	0.473	0.546	0.527	0.550	0.516	0.505
ρ_{28}	5.68	5.33	6.41	6.14	6.46	5.83	5.69
δ_{25}	0.316	0.311	0.328	0.325	0.328	0.294	0.294
FTC (pcm/K)	–3.60	–3.29	–4.73	—	–4.70	–4.96	–4.48
MTC (pcm/K)	–86.3	–78.7	–82.0	–75.9	–84.6	—	–78.2

[a] The fast fission factor, ε, is defined as the ratio of the total rate of production of fission neutrons to the rate of production in the thermal energy range with cutoff energy 0.5 eV, which includes epithermal fission contributions [122].

[b] The eta factor η, the thermal utilization factor f, and the resonance-escape probability p are defined in the usual way as in Ref. 5.

[c] The ICR refers to the initial conversion ratio, i.e., the ratio of U-238 captures to U-235 absorptions.

[d] The quantity C^* is the ratio of U-238 captures to U-235 fissions. Therefore, $C^* \geq$ ICR.

[e] The quantity ρ_{28} refers to the ratio of epithermal to thermal U-238 captures. Again the energy boundary between thermal and epithermal is defined as 0.5 eV.

[f] The quantity δ_{25} is the ratio of epithermal to thermal U-235 fissions.

[g] The FTC (Doppler coefficient) and MTC are computed as $\frac{\Delta k}{\Delta T}$ respectively. The fuel temperatures are 600 K and 900 K, and the moderator temperatures are 583.1 K and 600 K. Note that these coefficients are free-of-poison values.

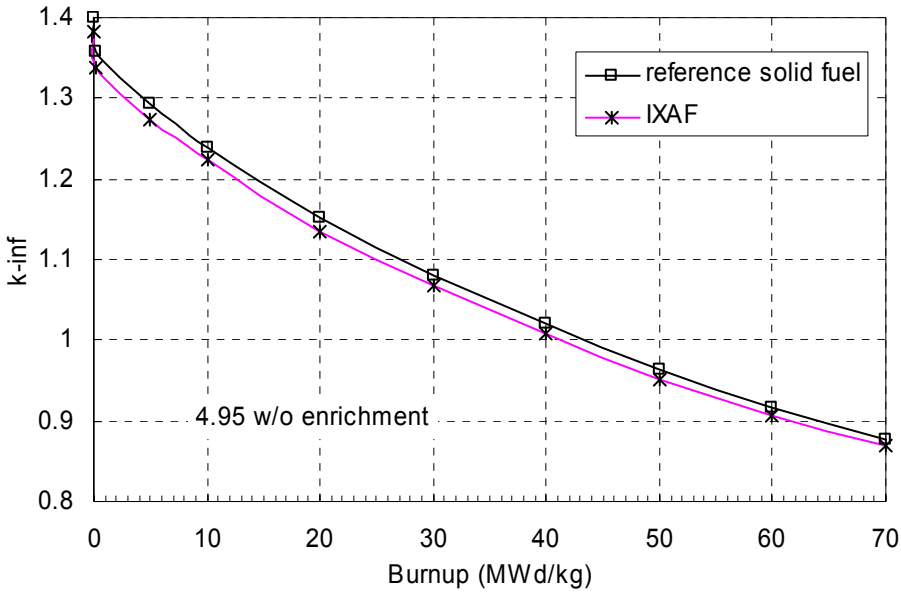

Figure 5.11 Reactivity change versus burnup for solid and IXAF cases.

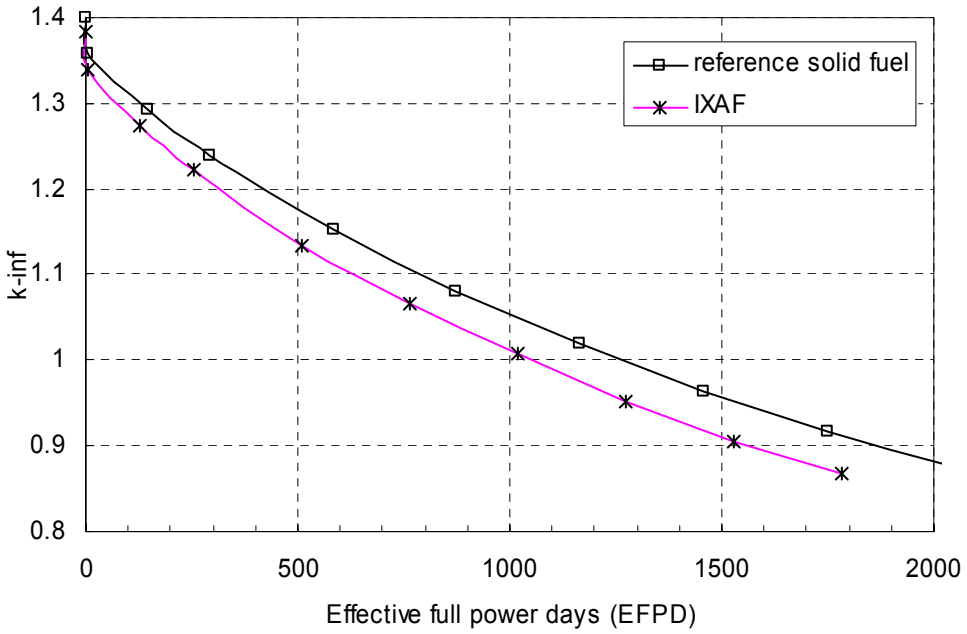

Figure 5.12 Reactivity change versus time for solid and IXAF cases.

5.4.5 The Eigenvalue Ladder

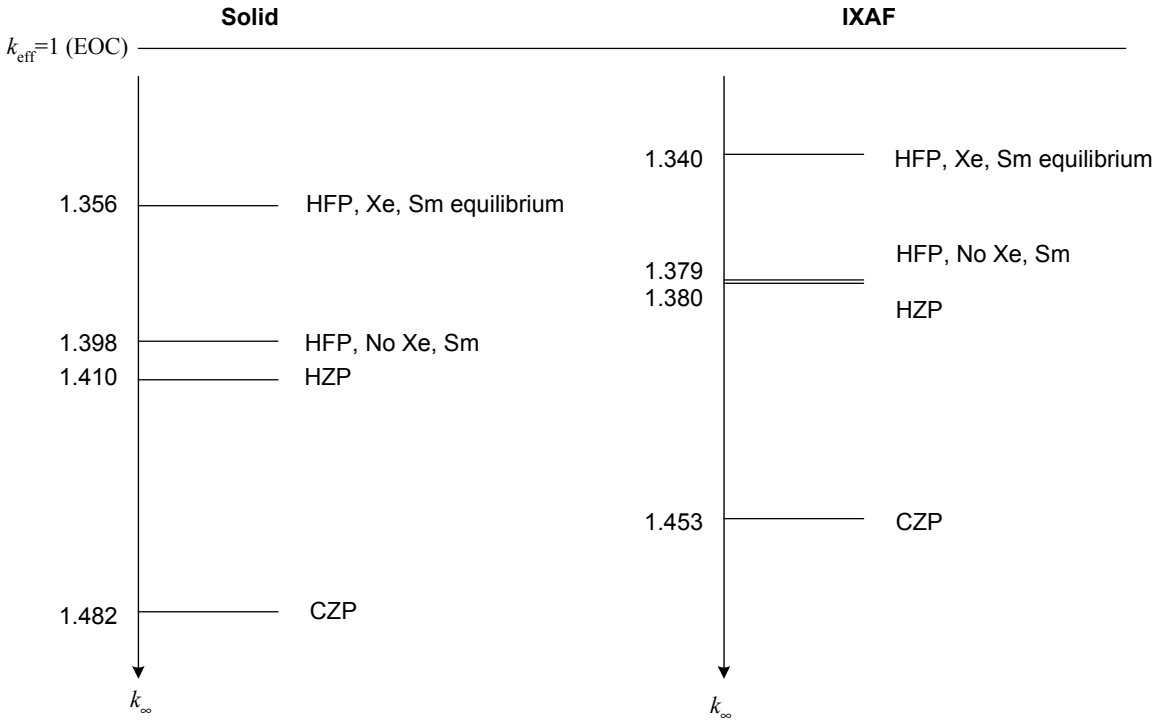

Figure 5.13 The eigenvalue ladder for solid and annular IXAF fuels.

During the core startup process, the core reactivity (eigenvalue) changes step by step, eventually reaching critical. The sequence of events for PWR core startup can be generally summarized as followings:

1. The core is initially at cold zero power (CZP) with all control rods inserted and the water highly borated.
2. The primary coolant pumps are used to raise the temperature to operating conditions (HZP). This reduces reactivity.
3. The shutdown control rods are withdrawn and the full length control rods withdrawn to take the reactor to critical.
4. The core power is gradually raised to full power (HFP, no Xe, Sm). This also reduces reactivity.
5. After a short period of running (about 3 days for a typical Westinghouse PWR) fission products reach equilibrium (HFP, Xe, Sm equilibrium), in the process also reducing reactivity.

6. The loss of reactivity in steps 4 and 5 is compensated for by control rod movement. Long term fuel depletion is compensated for mainly by reducing the soluble boron concentration in the primary coolant.

In order to compare the startup performance of the reference solid fuel and the annular fuel, an eigenvalue ladder showing the above processes has been prepared (see Figure 5.13). The infinite multiplication factor is simulated at different stages. This calculation is based on the unit cell model with parameters listed in Table 5.4. Overall, the reactivity control requirement for annular fuel is less than for the reference solid fuel primarily due to the stronger resonance absorption of annular fuel. When comparing the eigenvalue differences in detail, only the transition from HZP to HFP without Xe, Sm is found to differ significantly. This is to be expected because the fuel temperature rise of annular fuel is much lower than that of the solid reference case. The consequence of this difference might lead to re-examination of PWR startup procedures if annular fuel is to be used. The need for precautions on control rod removal when making transitions should be examined.

Other than that, these two fuels show comparable characteristics. The initially lower eigenvalue under HFP with Xe, Sm implies easier control (smaller boron concentrations) and a larger conversion ratio. The eventual burnup, however, is similar to that of the reference solid case as found in previous sections. To gain the same cycle length as the reference solid fuel, future designs of higher enrichment or higher fuel volume should be examined.

An important difference is in the ability of the IXAF to operate at higher core power densities, which would be hard to achieve with the solid pins. This is due to the lower heat flux to the coolant in the IXAF design.

5.4.6 RIM Effects

Due to strong epithermal U-238 resonance absorption in the epithermal range, plutonium formation on the UO_2 fuel surface is distinctly higher than the rest of the pellet. The phenomenon is known as the RIM effect. This plutonium formation contributes to a very high local burnup in the RIM region. Another issue with the RIM region is that the fuel temperature there is usually low, which makes the RIM modeling a key issue for fuel

performance analysis, especially for high burnup. Unfortunately, the mechanism and consequence of a distinct RIM region in fuel modeling is still unknown.

The IXAF fuel was compared to the solid fuel in terms of RIM effects. A series of plutonium distributions and the power profiles were calculated using MCODE for the reference and the IXAF cases. Note that a high enrichment of 9.75 w/o is used here.

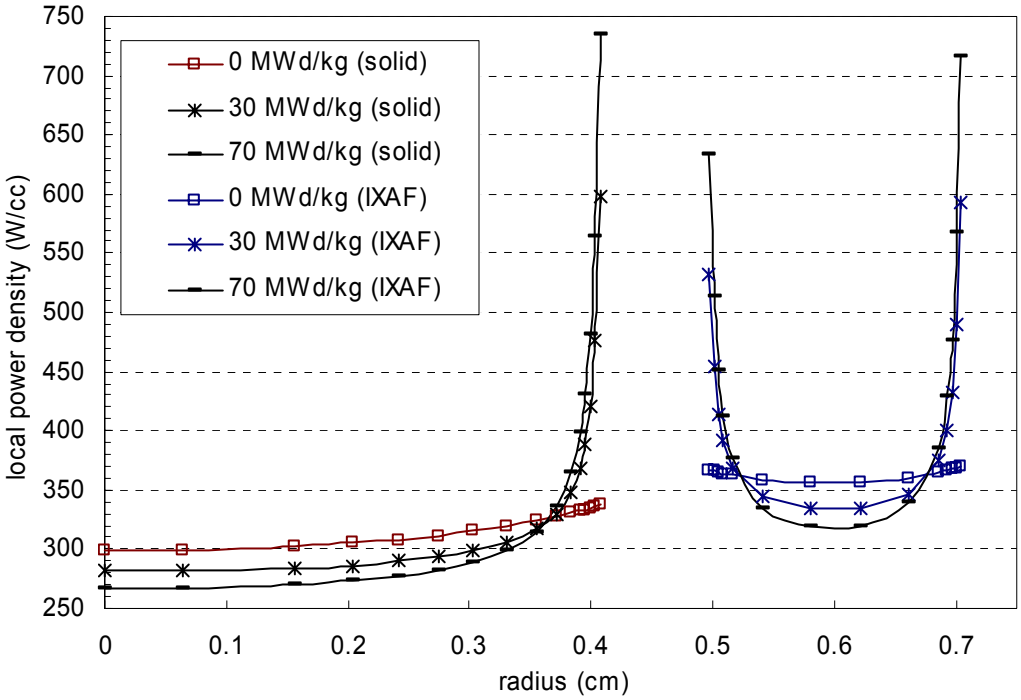

Figure 5.14 Power distributions in IXAF and solid fuel.

Figure 5.14 shows the local power density inside the fuel pellet for the reference and the IXAF fuels. The thickness of the RIM region is about the same (~200μm) for these two cases. However, the volume of the RIM region is significantly different. For solid fuel the fraction of RIM region is ~10%. For the IXAF fuel, the RIM fraction is as high as ~20%. RIM effects are more important to the IXAF fuel. Also it can be seen from Fig. 5.14 that on average the IXAF fuel operates at a higher specific power since there is less fuel loaded in the core. The peak-to-average power is less for the IXAF case. Once the power profile evolution with time is given, one can readily compute the local fuel burnup by integrating the power profile with time. Figure 5.15 shows the local burnup distribution inside the fuel pellet at different average burnup values. It is observed that

compared to solid fuel, the IXAF fuel has a smaller peak burnup. For example, at an average of 50 MWd/kg, the peak RIM burnup of solid and IXAF fuel are ~90 MWd/kg and ~75 MWd/kg. This appears to be an advantage of IXAF fuel since the burnup-related microstructure evolution in the IXAF fuel is slower than that of the solid fuel. The threshold of the average fuel burnup is therefore expected to be higher for the IXAF case.

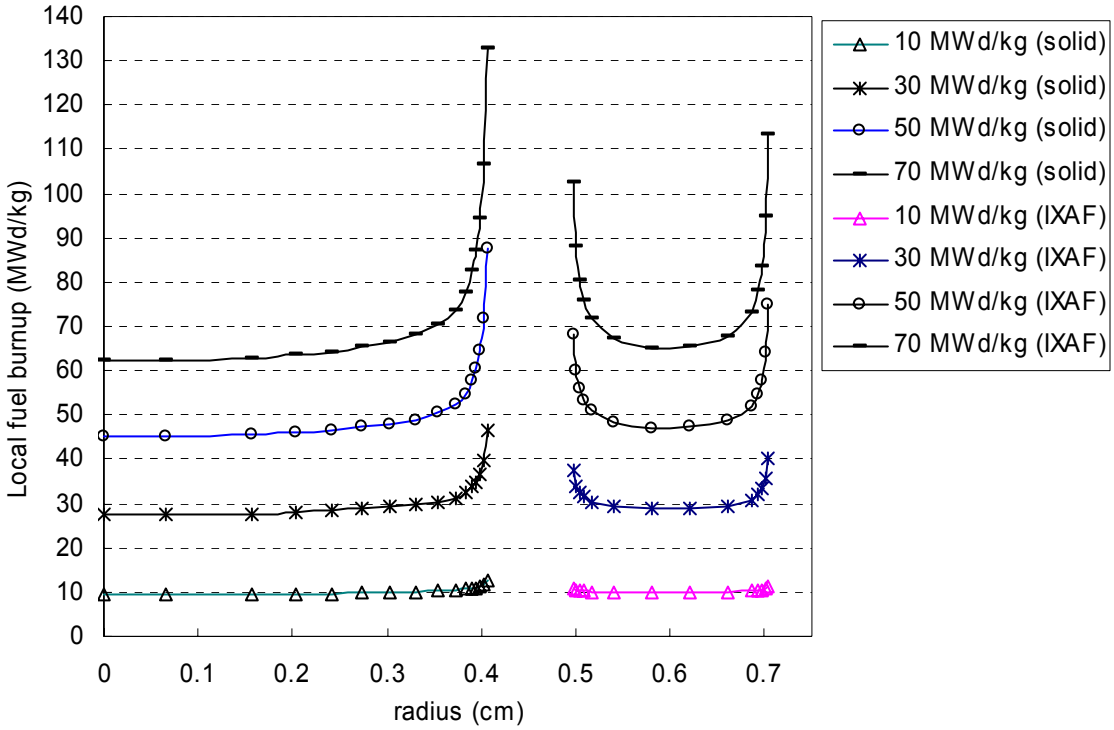

Figure 5.15 Local burnup distribution in the fuel pellet.

In fact the small peak-to-average local power/burnup is expected for the IXAF fuel. Since the moderator (water) is now divided into two separate channels, the slowing down power of each channel will be weaker compared to the solid fuel pin. Hence the epithermal neutron flux on each side of fuel surface will be smaller. Figure 5.16 shows the local conversion ratio at BOL. Although the IXAF fuel has an average CR of 0.414 (greater than that of the reference solid fuel), the peak CR in the RIM region is nevertheless smaller than that of the solid fuel.

Similarly a series of plutonium profiles is shown in Fig. 5.17(a)-(c) at various burnups. All calculations are with MCODE (MCNP+ORIGEN) since CASMO-4 cannot predict the plutonium formation on the inner fuel surface.

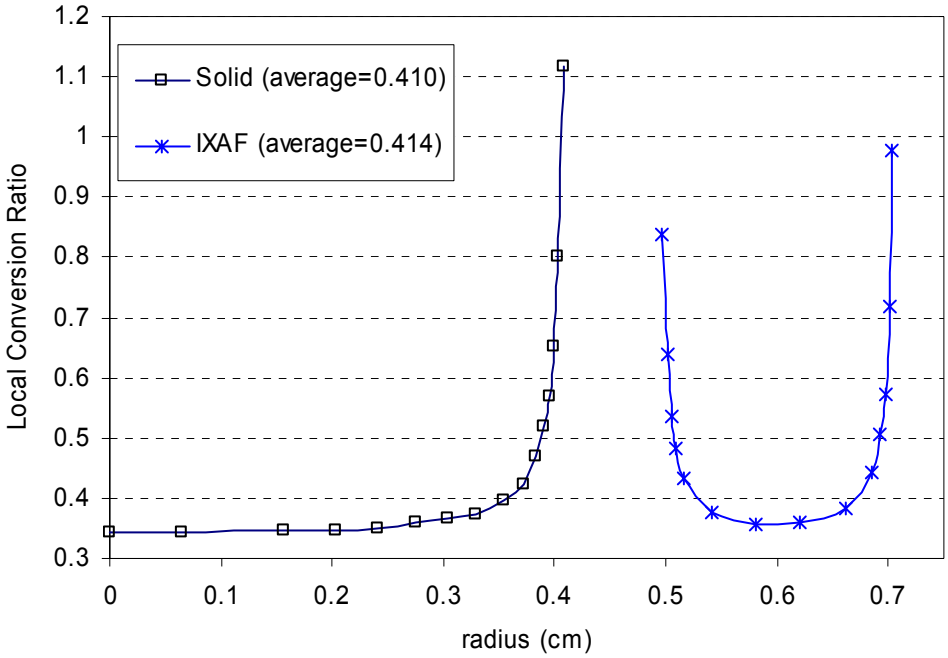

Figure 5.16 Local conversion ratio at BOL for the solid and IXAF cases.

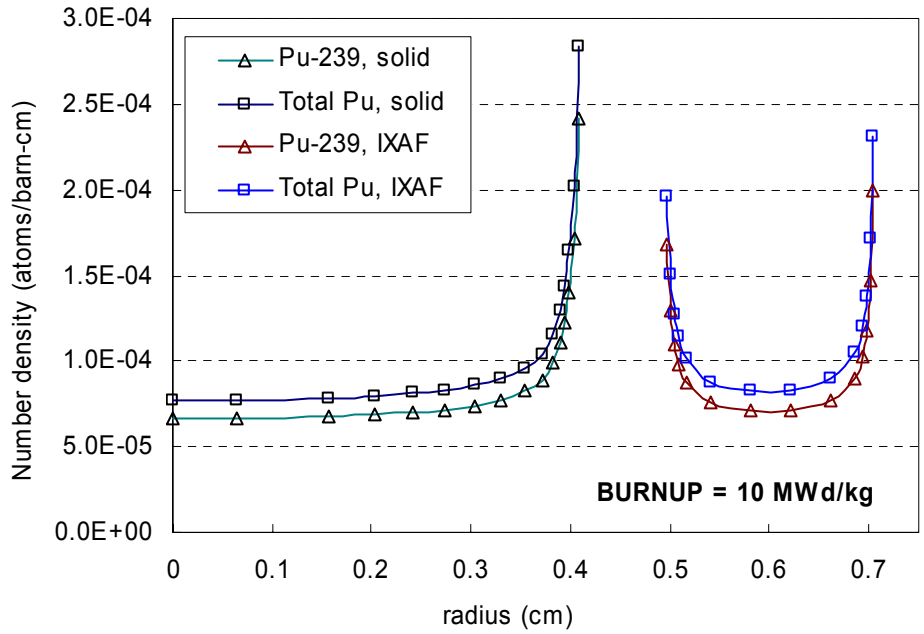

Figure 5.17 (a) Plutonium distribution at 10 MWd/kg.

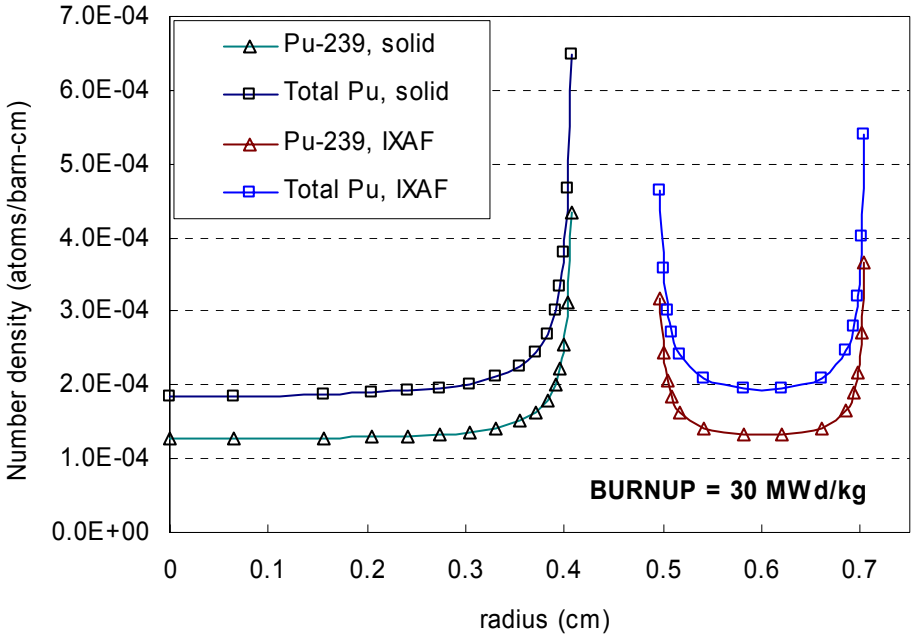

Figure 5.17 (b) Plutonium distribution at 30 MWd/kg.

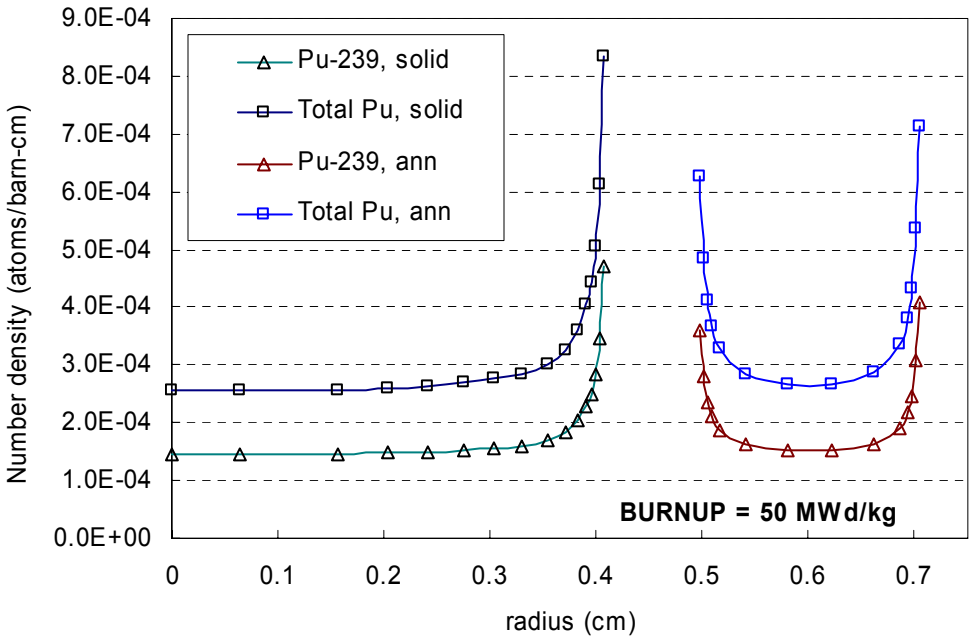

Figure 5.17 (c) Plutonium distribution at 50 MWd/kg.

5.5 Chapter Summary

Three new fuel forms were discussed in this chapter, all of which can be used to achieve a wetter lattice. The IMF approach is still undergoing R&D and testing. The fabrication cost of this fuel is of considerable uncertainty. Currently the main application of the IMF is for plutonium burning and minor actinides transmutation. Annular pellets with a central void have been used in industry, but it appears that optimizing the solid pellet and pin diameter is better than this approach in terms of economics. However, if thermal hydraulic constraints are of concern, the annular pellet can still provide certain advantages since it avoids the loss of heat transfer area. The IXAF fuel is a recent development which can significantly lower the fuel temperature. While its reactivity (neutronically) is somewhat inferior to solid fuel pellets, its conversion ratio is higher and the optimization space for IXAF fuel is larger than that for solid fuel.

The traditional design trend of implementing a wetter lattice is to increase the number of pin cells in an assembly (but with a smaller-diameter fuel rod). Further increasing the number of fuel pins from the current 17×17 lattice leads to mechanical problems in assembly structural design. However, under the future deregulated electricity market, power uprate is an attractive option to improve economics, which requires more margins to operate the core. The IXAF fuel is a promising candidate to provide the capability of operating at a high power level. The annular fuel without internal cooling has a narrower range for upgrading power. Therefore, although neutronically not advantageous compared to other options, the IXAF design is still the most attractive. Its low fuel temperature and distinct RIM characteristics are helpful to withstanding high burnup.

6. Practical Issues of High Burnup in Wetter Lattices

"Reality is a sliding door"
— R. W. Emerson (1803-1882)

6.1 Introduction

Following the preceding neutronic investigation of several candidate wetter lattice designs, practical issues and constraints are considered in this chapter which includes reactivity control and engineering constraints (heat transfer and fuel performance) affecting lattice optimization.

As discussed in Chapter 2, three means of control are available in typical PWRs. However, burnable poison and soluble poison issues are the main focus here. The control rods, although important, are not discussed. Since only about one quarter of the fuel assemblies have control rods in a typical PWR core, one can in future designs potentially increase the number of control rods significantly (a much larger option space). Blacker materials than the traditional Ag-In-Cd (AIC) alloy, such as B_4C with enriched B-10, are also available for use. Therefore, the preservation of shutdown margins in high burnup cores does not appear to be a problem from the control rod perspective. One should also be aware that the fuel lattice design can affect the reactivity control. Wetter lattices have a higher initial excess reactivity due to their reduced conversion ratio. Higher burnup itself is also a challenging problem in terms of reactivity control.

The engineering aspects of wetter lattices are also of concern. Although more water is available for wetter lattices, the heat transfer margin, MDNBR, is more affected by the heat transfer area. For the same thermal energy output, there are certain constraints associated with each variation of wetter lattice implementation. Generally the major engineering constraints on thermal power output of a PWR include [123]:

- fuel centerline melting
- heat transfer limit expressed as DNB ratio (DNBR) under both normal and anticipated transient occurrences

- burnup and fission gas release limits.

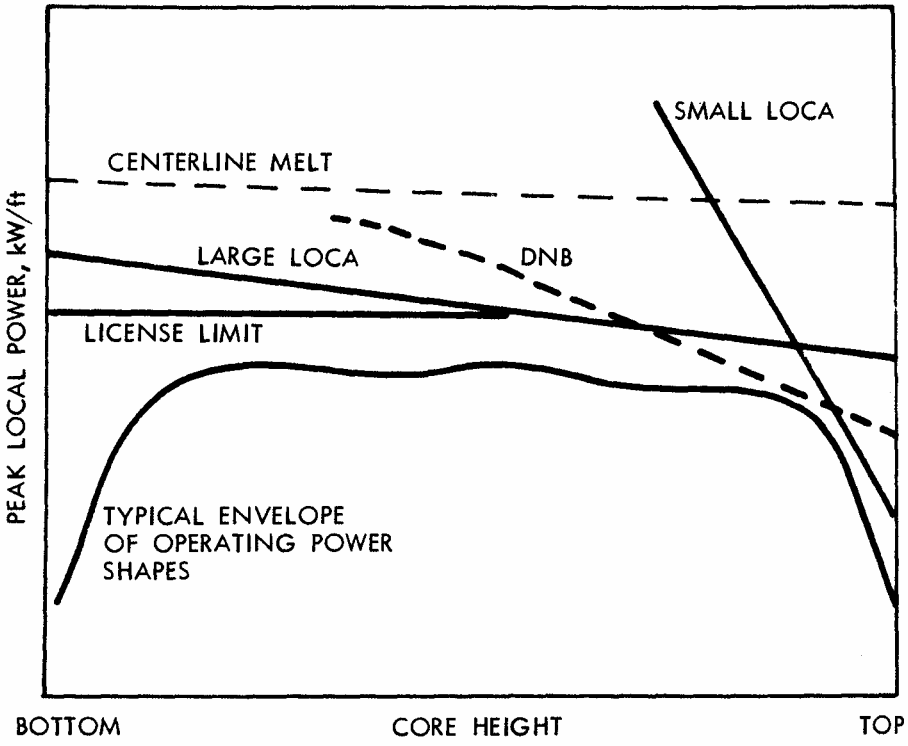

Figure 6.1 Schematic demonstration of various linear power limits [123].

Fig. 6.1 shows typical linear power limits related to heat transfer margin (both steady-state and transient conditions) and fuel centerline melting. It is seen that for conventional PWRs fuel centerline melting is not a limiting factor (well above the large LOCA limit).

An exploration of wetter lattice properties is described, dealing with engineering constraints on allowable operating regimes. Several design variations, including varying pin pitch, rod diameter, using annular fuel (central void), and using IXAF fuel, are considered based on UO_2 fuel. Those options were then examined using VIPRE and FRAPCON to quantitatively determine allowable operating regimes. Heat transfer limits (MDNBR), coolant pressure drop across the core, fuel pin internal pressure, and maximum fuel temperature are taken as basic criteria to judge the practicality of operating regimes assuming that 1) the average core power density is conserved; and 2) the same coolant conditions (same inlet/outlet water temperature) are specified. It should be noted that there is a large technical improvement potential in fuel design, such as the fuel and

cladding material. Some situations, although not practical today, might become promising in the future.

6.2 Neutronic Reactivity Control

6.2.1 Introduction

The first important factor in considering reactivity control is the fuel management scheme. As mentioned in Chapter 1, there are four principal specific options by which to exploit high burnup capabilities:

1. Increase cycle length at the same linear power, use current 3-batch fuel management;
2. Keep current cycle length and linear power, increase the number of staggered batches;
3. Design a very long life core, single-batch refuel at a reduced power density;
4. Increase power density (burn faster) and keep the same cycle length and refueling rate.

The primary goal of neutronic reactivity control is to maintain a critical core condition, i.e., $k_{\text{eff}} = 1$. The beginning-of-cycle (BOC), free-of-poison excess reactivity roughly gives the maximum amount of poison required, which is estimated according to the linear reactivity model as [49]:

$$\Delta\rho_{\text{c}} = AB_{\text{c}} = \frac{2}{n+1}\rho_0, \tag{6.1}$$

where A = the slope of the burnup curve ($|d\rho/dB|$),

B_{c} = the cycle burnup,

n = number of batches,

ρ_0 = the free-of-poison reactivity of a fresh batch.

For PWRs having the same fuel design, the conversion ratio variations are small. Therefore, as a first order approximation, the cycle excess reactivity is proportional to the cycle burnup. Eq. (6.1) also suggests that for a fixed ρ_0 (same fuel type) the larger the number n the smaller is the BOC reactivity. From this perspective a continuous refueling scheme ($n\rightarrow\infty$) is best (easiest to control).

For current PWRs, the cycle length is 12, 18, or 24 months (mostly 18 months in the US). Going to a wetter lattice (reduced fuel loading) at a fixed cycle length leads to a higher cycle burnup than the conventional lattice. Usually more fuel loading or higher

enrichment is required to compensate for the loss of the energy production in a wetter lattice. In addition the conversion ratio is slightly reduced (larger A) in wetter lattices. In combination, the BOC excess reactivity is larger for wetter lattices. In this regard, options 1, 3, and 4 all have a difficult control problem. In particular, option 3 — a single-batch core with a very high cycle burnup — poses a challenge as demonstrated in Refs. [8, 12]. To date, there have been no commercial PWRs operating with a longer cycle than 24 months. Hence, it turns out that option 2 (same cycle length) is the most practical approach. Besides BOC reactivity control, other limitations of neutronic character such as the need to have a negative MTC are imposed throughout the entire cycle. Since the soluble boron is limited to ~2000 ppm from both technical reasons involving water chemistry and the safety implications of MTC, burnable poison is usually needed for current core designs. Burnable poison is also used to control the power distribution between fresh and burnt assemblies.

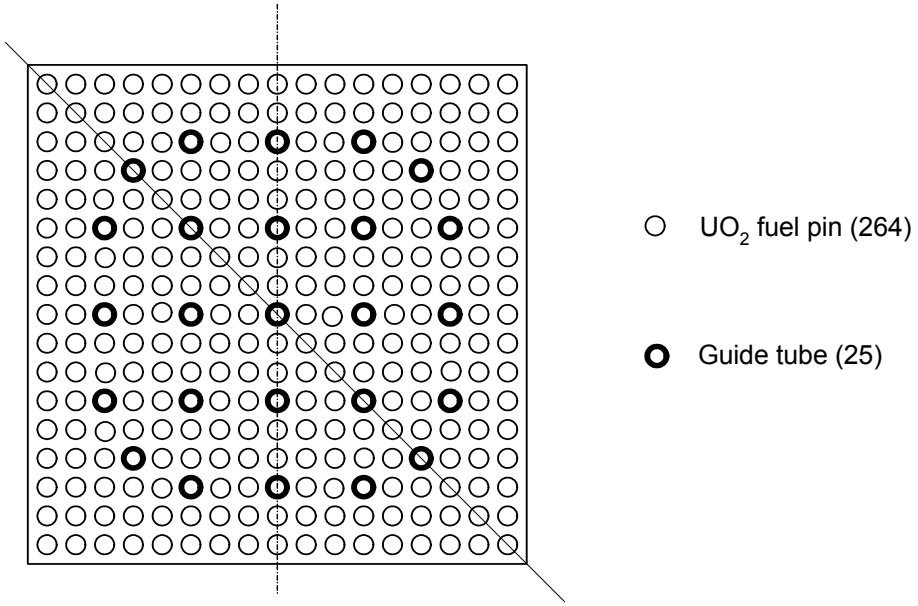

Figure 6.2 Standard Westinghouse 17×17 assembly model.

Calculations reported here are based on a 4-Loop Westinghouse PWR assembly model (17×17 lattice as shown in Fig. 6.2). The CASMO-4 code actually uses one eighth of the whole assembly to do transport calculations. Various H/HM values are achieved only by varying the rod diameter. The reference 18-month PWR assembly uses 4.5 w/o

UO_2 fuel, and the high burnup assembly uses 9.75 w/o UO_2 fuel. The high burnup case is also based on an 18 month cycle with the same thermal energy output (option 2, the most practical approach from a reactivity control point of view). The assembly power is conserved for all calculations. Therefore, the energy production can be expressed as the effective full power cycle length. Note that the reference design H/HM for an assembly is 4.1 rather than 3.4 (pin value) because of additional water in the guide tubes. Figure 6.3 shows the poison-free burnup curves for 4.5 w/o and 9.75 w/o UO_2 cases based on the conventional assembly design (H/HM = 4.1). It can be seen that the 9.75 w/o case roughly doubles the burnup of the 4.5 w/o case. Figure 6.3 also suggests that if the cycle length (cycle burnup) is kept the same as the typical 18 month cycle, the BOC reactivity will be smaller in magnitude due to an increased conversion ratio (harder spectrum).

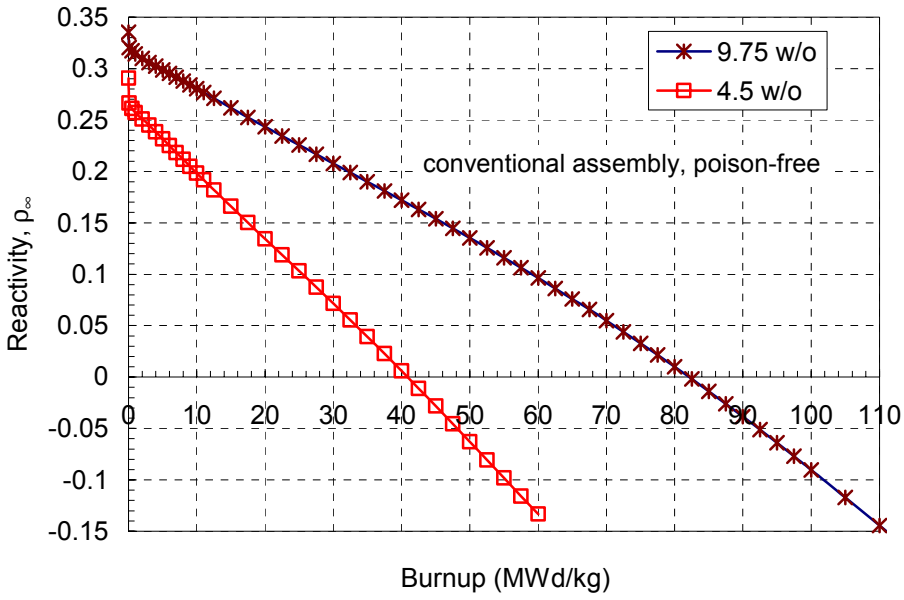

Figure 6.3 Depletion histories of 18-month PWR fuel and high burnup fuel.

6.2.2 Burnable-Poison-Free Core Analysis

It was shown in Chapters 4 and 5 that a wetter lattice leads to a shortened cycle length although the burnup potential is increased. The BOC reactivity is larger for a wetter lattice. However, it is not clear that the BOC core reactivity control will be more difficult because the softer neutron spectrum of a wetter lattice increases the poison worth. In this

section, the neutron spectrum effects of wetter lattices are investigated from the reactivity control point of view. Burnable poison is not considered in this section.

Starting with the conventional assembly design, one can increase H/HM values by reducing the fuel rod diameter to achieve wetter lattices. In this variation, the gap and clad thicknesses are kept constant. The guide tubes also remain the same. The core is operating on an 18 month cycle with a capacity factor of 87%, i.e.,

$$(30.44\,\text{days/month})\times(18\,\text{months/cycle})\times 87\% = 476.7\,\text{EFPD/cycle}.$$

The cycle burnup is then calculated as follows:

$$B_c = 30.44\times 10^{-3}\,\frac{q_P}{\rho_{IHM}}\,T_c L\,, \tag{6.2}$$

where q_P = the core average power density (104.5 kW/liter-core),

ρ_{IHM} = the initial heavy metal density averaged over the core volume (g/cm^3-core),

T_c = the calendar cycle length (18 months, defined as 30.44 days/month),

L = the capacity factor (87%).

The ρ_{IHM} depends on the fuel design. Wetter lattices have smaller ρ_{IHM}. It can be expressed as the ratio between the power density and the specific power (burnup rate):

$$\rho_{IHM} = \frac{q_P}{q_{SP}}\,, \tag{6.3}$$

where q_{SP} = the specific power (W/gIHM ≡ kW/kgIHM).

The single batch discharge burnup, B_1, is estimated from the assembly burnup curve where $\rho_\infty = 0.03$ (3% leakage). The discharge burnup and the number of batches are then computed by:

$$B_d = 2B_1 - B_c\,, \tag{6.4}$$

$$n = \frac{B_d}{B_c}\,. \tag{6.5}$$

The BOC, poison-free core reactivity is estimated as

$$\Delta\rho_c = \frac{1}{n}\left[\rho_\infty(0) + \rho_\infty(B_c) + \cdots + \rho_\infty\left((n-1)B_c\right)\right] - 0.03\,. \tag{6.6}$$

Similarly one can calculate other neutronic parameters at BOC (poison-free) such as:

- the core critical boron concentration (CBC), i.e., the amount of soluble boron required to make $\rho_\infty = 0.03$;

- the moderator temperature coefficient and the Doppler coefficient.

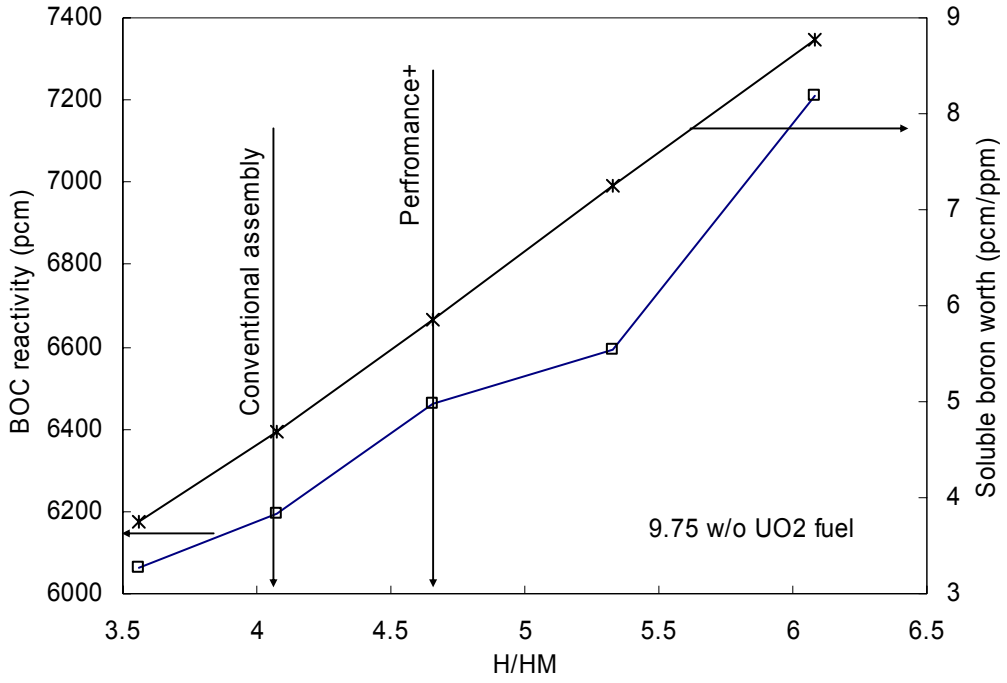

Figure 6.4 BOC reactivity and boron worth as a function of H/HM.

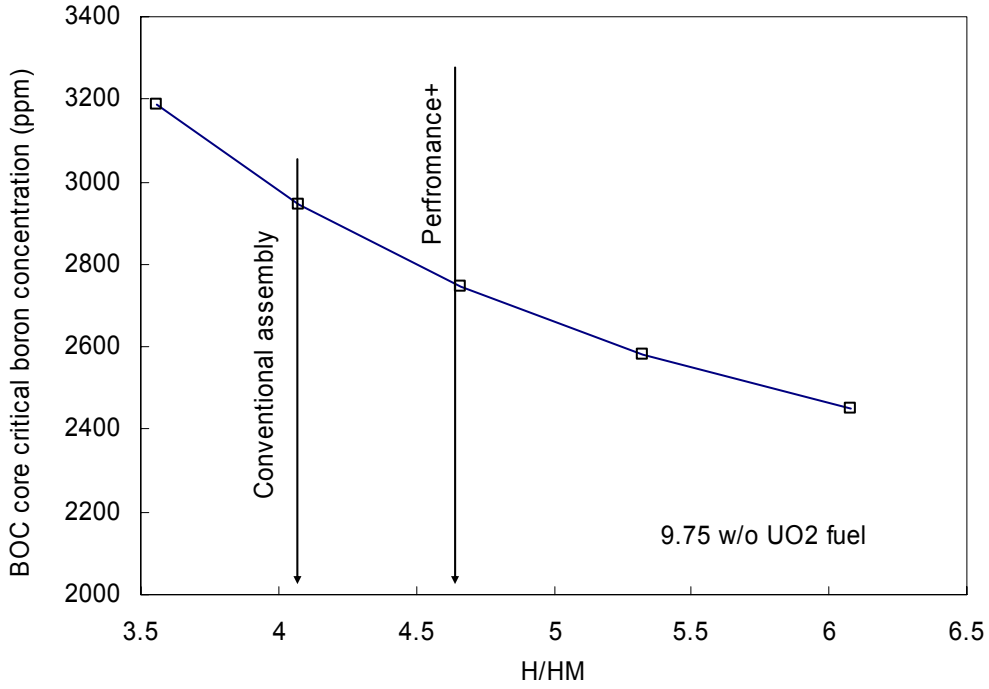

Figure 6.5 BOC core critical boron concentration as a function of H/HM.

Figs. 6.4 and 6.5 show the 18-month-cycle, fresh core boron requirement as a function of H/HM. Both the BOC reactivity and boron worth increase with H/HM. However, the core critical boron concentration decreases with H/HM, which recommends wetter lattices for high burnup cases from a control point of view. In these figures, the Performance+ designation refers to the assembly design with reduced rod diameter by Westinghouse.

Table 6.1 Poison-free, BOC core parameters for various designs (18-month cycle).

	Conventional assembly design		Wetter lattice*
	Conventional PWR	High burnup	High burnup
Enrichment (w/o)	4.5	9.75	9.75
H/HM	4.07	4.07	4.66
Specific power (W/gIHM)	38.2	38.2	41.7
B_c (MWd/kg)	18.23	18.23	19.88
Number of batches, n	3.0	7.3	6.9
BOC reactivity, $\Delta\rho_c$ (pcm)	12,555	6,193	6,463
Boron worth (pcm/ppm)	6.7	4.7	5.9
Critical boron (ppm)	2,164	2,944	2,745
Max boron (MTC=0) (ppm)	2,260	4,037	3,082
MTC (pcm/K)	−52.2	−67.2	−62.0
FTC (pcm/K)	−2.2	−2.4	−2.3

∗ This is the optimized Westinghouse Performance+ design.

Table 6.1 summarizes the BOC neutronic parameters for high burnup cases and the reference conventional 18-month cycle PWR. The wetter lattice here refers to the Westinghouse Performance+ design. An increased specific power (burnup rate) is observed for the wetter lattice, which consequently increases the cycle burnup for the 18-month cycle. Although both high burnup cases use the same 9.75 w/o UO_2 fuel, the wetter lattice has a slightly smaller value of n, i.e., more fresh fuel assemblies are needed during the refueling.

Due to the much smaller conversion ratio of high burnup cores (9.75 w/o), i.e., a smaller $|\Delta\rho/\Delta B|$, the BOC reactivity of a conventional core is twice that of the high burnup cases. The neutron spectrum of the high burnup cases, in general, is harder than the conventional core due to their high fissile contents (in order to compensate for their increased fission product inventory). Therefore, the boron worth is lower for the high

burnup cases. The wetter lattice improves the effectiveness of the poison. Overall the critical boron concentration of the high burnup cases is still larger than that of the conventional core. The wetter-lattice high burnup case, however, has a smaller critical boron concentration than the normal-lattice high burnup case. It should also be noted that there is more room for soluble boron addition in a wetter lattice. The critical boron concentrations are all under the maximum allowable boron concentration in terms of MTC.

The MTC for high burnup cases (harder spectrum) is more negative than that of the conventional core. The impact of soluble boron on the MTC is expected to be smaller for the high burnup cases because of their harder spectrum (reduced boron worth). Typically it is desired to ensure the MTC be within a certain window compared to the conventional core since both too large and too small MTC values might aggravate accidents under different scenarios. For 9.75 w/o fuel, there is still room to be wetter in order to have a comparable MTC to the conventional core. The FTC is almost the same for all cases.

6.2.3 Poisoning the Core

Table 6.1 shows that a burnable poison is necessary to reduce the soluble boron concentration (hence achieve an acceptable MTC) even for a conventional PWR design. Besides reactivity control, burnable poison is also required for the purpose of power peaking control. To get a higher discharge burnup for the same cycle energy production, a higher enrichment is needed. This increases the reactivity difference (poison-free) between the fresh and most burned fuel in the core. Therefore power peaking control by burnable poison is necessary. According to Ref. [124], for a typical large Westinghouse PWR core with discharge burnups of 40 to 50 MWd/kg, it is power peaking that determined equilibrium burnable poison requirements for a 12 month cycle using IFBA, but MTC that determines burnable poison for an 18 month cycle using gadolinium. Table 6.2 summarizes the limiting criteria encountered in low-leakage loading pattern (L^3P) PWR cores when determining the equilibrium fuel cycle plans for various burnable absorber designs.

Table 6.2 Fuel cycle limiting criteria [124].

Burnable Absorber	12-month	18-month	24-month
IFBA	Power Peaking	Power Peaking	MTC
Erbium	Power Peaking	MTC	MTC
Gadolinium	Power Peaking	MTC	MTC

Whether MTC or power peaking is the controlling factor has an interesting effect on how long the burnable poison must control the reactivity. Since unpoisoned excess reactivity decreases continuously as the cycle depletes, the need for MTC control disappears within the first 25 or 50% of the cycle length except for an ultra long cycle. The need for power peaking control usually lasts over the entire cycle, and is occasionally worse toward the end of cycle if the reactivity of the fresh fuel actually rises during depletion. Note, however, that a core whose burnable poison requirement is MTC controlled at BOC may be peaking controlled starting some time in the middle of the cycle.

The longest period the burnable poison has to control reactivity is the burnup achieved by an assembly during its first cycle in core. If the burnable poison takes longer to burn out, it would be holding down unnecessary residual reactivity at EOC and thereby shortening the cycle. For large, non-uprated, Westinghouse PWRs, a conservatively large cycle burnup for a high capacity factor plant is about 20 MWd/kg. The hot assembly might have a relative power of 1.5. Thus the hot assembly would achieve a burnup of about 30 MWd/kg. So to control power for the entire cycle, the burnable poison should not burn out before this burnup. If axial peaking is important, one can raise this by perhaps another 25%, in which case, the burnable poison has to last for 30 to 40 MWd/kg.

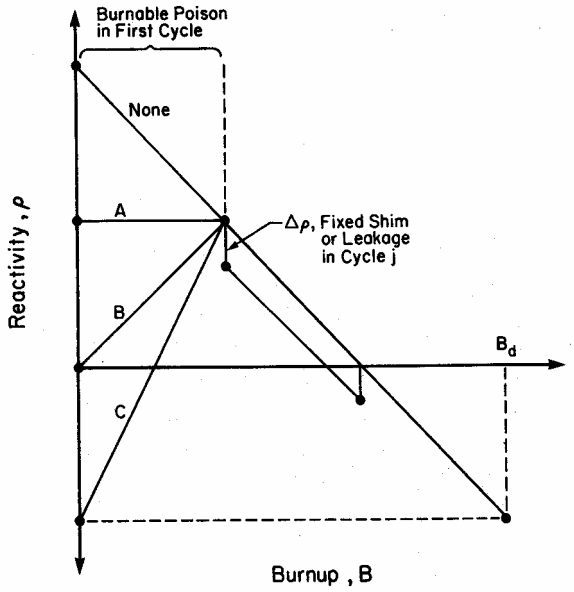

Figure 6.6 Range of burnable poison control trajectories using LRM [49].

Using the linear reactivity model [49], one can understand burnable poison usage from Fig. 6.6 (a typical 3-batch PWR core). Three burnable poison traces are shown as A, B, and C. If about same amount of burnable poison material is used,

$$\sigma_a^{BP}(A) < \sigma_a^{BP}(B) < \sigma_a^{BP}(C).$$

Trace A has the most uniform power history while trace C has the highest discharge burnup. In principle, the equilibrium cycle core reactivity can be controlled entirely by burnable poison for trace C, resulting in the elimination of the soluble boron system, which represents a considerable saving in both capital and operating costs [125, 126]. With no soluble boron in water, the core has a strong negative MTC. However, there are other considerations in core design. The assembly reactivity (hence power) swing is the largest for trace C. An actual assembly with such heavy poison loading will suffer from the reduction of power-generating pins. Hence the peak unpoisoned pin in the assembly runs hotter. Current industry practice all aims at achieving trace A, which has a flat power shape. Upon selection of an appropriate burnable poison loading pattern, depletion histories similar to trace A will be chosen.

In general, the neutronic requirements of burnable poison are: (1) strong neutron absorption to reduce the BOC reactivity; (2) suitable burnup time dependence during core operation; (3) minimal residual at the EOC. Although the amount of burnable poison is usually set based on the initial excess reactivity, the type and distribution of the burnable poison are open to discussion. For wetter lattices burnable poison usage is a crucial factor and has not been fully addressed in the past.

Three burnable poison candidates are under consideration: Integral Fuel Burnable Absorbers (IFBA), Gd_2O_3, and Er_2O_3. The key absorbers are boron, gadolinium, and erbium. The neutronic characteristics for these three elements are shown in Table 6.3 [127]. It is seen that the neutron absorbers are B-10, Gd-155, Gd-157, and Er-167; each of these nuclides has its particular characteristics.

- Gd-155, Gd-157 [128]
  - — Widely used in industry, especially in BWRs; hence has a mature manufacturing technology

— Large absorption cross section, which makes the material thermally "black". The required loading to hold down the initial reactivity is minimum. Therefore, fuel displacement can be reduced.

— Depletion rate might be too fast in an inappropriate burnable poison design.

— Degradation of material properties (the thermal conductivity and the melting temperature) when mixed with UO_2. Common design practice is to maintain the power in the gadolinium bearing fuel 10% to 15% below the hottest UO_2 fuel pin.

- B-10
  — With much lower cross section than Gd-155/Gd-157, some thermal neutrons are allowed to penetrate (a "gray" absorber).
  — The difficulty for B-10 is that the predominant type of neutron absorption is (n,α). The released helium gas results in an increase of internal rod pressure, which imposes a constraint on the amount of B-10 loading.
- Er-167
  — Relatively low thermal absorption and high resonance integral, which is beneficial for improving the MTC and more suitable for long cycles.

Table 6.3 Properties of boron, gadolinium, and erbium [127].

Element	Isotope	Half-life	Abundance (atom%)	Thermal* σ_a (barns)	Resonance Integral (barns)
Boron	——	——	100	760	343
	B-10	Stable	19.9	3840	1730
	B-11	Stable	80.1	0.005	0.002
Gadolinium	——	——	100	49000	400
	Gd-152	1.1×10^{14} yr	0.20	700	700
	Gd-154	Stable	2.18	60	230
	Gd-155	Stable	14.80	61000	1540
	Gd-156	Stable	20.47	2	100
	Gd-157	Stable	15.65	255000	800
	Gd-158	Stable	24.84	2.4	70
	Gd-160	Stable	21.86	1	8
Erbium	——	——	100	160	740
	Er-162	Stable	0.14	19	500
	Er-164	Stable	1.61	13	110
	Er-166	Stable	33.6	20	100
	Er-167	Stable	22.95	670	3000
	Er-168	Stable	26.8	2.3	37
	Er-170	Stable	14.9	6	30

∗ Thermal refers to thermal neutrons at 2200 m/sec or 0.025 eV.

Figure 6.7 shows detailed absorption cross sections for these nuclides in the thermal energy range. At 0.025 eV, Gd-157 has a higher capture cross section: two orders of magnitude larger than B-10.

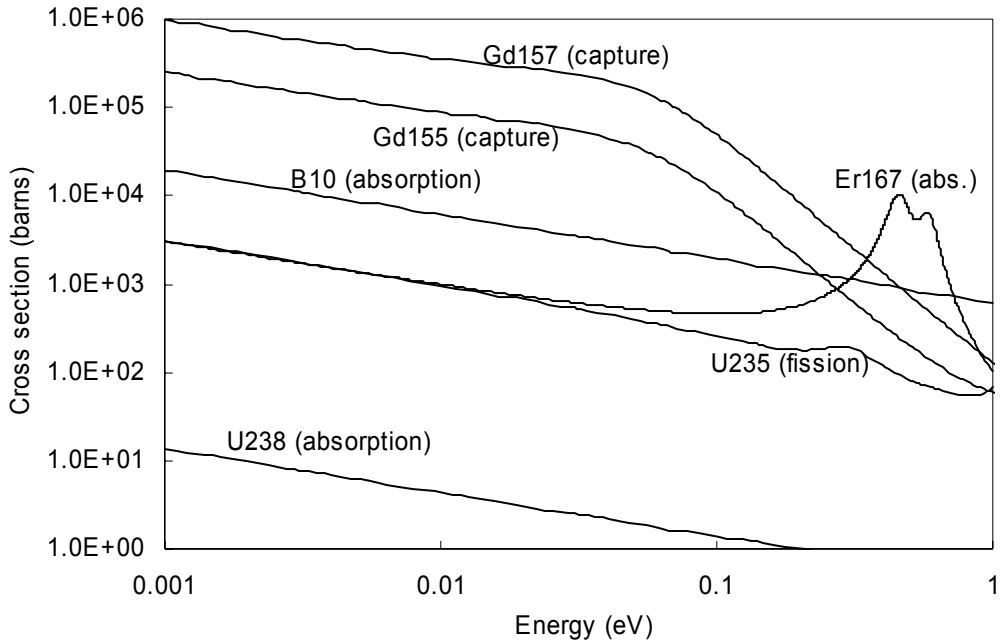

Figure 6.7 Cross sections of various nuclides in the thermal energy range (ENDF/B-IV).

Three types of fuel assemblies are modeled and compared to estimate core performance of burnable poison usage in an 18-month cycle:

- conventional PWR fuel assembly (H/HM=4.07), with 4.5 w/o UO_2, (denoted as REF);
- conventional fuel assembly design (H/HM=4.07), high burnup case with 9.75 w/o UO_2 (denoted as HB-REF);
- wetter lattice design (Westinghouse Performance+, H/HM=4.66), high burnup case with 9.75 w/o UO_2 (denoted as HB-WET).

As shown in Fig. 6.6, the poisoned fuel has a higher than core-average reactivity (trace A, current industry practice), which leads to a higher relative power for fresh fuel assemblies (1.2 for typical Westinghouse PWRs). The relative power of hot fresh fuel assemblies depends on the specific fuel loading patterns and can be as high as 1.5 for a low leakage loading pattern. This value is assumed to be 1.4 for estimation of BP requirements. Thus the burn-out point of burnable poison is $1.4B_c$. Using the poison-free cycle burnup values

in Table 6.1, the burn-out points of these three fuel assemblies are 25.5 MWd/kg (for REF and HB-REF) and 27.8 MWd/kg (for HB-WET). Calculations for the high burnup case with a conventional fuel assembly (HB-REF) are first made for each individual BP candidate to illustrate basic physics characteristics. An intercomparison among the three BP candidates then follows.

IFBA

Westinghouse manufactures IFBAs by applying a thin layer of zirconium diboride (ZrB_2) to fuel pellets using a self-designed, patented process. The coating adheres strongly and is highly compatible with the fuel pellet and cladding. The IFBA coating does not affect pellet manufacturing or enrichment, since it is applied to otherwise finished pellets. Compared to Gd_2O_3 or Er_2O_3, it burns out completely at EOC (essentially no residual absorption penalty). IFBA doesn't occupy guide thimbles so that the core-loading pattern is very flexible. It has been widely used in current nuclear power plants. The IFBA experience in PWRs is substantially greater than the industry-wide use of gadolinia and erbia. For high burnup cores, IFBA is a good choice if it is capable of controlling the initial excessive reactivity.

A significant drawback of IFBA is its helium production via the (n, α) helium-producing reaction of B-10, which exerts an additional pressure on the cladding. Hence, Westinghouse limits the IFBA loading to below 2X (1X corresponds to 1.545 mg-B^{10}/inch). In our calculations, the ZrB_2 layer thickness is taken as 0.015 mm.

Two IFBA loading patterns are considered for the high burnup case (HB-REF): one with 156 IFBA rods and other with all IFBA rods (264). Results are shown in Figs. 6.8 and 6.9 respectively. As far as the holddown time is concerned, it appears that 0.5X or 1.0X would be adequate for the 18-month cycle. Comparing these two BP loadings, the burn-out time for the same amount of B-10 loading is roughly the same, which is due to the gray absorber nature of B-10.

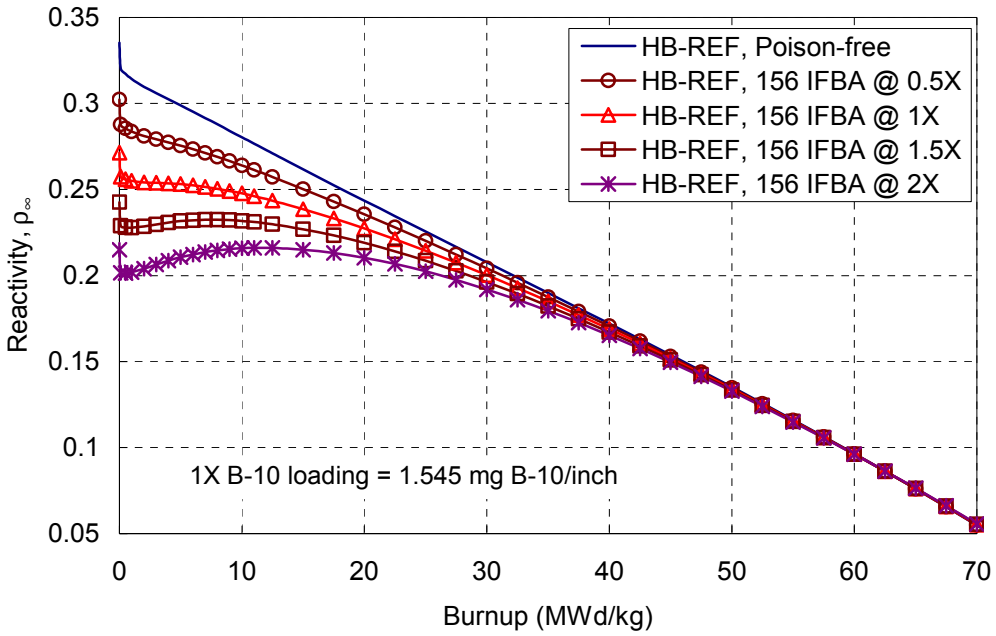

Figure 6.8 Depletion curves for HB-REF case with 156 IFBA rods.

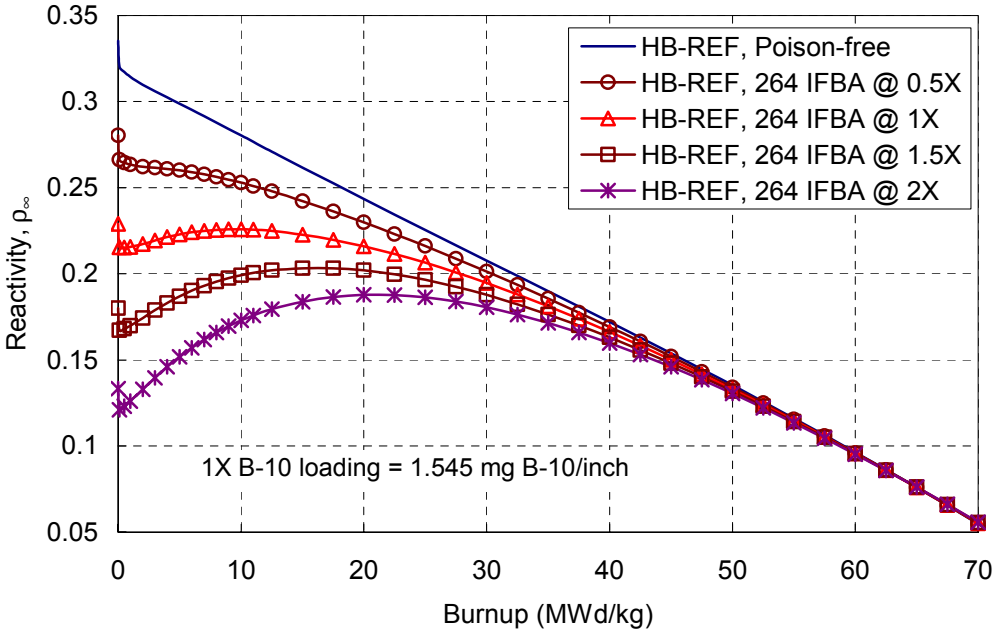

Figure 6.9 Depletion curves for HB-REF case with all IFBA rods.

Gadolinium Oxide (Gd_2O_3)

Gadolinium has a large absorption cross section as shown in Fig. 6.7. As a burnable poison, it is used in the form of its oxide (Gd_2O_3) at a density of 7.64 g/cm^3. Since gadolinium is a very strong thermal absorber, the number of gadolinium BP pins needed (typically 12 BP pins) is typically small compared to IFBA loading (typically ~100 pins). This provides operational flexibilities when some under-burned pins need to be re-inserted into the core to replace the BP pins in the once-burned assembly during a refueling outage.

As far as the hot-to-cold reactivity swing is concerned, gadolinia is also a better choice than boron. As water cools down and the spectrum is softer (more thermal neutrons), gadolinia remains as a surface absorber, while boron, as a $1/v$ absorber, loses some poison worth as its volume absorption is replaced with surface absorption [129].

One interesting point about gadolinia is that the gadolinia content (in w/o) governs the length of the burnup cycle. The number of BP rods governs the initial negative reactivity. Moreover, only in the case of gadolinia, are these two factors nearly totally unconnected as regards physics [130].

Four types of gadolinia loading layouts are considered: 12, 24, 36, and 48 BP pins (Fig. 6.10). The series of gadolinia contents include 6 wt%, 8 wt%, and 10 wt% loadings, which are shown in Figs. 6.11 to 6.13. The time to burn out gadolinia only depends on the gadolinia content (regardless of the number of gadolinia pins used), whereas more gadolinia pins holds down more reactivity at BOC. The residual burnable poison, however, is roughly proportional to the initial amount of gadolinia.

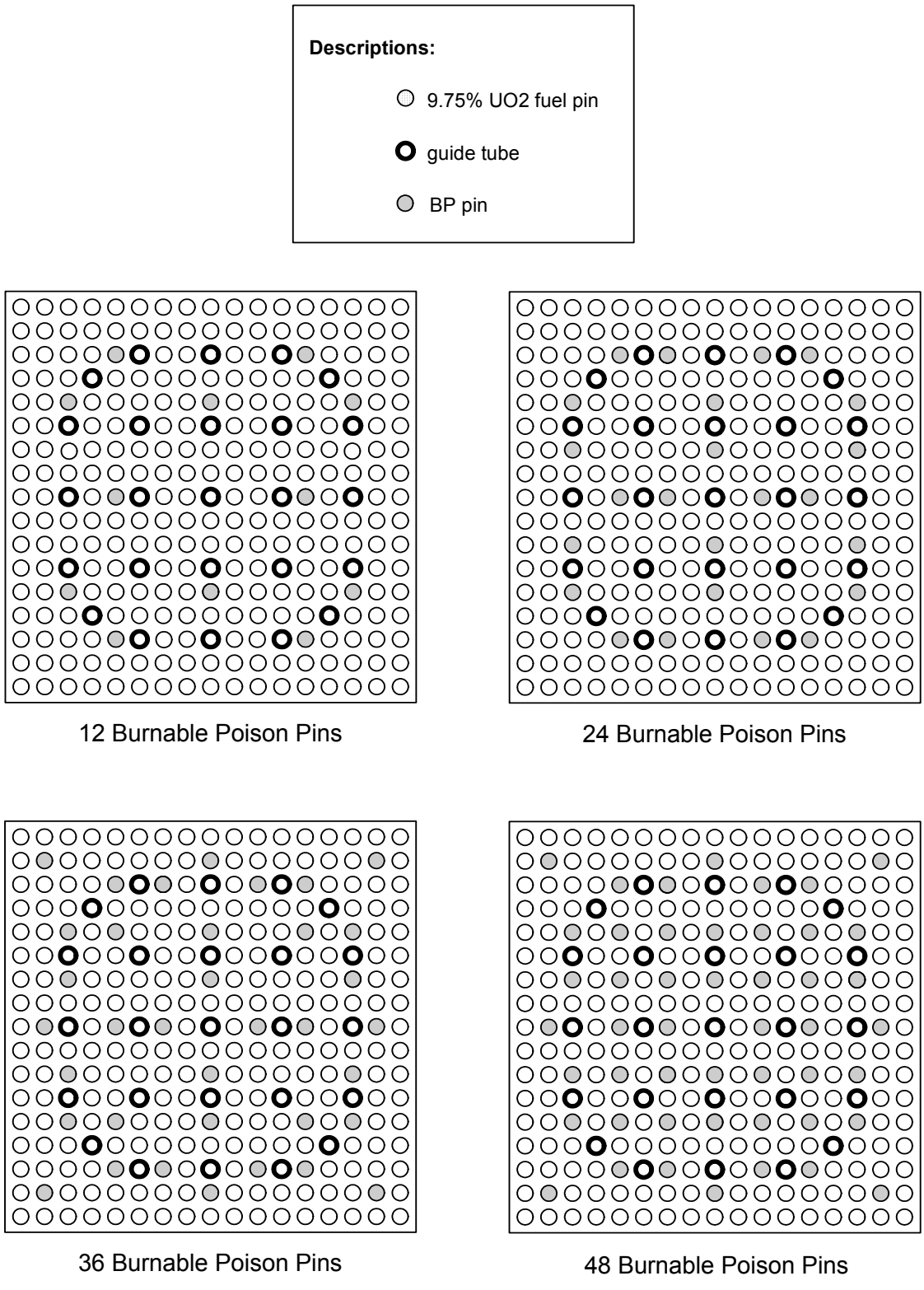

Figure 6.10 Burnable-poison pin layouts.

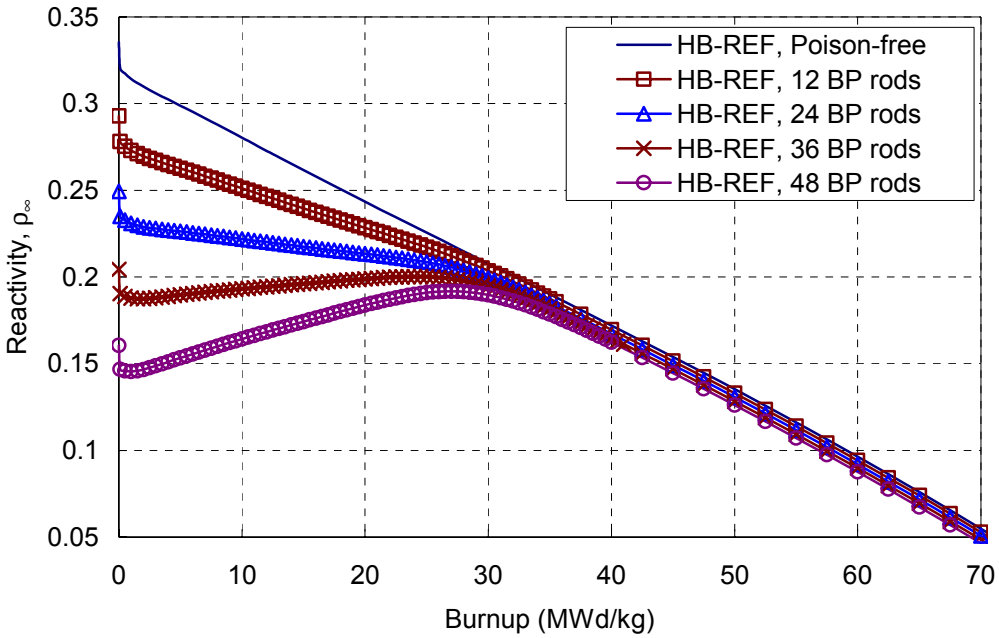

Figure 6.11 $\rho(B)$ histories for burnable poison pins with 6 wt% Gd_2O_3 (9.75 w/o UO2).

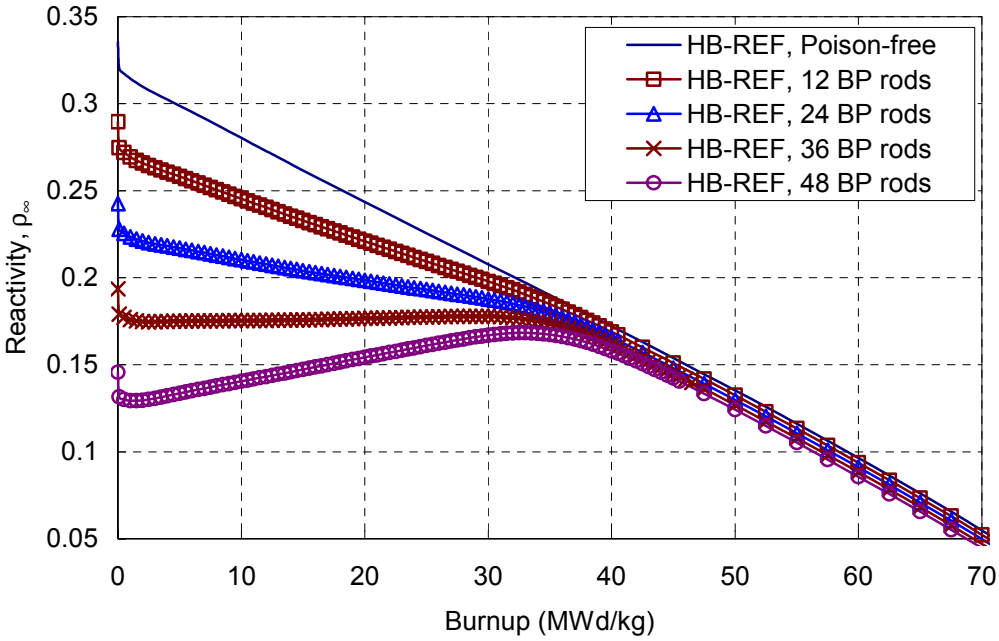

Figure 6.12 $\rho(B)$ histories for burnable poison pins with 8 wt% Gd_2O_3 (9.75 w/o UO2).

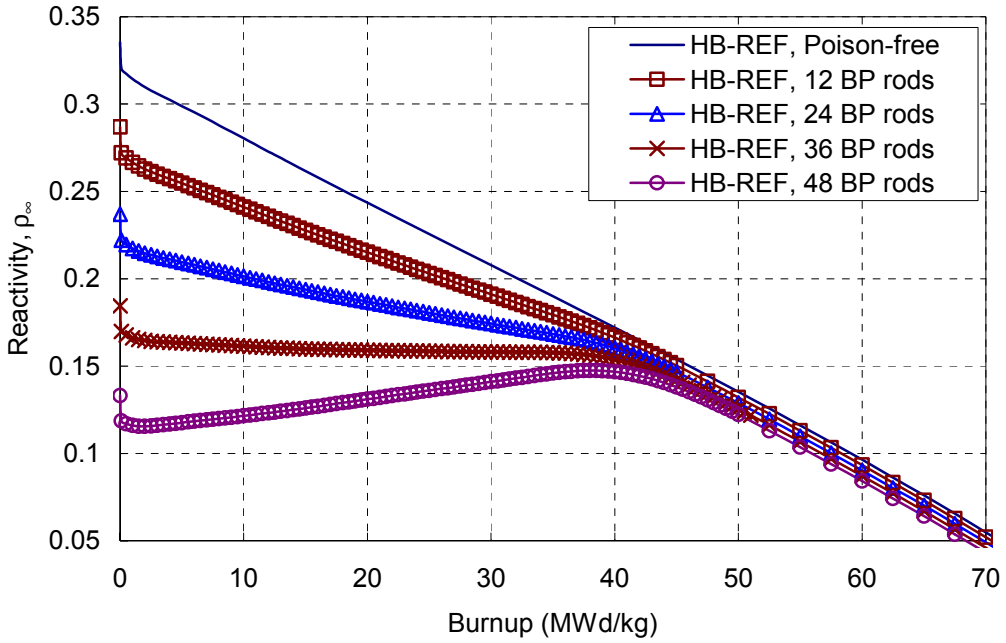

Figure 6.13 $\rho(B)$ histories for burnable poison pins with 10 wt% Gd_2O_3 (9.75 w/o UO2).

Erbium Oxide (Er_2O_3)

The density of erbia is 8.64 g/cm^3 at room temperature. As a primarily resonance absorber, erbia has a relatively small thermal absorption cross section. An appreciable amount of erbia is needed in order to suppress the initial excessive reactivity compared to gadolinium. The EOC residual poison is largest among the three candidates considered here for 18-month cycles. It is preferable to use erbia in a more homogeneous way, i.e., highly diluted but in a large number of rods. Due to its resonance absorption near the 0.3 eV resonance in Pu-239, the MTC can be improved using erbia as BP [130]. This poison is suitable for long cycle control since the burning rate is slow [131].

Based on the above discussion, calculations are made such that all fuel rods in the assembly are poisoned, but with a low erbia content: 0.5 wt%, 1.0 wt%, and 2.0 wt%. Depletion curves are shown in Fig. 6.14. The residual is also seen to be proportional to the amount of erbia loading.

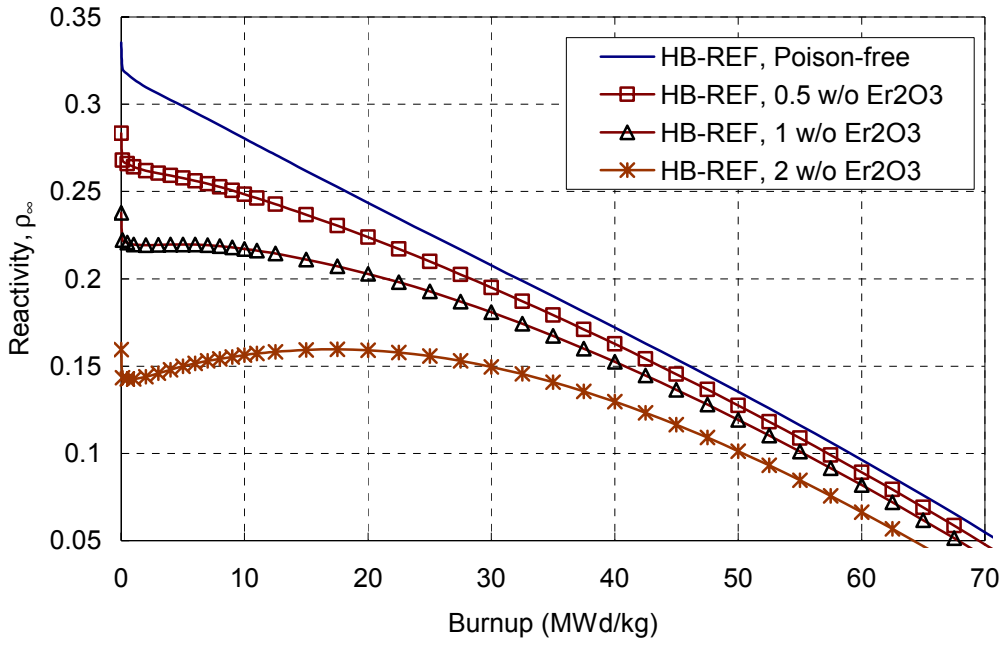

Figure 6.14 $\rho(B)$ histories for all fuel (9.75 w/o UO_2) pins poisoned with erbia.

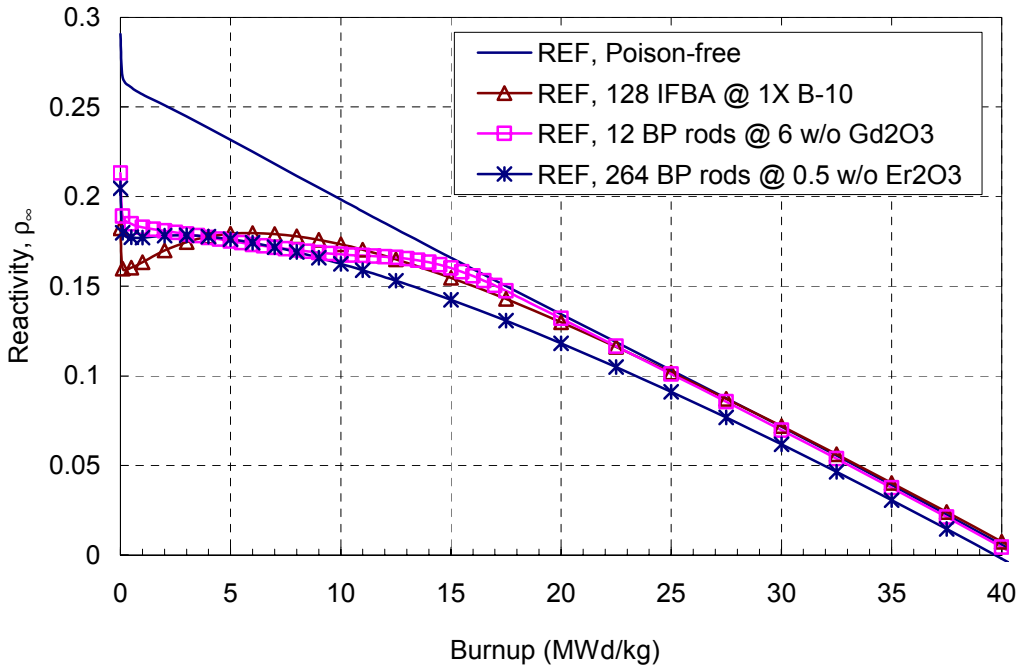

Figure 6.15 Comparisons of burnable poisons in a conventional PWR assembly (4.5 w/o).

An intercomparison of BP candidates in three types of assemblies (REF, HB-REF, HB-WET) has been made.

Figure 6.15 shows depletions of the reference conventional PWR assembly (4.5 w/o UO_2) with different BP candidates. It is seen that both gadolinia and IFBA have a very small EOC residual (they burn out completely) while erbia has a relatively large EOC residual. The neutronic performance of gadolinia is close to IFBA. In industry practice both gadolinia and IFBA are widely used to control 18-month PWR operation. Suffering from a sizable penalty in cycle length, erbia is not as attractive for the conventional PWR 18-month cycle.

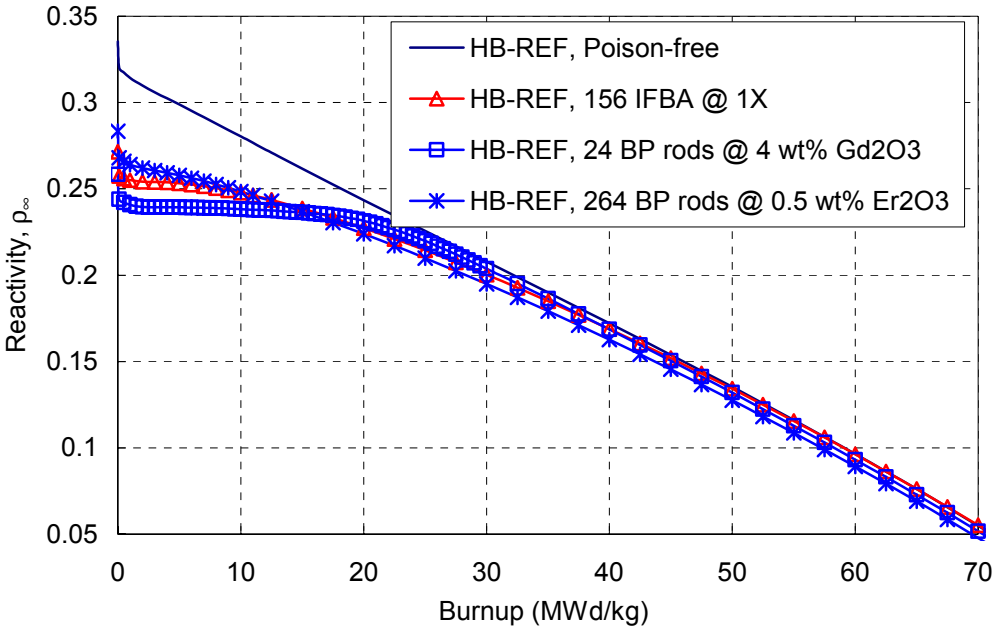

Figure 6.16 Comparison of burnable poisons in a high burnup, conventional PWR assembly (9.75 w/o).

The high burnup case with conventional PWR assembly design (HB-REF) is an interesting case (Fig. 6.16). Due to high enrichment, the spectrum is harder. Hence the IFBA depletion appears slower than that in the REF case. Gadolinia, as a very strong absorber, is almost not affected. Precise cycle length control can be satisfied using gadolinia by optimizing the gadolinia content in each poisoned rod and the number of poisoned rods. The erbia option still leads to large residual reactivity, but the difference between gadolinia and erbia is smaller compared to the REF case. In this situation, gado-

linia might be preferred due to its ability to suppress the initial BOC reactivity while still burning out fairly completely at EOC.

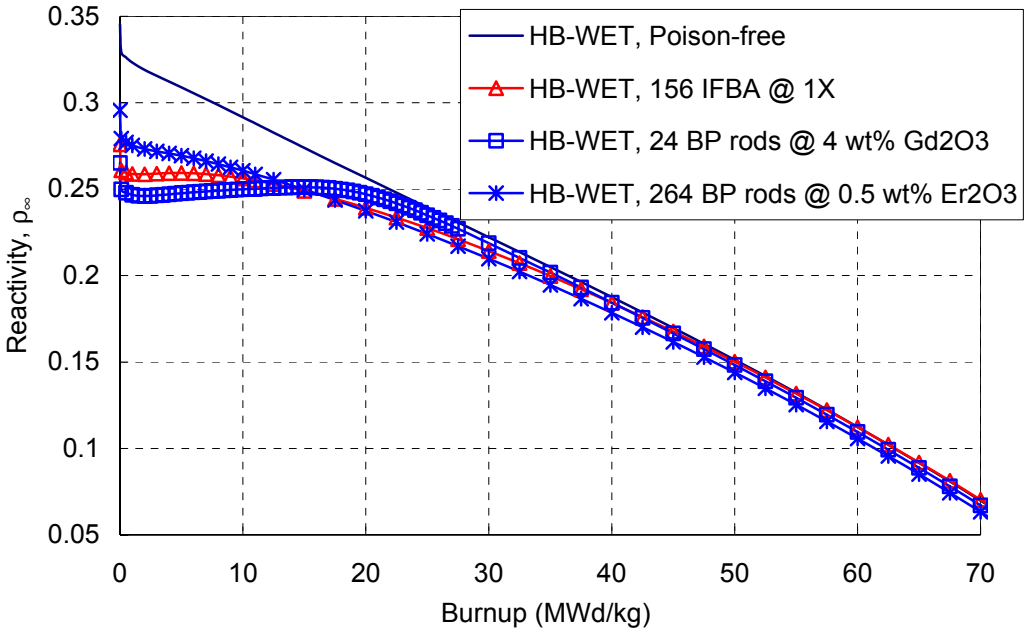

Figure 6.17 Poisoning the high burnup assembly with a wet lattice (9.75 w/o UO_2).

For high burnup with a wet lattice (Fig. 6.17), the behavior is similar to the HB-REF case. Gadolinia burns out almost completely at EOC (~30 MWd/kg). The erbia option still has the largest residual.

In conclusion, gadolinia shows promising results in controlling the 18-month cycle of the various cases considered. It is a neutronically versatile option while the IFBA might not be a good candidate for high burnup cases. Erbia is not as advantageous as the other two options. However, the BP situation is a complex issue which depends on specific core design requirements. There are, in turn, no universally best BP candidates.

There are some ideas for improving burnable poison usage in PWRs. Both gadolinium and erbium are seen to have a larger residual reactivity at EOC since the naturally occurring elements contain a chain of isotopes. It can be demonstrated that there is potential savings of several million dollars over a 4 year period (fuel irradiation life) by using separated absorber isotopes [132]. Another interesting possibility is the polymer material containing carbon, oxygen, hydrogen, silicon and boron discussed in Ref. [133]. It is de-

signed for use in heterogeneous poison rods, but has the advantage that it provides added moderation when the boron is burned out. This contrasts with the use of B_4C in alumina, which pretty much leaves a neutronic void when the boron burns out.

6.2.4 Design Considerations

As shown in Eq. (6.1), the BOC excess reactivity is also affected by the slope A (reactivity versus burnup), which can be reduced by increasing the conversion ratio via a design change. In fact, high conversion cores were intensively studied in the 1970s and 1980s with the major objective of saving uranium ore.

Several variants of design changes can be adopted to increase the conversion ratio. A basic approach is to turn to a harder neutron spectrum, i.e., poorer moderation than a conventional core, in which an epithermal spectrum is created by reducing H/HM, e.g., in an evaluation of tight-pitch PWR cores carried out at MIT in Ref. [134]. Typically recycling of plutonium is needed in close-packed lattices to take advantage of their high conversion ratio (more plutonium production) [135]. In addition to an H/HM change, heavy water can also be used to further harden the spectrum. The spectrum-shift control concept of varying the moderator density (small H/HM in the BOC and large H/HM near EOC) is another way to increase the conversion ratio.

Besides neutron spectrum modification there are other design changes which can increase conversion ratio. The use of annular fuel with internal cooling is one example. As discussed in Chapter 5, the conversion ratio is increased due to an increased fuel surface-to-volume ratio. Another interesting approach is to use axial fuel zoning, the so-called "Big Mac" core described by Y. Ronen in Ref. [136]. This option will be the main consideration in this section.

Usually less attention is paid to axial zoning for PWRs than for BWRs since the H/HM ratio remains almost the same along the length of the coolant channel. Figure 6.18 illustrates the idea of axial zoning of the fuel. In Fig. 6.18(a), a typical solid UO_2 fuel rod with enrichment of X_P is shown (denoted as HOM). It is possible to axially zone the fuel rod with different enrichments. A simple version shown in Fig. 6.18(b) illustrates two alternative layers: a higher-enriched UO_2 (HEU) fuel segment with height h_1 and enrichment X_{P1} and a lower-enriched UO_2 (LEU) fuel segment with height h_2 and enrichment X_{P2}.

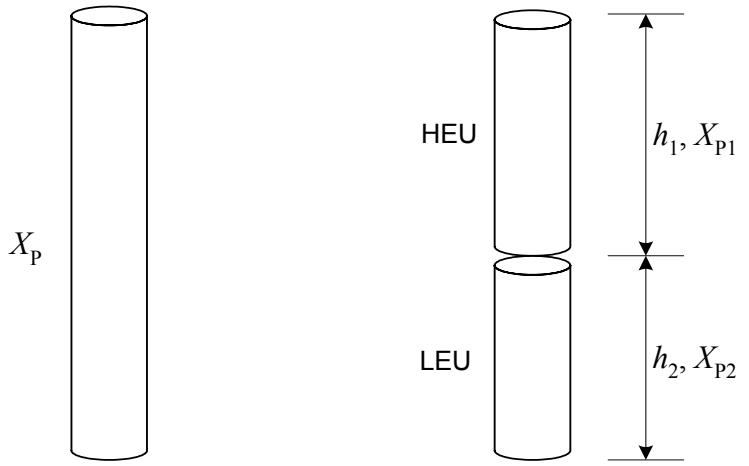

Figure 6.18 Schematic of axial heterogeneous fuel loading.

Assuming the same U-235 contents for these two cases, i.e.,

$$\left(h_1 + h_2\right) X_P = h_1 X_{P1} + h_2 X_{P2}\,, \tag{6.7}$$

one can show that the natural uranium and SWU requirements for these two cases are roughly the same:

$$\left(\frac{F}{P}\right)_{HOM} = aX_P + b\,,$$

$$\left(\frac{F}{P}\right)_{AxH} = \frac{h_1}{h_1 + h_2}\left(\frac{F}{P}\right)_{HEU} + \frac{h_2}{h_1 + h_2}\left(\frac{F}{P}\right)_{LEU}$$

$$= \frac{h_1}{h_1 + h_2}\left(aX_{P1} + b\right) + \frac{h_2}{h_1 + h_2}\left(aX_{P2} + b\right)$$

$$= a\frac{h_1 X_{P1} + h_2 X_{P2}}{h_1 + h_2} + b$$

$$= aX_P + b\,,$$

where a and b are constants. Similarly the SWU requirement is about the same given a linearized approximation of S/P. Even for such a simple axial heterogeneous configuration, many parameters are open to variation, such as the height and enrichment of each layer. For an illustration of reactivity control effects, equal thickness layers are assumed, i.e., h_1=h_2. The homogeneous reference case employs 9.75 w/o U-235, and the axial het-

erogeneous case uses 19.5 w/o and 0 w/o enrichments respectively. MCODE was used to model the axially heterogeneous case and the input files for the case of 6 cm of axial layer thickness are included in Appendix D. Note that the homogeneous case is actually the special case of the axially heterogeneous case with the layer thickness equal to zero.

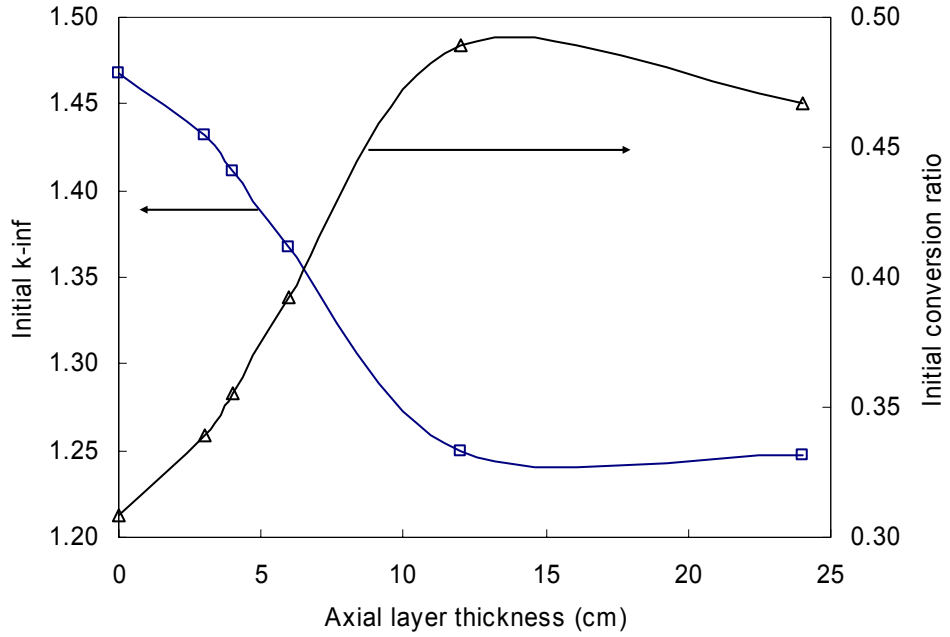

Figure 6.19 The effect of axially heterogeneous fissile distribution on initial neutronic parameters.

As shown in Fig. 6.19, the initial k_∞ decreases as the axial heterogeneous layer thickness increases. After about 10 cm of axial layer thickness, the initial k_∞ approaches a constant value. For PWR lattices with 9.75 w/o UO_2 fuel, the neutron migration length is ~8 cm, which agrees with that thickness value. Thus, in terms of reactivity control, one might limit the layer thickness variation to below 10 cm for this case. The initial conversion ratio increases with axial layer thickness due to increased fast neutron diffusion from the HEU to the LEU segment. The depletion curves are then shown in Fig. 6.20. Although the initial reactivity is suppressed substantially the burnup potential is reduced as the axial layer thickness increases. In a recent neutronic design for thorium fuel, a similar arrangement, however, yields a 10% increase in burnup potential due to the superior fissile material, U-233, bred from Th-232 [106].

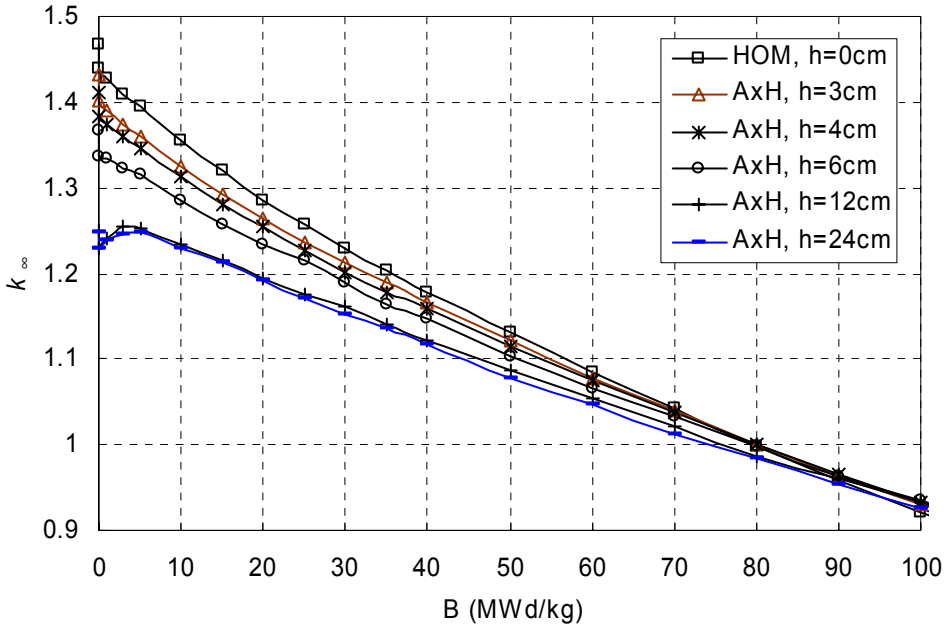

Figure 6.20 Depletion curves for axial zoning cases.

The challenge of this axial enrichment-zoning design is the high power peaking, which seems to emphasize that there may always be a trade-off between thermal hydraulics and neutronics. More than 97% of the thermal energy is produced in the HEU segment at the BOC, which roughly doubles the linear power of the HEU segment. Only at very small axial layer thickness, is axial heat transfer between adjacent HEU and LEU segments helpful. Furthermore, critical heat flux is likely to be governed by the average, not the peak condition [106]. As the layer thickness increases, this power peaking poses an even more severe problem. Eventually the layer thickness will be determined by the heat removal capability rather than the 10 cm recommended from the neutronic reactivity control point of view.

In conclusion the axial enrichment zoning approach might not be limited in its benefit at this moment from a heat transfer point of view. However, it is a neutronically interesting design which can theoretically increase the conversion ratio by 50%. It was demonstrated here that separation of fissile and fertile species (more heterogeneity in the core) reduced the reactivity while increasing the conversion ratio. However, the burnup potential may be reduced for the higher conversion ratio LWR core design. Under current

once-through fuel cycle practice, it is therefore not worthwhile to adopt this approach since no reprocessing is available to take advantage of the increase in bred plutonium. Also, such design changes alone are not expected to fulfill the neutronic reactivity control requirement.

6.3 Heat Transfer Considerations

6.3.1 Introduction

Wetter lattices, even with increased water in the lattice, do not necessarily have a better thermal margin. To examine the heat transfer limits, a qualitative scoping study of heat removal capability has been carried out for various options for H/HM variations as summarized in Table 6.4.

Table 6.4 Practically-considered ways of varying H/HM.

No.	Variations	Comments
1	Rod diameter	• primary way of lattice optimization while assembly design is maintained • geometrically-limited by the pin pitch
2	Pin pitch	• changes lattice structure as well if assembly dimension is to be conserved • geometrically-limited by rod diameter
3	Annular fuel pellet (central-voided)	• varying H/HM without affecting heat transfer • central plug needed to maintain the pellet geometry • a reduction of fuel temperature due to geometry
4	Annular fuel with internal cooling (IXAF)	• a significant fuel temperature reduction • doubling of heat transfer surface area • doubling of the clad material

The first three variations all use a solid fuel pin while the last one uses an annular fuel pin. Various H/HM ratios are achieved using the first three ways starting from a standard PWR 17×17 lattice. Only one design (13×13 lattice) of the annular fuel with internal cooling is calculated (the so-called the IXAF concept with parameters shown in Table 5.4, Chapter 5). Three general assumptions are made: (1) the core volume is fixed, (2) the total core power is fixed, and (3) the coolant condition in the core is the same. Consequently the power density for all cases will be the same. Note that the specific power

(kW/kgIHM) varies, however. A single pin cell model is used for thermal hydraulic analysis. The rod power can be written as

$$\dot{q} = \left(P^2 L\right) q'''_{\text{core}} = c_p \dot{m} \left(T_{\text{out}} - T_{\text{in}}\right), \tag{6.8}$$

where P is the pitch pitch (1.26 cm for reference PWRs),

L is the active fuel height (3.66 m for reference PWRs),

q'''_{core} is the core average power density,

$\dot{m}$ is the mass flow rate and $\dot{m} = (\text{flow area}) \times (\text{mass flux}) = \left(P^2 - \frac{\pi}{4} D^2\right) G$.

By assumption, four quantities in Eq. (6.8) remain unchanged for all cases: q'''_{core}, c_p, T_{in}, and T_{out}. Conceptual thermal hydraulics analysis is provided case by case:

- *Rod diameter variation* The rod power, $\dot{q}$, is conserved. According to Eq. (6.8), the mass flow rate will also be constant for various H/HM values. The flow cross sectional area increases resulting in a reduced mass flux, i.e., flow velocity decrease (hence a reduced heat transfer coefficient). In addition, the heat transfer (rod surface) area decreases resulting in heat flux increase. The heat transfer margin for a wetter lattice is therefore reduced [137].
- *Pitch variation* In the reactor core, increasing pin pitch will reduce the number of pins, and thus, the individual pin power will rise. Since the rod surface area is the same for various H/HM values, the heat flux will rise. There will be also a reduced heat transfer margin.
- *Annular fuel pellet with central void* The heat transfer is not affected. However, the fuel temperature is reduced.
- *The IXAF case* Doubling of the heat transfer surface for this internally and externally cooled fuel reduces the heat flux by a factor of 2, which significantly improves the thermal margin.

6.3.2 Hot Channel Analysis

A single, hot channel analysis was made using VIPRE [26] for varying rod diameter to change H/HM. The radial peaking factor, $F_{\Delta h}$, is taken as in the conventional PWR, i.e., 1.65. The axial power employs a chopped cosine shape with peak to average value of

1.55. Hence, the hot spot factor is 2.56, which is 2.3% larger than the typical maximum value, 2.5.

For the reference PWR solid pin, the average linear rod power in the hottest assembly is

$$\dot{q}_{\mathrm{REF}} = \frac{3411\mathrm{MW}}{193\mathrm{assemblies}\times 264\mathrm{rods}\times 3.66\mathrm{m}}\times 1.65 = 30.18\frac{\mathrm{kW}}{\mathrm{m}}.$$

When varying H/HM value for solid fuel pins, the rod power is adjusted according to

$$\dot{q} = \left(\frac{P}{P_{\mathrm{REF}}}\right)^2 \dot{q}_{\mathrm{REF}}, \tag{6.9}$$

where P and P_{REF} are the pitches of the current H/HM value and the reference H/HM value (~3.4 for pin cell).

The mass flow rate, however, doesn't take into consideration the flow redistribution resulting from the core thermal hydraulics balance. It is simply the average flow rate (product of the average mass flux, 3729 kg/m^2-sec for the reference PWR solid pin, and the flow area), which is actually an overestimate since the hot channel subcooled boiling usually directs the flow out of that channel. This over-estimation becomes more obvious as one increases the core power. On the other hand, cross flow (a beneficial factor) is ignored in the single hot channel analysis. These two factors therefore cancel each other in part. In the following calculations, the mass flow rate is a constant for various rod diameters (given the same pitch).

The gap conductance for all cases is assumed to be 6000 W/(m^2·K); and the Westinghouse CHF correlation, W-3L, is used for all cases except that the IXAF inner channel uses W-3S since there is no grid inside.

Two VIPRE input files are included in Appendix E: one for the reference PWR lattice and the other for the IXAF pin cell.

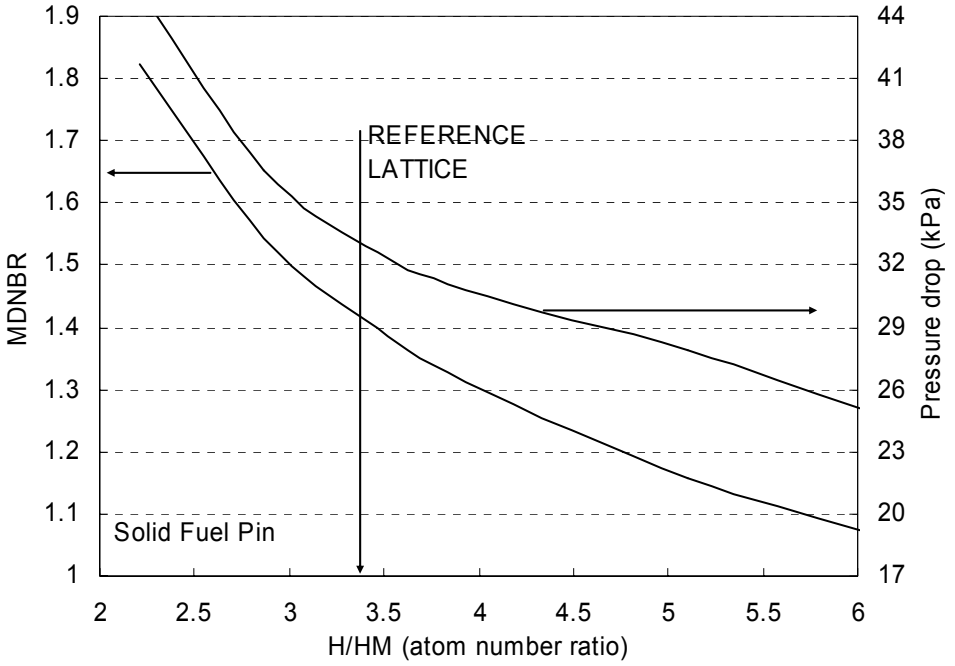

Figure 6.21 MDNBR and pressure drop as a function of H/HM for solid fuel pin.

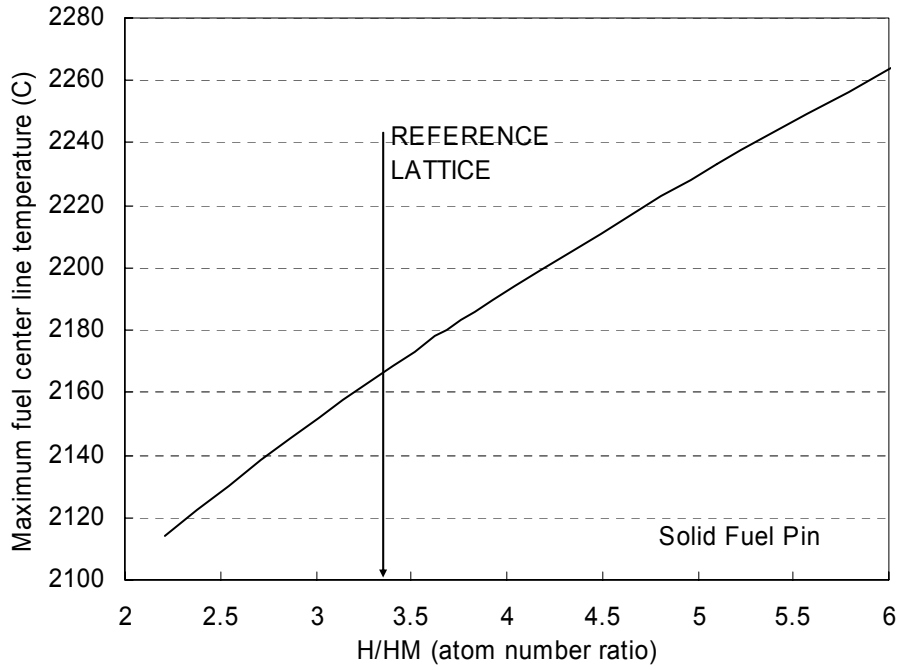

Figure 6.22 Maximum fuel temperature (centerline) as H/HM increases (rod diameter).

Fig. 6.21 shows that when varying rod diameter, the MDNBR decreases as the lattice becomes wetter. Meanwhile the pumping power requirement decreases. For fat pins, however, more powerful pumps are needed to maintain the same core coolant conditions. Figure 6.22 shows that the maximum temperature in the fuel is higher for wetter lattices, primarily due to the increased pin power. It is seen that the margin to melting (melting point at 2800°C) is large compared to the margin to DNBR.

Figure 6.23 shows the significant thermal margin of the IXAF concept compared to the reference PWR.

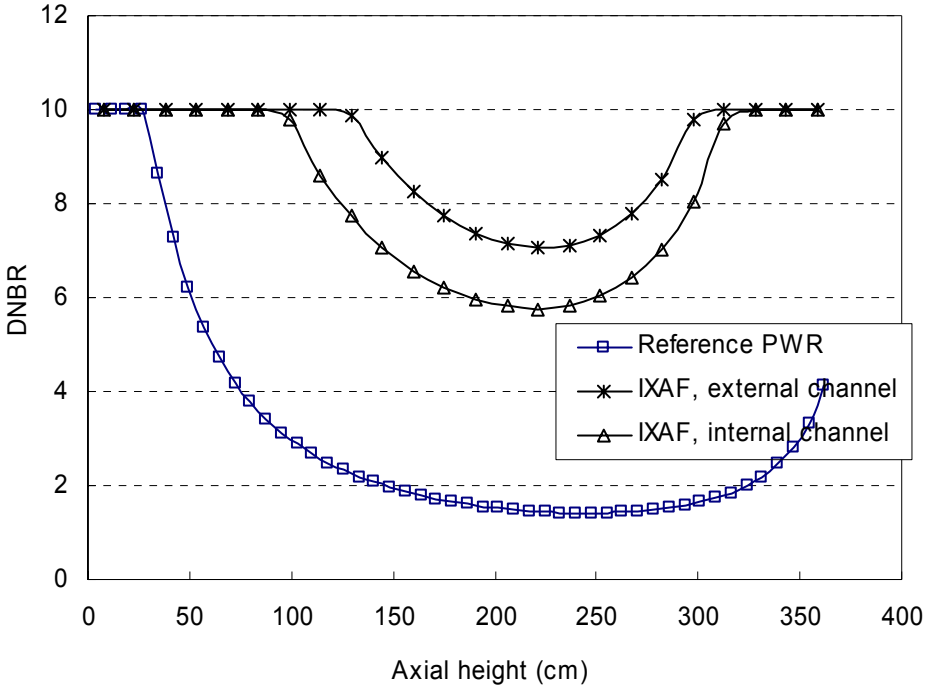

Figure 6.23 MDNBR comparison in hot channel for the IXAF and reference solid pin.

6.3.3 Discussion

Wetter lattices using solid fuel rods reduce the MDNBR. In order to remedy this shortcoming, two options are possible. One is to use more mixing vanes to promote heat transfer. The other is to use more pins in the assembly, for example, a 19×19 lattice.

From the industrial side, the thermal margins in conventional PWRs are known and exploitable. There have been two approaches to utilize that margin: (1) going to wetter lattices, as in Westinghouse's Performance+ fuel; (2) power uprating based on con-

ventionally designed fuel. Recently due to the impact of the de-regulated electricity market, it appears that power uprating is more attractive. However, for a wetter lattice with solid fuel, it is difficult to do power uprating due to its more limited thermal margin. Only the newly-developed IXAF fuel concept holds the promise of going to wetter lattices while still respecting thermal margins. Therefore, the IXAF design is recommended as a candidate to implement wetter lattices with power uprating. In fact a wetter lattice is beneficial for this concept to recover neutronic reactivity loss due to the double cladding and fuel surface resonance capture.

6.4 Fuel Performance Considerations

Another practical consideration is the fuel performance in the core, which relates more to material issues. The primary concern is the fission gas release from the UO_2 fuel pellet and the resulting internal pressure. During operation in the core, some of the gaseous fission products are released to the free space in the pin. Most of these are inert gases, such as xenon, krypton, and helium. The rod internal pressure builds up due to the released gases. The insoluble fission products accumulate in the fuel and cause fuel swelling (which plays a role in gap closing). The gas bubbles formed will deteriorate the fuel thermal conductivity. Mainly, there are two mechanisms for fission gas release: an athermal mechanism and a thermally activated mechanism. The athermal mechanism is primarily due to the recoil and knockout at low temperatures. It depends on the surface area of the fuel pellet and increases with burnup. The thermally activated mechanism is responsible for most of the gas release at high power. The central hot zone in the pellet forms a peculiar microstructure characterized by intragranular gas bubble formation and by intergranular bubble interconnection. The fission gas is mainly released from this zone. The threshold for the temperature at low burnup is 1200°C and probably decreases with burnup. However, at high burnup, the thermal mechanism and the athermal mechanism interact with each other, which requires experiments to verify the fission gas release models.

The IXAF demonstrates very low fuel temperature. Therefore, the thermally activated mechanism is essentially stopped. The dominant fission gas release contribution

comes from the athermal mechanism. The FRAPCON-3 [27] code is used here to obtain the fission gas release. Because the code cannot represent the IXAF case, an equivalent solid fuel pin is made based on the same fuel surface-to-mass ratio. Under the same moderator-to-fuel ratio, the same power density is maintained, i.e.,

$$\frac{q'_{\text{eq}}}{P_{\text{eq}}{}^2} = \frac{q'_{\text{IXAF}}}{P_{\text{IXAF}}{}^2}, \tag{6.10}$$

where the subscript "eq" means equivalent solid fuel pin, and the symbol P refers to the lattice pitch. The reference PWR rod is then compared to this IXAF-equivalent solid rod case. Note that 9.75 w/o UO_2 is used here to achieve a burnup of ~100MWd/kg.

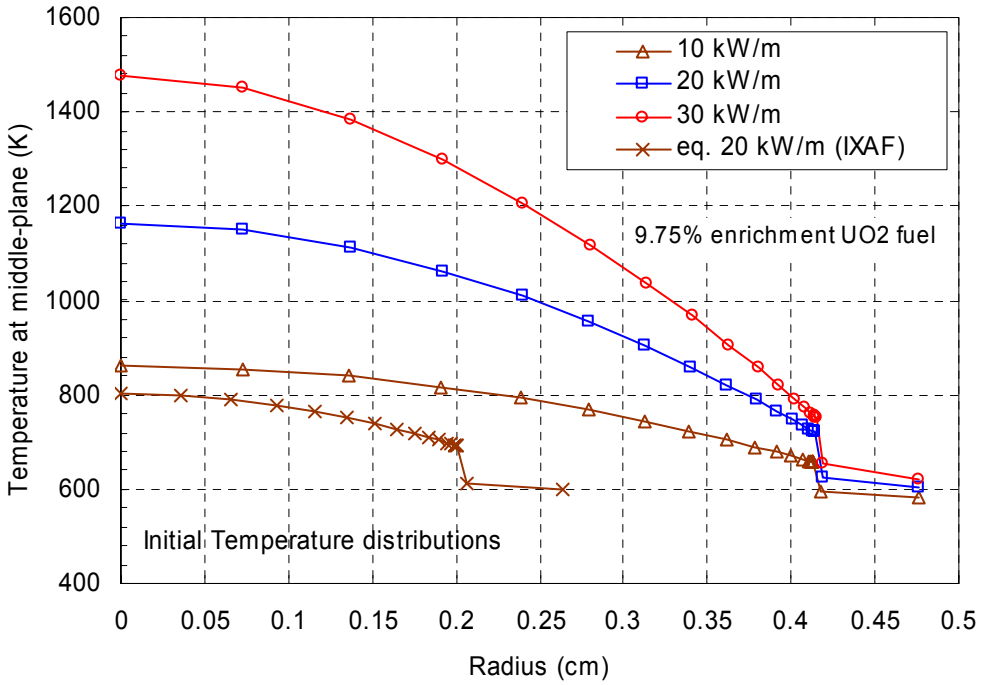

Figure 6.24 Fuel temperature distributions at BOC.

Figure 6.24 shows the initial fuel temperature distribution in the pin. It is noted that the IXAF-equivalent solid pin operates at a very low fuel temperature. The equivalent solid pin can be viewed as half of the IXAF pin, i.e., the centerline of the solid pin is equivalent to the maximum-temperature radius in the IXAF pin. Although this analog is not exact, some similarity exists which allows qualitative representation of the behavior of the IXAF pin.

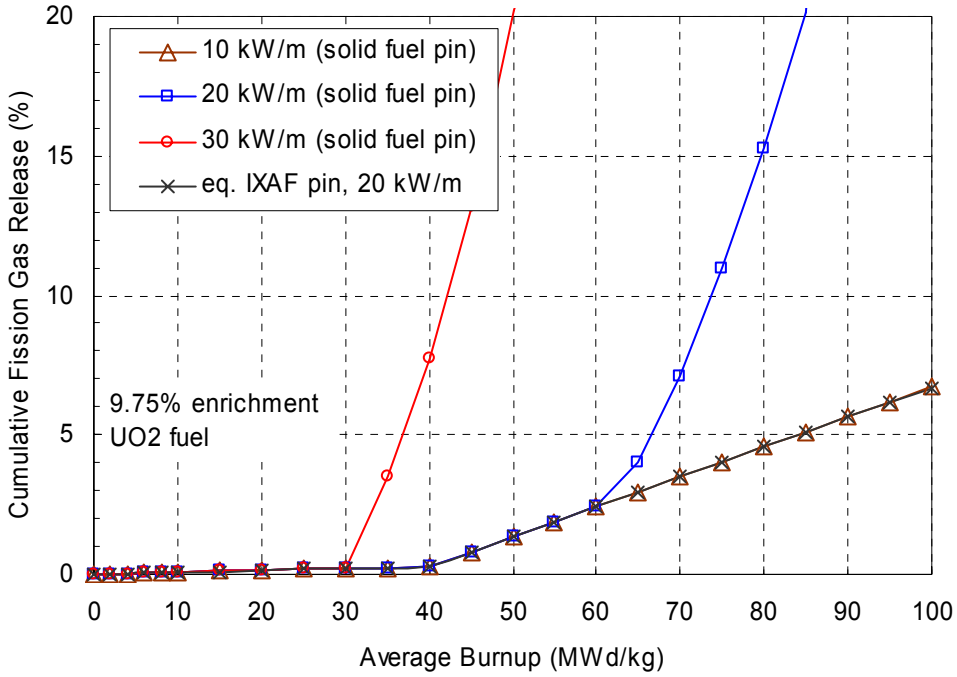

Figure 6.25 Fission gas release calculations for various fuel pins.

The cumulative fission gas release is shown in Fig. 6.25 for various fuel pins. The fission gas release limit for the current fuel rod design is about 5% [44]. The fission gas release strongly depends on the operating fuel temperatures. For the 10 kW/m case, it takes three times longer to reach the same burnup as the 30 kW/m case. However, at the same burnup the cumulative fission release for 30 kW/m is still larger than that of the 10 kW/m case. The burnup threshold for athermal gas release in the current FRAPCON3 model is seen from Fig. 6.25 as 40 MWd/kg. For the IXAF pin, only athermal gas release is present. In fact, the linear release predicted is an extrapolation of the current athermal release model, which needs further investigation. Based on current knowledge, the IXAF fuel, with its very low fuel temperature, should release less fission gases compared to any other operating solid pin. Additionally, the RIM calculations in Chapter 5 show that the RIM region of the IXAF has a smaller peak-to-average power ratio. Hence the burnup in the RIM region is smaller compared to the RIM region of the solid fuel pellet. The fuel performance issue therefore favors the IXAF concept. Again the IXAF appears to be an excellent candidate for high burnup applications.

6.5 Chapter Summary

Several practical issues related to high burnup were discussed in this Chapter. The neutronic reactivity control of high burnup cores, even with the same cycle length as the current 18-month core, shows an increased requirement for poison control. The basic physics characteristic of high burnup cores is a harder neutron spectrum, hence a reduced poison worth. Burnable poisons are a must for such cores. Among the BPs evaluated, gadolinia shows promising results for an 18-month cycle. It is also interesting to note that the use of IFBA leads to larger EOC residual compared to gadolinia for high burnup cores. A design change of axial enrichment zoning was evaluated, which is however limited by heat removal capability. The burnup potential was also diminished in such a configuration. It is therefore concluded that axial enrichment zoning is not a worthwhile undertaking. The IXAF concept has certain gains in terms of reactivity control due to its doubling of fuel surface-to-volume ratio. The reactivity control issue for the IXAF, however, was not addressed. It is clear that there is more room for the IXAF design to hold the IFBA poison (more fuel surface area), but the total IFBA loading is still limited by the helium produced.

Other practical implications such as thermal hydraulics and fuel performance issues were also addressed. A wetter lattice with a solid fuel rod leads to reduced thermal margins, which motivates either more fuel pins or the IXAF concept. However, the current industrial trend of pursuing higher power density seems inconsistent with the wetter lattice approach. It is more difficult for utilities with wetter lattices (such as adoption of the Westinghouse Performance+ fuel) to do power upgrade. The technical flexibility of solid fuel pins has been almost used up in LWR designs, i.e., there is very little room to increase moderation while satisfying all thermal margins particularly under the power uprating case. In this regard, only the IXAF concept is a promising candidate since it excels in nearly all practical considerations primarily due to its very low fuel temperature and doubling of the heat transfer surface.

Future work on global optimization is needed in the process of designing high burnup advanced PWRs. Particularly for the IXAF concept, many variables are open to

optimization, such as the rod dimensions (inner & outer radii) and the lattice structure (pitch).

7. High Burnup Effects on Spent Fuel Characteristics

"You may delay, but time will not"
— B. Franklin (1706-1790)

7.1 Introduction

Disposal of nuclear spent fuel has been a public concern for decades ever since the birth of nuclear power. It is commonly recognized by the scientific & engineering community that spent nuclear fuel storage and disposal can be done safely, i.e., current technology should be more than adequate for isolating radioactive wastes from the biosphere and for protecting public health and safety. The problem, therefore, is largely political rather than technical. The Nuclear Waste Policy Act (NWPA) was passed by the US Congress in 1982 and was signed by the president later in 1983. According to NWPA, nuclear utilities have no responsibility for ultimate spent fuel disposal except for paying 1 mill per kW-hr(e) generated after April 7, 1983 into a special fund controlled by Congress. However, storage of spent fuel prior to waste disposal is still the responsibility of the individual utility. The opening of the first US repository at Yucca Mountain, Nevada is now expected to be in 2010 (refer to [138] for up-to-date information).

When early commercial power plants were built in the US, it was expected that the spent fuel would be reprocessed within a few years after discharge. The spent fuel pools were generally designed to hold two or three cores (one to accommodate a whole core if needed during operation). However, under the once-through fuel cycle constraint imposed since 1977, the storage of spent fuel has become a serious issue as the spent fuel pool capacity is being used up. The average annual discharge of spent fuel in the US is about 2000 metric tons of heavy metal (about 7000 assemblies). By 2030, accumulation of spent fuel will reach 80,000 metric tons of heavy metal (or 293,000 assemblies) [139]. Although NWPA states clearly that the federal government shall eventually take custody of these spent fuel assemblies, it is highly uncertain when that will happen. Consequently the expansion of spent fuel storage capability is of strong interest to utilities. There are

currently two storage options: wet and dry. The wet option is only economical if practical with on-site nuclear spent fuel pools. The pool capacity can be expanded by reracking (closer assembly spacings), which makes it possible to store up to three times as much fuel in the same spent fuel pool while still satisfying the spent fuel storage requirements [140]. Also considered but not practiced due to cost is the possibility of fuel consolidation, i.e., dismantle the fuel assembly, consolidate the rod bundle, and compact the fuel assembly skeleton. The dry storage option involves storing the spent fuel in a properly shielded canister cooled by air natural convection flow. In the US some 12 reactors now practice this option that is competitive with wet storage in terms of cost, maintenance, expandability, and transportability.

Although higher burnup can reduce the spent fuel generation (both volume and mass), it is important to quantify/assess other impacts (such as the heat load requirement and radiotoxicity) when considering its different isotopic composition (more actinides and fission products per MTIHM) due to the higher neutron fluence. These quantities affect both storage and repository designs. The high-burnup spent fuel fissile content also needs to be investigated. One concern is repository criticality. There are other nuclear fuel cycle possibilities for utilizing high-burnup fuel, e.g., DUPIC.

The proliferation worry associated with spent fuel is another important issue, which is largely characterized by the plutonium vector in the nuclear spent fuel. The plutonium contents relate directly to weapons proliferation vulnerability.

7.2 Waste Disposal Characteristics

7.2.1 Characteristics of Today's Discharged Fuel

The nuclear spent fuel belongs to the category of high-level waste (HLW) according to the NRC definition of waste categories. It consists of three components:

- actinides and their decay daughters (ACT);
- fission products (FP) from splitting of heavy metal atoms (mainly U-235 and Pu-239);
- activation products (AP), which result from neutron capture in structural materials.

Among the above three groups of nuclides, the activation products have much smaller contributions to in-situ toxicity and heat load compared to the actinides and fission products. Therefore they are ignored in the following discussions.

Generally speaking actinides have very long half lives (even millions of years) and long decay chains. On the other hand, the fission products typically have short half lives (tens of years) and short decay chains. Therefore, conceptually the short-term nuclear spent fuel radioactivity is governed more by fission products, and the long-term behavior by actinides. The spent fuel at 33 MWd/kg discharge burnup using 3.1 w/o initially enriched UO_2 fuel for a typical PWR lattice was chosen as the reference case. Depletion calculations were entirely based on MCODE. ORIGEN2 was then used to compute the decay process of the spent fuel. The in-situ radioactivity of nuclear spent fuel is shown in Figure 7.1. Note that the repository hazard to the biosphere in reality should also consider the transportability of nuclides, several of which are of interest including Tc-99, I-129, and Np-237.

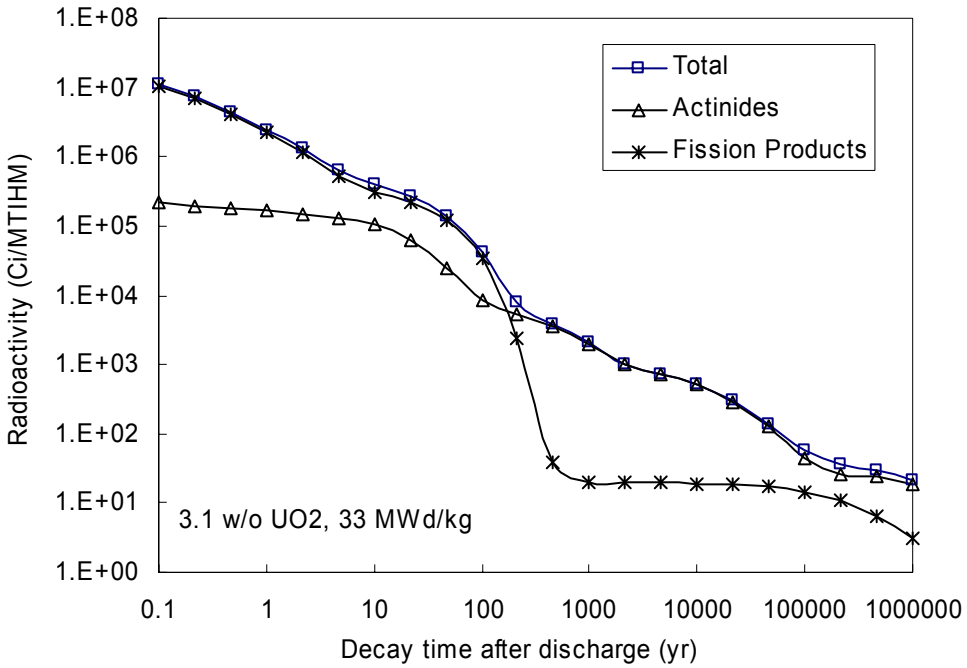

Figure 7.1 In-situ radioactivity for typical PWR spent fuel as a function of time.

As discussed in Chapter 4, the neutron spectrum can significantly affect the reactivity-limited burnup capability. In addition, it is also observed that higher enrichment always enables a higher burnup under any H/HM ratio. It is therefore necessary to separate these two effects. Based on the reference PWR thermal lattice (H/HM=3.4), a series of cases with different discharge burnup values have been evaluated as the basis to study spent fuel behavior. Then lattices with different H/HM ratios but the same discharge burnup value are studied focusing on the spectrum effects.

7.2.2 High Burnup via Higher-Enriched Uranium

A higher discharge burnup is primarily achieved via a higher reload fuel enrichment. Based on the burnup-enrichment correlation developed in Chapter 2, i.e., Eq. (2.8), estimates of reload fuel enrichment can be made for various discharge burnup levels. Three-batch fuel management is assumed for all cases under consideration. Table 7.1 shows the range of discharge burnup values.

Table 7.1 High burnup spent fuel under consideration.

No.	B_d (MWd/kg)	B_1 (MWd/kg)*	X_P (w/o)**	Comment
1	33	22	3.1	Early-days discharge burnup
2	50	33.33	4.5	Present burnup level
3	70	46.67	6.3	Foreseeable future
4	100	66.67	9.1	Future burnup level
5	120	80	11.2	Far future burnup
6	150	100	14.3	Remote future

* Assuming three-batch management, $B_1 = \frac{2}{3} B_d$

** $X_P = 0.41201 + 0.11508 B_1 + 0.00023937 B_1^2$, from Eq. (2.8).

Burnup calculations have been carried out for the above 6 cases using MCODE. A complete nuclide representation containing 130 fission products and 23 actinides was employed. The varying power history effect and the refueling outage decay are ignored.

Two comparison bases are considered: per MTIHM and per GW·yr(e). The first comparison is based on the unit mass of the initial heavy metal loading. Given the same assembly design, each assembly has the same fuel loading although the enrichment might be different in order to achieve different burnup levels. The second comparison is based on the unit energy produced in the reactor core. This reflects the amount of the spent fuel

generation per unit time of reactor operation. The transformation between two bases (X_1 as per MTIHM and X_2 as per GW·yr(e)) is:

$$X_2 = \frac{365}{\eta B_d} X_1, \tag{7.1}$$

where η is plant thermodynamic efficiency, i.e., 1150MW(e)/3411MW(th) = 33.7%

B_d is the discharge burnup, MWd/kgIHM (same as GWD/MTIHM).

Radioactivity

Radioactivity after discharge is shown in Figs. 7.2 and 7.3. The higher the discharge burnup, the more radioactive is the spent fuel. Within 100,000 years, the radioactivity generated in the spent fuel per unit electricity production always favors going to high burnup. It is interesting to note that, at 100 years after discharge, the radioactivity per unit electricity is relatively independent of the discharge burnup.

Figure 7.8 reveals the correlation between the decay power and the radioactivity. Roughly speaking these two quantities are proportional, but at quite different ratios below and above 100 years. However, around 10 years, there are moderate differences between the different cases. This explains the difference in decay heat power versus time: the radioactivity decreases very fast in the time frame of 100 to 1000 years after discharge because the fission products decay out.

Figure 7.9 shows the correlation between the radioactivity and the decay energy. Note that the decay thermal energy, $E(t)$, is calculated as an integration of the decay power, $P(t)$, since discharge:

$$E(t) = \int_0^t P(\tau)\, d\tau\,. \tag{7.2}$$

Since the thermal energy increases with time, the ratio between the thermal energy and the radioactivity also increases as a function of time.

Heat Load

It is seen as expected, from Fig. 7.4, that higher burnup leads to a higher decay heat generation rate per MTIHM (or per assembly if the initial heavy metal loading is the same). But, based on the unit electricity generation (Fig. 7.5), the decay power of high burnup spent fuel is only larger than the reference fuel within two time periods: (1) 4 years to 150 years; and (2) 150,000 years to 700,000 years. The long time frame differ-

ence is probably not important since (1) tremendous amount of uncertainties, including both the calculations and the future world, exist; (2) the decay power is about 5 orders of magnitude lower than the short term. The short time frame difference suggests that high-burnup spent fuel might need a longer time in the storage before the final disposal. Of course, based on a per assembly basis, the high burnup spent fuel assembly will be hotter (hence a higher surface heat flux), thus more expensive to handle. Each cask holds fewer assemblies of the higher burnup.

Based on unit energy production, the high burnup approach has certain advantages since the accumulated decay heat is reduced. Typically fuel disposal repository design is heat-transfer limited, i.e., the cost depends on the extent of cooling needed. For high burnup cases, the heat load from a single assembly will be higher (Fig. 7.6); however, fewer assemblies will be discharged per unit energy production. Furthermore, Fig. 7.7 shows that there will be also somewhat reduced heat load (total decay heat generation).

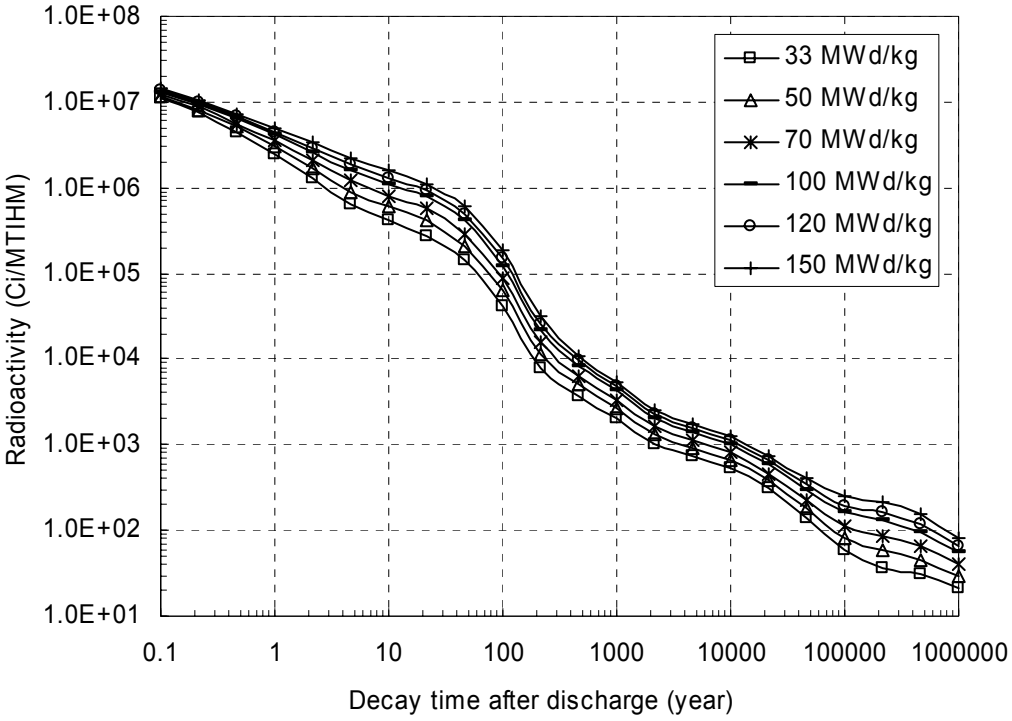

(a) Absolute magnitude

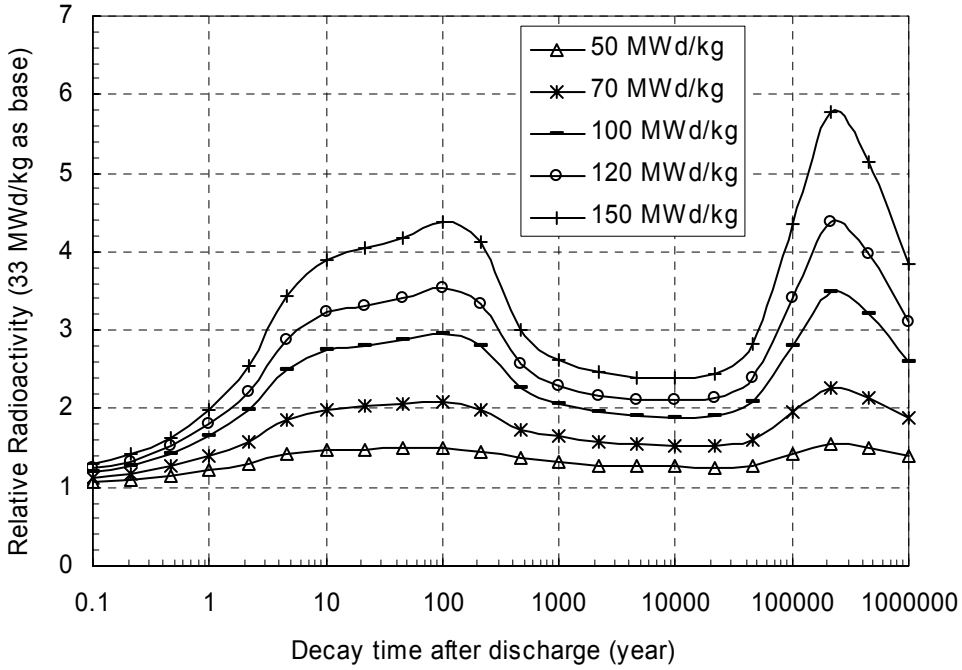

(b) Relative magnitude.

Figure 7.2 Radioactivity per MTIHM versus time after discharge.

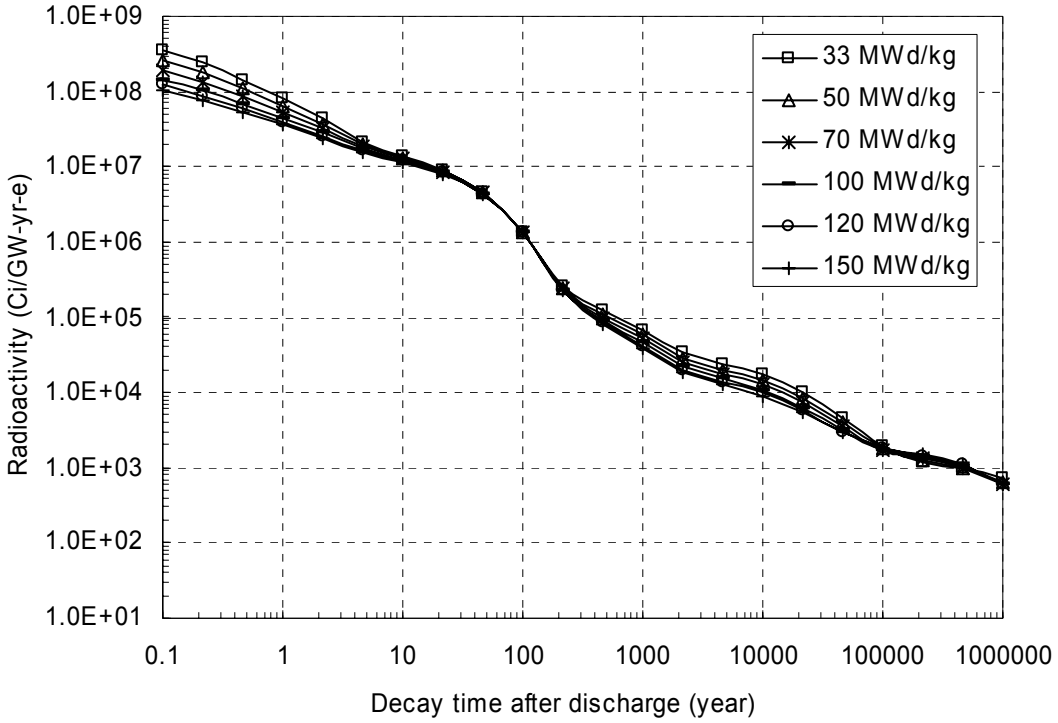

(a) Absolute magnitude.

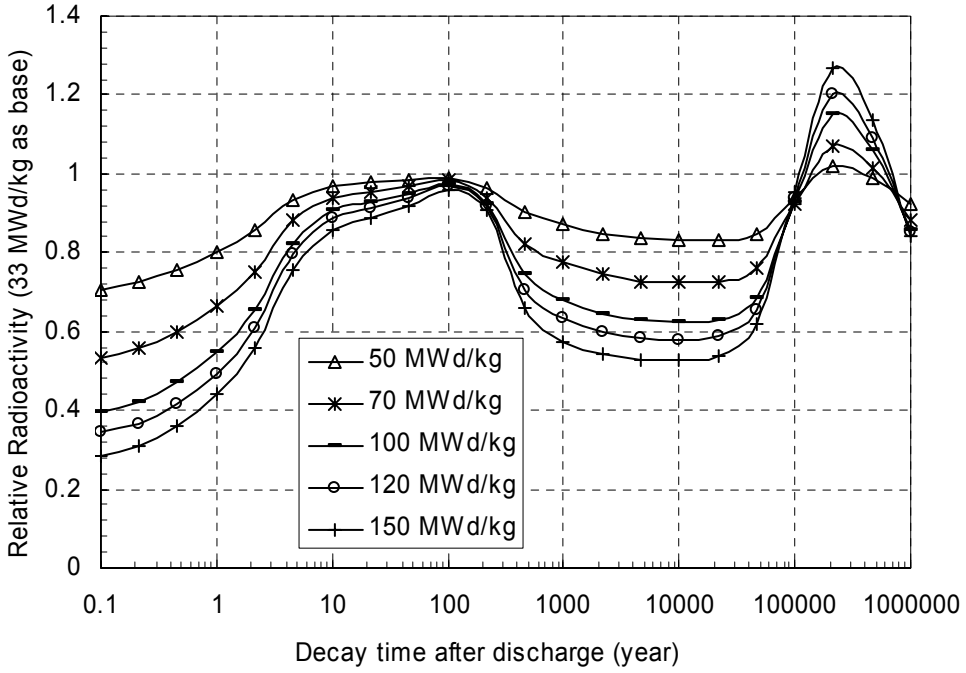

(b) Relative magnitude.

Figure 7.3 Radioactivity per GW·yr(e) versus time after discharge.

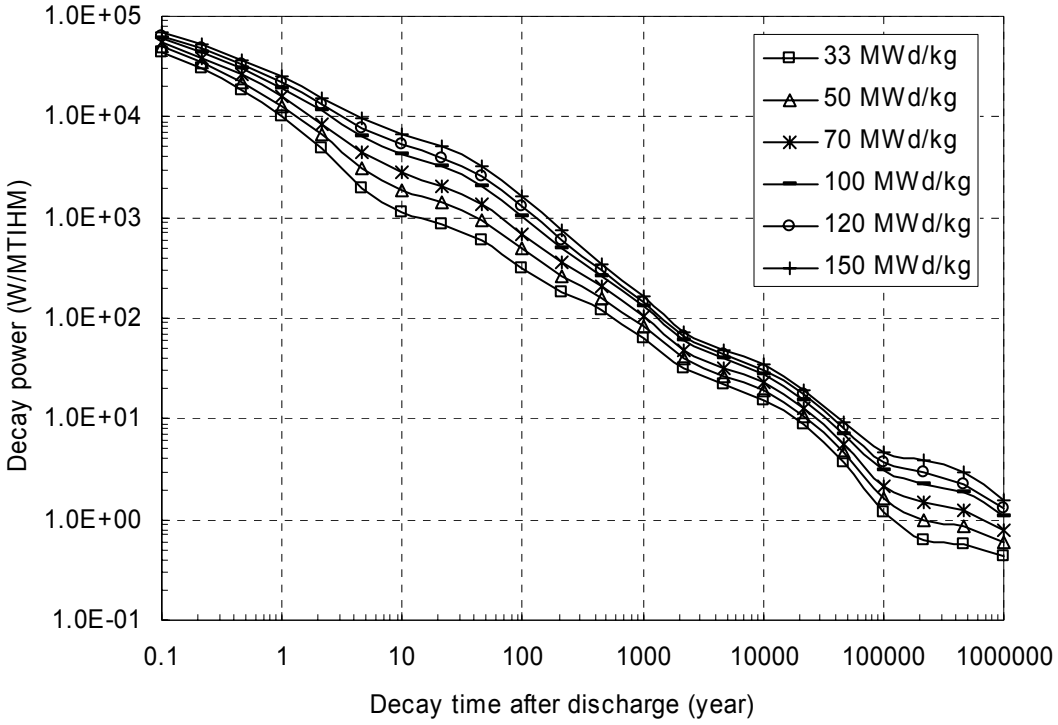

(a) Absolute magnitude

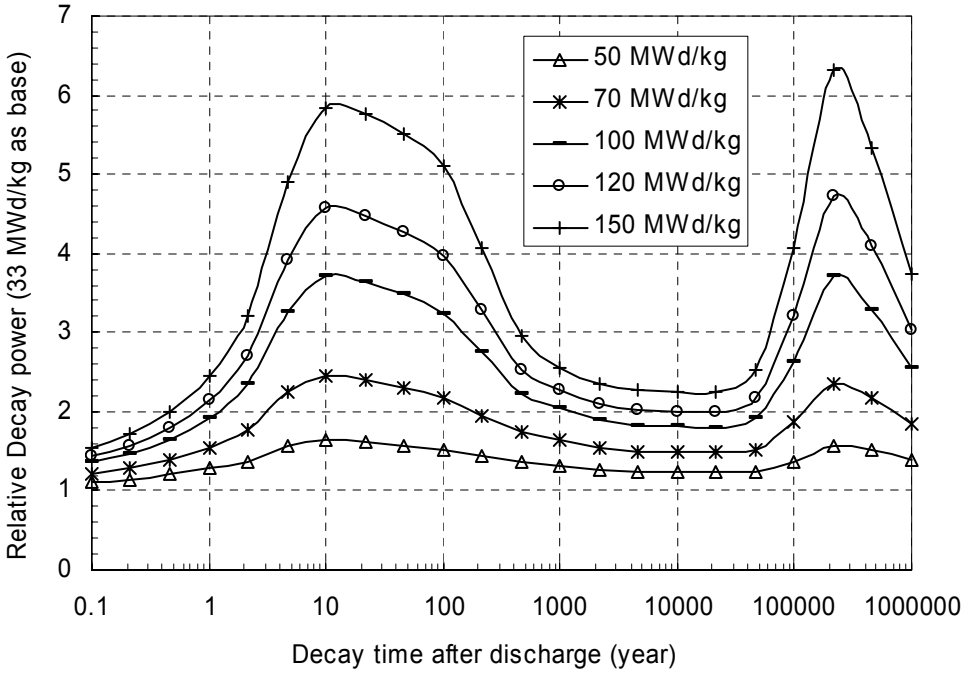

(b) Relative magnitude.

Figure 7.4 Decay power per MTIHM after discharge.

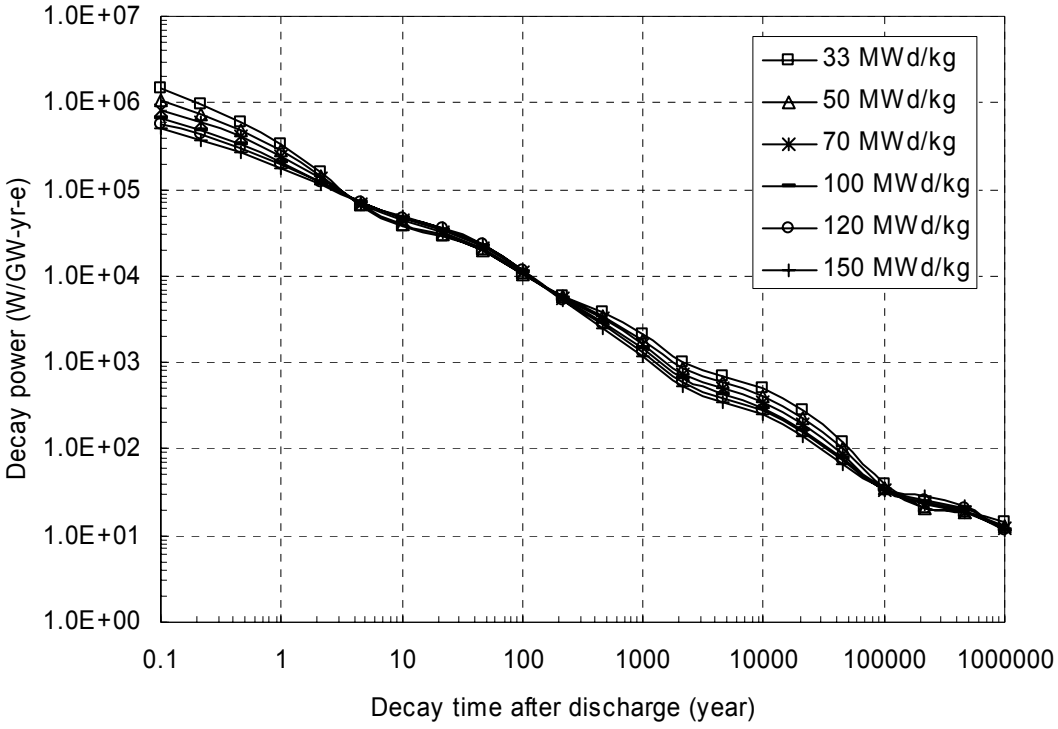

(a) Absolute magnitude.

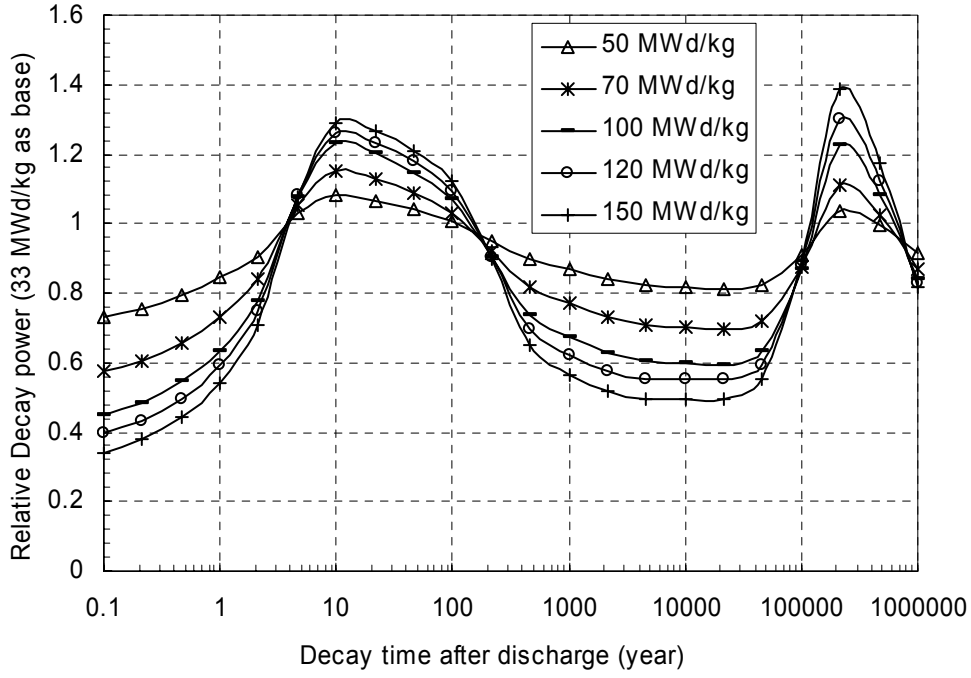

(b) Relative magnitude

Figure 7.5 Decay power per GW-yr(e) after discharge.

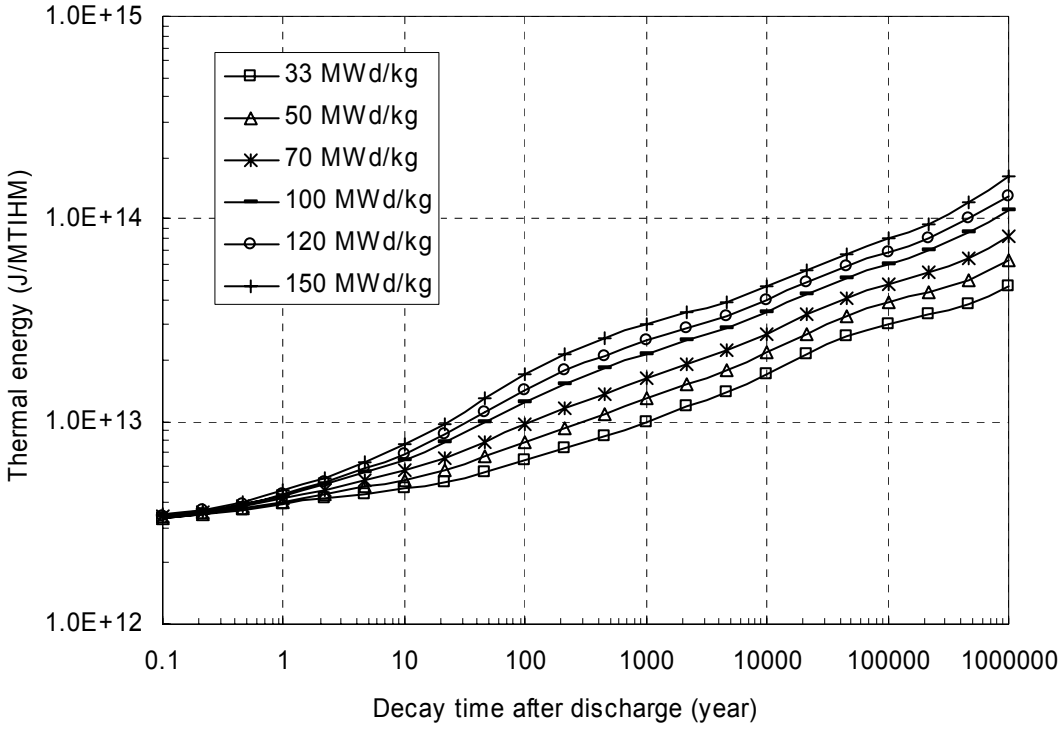

(a) Absolute magnitude.

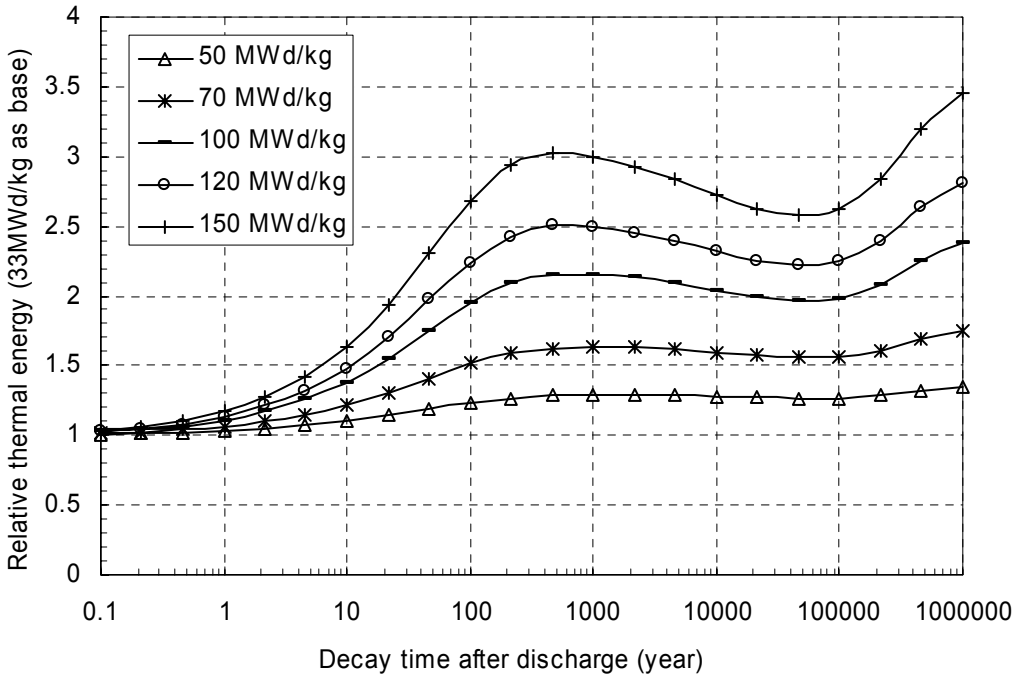

(b) Relative magnitude

Figure 7.6 Accumulated decay heat per MTIHM after discharge.

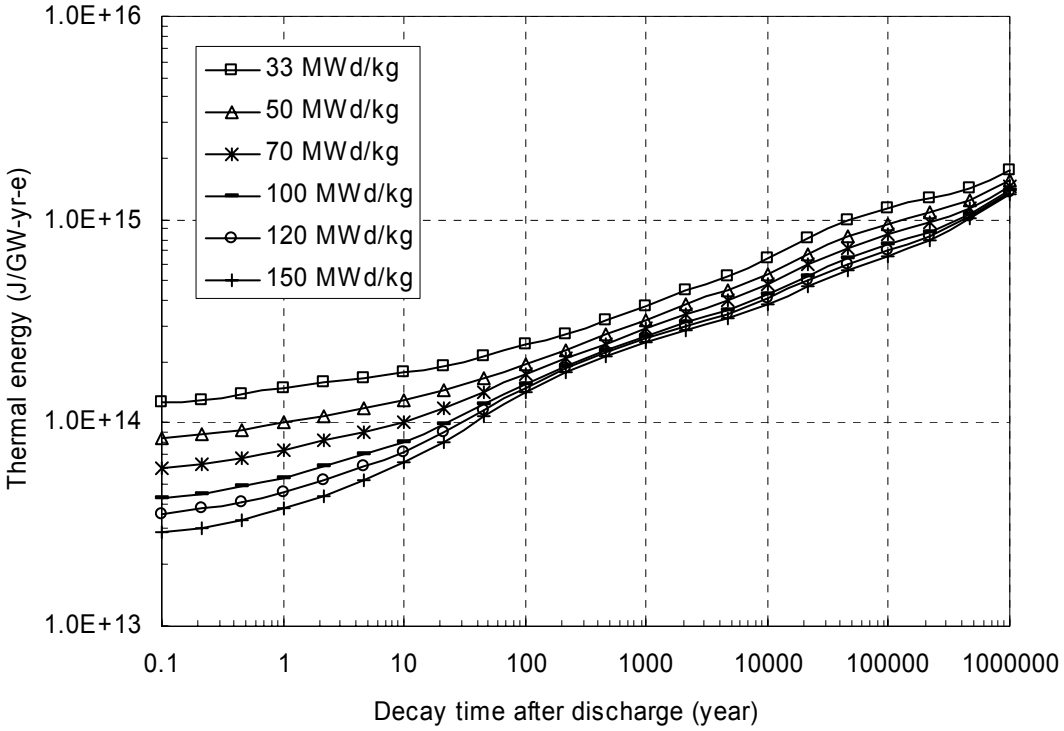

(a) Absolute magnitude

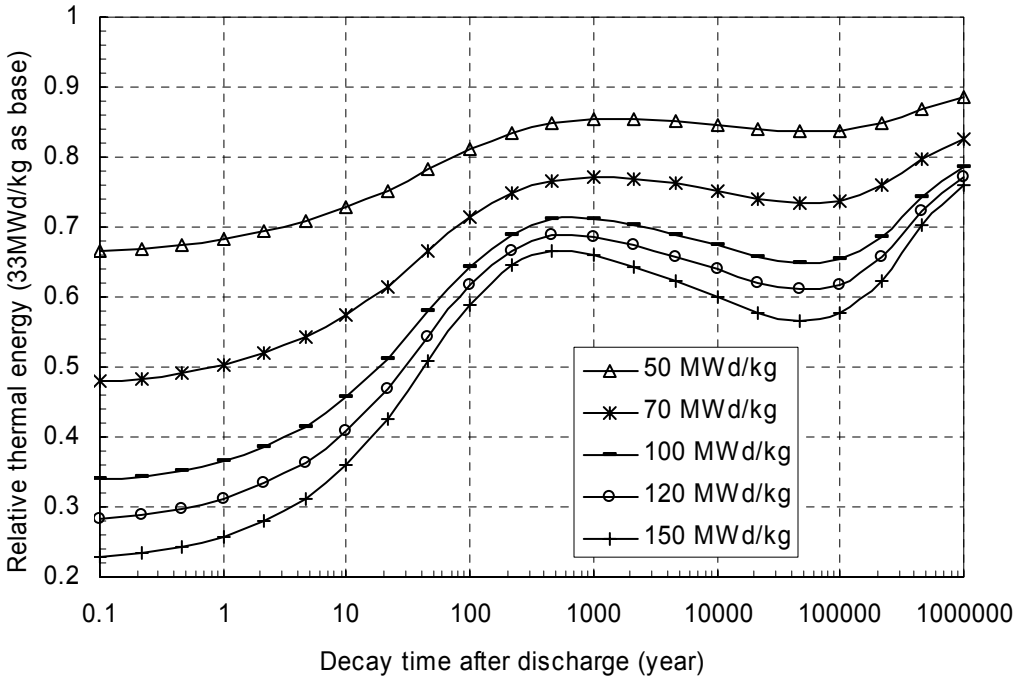

(a) Relative magnitude

Figure 7.7 Accumulated decay heat per GW-yr(e) after discharge.

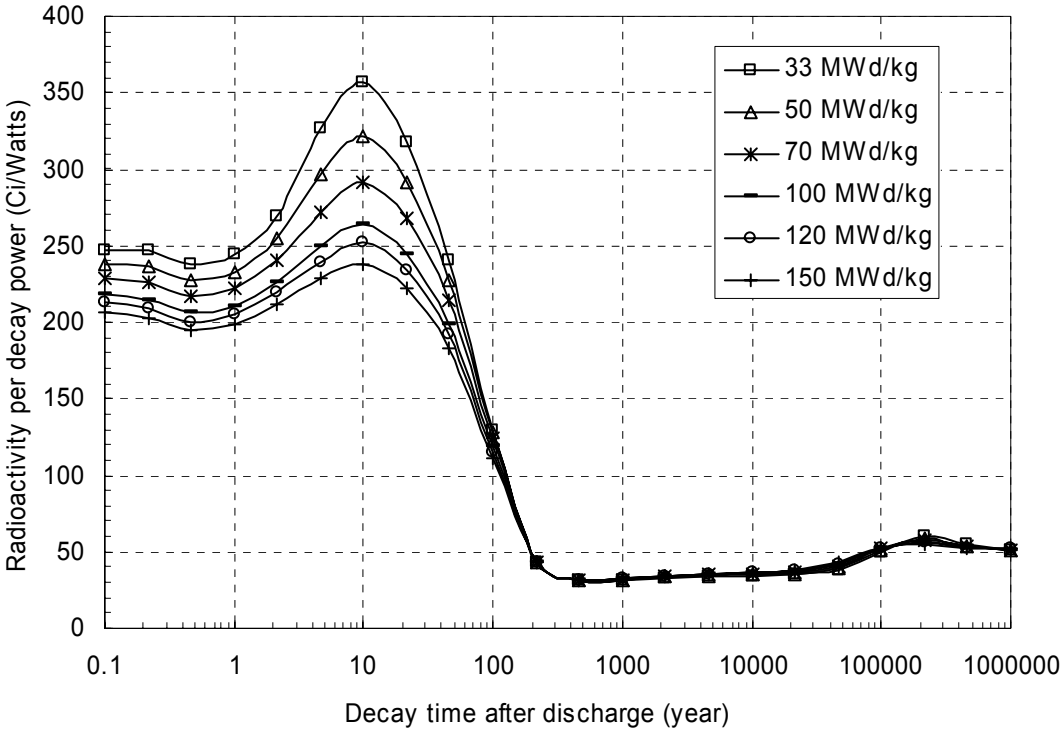

Figure 7.8 Correlation between decay power and radioactivity.

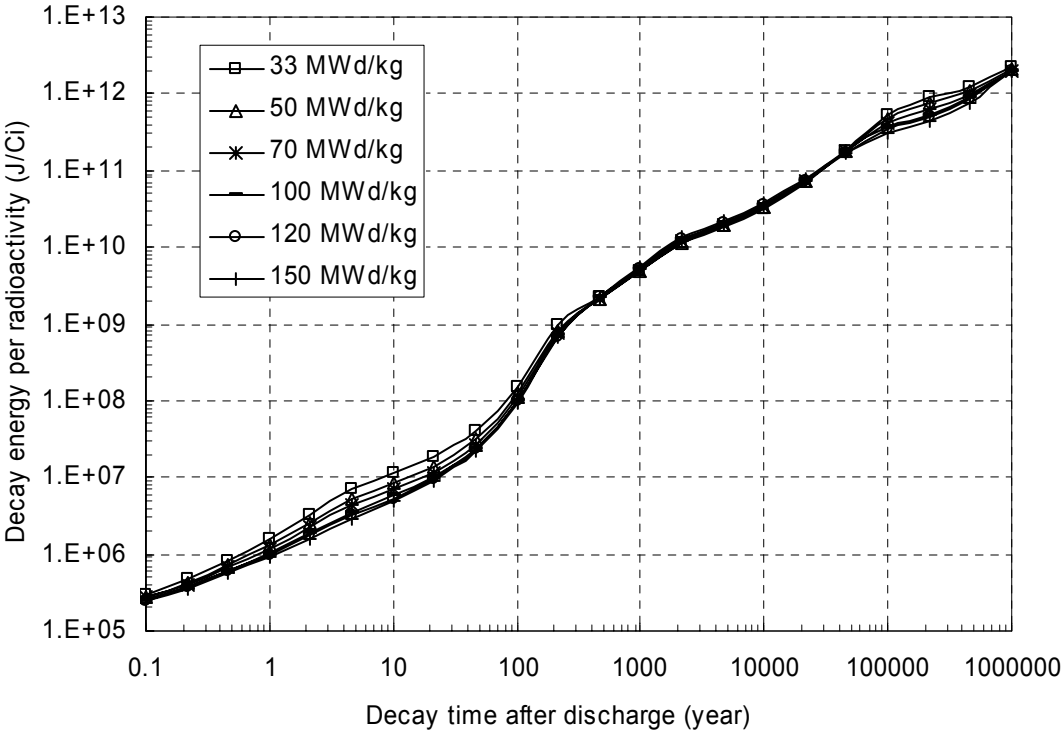

Figure 7.9 Correlation between decay energy and radioactivity.

A specific example is given here (Table 7.2): 100 MWd/kg versus 50 MWd/kg, hence 2 assemblies versus 1 assembly for storage, transportation, and disposal for the same electricity generation. One has criteria which might depend on per assembly (local effect) or total (global effect), e.g., the heat flux for cooling is per assembly as is the radioactivity for handling, but cask capacity is more dependent on total decay power for cooling and total radioactivity for shielding.

Table 7.2 Comparison of 100 and 50 MWd/kg spent fuel parameters.

		LOCAL EFFECT	GLOBAL EFFECT
		1 assembly@100 MWd/kg / 1 assembly@50 MWd/kg	1 assembly@100 MWd/kg / 2 assemblies@50 MWd/kg
Storage (@ 1 year)	Radioactivity	1.36	0.68
	Decay power	1.51	0.75
Transportation (@ 10 years)	Radioactivity	1.87	0.94
	Decay power	2.28	1.14
Disposal (@ 100 years)	Radioactivity	1.97	0.98
	Decay power	2.12	1.06
	Heat load (10 to 100 yr)*	2.22	1.11
Repository (@ 1000 years)	Radioactivity	1.56	0.78
	Decay power	1.54	0.77
	Heat load (100 to 1000 yr)	1.79	0.89

* Calculated as the integration of decay power between interval of 10 to 100 years.

Spent Fuel Isotopics

Criticality control is an important issue which depends on the specific spent fuel waste package design and the geometric configuration. The criticality in a repository needs to be avoided because it might accelerate long-term radionuclide releases to the environment. A criticality safety requires that $k_{\text{eff}} \leq 0.95$. It was proposed in Ref. [141] that depleted uranium dioxide particulates made from enrichment plant tails can be added in the LWR waste package for long-term repository criticality control.

The actinides of the spent fuel at different discharge burnups are examined in this part. Since some actinides have relatively short half lives, such as 13.2 years for Pu-241, the isotopics are compared at 10 and 1000 years after discharge (Table 7.3). There are more minor actinides generated as the discharge burnup increases. The residual U-235 enrichment in the spent fuel increases with burnup. However, U-236 also increases significantly. In a LWR the burnup-reactivity worth of U-236 is approximately –0.24 rela-

tive to U-235 at +1.0. Therefore this makes the uranium worth less. This feature is beneficial when considering the repository criticality issue. But, on the other hand, the degraded uranium discourages reprocessing & recycling of the uranium in the high burnup fuel especially since enrichment using gaseous diffusion or centrifuge technology will further increase the U-236/U-235 ratio by another factor of 3 or so. The irradiation of U-236 produces Np-237, which is the limiting actinide for waste disposal in the Yucca Mountain assessment. Hence further irradiation (recycling of uranium) is unwise.

Table 7.3 Actinide compositions (wt%) in high-burnup spent fuels.

B_d	33 MWd/kg	50 MWd/kg	100 MWd/kg	150 MWd/kg
10 years after discharge				
U-234	0.02	0.02	0.04	0.06
U-235	0.90	1.07	1.62	2.21
U-236	0.38	0.61	1.47	2.60
U-238	97.54	96.77	94.33	91.66
Np-237	0.04	0.08	0.20	0.34
Pu-238	0.01	0.03	0.14	0.29
Pu-239	0.65	0.78	1.12	1.42
Pu-240	0.24	0.31	0.46	0.58
Pu-241	0.10	0.13	0.22	0.29
Pu-242	0.05	0.08	0.15	0.19
Am-241	0.06	0.09	0.16	0.21
Am-242m	—	—	—	0.01
Am-243	0.01	0.02	0.05	0.08
Cm-244	—	0.01	0.03	0.05
Cm-245	—	—	0.01	0.01
Pu-239/(Pu_{total})	62%	57%	54%	51%
1000 years after discharge				
U-234	0.03	0.06	0.17	0.35
U-235	1.06	1.10	1.65	2.25
U-236	0.54	0.64	1.52	2.66
U-238	97.54	96.76	94.36	91.66
Np-237	0.20	0.25	0.49	0.74
Pu-238	—	—	—	—
Pu-239	0.49	0.76	1.09	1.39
Pu-240	0.09	0.28	0.44	0.57
Pu-241	—	—	—	—
Pu-242	0.05	0.08	0.15	0.19
Am-241	—	0.05	0.08	0.11
Am-242m	—	—	—	—
Am-243	—	0.02	0.05	0.07
Cm-244	—	—	—	—
Cm-245	—	—	—	0.01

7.2.3 Neutron Spectrum Effects (H/HM)

Np-237 production, also as a function of hydrogen-to-heavy-metal ratio (H/HM), has been computed as a measure of long-term radiological hazard for high-level-waste (HLW) disposal. Figure 7.10 [142] shows the water dilution volume (WDV) needed to reach acceptable concentration levels, which characterize the in-situ hazard of different elements. After one million years the preponderant contribution comes from Np-237. Thus, the concentration of Np-237 should be tracked in the high-burnup spent fuel.

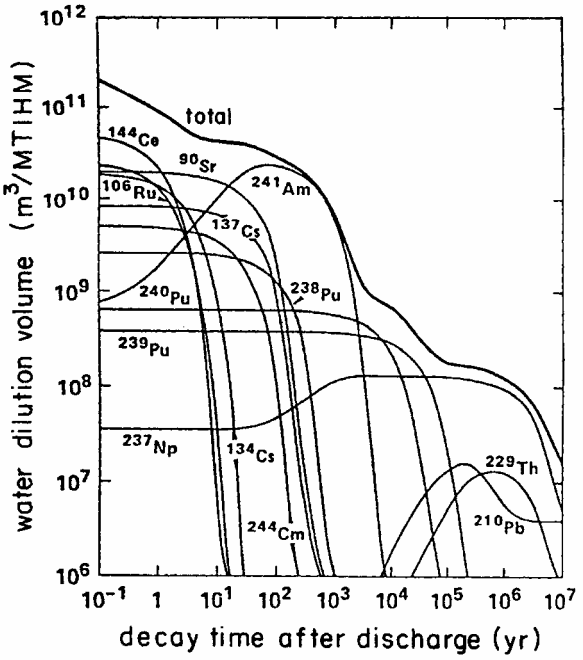

Figure 7.10 The WDV of nuclides in PWR spent fuel as a function of time [142].

Fig. 7.11 also shows a small peak for the Np-237 production in the epithermal range where H/HM is about 1.4. Here we plot a *maximum* Np-237 inventory defined as the sum of Np-237, Pu-241, and Am-241 present at discharge, since the latter two decay into the former, to roughly double the amount at time of discharge. Figure 7.11 demonstrates that high H/HM lattices are beneficial to reducing long-term radiotoxicity. Although the hard spectra region (low H/HM value) has roughly the same long-term radiotoxicity as the high H/HM lattices, both the plutonium quantity and quality are worse for the low H/HM lattices in terms of proliferation resistance.

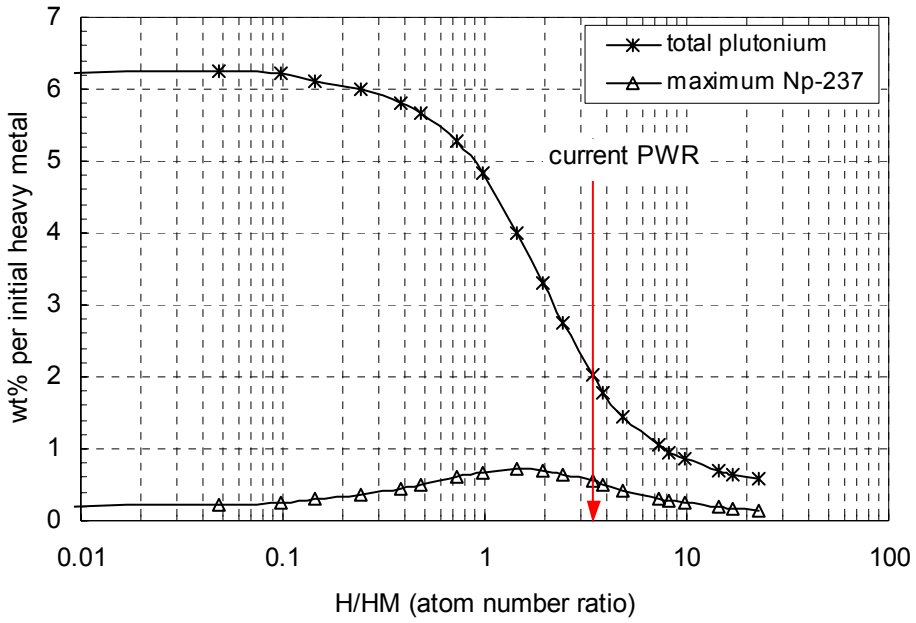

Figure 7.11 Total plutonium and maximum Np-237 for spent fuel with 100 MWd/kg, 12% initial U-235 enrichment.

7.2.4 Power Density Effect

Recently power uprating has been an attractive option for nuclear utilities to increase revenues. However, its impact on the spent fuel characteristics has not been studied. Neutronically a power uprate leads to several detrimental effects:

- *Xenon poison* The specific power of the fuel increases. Hence, the xenon concentration increases correspondingly which contributes a negative reactivity penalty.
- *fuel temperature* The fuel temperature is usually increased by power uprating, which increases the Doppler absorption, hence again reducing reactivity.
- *moderator temperature* In some power uprating approaches, the outlet temperature is raised. The average moderator temperature is thus higher in the core, which again adds a negative reactivity due to the negative MTC.

A power uprate inevitably shortens the cycle length. However, power uprating is attractive under current market conditions because more electricity is produced sooner with small added penalties. In this section, the case of doubling the power density is investigated and the spent fuel characteristics are studied.

A reference PWR pin with 4.5 w/o UO_2 is calculated: one with nominal power density and the other with doubling of the power density. Both types of spent fuel achieve 50 MWd/kg discharge burnup and no neutronic penalties are taken into consideration. Figure 7.12 shows the ratio between the case with double power density and the reference case. Doubling of the power density is seen to have a 10 year effect on both the radioactivity and the decay heat generation. This is due to the decay of the flux-dependent fission products. It is concluded that doubling the core power density is not an issue for repository considerations. But it needs to be considered for utility on-site storage (more demanding spent fuel cooling).

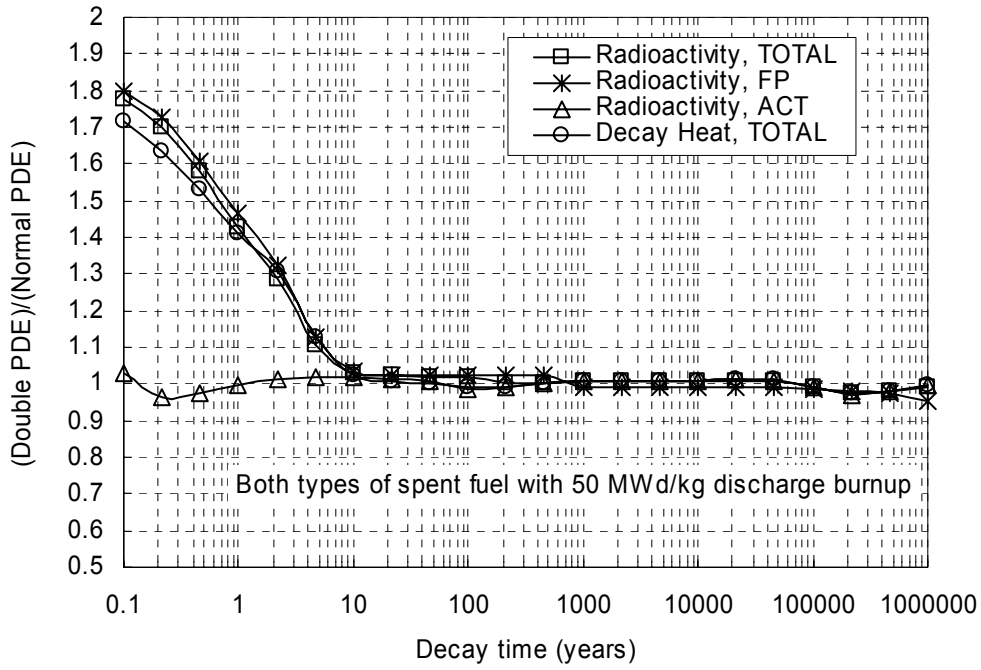

Figure 7.12 Power density effect on spent fuel characteristics.

7.3 Proliferation Resistance

7.3.1 Introduction

Plutonium is a sensitive nuclear-weapon material. Its content in the spent fuel poses a certain degree of proliferation potential. Fifteen isotopes of plutonium are known, all are

radioactive. The principle ones of interest to the design of nuclear weapons, and their half-lives/decay modes, are:

$$\text{Pu-238} \xrightarrow[87.7 \text{ years}]{\alpha} \text{U-234}$$

$$\text{Pu-239} \xrightarrow[24{,}100 \text{ years}]{\alpha} \text{U-235}$$

$$\text{Pu-240} \xrightarrow[6{,}560 \text{ years}]{\alpha} \text{U-236}$$

$$\text{Pu-241} \xrightarrow[14.4 \text{ years}]{\beta^-} \text{Am-241}$$

$$\text{Pu-242} \xrightarrow[375{,}000 \text{ years}]{\alpha} \text{U-238}$$

Based on critical mass considerations, the U-235 enrichment limit from proliferation resistance is 20 w/o, and the U-233 concentration limit in the uranium is 12 w/o [143]. However, unlike uranium, any isotopic mix of plutonium has a finite critical mass, i.e., a potential explosive material. Hence, there is no general isotopic concentration threshold for plutonium isotopes from a critical mass point of view. Nevertheless, the suitability for weapons usage varies significantly for plutonium isotopes. Table 7.4 lists the important characteristics of plutonium isotopes [144]. Pu-238, Pu-240, and Pu-242 have high spontaneous neutron generation, which reduces the bomb yield significantly. Pu-238 also has a large decay heat, which further complicates the design of an explosive device. Pu-241, although a suitable material for weapons, has a relatively short half life. If a weapon does include Pu-241 initially over several years or even decades, the reactivity worth will decline with time (note that the daughter nuclide, Am-241, is non-fissile). In conclusion, Pu-239 is the only desired isotope for weapons use, and other isotopes are important through their adverse effects.

Table 7.4 Plutonium isotope properties important to proliferation resistance [144].

	Half-life (years)	Spontaneous fission neutrons (n/kg/sec)	Decay heat (Watt/kg)	Bare critical mass (kg)
Pu-238	87.7	2,600,000	560	10
Pu-239	24,100	22	1.9	10
Pu-240	6,560	910,000	6.8	40
Pu-241	14.4	49	4.2	10
Pu-242	376,000	1,700,000	0.1	100

It was proposed in Ref. [145] a distinction be made between plutonium of different isotopic grades as shown in Table 7.5. The adoption of several categories of plutonium, as for uranium case, was proposed to promote the security and safeguards.

Table 7.5 Plutonium category divisions [145].

Categories	Pu-240 fraction	Significant quantity *	Timeliness ** (separated)	Timeliness (unseparated)
High grade	<17 percent	8 kilograms	Two weeks	One month
Low grade	17-30 percent	16 kilograms	Three months	One year
Depleted grade	>30 percent	—	One year	—

∗ The significant quantity is the approximate quantity of nuclear materials needed to manufacture a first nuclear device, taking into account losses in conversion and in manufacturing.

∗∗ Timeliness is a component of inspection goals related to the conversion time, that is the time required to convert a given nuclear material into metallic components for an explosive device.

Table 7.6 Approximate isotopic composition correlations for current PWR lattices with H/HM ≈ 3.4.

For total plutonium:

$$\frac{\text{kg Pu}}{\text{kg initial heavy metal}} = 0.0193\left(\frac{\text{B}}{100}\right)^{0.565}$$

$$\frac{\text{kg Pu}}{\text{GWe}\cdot\text{yr}} = \frac{70.45}{\eta\left(\frac{\text{B}}{100}\right)^{0.435}}$$

where B = burnup, MWd/kg;
η = thermodynamic efficiency.

For individual isotopes:

$$\frac{\text{X48}}{\text{X49}} = \left(\frac{0.0125}{\text{X25(0)}}\right)\left(\frac{\text{B}}{100}\right)^{2.47}$$

$$\frac{\text{X48}}{\text{X42}} = 9.73\left(\frac{\text{X25(0)}}{1-\text{X25(0)}}\right)\left(\frac{\text{B}}{100}\right)^{0.0339}$$

$$\frac{\text{X40}}{\text{X49}} = \frac{0.0354}{\text{X25(0)}}\left(\frac{\text{B}}{100}\right)^{1.01}$$

$$\frac{\text{X41}}{\text{X49}} = 1.47\left(1-\text{X25(0)}\right)\left(\frac{\text{B}}{100}\right)^{0.152} - 1$$

where X4z = weight fraction of plutonium isotope of mass number ending in "z";
X25(0) = U-235 weight fraction in initial heavy metal.

The applicable range of the above approximations is for burnup values 8 to 12 times initial U-235 enrichment, w/o; and X25(0) enrichments between 3 and 20 w/o. Representative average error is ≤ 5% and maximum error is ≤ 10%.
(See Ref. [146] for an alternative set of relations)

7.3.2 Higher Discharge Burnup

Increasing the discharge burnup is advantageous in improving the proliferation resistance. Table 7.6 gives correlations that relate the isotopic composition with burnup and enrichment for current design PWR lattice pin cell calculations based on the CASMO-4 data, which is an updated version of correlations given in [146]. From Table 7.6, the total plutonium accumulates approximately as the square root of burnup; hence less is produced per GWe·yr at higher burnup. For example, doubling the discharge burnup from 50 to 100 MWd/kg decreases the plutonium content by about 25%. The ratio of Pu-238 to Pu-239 increases approximately as burnup to the 2.5 power, whereas the ratio of Pu-240 to Pu-239 increases approximately proportional to the burnup.

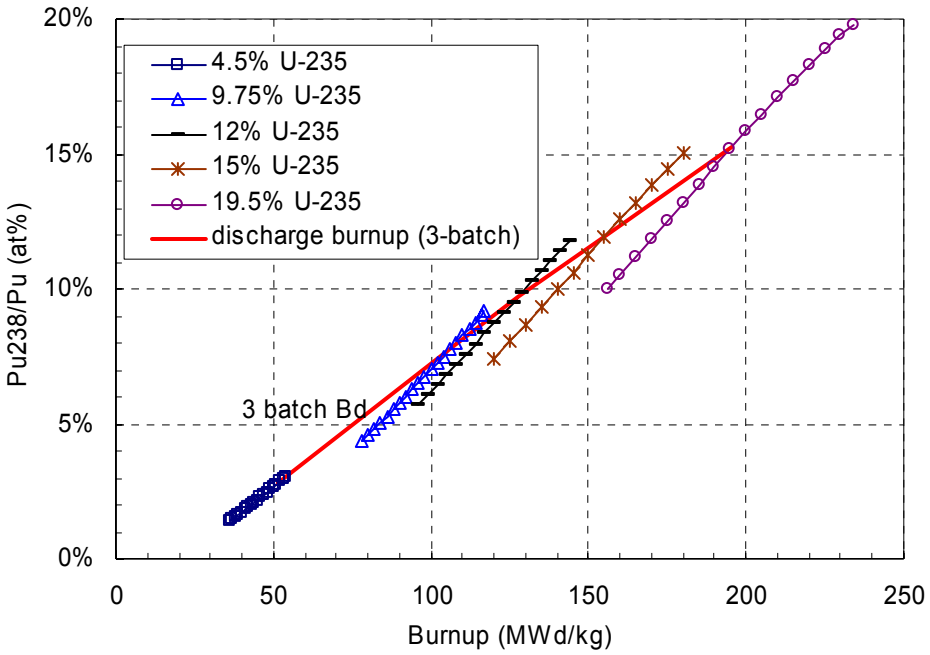

Figure 7.13 Plutonium 238 fraction versus burnup for several initial U-235 enrichments.

As an example, the fraction of Pu-238 in the plutonium is examined. Figure 7.13 shows that the fraction of Pu-238 in the discharged fuel increases slightly faster than linearly with burnup. This is represented by the intersection of the heavy line showing discharge burnup, with the marked lines showing Pu-238 content for various initial enrichments. For example, doubling the burnup (from 50 MWd/kg using 4.5 w/o to 100 MWd/kg using 9.75 w/o assuming three batches) would increase the Pu-238 fraction to

about 7%. Pu-238 is so undesirable that some authors see too many difficulties beyond a 2 percent fraction of the total plutonium [145]. The figure also demonstrates the importance of using an appropriate initial U-235 enrichment when calculating Pu-238 content. Note that for a fixed discharge burnup (corresponding to a vertical line in Fig. 7.13), increases in the initial U-235 enrichment actually reduce the Pu-238 content at discharge.

In conclusion, the isotopic mix of plutonium is less weapons usable at higher burnup while the total plutonium production is reduced. However, it is conceded that any composition of plutonium can be fabricated into a crude, low yield bomb in the kiloton range given sufficient determination and ingenuity [144]. Nevertheless, a recent assessment [147] assigns Pu-239 ~ 40% to a category one step down in weapons usability compared to the 60% representative of current LWR spent fuel; this favors higher burnup.

7.3.3 Neutron Spectrum Effect (H/HM Variation)

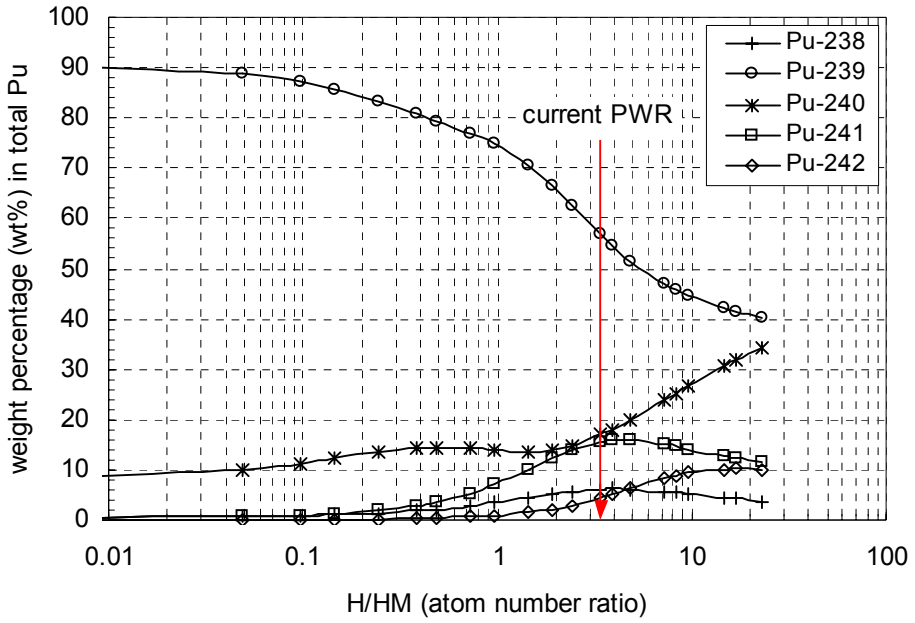

Figure 7.14 CASMO-4 pin-cell predictions of isotopic composition of Pu in spent fuel at 100 MWd/kg for lattices with initial enrichment of 12%.

Figure 7.14 shows the results of CASMO-4 calculations of the isotopic composition of plutonium as H/HM is varied above and below the value of 3.4, typical of current PWRs, for a specific uranium enrichment (12%) and burnup (100 MWd/kg).

The plutonium production at a given burnup increases monotonically as H/HM decreases (Fig. 7.11), while weapon usability increases (Fig. 7.14). In particular spontaneous fission neutron emission, which is dominated by Pu-238 concentration, is reduced as the lattice becomes progressively drier. The same is true of Pu-240 and Pu-242, which also help spoil the plutonium mix as potential weapon material. Thus, current H/HM value (~3.4), or slightly wetter lattices generate the most proliferation-resistant spent fuel from PWRs.

The heat generation per unit mass of plutonium peaks fortuitously in the neighborhood of the present design, as shown in Figure 7.15 [148]. In contrast to this behavior, the neutron source per mass of plutonium rises monotonically with H/HM. Overall the present design point appears near optimum with regard to neutron and heat barriers to proliferation.

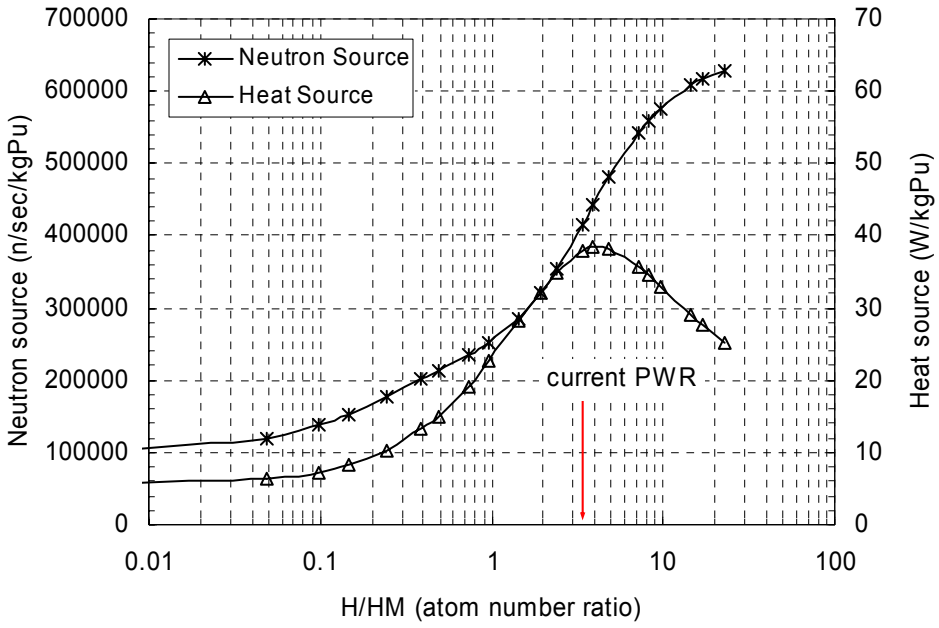

Figure 7.15 Spontaneous neutron and heat generation rates vs. H/HM at 100 MWd/kg, 12 w/o initial U-235 enrichment [148].

7.4 Other Considerations

While focused on UO_2-fueled water moderated reactors, the trends noted above also apply to other coolants if one defines an equivalent H/HM value which accounts for their reduced slowing down power.

Also note that plutonium fueling was not considered in this study since a fresh core of even a small power reactor would contain more than one hundred weapons worth of plutonium and thereby defeat the overarching purpose of this exercise. Similarly, a once-through fuel cycle minimizes the transuranics content in the core.

7.5 Chapter Summary

Overall it is concluded that wetter lattices offer a better approach for reducing the amount and weapons usability of plutonium in spent nuclear reactor fuel. Considerable benefits to the volume of spent fuel and its heat load can be achieved if higher burnup is also pursued as a strategy.

8. Economics Aspects of High Burnup

"He intends only his own gain, and he is in this, as in many other cases, led by an invisible hand to promote an end which was no part of his intention"
— A. Smith (1723-1790)

8.1 Introduction

The current nuclear fuel cycle practice in the US is the once-though fuel cycle. Thus one goal of high burnup is to promote better fuel utilization in this mode, since the fuel will not be recycled. Recent developments in the nuclear fuel cycle have been motivated by combined environmental, economic, and social considerations [30]. Only the economic aspect of high burnup options is addressed in this chapter. The primary focus is on nuclear fuel cycle economics although other considerations, such as refueling outages and power uprating, are also considered. A typical cost breakdown in OECD countries shows that the fuel cycle cost accounts for about 20% of the busbar cost (Fig. 8.1 [30]). Advanced LWRs, however, are expected to have a lower capital cost compared to conventional reactors; hence a larger fraction of nuclear fuel cycle cost.

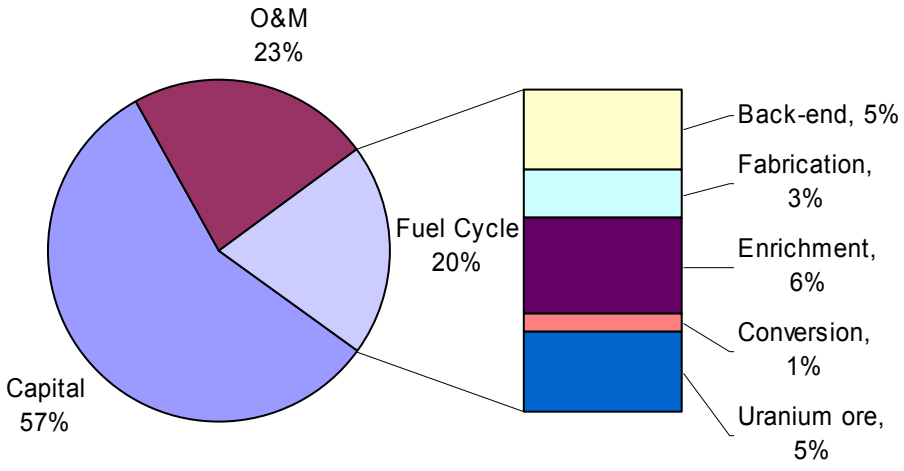

Figure 8.1 Nuclear electricity generation cost breakdown [30].

For existing conventional PWRs, higher discharge burnup implies longer in-core residence time for the fuel, which raises series concerns such as increased cladding corrosion and more gaseous fission product production/release. A typical licensed limit of the rod-average burnup is 62 MWd/kg for some PWR fuels in the US [37] while the current batch-averaged discharge burnup is already around 50 MWd/kg. Hence there is limited option space for further burnup increase while satisfying material limits and regulatory requirements based on current fuel technologies. In this chapter, however, the high burnup discussion assumes going beyond the current fuel enrichment licensing and burnup limits in recognition of the likelihood that achieving a higher burnup will be easier for future non-retrofit PWR designs.

8.2 Nuclear Fuel Cycle Economics

8.2.1 Introduction

The flow chart of the current once-through nuclear fuel cycle in the US is shown in Fig. 8.2. Transportation of the fuel is usually needed between two consecutive process steps, and it is assumed that there is no loss of material due to transportation. For example, the product of the enrichment plant is the same as the feed into the fabrication plant. The fuel cycle can be divided into three stages:

- *the front end* including uranium ore mining & milling, conversion, enrichment, and fuel fabrication;
- *reactor irradiation* during which the electricity is produced;
- *the back end* including spent fuel storage and final disposal.

Generally speaking, the front end is a mature commercial market, but there are considerable uncertainties about the back-end of the fuel cycle, e.g., final disposal of wastes remains undemonstrated in most countries. The most significant feature of the current fuel cycle in the US is the planned direct disposal of the spent fuel, i.e., no reprocessing, which originated from political consideration of weapons proliferation in the late 1970s. Although better uranium resource utilization can be achieved by reprocessing (sustain-

ability), there is still considerable skepticism about reprocessing nowadays for a variety of reasons:

- The use of virgin uranium is quite likely to be made an even more economic option by inevitable future improvements in ore recovery and enrichment technology. One should note that over the past century, the average cost of all minerals has, as a long term trend, decreased (in constant dollars). This is largely due to progressive improvements in exploration and extraction technology. While average ore grade may have declined, scarcity has been offset by ingenuity. Improved centrifuges are continuously being developed and deployed. Laser methods are in the R&D phase and molecular nano-technology is growing as a sub-discipline of physics and chemistry. The theoretical minimum work of separation is approximately six orders of magnitude lower than that expended in current processes! Therefore, it is not prudent to assume that costs must surely escalate, much less rapidly so, in the foreseeable future. The threat of "running out" of a mineral within a few decades is a consequence of free market behavior, since expenditures proving out reserves are hard to justify more than about two decades in advance at commercially interesting rates of return. Therefore, resource conservation via reprocessing of spent fuel might not be economically attractive.
- Reprocessing is not needed to permit production of a more robust waste form since other alternatives are available to reduce the probability of the escape of radionuclides from a repository. For example, adding a backfill containing depleted uranium (available in accumulated enrichment plant tails at more than 5 kg per kg of spent LWR fuel) can alter the local chemical environment to reduce the rate of dissolution of the spent fuel. Adding another overpack canister and/or clay with ion exchange capability has also been proposed as palliative measures.
- Reprocessing is not currently economic nor is it likely to become so, particularly given public pressure for "zero-release" operations. Current MOX users usually treat their recycled plutonium as "free", and reprocessing costs are charged off to other accounts, such as the postulated need to turn the spent fuel into a more robust waste form of glass or synrock.

In conclusion, reprocessing, although it might be more interesting for high burnup studies due to higher residual fissile content, is not considered in the current economic evaluation.

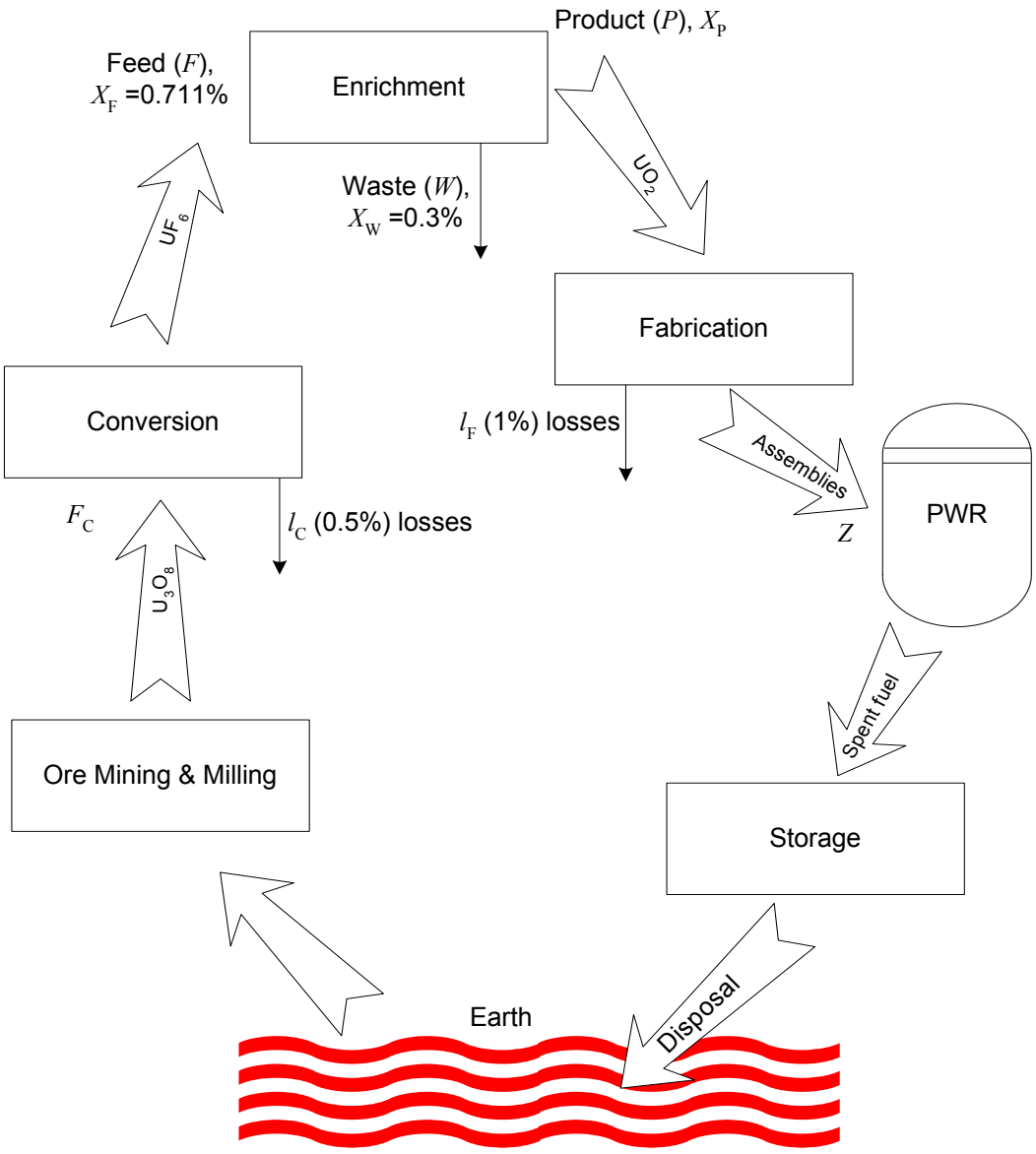

Figure 8.2 Flow chart of current once-through fuel cycle.

8.2.2 The Fuel Cycle Cost Calculation

Corresponding to the current fuel cycle flow chart (Fig. 8.2), a cash flow diagram (Fig. 8.3) shows all cost vectors as a function of time. It is assumed that the cost of transportation is already included in individual process steps. The fuel cycle cost is then calculated as the ratio of the present value of the dollars expended on the batch to the present value of the energy generated by the batch.

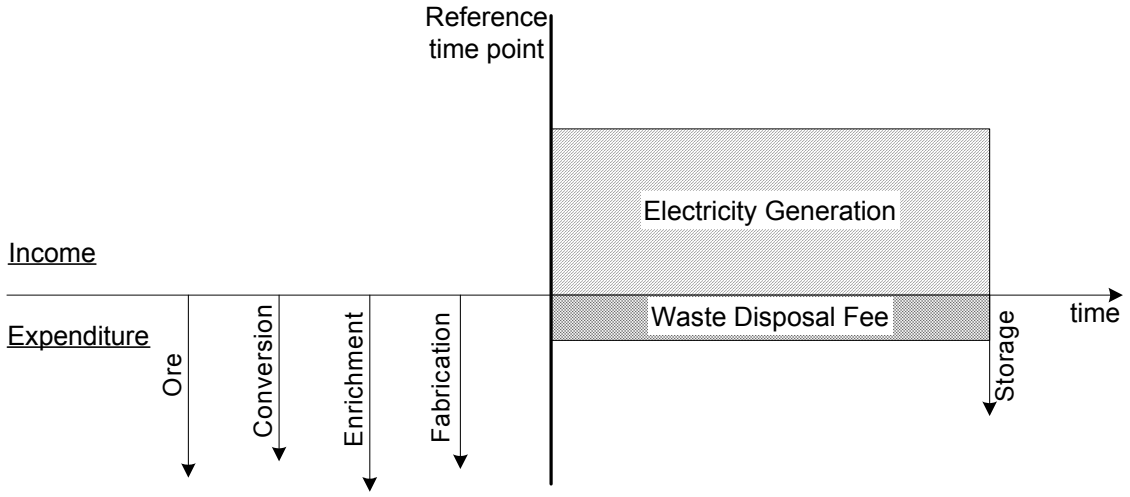

Figure 8.3 A schematic cash flow diagram for the current once-through fuel cycle.

Several points should be noted:

- A continuously compounded model is employed and the reference time is set at the beginning of irradiation (Fig. 8.3). The equivalence between the continuous and discrete rates is

$$i_c = \ln\left(1 + i_d\right), \tag{8.1}$$

  in which i_c = continuous compounding rate, (%/year)/100

  i_d = discrete compounding rate, (%/year)/100.

  Thus, if i_d = 10% per year, the continuous compounding rate, i_c = 9.53% per year.
- The fuel cycle cost is calculated for the energy generated by that batch only, not the rated core power output. The power history shape of the specific batch of the fuel is ignored. In addition the refueling downtime is ignored. Thus the energy generation is assumed to be uniform over the fuel residence time in the core.
- Evaluation of the fuel cycle cost will be based on an equilibrium basis, which provides a reasonable basis for comparison between existing fuel types or other new types. For economics purposes, an "equilibrium" requires both a technical equilibrium (all batches are identical and have identical operating histories) and an economic equilibrium (no escalation — all batches require the same dollar expenditure).
- Price escalation, including inflation (loss in the value of the dollar as time passes), is excluded. To include inflation and escalation usually leads to interminable arguments about how much inflation and escalation is appropriate. However, escalation and in-

flation can be added when calculating fuel costs for specific transition and operating cycles under specified economic and contracting situations. Another argument in favor of this approach is that cost can decrease with time due to processing improvements.

The overall nuclear fuel cycle cost, including both the front end and the back end, can be written as:

$$e_{\mathrm{NFC}} = \frac{C_{\mathrm{fuel}}}{24\eta B_{\mathrm{d}}} \cdot \left(\frac{i_{\mathrm{c}} T_{\mathrm{res}}}{1 - e^{-i_{\mathrm{c}} T_{\mathrm{res}}}} \right) + e_{\mathrm{disposal}}\,, \tag{8.2}$$

where e_{NFC} = the fuel cycle cost, mills/kW·hr(e)

C_{fuel} = total fuel cost (excluding disposal) at beginning-of-irradiation, $/kgIHM

η = plant thermodynamic efficiency, i.e., 1150MW(e)/3411MW(th) = 33.7%

B_{d} = batch-average discharge burnup, MWd/kgIHM

i_{c} = continuous compounding rate per year

T_{res} = fuel residence time in the core, years

$= nT_{\mathrm{c}}$, (n is number of batches and T_{c} is cycle length in calendar years)

e_{disposal} = federal waste disposal fee, 1 mill/kW·hr(e).

The fuel cost (excluding disposal), C_{fuel}, in Eq. (8.2) can be further decomposed as:

$$C_{\mathrm{fuel}} = C_{\mathrm{ore}} + C_{\mathrm{conv}} + C_{\mathrm{SWU}} + C_{\mathrm{fab}} + C_{\mathrm{storage}}\,, \tag{8.3}$$

where all cost terms are in units of $/kgIHM at the beginning-of-irradiation. Two factors need to be considered then: (1) the material flow based on one kg IHM at the beginning of irradiation; (2) the lead time of each process.

Denote mass flow rates (kg/kgIHM) for each process as M_{ore}, M_{conv}, M_{SWU}, M_{fab}, and M_{storage}. Assuming that the reactor requires Z kg of IHM (Fig. 8.2), i.e., the mass flow from the fabrication process is also Z kg IHM (no loss in transportation). Thus,

$$M_{\mathrm{fab}} = \frac{Z}{Z} = 1\,. \tag{8.4}$$

In the enrichment process, the product uranium, P, is

$$P = \frac{Z}{1 - l_{\mathrm{F}}}\,, \tag{8.5}$$

where l_{F} is the fabrication loss, 1%. The SWU requirement is then

$$M_{\mathrm{SWU}} = \frac{S}{Z} = \frac{1}{1 - l_{\mathrm{F}}} \left[V\left(X_{\mathrm{P}}\right) - V\left(X_{\mathrm{W}}\right) - \left(X_{\mathrm{P}} - X_{\mathrm{W}}\right) \frac{V\left(X_{\mathrm{F}}\right) - V\left(X_{\mathrm{W}}\right)}{X_{\mathrm{F}} - X_{\mathrm{W}}} \right], \tag{8.6}$$

where S = the separative work requirement, kgSWU

$V(X_i) \equiv (1-2X_i)\ln\frac{1-X_i}{X_i}$ for X_i expressed as weight fractions. The subscript i represents P (product), F (natural uranium feed), or W (waste tails). Note that the tails enrichment is assumed 0.3% in the following calculations.

The conversion process mass flow is

$$M_{\text{conv}} = \frac{F}{Z} = \frac{1}{1-l_{\text{F}}}\left(\frac{X_{\text{P}} - X_{\text{W}}}{X_{\text{F}} - X_{\text{W}}}\right). \tag{8.7}$$

After considering the conversion loss, the uranium ore flow rate is

$$M_{\text{ore}} = \frac{F_{\text{C}}}{Z} = \frac{1}{1-l_{\text{C}}}\frac{1}{1-l_{\text{F}}}\left(\frac{X_{\text{P}} - X_{\text{W}}}{X_{\text{F}} - X_{\text{W}}}\right), \tag{8.8}$$

where l_{C} is the conversion loss, 0.5%.

For the back-end storage, the mass flow rate should be the same as the fuel discharged from the reactor, i.e.,

$$M_{\text{storage}} = \frac{Z}{Z} = 1. \tag{8.9}$$

With mass flow rates given as Eqs. (8.4) to (8.9), the lead time of each process also needs to be taken into consideration. Final costs of each process discounted to the beginning of irradiation are as follows:

$$\begin{cases} C_{\text{ore}} = c_{\text{ore}} M_{\text{ore}} e^{i_{\text{c}} T_{\text{L,ore}}} \\ C_{\text{conv}} = c_{\text{conv}} M_{\text{conv}} e^{i_{\text{c}} T_{\text{L,conv}}} \\ C_{\text{SWU}} = c_{\text{SWU}} M_{\text{SWU}} e^{i_{\text{c}} T_{\text{L,SWU}}} \\ C_{\text{fab}} = c_{\text{fab}} M_{\text{fab}} e^{i_{\text{c}} T_{\text{L,fab}}} \\ C_{\text{storage}} = c_{\text{storage}} M_{\text{storage}} e^{-i_{\text{c}} T_{\text{res}}} \end{cases}, \tag{8.10}$$

where c_{ore}, c_{conv}, c_{SWU}, c_{fab}, c_{storage} are unit costs for each process and $T_{\text{L,ore}}$, $T_{\text{L,conv}}$, $T_{\text{L,SWU}}$, $T_{\text{L,fab}}$ are lead times. Note that the storage cost is assumed to be spent at the end of irradiation, which is therefore discounted back to the beginning of irradiation.

The fuel cycle economic parameters, such as the unit cost of each process, vary with market conditions at different time periods and in different countries. The reference parameters are summarized in Table 8.1 from the 1994 OECD report [149]. Some more recent estimates of the lower and upper bounds of unit costs as expected to be applicable

in the short to medium term are also included [30]. Significant uncertainties can be seen from the lower and upper bound estimates, particularly for the uranium ore purchase.

Table 8.1 The fuel cycle economics parameters [30, 149].

Parameters	Reference	Lower bound	Upper bound
Unit costs:			
— uranium ore purchase ($/kg$U_{NAT}$)	50	24	94
— conversion ($/kgU)	8	3	8
— enrichment ($/kgSWU)	110	80	120
— fuel fabrication ($/kgU)	275	200	300
— spent fuel storage ($/kgU)	120	100	300
— waste disposal fee (mills/kW·hr-e)	1.0 (US)		
Lead time prior to irradiation:			
— uranium ore purchase (months)	24		
— conversion (months)	18		
— enrichment (months)	12		
— fabrication (months)	6		
Other fuel cycle data:			
— carrying charge rate per year	10%		
— tails assay enrichment (w/o)	0.3		
— conversion loss	0.5%		
— fabrication loss	1.0%		

8.2.3 High Burnup for Conventional PWRs

8.2.3.1 Enrichment Increase

For existing PWRs, the traditional way of enhancing fuel utilization is to increase the burnup via higher reload fuel enrichment, hence better fuel cycle economics. However, it is questionable whether it is still economic to continue to increase enrichment beyond the current licensing level of 5 w/o. The uranium and SWU utilizations are shown in Chapter 2, which suggests that current discharge burnup is close to optimum. Here a detailed fuel cycle cost analysis is demonstrated for discharge burnup between 40 MWd/kg and 100 MWd/kg. The linear reactivity model is assumed, and the burnup-enrichment correlation is taken from Eq. (2.8) in Chapter 2. The reference PWR parameters are taken from Table 2.2, and the capacity factor is taken as 87%. In this study the cycle length is fixed as 18 months. This is different from previous economic analysis where the number of batches is fixed [9]. Hence higher burnup can be achieved due to larger n.

The nuclear fuel cycle cost is computed for conventional PWRs with a fixed 18-month cycle (Fig. 8.4). Besides the total fuel cycle cost, the six cost components are also shown individually in Fig. 8.4. The current PWR with a discharge burnup of 50 MWd/kg has a fuel cycle cost of 6.8 mills/kWhr-e, which is close to the weak optimum of ~6.7 mills/kWhr-e at ~65 MWd/kg. In view of large uncertainties about the economic parameters, there is no strong economic incentive for current PWRs to go beyond 50 MWd/kg from the nuclear fuel cycle cost perspective. Neither, on the other hand, is there a large disincentive. Section 8.3 discusses economic factors other than fuel cycle cost which could favor high burnup.

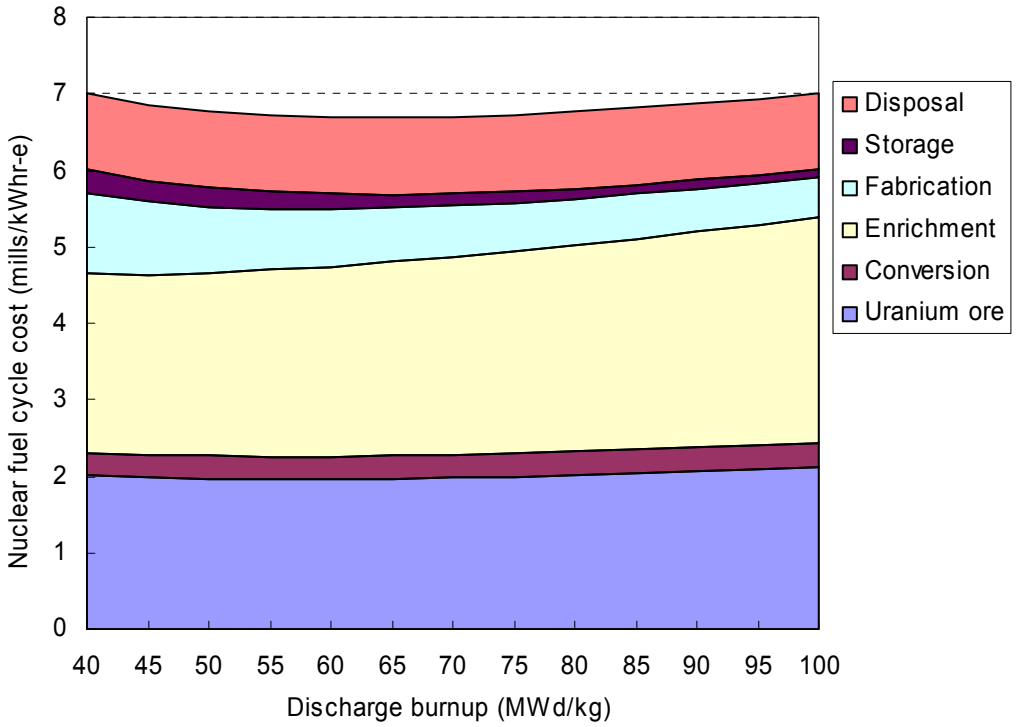

Figure 8.4 Fuel cycle cost for 18-month conventional PWRs.

The uranium ore purchase and the SWU cost are the dominant factors in the fuel cycle cost. The uranium ore purchase and the conversion cost appear to be almost constant for the various discharge burnup values, from which it can be inferred that the natural uranium requirement is almost the same between 40 MWd/kg and 100 MWd/kg.

The enrichment cost shows a sizable increase with burnup due to the need for higher reload fuel enrichment. The enrichment price of 110 $/kgSWU might need to be

revised for enrichment above 5 w/o due to the re-licensing and design costs of the enrichment facilities. Within the current 5 w/o limit, the discharge burnup can reach about 55 MWd/kg for an 18-month-cycle PWR. Future technology innovations will eventually push the SWU cost down since the current enrichment process is six orders of magnitude more expensive compared to the minimum separation work (energy usage), which favors high burnup. A sensitivity calculation is performed for different SWU costs (Figure 8.5). The minimum fuel cycle cost is pushed to higher burnup as the SWU cost decreases.

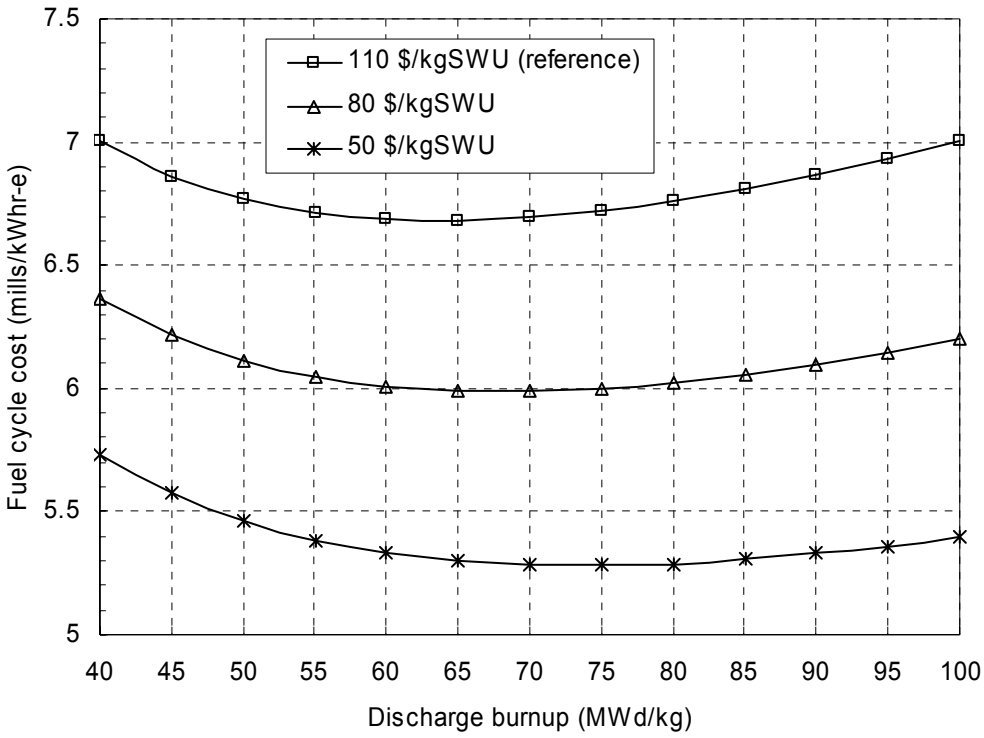

Figure 8.5 Sensitivity to SWU costs for 18-month-cycle PWRs.

In spite of their smaller fractions compared to the SWU cost, the fabrication and storage costs decrease monotonically with burnup, which cancels part of the increasing SWU cost. The primary reason is the fewer fuel assemblies needed per reload. However, for high burnup assemblies, the fabrication cost might well be more expensive due to the need to make them more robust. The increased burnable poison addition, as needed for high burnup cores, also raises the fabrication cost. Another point to note is that there are

limited incentives for fuel vendors to greatly increase product burnup since it reduces the number of assemblies ordered.

The spent fuel storage component is a relatively small contributor. Therefore, the savings due to fewer discharged spent fuel assemblies are small. Since the storage cost occurs after the fuel irradiation, it needs to be discounted back to the beginning of irradiation; that alone lowers the direct cost by a factor of ~0.6. On the contrary there are other considerations increasing the storage cost: higher-burnup fuel assemblies generally have higher decay heat levels and are more radioactive as shown in Chapter 7, which would increase the storage cost. Hence actual storage costs might not decrease much with burnup.

The current disposal cost in the US is 1 mills/kWhr-e, which is a constant contributor to the total fuel cycle cost. However, as shown in Chapter 7, the higher-burnup spent fuel has better proliferation-resistance characteristics, e.g., a degraded plutonium vector. The ^{240}Pu-to-^{239}Pu atom number ratio in the spent fuel is roughly proportional to the burnup whereas the ^{238}Pu-to-^{239}Pu ratio is proportional to the 2.5 power of the burnup. Credits for better proliferation resistance and fewer spent fuel assemblies need to be reflected back to the fuel cycle cost. If the waste fee was to be based on $ per kg initial heavy metal (IHM), the disposal cost would actually decrease with burnup. Hence the regulation for collecting waste fees could be revised by the government to reflect these credits. An increased incentive for high burnup would be provided if the spent fuel disposal fees were simply based on the spent fuel mass rather than on electricity sales.

In summary, from a utility's point of view, there is really not much incentive to go beyond current practice. The option space is also limited, i.e., below 5 w/o, the discharge burnup is limited to ~55 MWd/kg. External incentives are needed for making the high burnup approach more attractive, e.g., switching to a waste fee based on per unit of mass of spent fuel.

8.2.3.2 Effect of a Wetter Lattice

A higher burnup can be achieved for a wetter lattice with the same fuel enrichment as discussed in Chapter 4. Two practical ways of increasing H/HM are considered here: reducing the rod diameter and employing an annular fuel pellet (center-voided). The reference PWR is an 18-month-cycle core with capacity factor of 87% and n = 2.71. When

varying H/HM, the cycle energy production is kept constant. Therefore, the reload fuel enrichment increases with H/HM to compensate for the loss of initial fuel loading as shown in Fig. 8.6. At the same final H/HM, varying the rod diameter requires lower-enriched fuel to maintain the same cycle length. In fact because of the central void, the effective fuel loading per unit core volume for the annular fuel pellet is smaller compared to the rod diameter variation case under the same H/HM. Therefore, a higher discharge burnup is required for the case of annular fuel pellets, which results in a worse utilization compared to the case of varying rod diameter. Under the same enrichment limit, varying the rod diameter has a larger option space for H/HM variation.

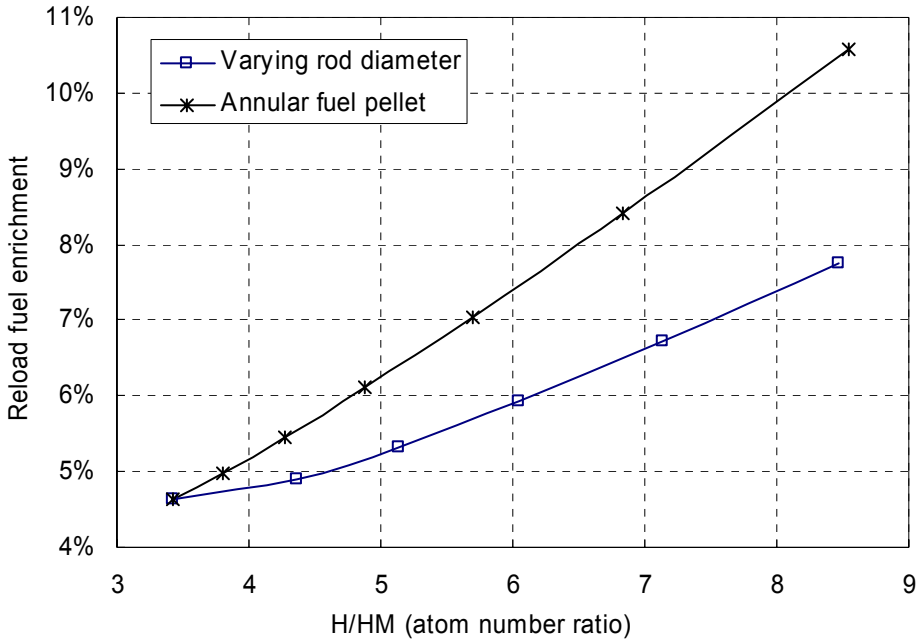

Figure 8.6 Reload fuel enrichment requirement with H/HM.

The fuel cycle costs at different H/HM values (or discharge burnup) are shown in Fig. 8.7. Varying rod diameter is better than using the annular fuel pellets because of a larger potential fuel cycle cost reduction when varying the rod diameter. In fact, the decrease of the fuel cycle cost is sizable (~10%) between 50 MWd/kg and 60 MWd/kg. The current Westinghouse optimized fuel design has a wetter lattice (~10% wetter than a normal lattice), which uses this feature to save the fuel. Based on Fig. 8.7 the optimum discharge burnup for varying rod diameters appears to be around 75 MWd/kg whereas

the optimum burnup for annular fuel pellets is around 90 MWd/kg. Note that manufacturing of the annular fuel pellets may be more expensive than the solid fuel, which exerts an additional penalty for the annular fuel pellet. On the other hand, decreasing the rod diameter would be limited by the DNBR consideration and may not be feasible beyond ~20%, i.e., beyond H/HM≈8.0 (corresponding to solid fuel burnup of 85 MWd/kg).

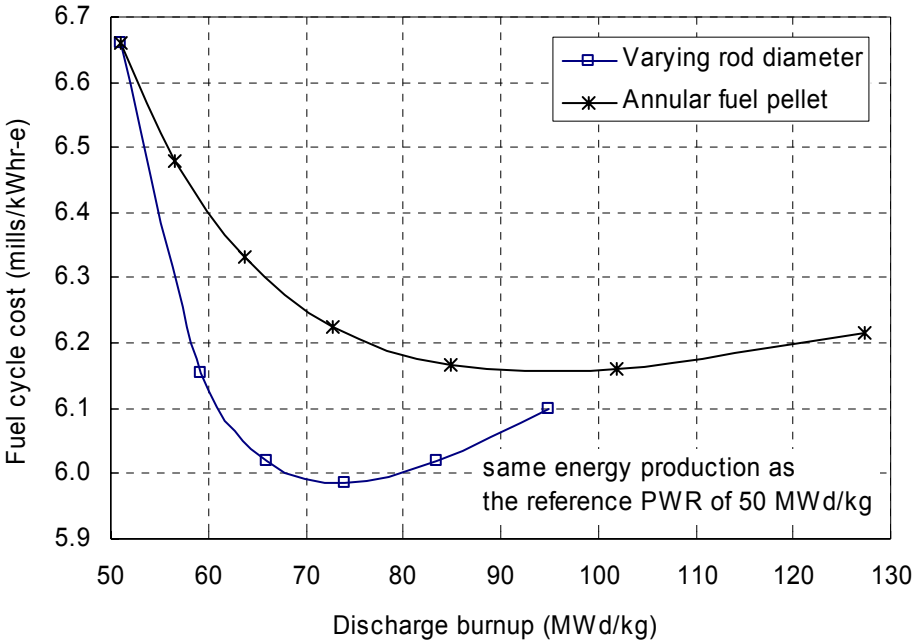

Figure 8.7 Fuel cycle costs with discharge burnup (same core energy production).

A detailed fuel cost decomposition is shown for the central-voided annular fuel in Fig. 8.8. Again the major decreasing component is the fabrication cost. The 10% void case (i.e., 10% wetter) has a fuel cycle cost decrease of ~3%. Although it appears to be a small gain, the fuel cycle cost saving will be about 1.5 million dollars per year for the current 18 month fuel cycle (which has about 50 million dollars per year of total fuel cost). In addition the introduction of the central-voided annular fuel essentially has no effect on the thermal margins, except to lower the fuel temperature by ~25%. Russian VVERs are actually operating with such fuel, having a 10% central void.

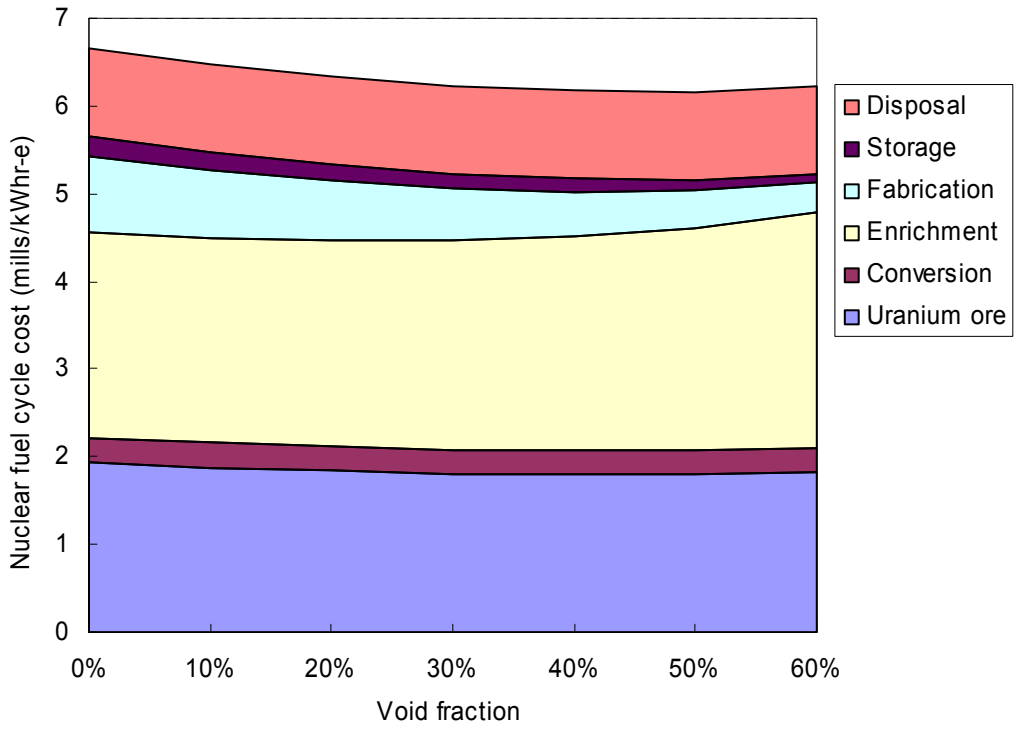

Figure 8.8 Fuel cycle decomposition for the central-voided annular fuel.

However, reducing the rod diameter reduces the thermal margin. This problem is particularly important if a core power upgrade is desired. Based on a solid fuel rod design, one solution is to increase the number of pins in the assembly, e.g., from 17×17 to 19×19. Also, one might modify the central-voided annular fuel design: either to use some moderating material, such as ZrH_2, to fill in the central hole for additional moderation or to use the IXAF concept with fuel cooled from both sides. However, the IXAF concept might have a worse fuel cycle cost compared to the solid fuel pin or the ZrH_2-filled annular fuel because of the increased parasitic absorption of the added cladding as discussed in Chapter 5.

8.2.4 Operational Strategies

High burnup fuel also provides more scope for optimization such as choosing the number of batches, cycle length; and the specific power (burnup rate) for a new core design. Several high burnup cases using 9.75 w/o UO_2 have been compared to the reference 18-month-cycle PWR using 4.63 w/o UO_2. The high burnup cases roughly double the refer-

ence PWR burnup (on a single batch reload basis, B_1). As described in Chapter 1, four principal specific options are considered to exploit high burnup capability:

1. increase the cycle length and keep the same number of batches (longer cycle);
2. keep the 18 month cycle and increase the number of batches (more batches);
3. a very long life core with single-batch refueling (single batch);
4. 100% power uprating (burn faster), keep the same cycle length (power upgrade).

The first two options are retrofitable while the last two are probably for new cores only. Table 8.2 summarizes the fuel cycle cost comparisons among the four high burnup schemes.

Table 8.2 Fuel cycle cost comparison of different high burnup strategies.

	Reference PWR	High burnup schemes			
		Retrofit cores		New cores	
		Longer cycle	More batches	Single batch	Power upgrade
Operating parameters:					
Enrichment (w/o)	4.63	9.75			
B_1 (MWd/kg)	33.90	70.42			
Cycle burnup (MWd/kg)	18.28	37.96	18.28	70.42	36.55
B_d (MWd/kg)	49.53	102.9	122.6	70.42	104.3
Cycle length (month)	18	34.5	18	62.9	18.0
Number of batches, n	2.71	2.71	6.71	1	2.85
Specific power (W/gU)	38.7	38.7			77.4
Refueling outage (days)	45.5	40	45.5	40	45.5
Forced outage rate (%)	6	3	6	3	6
Capacity factor (%)	86.2	93.3	86.2	95.0	86.2
Fuel cycle cost (10% carrying charge per year):					
Levelizing factor*	1.217	1.440	1.586	1.285	1.229
Fuel cost ($/kgIHM)**	1917	4045	4033	4060	4068
e_{NFC} (mills/kWhr-e)***	6.82	8.00 (+17%)	7.45 (+9%)	10.2 (+50%)	6.93 (+2%)
Direct fuel cycle cost (no carrying charge):					
e_{NFC} (mills/kWhr-e)	5.33	5.34 (+0.2%)	4.64 (–13%)	7.34 (+38%)	5.28 (–1%)

* The levelizing factor is $\left(\frac{i_c T_{res}}{1-e^{-i_c T_{res}}}\right)$.

** The fuel cost is calculated at the beginning of irradiation.

*** The numbers in parentheses are changes relative to the reference PWR.

The capacity factor, L, is defined as the ratio of actual electricity produced to the amount of electricity which could be produced by continuous full-power operation:

$$L = \left(1 - \frac{T_R}{30.44 T_c}\right) L', \tag{8.11}$$

where L' = 1 – (Forced outage rate) = availability

T_R = refueling outage length, days (1 month equals 30.44 days)

T_c = calendar cycle length, months.

For longer cycles and the same n, the shutdown cost is saved. Table 8.2 shows an improved capacity factor compared to the reference PWR. However, previous analysis found no benefit in cycles ≥ 24 months, i.e., added enrichment costs offset the savings [10, 11]. The direct fuel cycle cost is almost the same as the reference PWR; hence the resource utilization is about the same.

For more batches and the same 18-month cycle, the number of batches increases from 2.71 to 6.71. The factor $\left(2n/(n+1)\right)$ goes from 1.46 to 1.74, i.e., an increase of ~19%. This extra burnup allows (almost) one more free cycle. However, the levelizing factor (at 10% carrying charge per year) increases from 1.217 to 1.586 (by ~30%), which penalizes the long in-core residence time in order to achieve high burnup by using more batches. The eventual fuel cycle cost is still 9% more expensive than the reference PWR. However, the direct fuel cycle cost shows that this approach actually has maximum utilization of the uranium resource, even when compared to the reference PWR. This could serve as the basis for governmental action to encourage high burnup.

The single batch, long life core suffers significantly from the loss of burnup. The resulting fuel cycle cost is almost prohibitive to be considered by utilities. If the core power densities need to be further reduced in order to achieve a really long core life, the fuel cycle cost will increase even more rapidly since the levelizing factor can be written as:

$$\left(\frac{i_c T_{res}}{1 - e^{-i_c T_{res}}}\right) \approx i_c T_{res} = i_c \frac{B_d}{q_{SP}} \propto \frac{1}{q_{SP}}, \tag{8.12}$$

where q_{SP} is the specific power. However, if other special considerations, e.g. the proliferation resistance, would ever dominate the economics, this approach can still be used.

For the 100% power uprate case in new core designs, one effectively reduces the fuel residence time in the core, e.g., at the same B_d, one can achieve it in 4.5 years instead of 9.0 years. The levelizing factor is comparable to the reference PWR. However, this also cuts the number of batches in half, which negates most of the rapid burn savings.

The final comparison between this approach and the reference PWR shows that they are closest in fuel cycle costs, whether for the 10%/year carrying charge rate or with no carrying charges. If the clad corrosion problem dominates, the rapid burn may be the only feasible option.

In conclusion, the high burnup approach under current market conditions doesn't offer much better fuel cycle economic performance compared to conventional practice even considering a wide range of strategies. Long core residence time penalizes the carrying charge via the levelizing factor while the increasing cycle burnup, including faster burning and cycle length extension, reduces the discharge burnup. From an operational strategy point of view, the current 3-batch, 18-month cycle core is about the optimum for the fuel cycle cost. This agrees with previous findings by M. V. McMahon, M. J. Driscoll, and E. E. Pilat that we are reaching the end of the era in which nuclear fuel cost can be significantly further reduced by innovative core design and in-core fuel management strategies [56]. Therefore, the cost-competitiveness of LWRs must be secured by other means. One only need to keep close to the current optimum fuel cycle cost for a new core design. Among the four high burnup strategies, power uprate and increased number of batches are recommended. Also more consideration should be given to action by the government to reflect high burnup advantages in their waste fee, i.e., for reduced back end assembly handling and better proliferation resistance.

8.2.5 High Burnup in Different Neutron Spectra

Up to now, the discussion is entirely based on an LWR thermal spectrum. However, as shown in Chapter 4, there exist significant variations of burnup capabilities depending on the neutron spectrum. In particular the fast region shows much larger burnup potentials compared to the epithermal and thermal regimes. Although not widely known, it is possible to design fast reactors which operate on a once-through fuel cycle mode. Such fast reactors are capable of extending economically exploitable uranium resources by an order of magnitude or more versus using only LWRs. (For comparison, LMFBRs in the recycle mode are another order of magnitude more resource-unlimited.) Hence four H/HM values are chosen from the unit cell calculations in Chapter 4 to represent typical neutron spectrums:

- H/HM=3.4, the reference PWR lattice, denoted as R

- H/HM=5.0, a wetter lattice with increased moderation, denoted as W
- H/HM=0.8, an epithermal-spectrum lattice, denoted as E
- H/HM=0.2, a fast-spectrum lattice, denoted as F.

Two resource utilization indices are considered: the natural uranium utilization and the SWU utilization. The definitions are the same as introduced in Chapter 2.

Figs. 8.9 and 8.10 show these two utilizations under different neutron spectrums. The fuel enrichment variation is limited to the proliferation limit of 20 w/o. Note that the calculation is based on unit cell calculations and the burnup is single batch burnup where k_∞ = 1.0 (no leakage considered). A wetter lattice (H/HM=5.0) shows better resource utilization compared to the reference PWR lattice (H/HM=3.4) below 20 w/o enrichment. Therefore, optimization of the fuel cycle cost favors a wetter lattice.

Both the epithermal-spectrum lattice (H/HM=0.8) and the fast-spectrum lattice (H/HM=0.2) need a higher enrichment for the fuel. Increasing the enrichment is more effective for the epithermal-spectrum lattice compared to thermal-spectrum lattices. Although the utilization below 20 w/o is always worse for the epithermal-spectrum compared to the thermal spectrum, the difference between them decreases as enrichment increases. In fact the epithermal lattice has not achieved the maximum utilization with respect to reload enrichments below 20 w/o.

The fast-spectrum lattice (H/HM=0.2) requires an even higher enrichment to go above critical. The increase in burnup is rapid between 8 and 10 w/o, which shows a quick increase of resource utilization. After the optimum enrichment (maximum utilization) at ~11 w/o, the resource utilization slowly decreases. This feature is reminiscent of the thermal lattice, where the initial increase of utilization is fairly fast while the decrease of utilization after the optimum value is slow. It is clear that above 10 w/o the fast-spectrum lattice has the best resource utilization among the four candidates. Although fast cores have a higher neutron leakage (which will increase the enrichment requirement), the fast spectrum lattice will still be the best performer above a certain enrichment. Hence, even for a once-through fuel cycle, the fast reactor, with its high conversion ratio, is still attractive in terms of maximizing resource utilization. An improved fuel cycle cost can in principle be achieved by a once-through fast reactor, provided the carrying charges of the large investment in the core are not excessive.

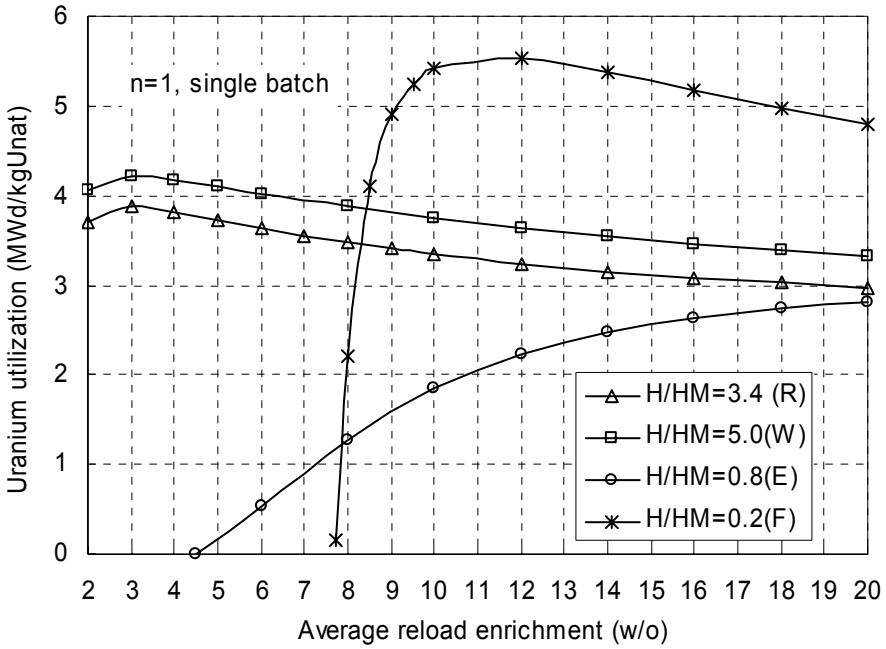

Figure 8.9 Uranium utilization for different neutron spectra.

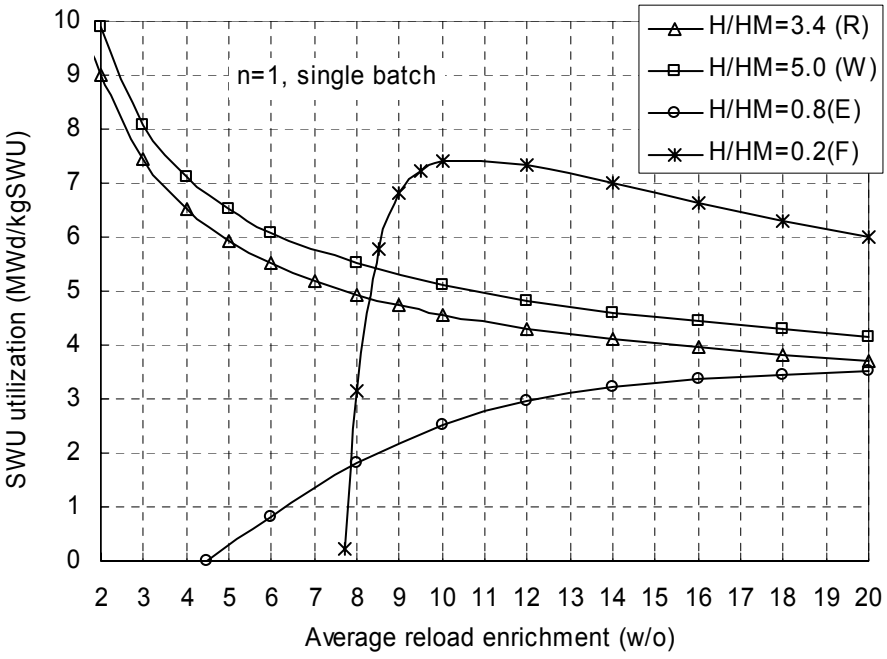

Figure 8.10 SWU utilization for different neutron spectra.

8.3 Operation and Maintenance Considerations

8.3.1 Introduction

The operation and maintenance (O&M) cost represents another component in the total electricity production cost. Since the capital cost is mainly a sunk cost, only two remaining components, the O&M cost and the fuel cycle cost, can be optimized by utilities. A positive trend in operational effectiveness has been observed in the recent past [139].

The O&M cost includes personnel and materials expenditures for operation, maintenance, and other administrative tasks. Staffing level, as a significant fraction of the cost, is higher than those in fossil power plants. The fuel cycle cost in the nuclear plant is about 20% of the total cost whereas the fuel cost is about 75% for a fossil plant. Therefore, it is probably tolerable for a fossil plant to be off-line for upgrade or repair for several months while unimaginable for nuclear plants because (1) there are fewer employees in the fossil plant; (2) the fuel cost dominates the electricity cost for fossil plants (no electricity generation, no fuel consumption). Of course one advantage of smaller fuel cost in the busbar cost for nuclear plants is that the electricity price will not be sensitive to short-range fluctuations of fuel cost in the market; hence nuclear power provides energy price security.

8.3.2 Refueling Outages

One issue in the O&M cost is the refueling outage. The historical transition from 12 month cycles to 18 month cycles is primarily driven by consideration of reduced refueling outages. Further extension of the cycle length can reduce the refueling shutdown cost.

The approximate cost of a refueling outage is $25 million [150]. In order to determine the contribution of this cost to the electricity generation, i.e., mills/kWhr-e, one can levelize the refueling shutdown cost over an entire operating cycle (Fig. 8.11).

$$C_{\mathrm{R}} = \int_0^{T_{\mathrm{c}}} \bar{C}_{\mathrm{R}} \exp\left(-i_{\mathrm{c}} t\right) dt\,, \tag{8.13}$$

where C_{R} = refueling shutdown cost, 25×10^6 dollars

i_{c} = discounting rate, 10% per year

T_{c} = cycle length, years

$\bar{C}_{\mathrm{R}}$ = levelized refueling cost, $/year.

Hence,

$$\bar{C}_{\mathrm{R}} = \frac{C_{\mathrm{R}}}{T_{\mathrm{c}}}\left(\frac{i_{\mathrm{c}}T_{\mathrm{c}}}{1-e^{-i_{\mathrm{c}}T_{\mathrm{c}}}}\right), \tag{8.14}$$

and the cost in mills/kWhr-e is

$$e_{\mathrm{RC}} = \frac{1}{24\times 365}\frac{1}{E}\frac{C_{\mathrm{R}}}{T_{\mathrm{c}}}\left(\frac{i_{\mathrm{c}}T_{\mathrm{c}}}{1-e^{-i_{\mathrm{c}}T_{\mathrm{c}}}}\right), \tag{8.15}$$

where E = rated electricity output, 1150 MW-e.

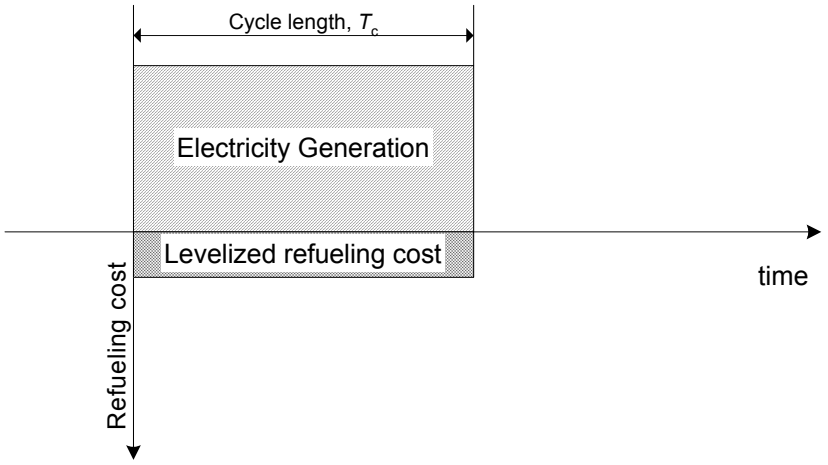

Figure 8.11 Refueling cost levelization.

Figure 8.12 shows the refueling cost for different cycle lengths. Sensitivity to the discount rate is also shown, which only shifts the absolute magnitude of the refueling cost. There is a ~1 mills/kWhr-e saving of refueling cost in transition from a 12 month cycle to an 18 month cycle. Further increases in the cycle length yields smaller cost reduction. For example, there is a ~0.5 mills/kWhr-e saving from an 18 month cycle to a 24 month cycle. Based on Fig. 8.12 (using 10% per year discounting rate), the Table 8.2 results are adjusted and re-assembled in Table 8.3. Although the single batch, high burnup strategy has a benefit of 1.2 mills/kWhr-e saving in refueling shutdown cost compared to 18-month cycle, this still can not offset the more expensive fuel cost. The longer cycle approach has a benefit of 0.8 mills/kWhr-e, which is enough to offset the higher fuel-only cost. However, under current market conditions, none of the high burnup schemes is better than the reference 18-month PWR.

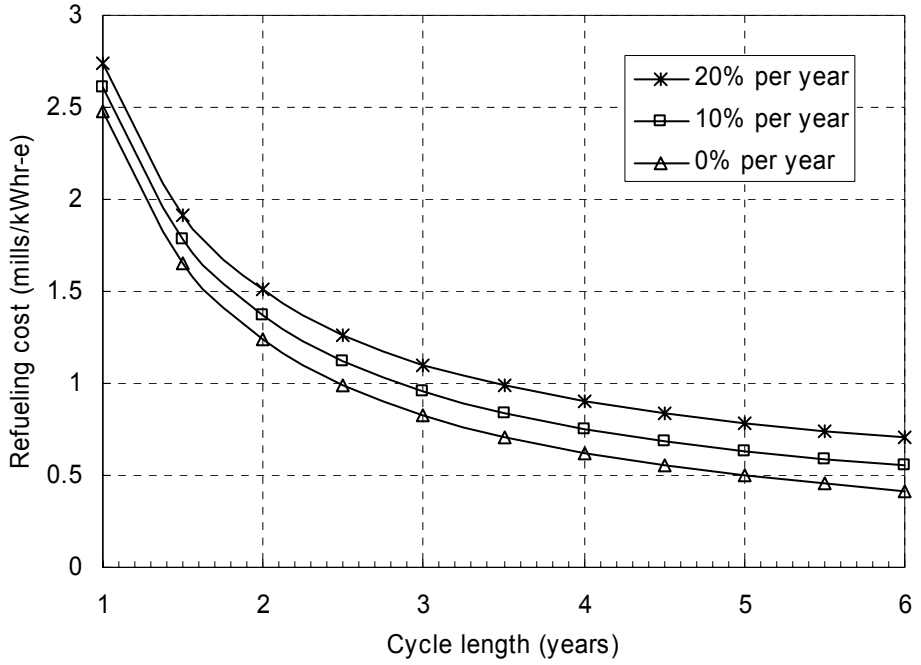

Figure 8.12 Refueling cost as a function of cycle length.

Table 8.3 Revised fuel cycle cost comparison of different high burnup strategies.

	Reference PWR	High burnup schemes			
		Retrofit cores		New cores	
		Longer cycle	More batches	Single batch	Power upgrade
Fuel cycle cost (10% carrying charge per year):					
e_{RC} (mills/kWhr-e)	1.78	0.99	1.78	0.61	1.78
e_{NFC} (mills/kWhr-e)	6.82	8.00	7.45	10.2	6.93
Total (mills/kWhr-e)	8.60	8.99 (+5%)	9.23 (+7%)	10.81 (+26%)	8.71 (+1%)
Direct fuel cycle cost (no carrying charge):					
e_{RC} (mills/kWhr-e)	1.65	0.86	1.65	0.47	1.65
e_{NFC} (mills/kWhr-e)	5.33	5.34	4.64	7.34	5.28
Total (mills/kWhr-e)	6.98	6.20 (–11%)	6.29 (–10%)	7.81 (+12%)	6.93 (–0.7%)
∗ The numbers in parentheses are changes relative to the reference PWR.					

The 24-month PWRs have a limited refueling shutdown cost savings compared to the current 18-month cycle. In addition the fuel cycle cost is more expensive for the 24 month cycle. Furthermore, the recent industry wave of power upratings significantly slows down the adoption of the 24 month cycle in PWRs. In the future, the 24-month

cycle might be of interest depending on the importance of the shutdown cost. It is, however, not attractive for PWRs now.

8.4 Case Study of Power Uprating

In recent years, power plant upratings have been very attractive to nuclear utilities as a measure to improve economic competitiveness. Two key driving factors include the deregulation of the electricity market and nuclear plant license extension. Typical Westinghouse plants have at least 5 to 10 percent available margin for uprate above the original rating; and in some cases 10 to 15 percent uprating can be justified [33]. For future reactor designs, an even higher core power density is realizable, e.g., a 50% core power density uprate for a Westinghouse 4-loop PWR can be achieved based on the use of IXAF fuel [102]. The economics implications of power uprating is investigated here as a case study.

The busbar electricity cost, e (mills/kWhr-e), can be written as

$$e = \frac{c_{\mathrm{CAP}} + c_{\mathrm{O\&M}} + c_{\mathrm{FUEL}}}{E}, \tag{8.16}$$

where E = the electricity generation, kWe

c_{CAP} = the capital cost, mills/hr

$c_{\mathrm{O\&M}}$ = the O&M cost, mills/hr

c_{FUEL} = the fuel cycle cost, mills/hr.

Using the typical breakeven numbers, the capital cost is 57%, the O&M cost is 23%, and the fuel cycle cost is 20%.

Now suppose the core power is uprated by 10%, i.e., the electricity generation increases by 10%. The fuel cost will increase proportionally to produce more energy. However, the O&M cost essentially doesn't change. The capital cost of course will increase to allow certain investments in the plant, such as steam generator upgrade. But this investment is typically 10-20 dollars per MWe (a small addition to the original 1000+ dollars per MWe). Hence the increase of capital cost is only ~2%. The relative cost for the 10%-uprate core is then

$$e_{10\%} = \frac{1.02c_{\mathrm{CAP}} + c_{\mathrm{O\&M}} + 1.1c_{\mathrm{FUEL}}}{1.1E} = \frac{1.02\times 57\% + 23\% + 1.1\times 20\%}{1.1} e = 0.94e\,. \tag{8.17}$$

The busbar cost decreases by about 6%, which reinforces the economic viability of nuclear power.

In this analysis, the fuel cycle cost doesn't improve. However, as electricity (product) increases by 10%, the O&M cost and the capital cost both improve. In particular, the O&M cost decreases by 10%. As long as the technical specifications of the core satisfy the regulatory requirements, power uprating is always desirable.

Another consequence of core power uprating is a high fuel burnup if the number of batches is kept the same. The increase of burnup will be proportional to the increase of power uprating. Since large savings are realized in the O&M cost and the capital cost, the increased fuel cost is not an issue. The range of burnup increase in this manner, however, is limited, e.g., for existing PWRs, at most 20% due to technical limitations. Hence the current PWR burnup of 50 MWd/kg might be stretched to 60 MWd/kg. There is still not much commercial incentive to go beyond that. In fact, high burnup is a consequence of rather than a motivation for the power uprating. Future core designs might allow a more drastic power increase, hence a much higher burnup. For a 100% power uprate, the current burnup of 50 MWd/kg will be doubled to 100 MWd/kg. The IXAF fuel concept is a promising candidate.

8.5 Chapter Summary & Recommendations

The economics of the fuel cycle are discussed in this chapter for high burnup. Nuclear fuel cycle cost is close to optimum for current practice, but there is room to improve it by stretching burnup by ~30% to 65 MWd/kg. Although a wetter lattice has a better fuel cycle cost compared to the reference case, the optimum range of burnup is still within 50 to 70 MWd/kg. Going beyond 70 MWd/kg, the principal benefits of high burnup appear to be ex-core, such as reduced spent fuel generation per MWe-yr, less plutonium per MWe-yr, dirtier plutonium mixture (less suitable for weapons), and longer duration of "self protection." These high burnup characteristics have a positive impact on the back-end fuel cycle and make it more proliferation resistant. However, these credits are not reflected in utility incentives. If high burnup is deemed important, changes such as the following should be considered:

- A waste fee based on the spent fuel mass instead of the electricity production
- Reduced carrying charges (cost of money) via changes in tax policy, depreciation regulations, and financing arrangements.

The savings in shutdown cost cannot compensate for the loss in fuel cycle cost during a cycle length extension. There are also other benefits for longer cycles, such as reduced low level wastes and lower doses to workers. In this aspect, the 24 month cycle is appealing.

Various once-though cycles have been compared under different neutron spectrums. A fast-spectrum lattice is seen to be the best performer above a certain enrichment (roughly ~9 w/o). Therefore, in terms of resource savings, fast reactors are potentially attractive although not technically as mature as the commercial LWRs. Fast reactors are also more expensive than LWRs due to higher capital cost. In addition the fissile content in the spent fuel of fast reactors is very large and the isotopic content of the fuel is closer to weapon usability.

A case study of power uprating is presented, which might lead to increased burnup (to 60 MWd/kg) for existing PWRs. Future PWR cores might have a much larger power density, hence a much higher burnup. Their economic viability actually comes from the savings in the capital cost and the O&M cost instead of the fuel cycle cost. Although the product generation (electricity) increases by 10%, the cost items do not increase linearly with the power increase. Hence, a busbar cost reduction is achieved.

Note that the economic considerations here are purely from a technical point of view. There is no attempt to model energy market behavior including the demand for energy. Utilities, however, need to consider all aspects such as the demand and the supply and the power plant operating strategies to maximize their profits.

9. Summary, Conclusions, and Recommendations

"And in the end, it's not the years in your life that count. It's the life in your years"
— A. Lincoln (1809-1865)

9.1 Summary of Motivation

The present work is a strategic study of the implication of high burnup fuel for PWRs, which scopes out the characteristics of reactor cores fueled with uranium fuel and outlines the best approach to high burnup service in a once-through fuel cycle. The historical increase in batch-averaged discharge fuel burnup, from ~30 MWd/kg in the 1970s to ~50 MWd/kg today, was achieved mainly by increasing the reload fuel enrichment to allow longer fuel cycles (from an average of 12 months to about 18 months). This improved fuel utilization also reduced operating costs by improving the plant capacity factor. Recently, because of proliferation concerns and limited spent fuel storage capacity, achieving burnup in the 70 to 100 MWd/kg has attracted considerable attention. However the implications of this initiative have not been fully explored; hence this work defines the practical issues for designing high-burnup PWR fuels based on neutronic, thermal hydraulic and economic considerations as well as spent fuel characteristics.

9.2 MCODE Development

The ability to carry out validated high-burnup physics calculations for various fuel options and moderator conditions as well as innovative heterogeneous designs is essential to achieving the goal of the present work. A new linkage program, MCODE (MCNP-ORIGEN DEpletion program), has been developed, which combines the continuous-energy Monte Carlo code, MCNP-4C, and the one-group depletion code, ORIGEN2, to perform burnup calculations. MCNP is capable of providing the neutron flux and effective one-group cross sections for different MCNP-defined regions.

ORIGEN, in turn, carries out multi-nuclide depletion calculations for each region and provides material compositions to update beginning-of-timestep MCNP input. This console program is entirely written in ANSI C (about 3000 lines) and is fully portable between Windows and UNIX environments. A standard burnup predictor-corrector algorithm is implemented, which distinguishes MCODE from other MCNP-ORIGEN linkage codes such as MOCUP and MONTEBURNS (Table 9.1).

Table 9.1 MCODE comparisons with MOCUP and MONTEBURNS.

	MCODE	MOCUP	MONTEBURNS
Developer	MIT	INEEL	LANL
Year	2001	1995	1999
Language	ANSI C	ANSI C	FORTRAN, PERL
Portability	excellent	Good	good
User involvement	Small	extensive	small
Running flexibility	excellent	excellent	good
Normalization	Power or flux	Flux	flux
Coupling manner	Standard predictor-corrector algorithm	Beginning-of-timestep representation	Middle of timestep representation

A single pin cell model with 9.75 w/o UO_2 fuel of a standard Westinghouse 17×17 PWR assembly has been employed to benchmark MCODE against CASMO-4 and HELIOS, which are licensing-level, industry standard burnup calculation tools for LWRs. Forty-nine burnup steps were chosen between 0 and 100 MWd/kg for the benchmarking calculations. The running options for MCODE are power normalization with burnup predictor-corrector algorithm on. There are 39 actinides (ACT) and 100 fission products (FP) considered in the burnup calculations, which accounts for ≥ 99.95% of total mass and neutron absorptions at 100 MWd/kg.

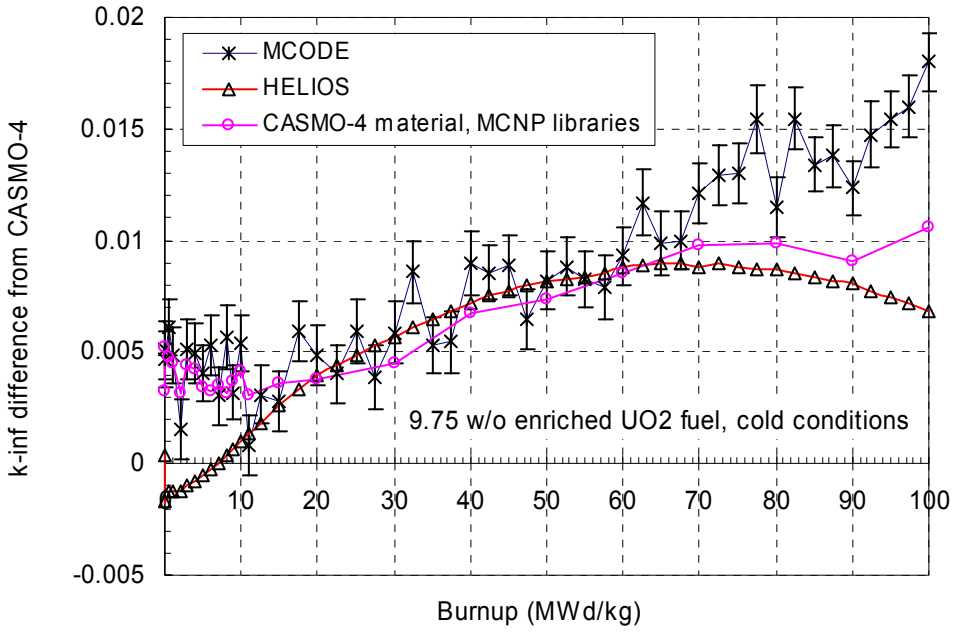

Figure 9.1 Eigenvalue difference from CASMO-4 as a function of burnup.

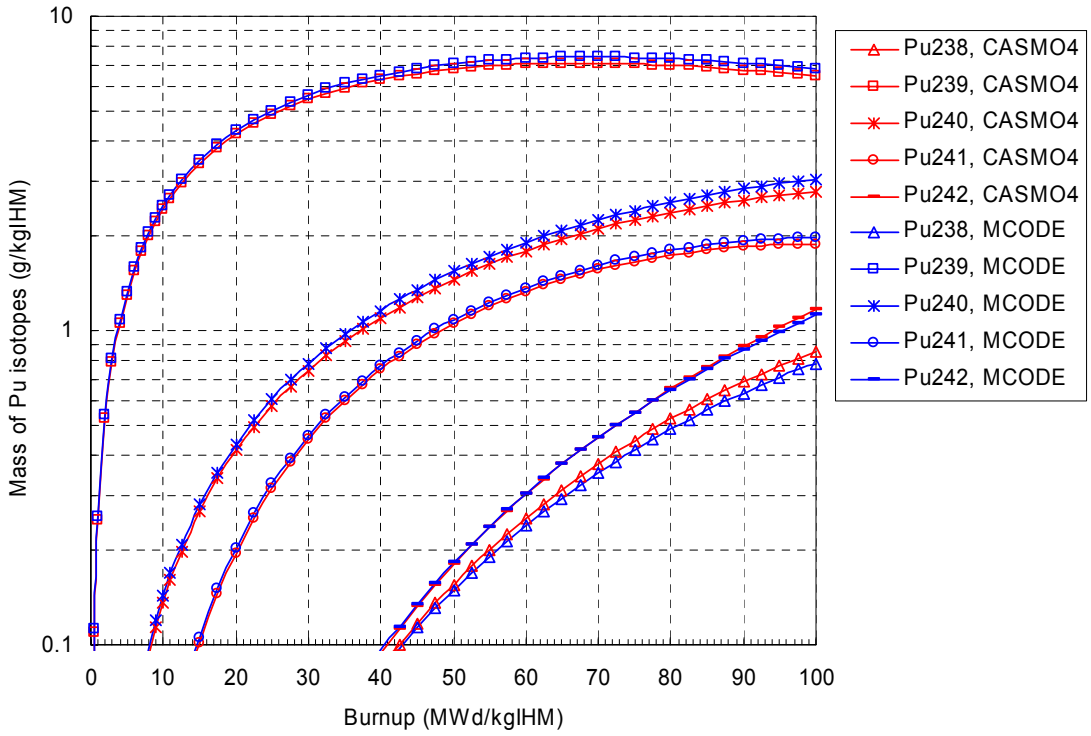

Figure 9.2 Plutonium vector comparison with CASMO-4 as a function of burnup.

Figure 9.1 shows the difference from CASMO-4. At 100 MWd/kg burnup, the eigenvalue difference is about 0.015. This result is excellent compared to previous benchmark efforts [69] where the eigenvalue difference reaches 0.01 at 60 MWd/kg. If one projects the burnup difference over one LWR 18-month cycle, the predicted cycle length difference translates into 3 days, less than the previous 1 week. Circled points indicate MCNP criticality calculations using the CASMO-4 output material vectors and MCNP ENDF-VI libraries. This isolates the static library difference and shows that the constant Δk before 80 MWd/kg is mainly due to the library difference. From an engineering point of view, MCODE is sufficiently accurate.

The predicted plutonium vectors by the two codes are also compared graphically as a function of burnup in Fig. 9.2, which indicates satisfactory agreement. From the code-vs-code benchmarking of the high burnup UO_2 lattice under cold conditions, it is concluded that MCODE is suitable and ready to be used in burnup calculations. Even for high burnup cases, the eigenvalue comparisons are still within ~0.02 of CASMO-4, and even closer to HELIOS. The material composition predictions are also acceptable compared to the comprehensive uranium benchmark reported by OECD in Ref. [70].

9.3 Neutron Spectrum Effects by H/HM Variations

The CASMO-4 code was used throughout this investigation. But since it is being exercised far beyond its intended scope of proven applicability, extensive confirmatory calibrations were carried out with the Monte Carlo code MCODE (MCNP + ORIGEN). The effect of lattice design (H/HM, hydrogen-to-heavy-metal atom number ratio) on overall strategic goals from a physics point of view has been explored. Table 9.2 compares "wet" lattices (25 to 50% higher H/HM than at present) to "dry" lattices (a factor of ≥ 3 lower H/HM). Based on these results the wet lattice is clearly preferable, particularly if one focuses on the objective of preserving or improving on the inherent weapons unsuitability of plutonium in spent fuel.

Table 9.2 Comparison of strategies to achieve high burnup in PWR cores.

CHARACTERISTIC	WET LATTICE VS. DRY LATTICE
▪ Reactivity-Limited Burnup	Wet is ~ 30% larger for same reload enrichment
▪ Coolant Void Worth	Wet is negative; dry may be positive
▪ Reactivity Loss vs. Burnup	Wet is much larger due to its lower conversion ratio
▪ Poison Worth	Wet is larger due to its more thermal spectrum
▪ Cycle Length	At the same burnup and core volume, wet is shorter due to its smaller core fuel inventory
▪ Core Leakage	Wet is smaller at the same volume
▪ Thermal Hydraulics	Wet is comparable to current fuel; dry has more challenging DNB and Post-LOCA reflood concerns
▪ Plutonium in Spent Fuel	Wet Lattice has a factor of ~ 3 less total Pu and higher fraction Pu-238 and Pu-242; hence, is considerably more proliferation resistant
▪ Retrofitability	Wet can be used in existing PWRs; Dry is suitable only for new plants

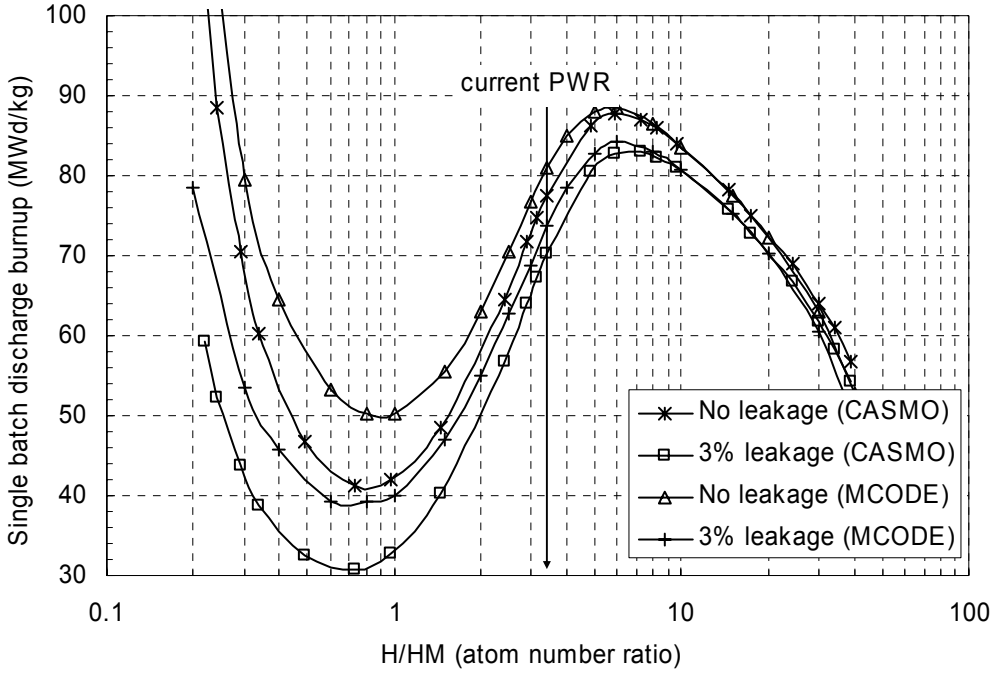

Figure 9.3 MCODE/CASMO results for 9.75 w/o enrichment.

Figure 9.3 shows that a higher reactivity-limited burnup is achievable in either a wetter than normal or much dryer than normal lattice, while epithermal lattices are distinctly inferior performers. There is another constraint of note: core endurance (cycle length), which is proportional to the product of burnup and core fuel inventory. For con-

stant core volume, the fuel inventory is less for wetter lattices. This will limit re-optimization of fuel assemblies for retrofit into current reactors.

9.4 Neutronic Considerations of Alternative Fuel Choices

In order to realize a wetter PWR lattice several fuel options with the same fuel enrichment were evaluated:

- Solid fuel pin with reduced rod diameter
- CERMET (60%Zr-40%UO_2)
- Central-voided annular fuel pellet
- Internally and eXternally cooled Annular Fuel (IXAF).

The smaller-diameter solid fuel pin was found to be the best neutronic performer, i.e., at the same H/HM and the same fuel enrichment, the largest energy production can be achieved among them. The next is the IXAF case. The CERMET and central-voided annular fuel are poorer performers compared to other cases. The primary reason is that for a solid fuel pin or the IXAF fuel, the core volume is (ignoring the cladding and gap volumes)

$$V_{\text{core}} \cong V_{\text{H}_2\text{O}} + V_{\text{UO}_2}; \tag{9.1}$$

while for the CERMET or the central-voided annular fuel,

$$V'_{\text{core}} \cong V'_{\text{H}_2\text{O}} + V'_{\text{UO}_2} + V'_{\text{other}}, \tag{9.2}$$

where the last item is the support matrix for the CERMET and is the void for the central-voided annular fuel. Given the same core volume and H/HM (same water to fuel volume ratio), one can write

$$\left(1+\frac{V_{\text{H}_2\text{O}}}{V_{\text{UO}_2}}\right)V_{\text{UO}_2} = \left(1+\frac{V_{\text{H}_2\text{O}}}{V_{\text{UO}_2}}\right)V'_{\text{UO}_2} + V'_{\text{other}}. \tag{9.3}$$

Hence the UO_2 volume is smaller for the CERMET and the central-voided case, which leads to smaller heavy metal loadings in the core even at the same H/HM compared to the solid pin and the IXAF cases.

In conclusion two parallel paths of achieving a wetter lattice are recommended: (1) to increase the number of solid fuel pins in an assembly (but with a smaller-diameter fuel

rod); (2) to use IXAF fuel pins in an assembly but in a wetter lattice. Neutronically the first option may be better (higher burnup potential), but thermally the second option is better.

9.5 Practical Issues

9.5.1 Reactivity Control

The first important factor in considering reactivity control is the fuel management scheme. The long cycle core often requires high fissile content at BOC (and more burnable poison as well). The hardened spectrum reduces control material worth. Hence the current control rods are usually found to be inadequate to provide shutdown margins [8, 12]. In a core design with more batches, however, it is easier to control the reduced BOC reactivity. All things considered, from a reactivity control point of view, the cycle length is recommended to be kept the same as the current 18 months.

Table 9.3 Poison-free, BOC core parameters for various designs (18-month cycle).

	Conventional assembly design		Wetter lattice*
	Conventional PWR	High burnup	High burnup
Enrichment (w/o)	4.5	9.75	9.75
H/HM	4.07	4.07	4.66
Specific power (W/gIHM)	38.2	38.2	41.7
B_c (MWd/kg)	18.23	18.23	19.88
Number of batches, n	3.0	7.3	6.9
BOC reactivity, $\Delta\rho_c$ (pcm)	12,555	6,193	6,463
Boron worth (pcm/ppm)	6.7	4.7	5.9
Critical boron (ppm)	2,164	2,944	2,745
Max boron (MTC=0) (ppm)	2,260	4,037	3,082
MTC (pcm/K)	–52.2	–67.2	–62.0
FTC (pcm/K)	–2.2	–2.4	–2.3

* This is the optimized Westinghouse Performance+ design.

Table 9.3 summarizes the BOC neutronic parameters for high burnup cases and the reference conventional 18-month cycle PWR. The wetter lattice here refers to the Westinghouse Performance+ design. An increased specific power (burnup rate) is observed for the wetter lattice, which consequently increases the cycle burnup for the 18-

month cycle. A wetter lattice offers the high burnup cases (here 18 month cycle) a softer neutron spectrum, hence better MTC and increased poison worth. Reactivity control is actually easier for a wetter lattice, particularly under high burnup. The critical boron concentration is reduced for the wetter lattice as shown in Table 9.3.

Burnable poison calculations were subsequently performed for different high burnup fuel assemblies. Gadolinia shows promising results in controlling the 18-month cycle of the various cases considered. It is a neutronically versatile option while IFBA did not appear to be a good candidate for the high burnup cases. Erbia is not found to be as advantageous as the other two options. However, the BP situation is a complex issue which depends on specific core design requirements. There is, in turn, no universally best BP candidate.

9.5..2 Thermal Hydraulics Considerations

Wetter lattices, even with increased water in the lattice, do not necessarily have a better thermal margin. To examine the heat transfer limits, a qualitative scoping study of heat removal capability has been carried out for various options of H/HM variations as summarized in Table 9.4.

Table 9.4 Practically-considered ways of varying H/HM.

No.	Variations	Comments
1	Rod diameter	• primary way of lattice optimization while assembly design is maintained • geometrically-limited by the pin pitch
2	Pin pitch	• changes lattice structure as well if assembly dimension is to be conserved • geometrically-limited by rod diameter
3	Annular fuel pellet (central-voided)	• varies H/HM without affecting heat flux to coolant • central plug needed to maintain the pellet geometry • reduced peak fuel temperature due to geometry
4	Annular fuel with internal cooling (IXAF)	• a significant average and peak fuel temperature reduction • doubling of heat transfer surface area • doubling of the clad material

Using the thermal hydraulic code, VIPRE, the solid fuel diameter variation was studied using a single-channel model. The MDNBR decreases (more demanding) as the lattice becomes wetter. Meanwhile the pumping power requirement is less.

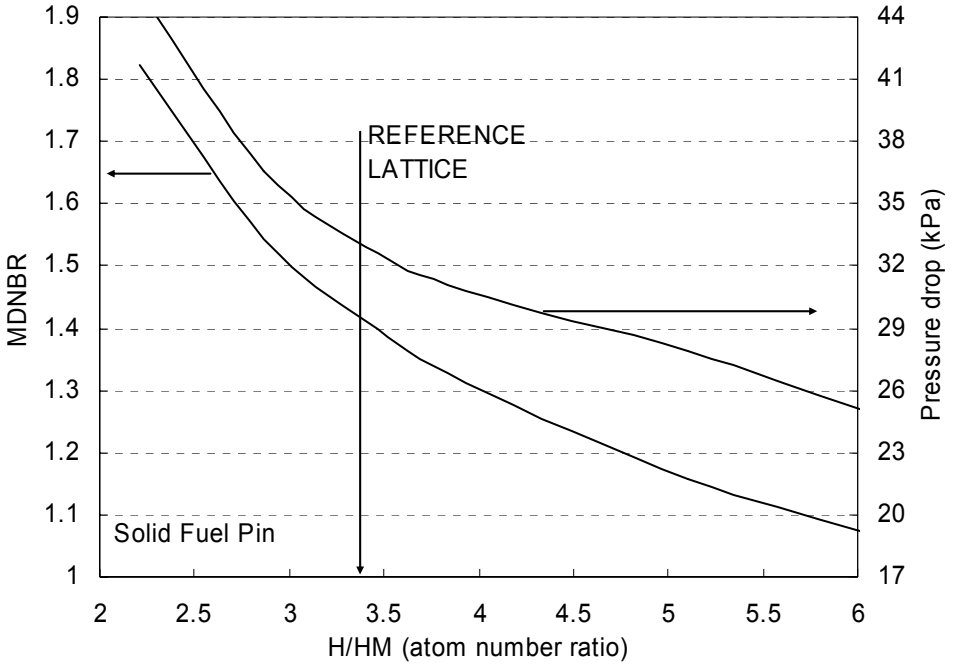

Figure 9.4 MDNBR and pressure drop as a function of H/HM for solid fuel pin.

Figure 9.5 shows the significant thermal margin of the IXAF concept compared to the reference PWR.

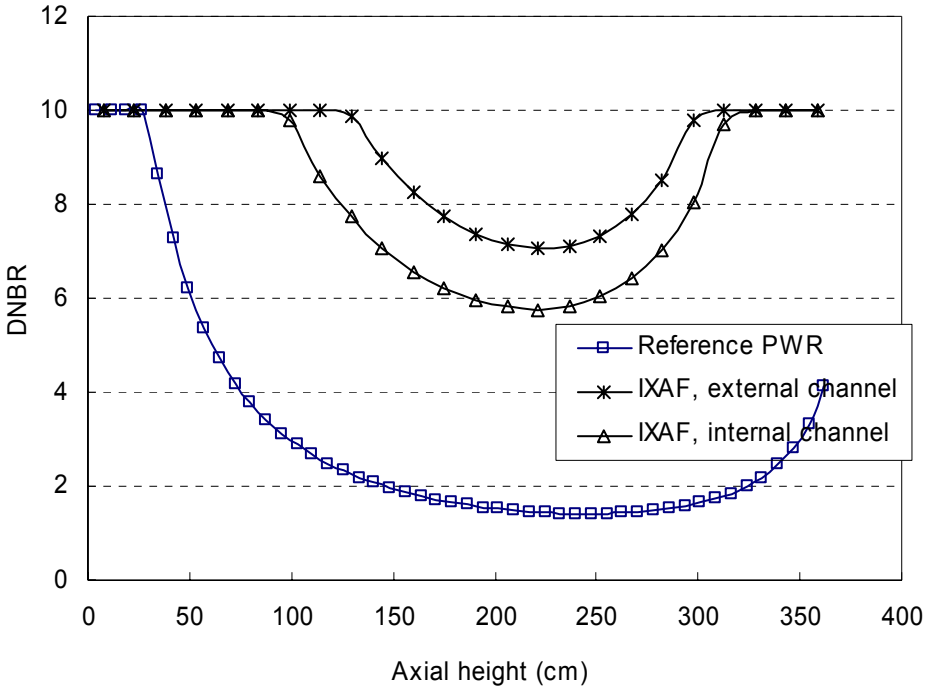

Figure 9.5 MDNBR comparison in hot channel for the IXAF and reference solid pin.

Therefore, the IXAF fuel is recommended because of its significant improvement of the thermal hydraulics (more DNBR margins, low fuel temperatures).

9.5.3 Fuel Performance

Another issue is the fuel rod performance in the core. One key quantity is the fission gas release. Since the current version of FRAPCON-3 cannot deal with the IXAF fuel, an equivalent solid pin is used based on the same fuel volume to surface ratio and power density. Figure 9.6 shows that the IXAF design has significantly lower fission gas release, almost entirely from the athermal gas release contribution. The fuel pellet rim calculations show that the rim region of the IXAF has a smaller peak-to-average power ratio. Hence the burnup in the rim region is smaller than for the solid fuel pellet. This fuel performance issue therefore favors the IXAF concept.

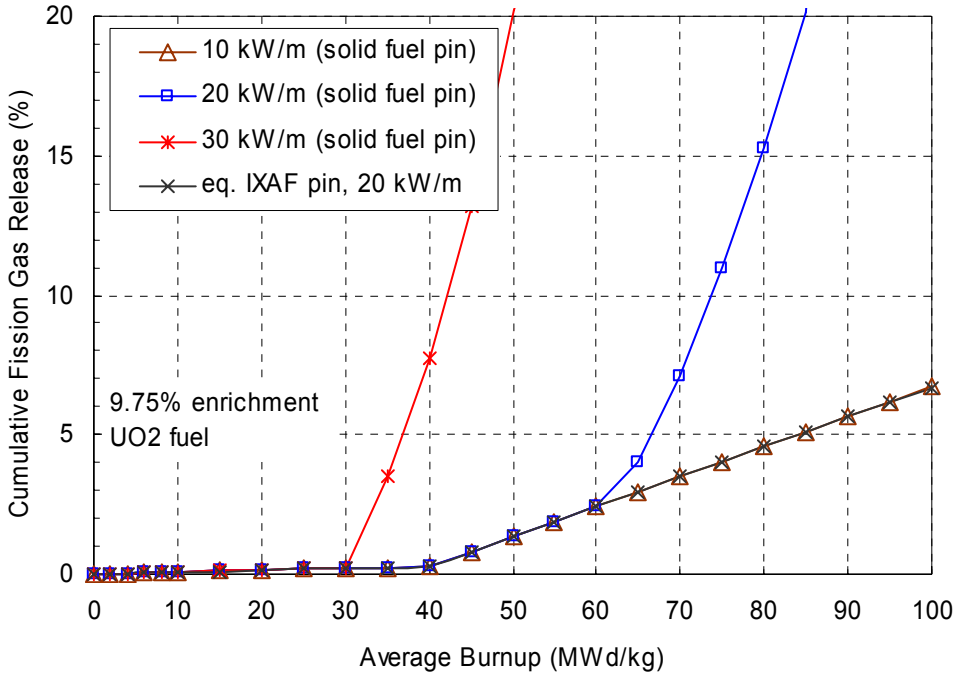

Figure 9.6 Fission gas release calculations for various fuel pins.

In conclusion, the IXAF fuel also appears to be a promising option from a fuel performance perspective.

9.6 High-Burnup Spent Fuel & Proliferation Resistance

Higher burnup leads to a higher decay heat generation rate per assembly. But, per unit electricity generation, the decay power of high burnup spent fuel is only larger than the reference fuel within two time periods: (1) 4 years to 150 years; and (2) 100,000 years to 1000,000 years (Fig. 9.7). The short time frame difference suggests that high-burnup spent fuel might need a longer time in the storage before the final disposal. However, based on unit electricity production, the high burnup approach has certain advantages since the accumulated decay heat is reduced.

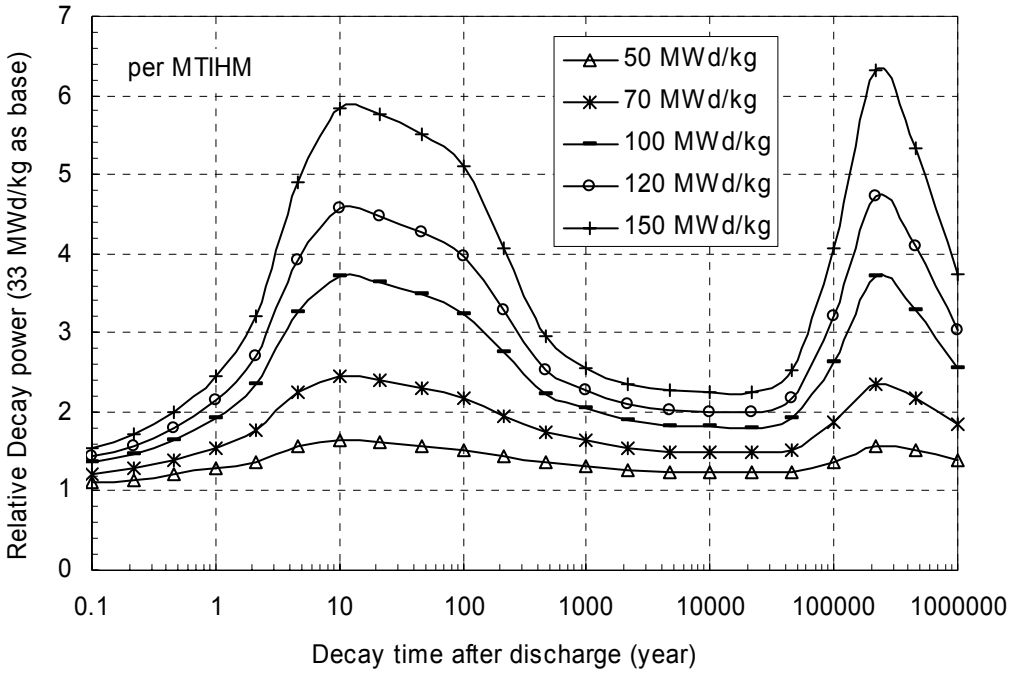

Figure 9.7 Relative decay power after discharge.

The plutonium production at a given burnup increases monotonically as H/HM decreases, while weapon usability increases. In particular spontaneous fission neutron emission, which is dominated by Pu-238 concentration, is reduced as the lattice becomes progressively drier. The same is true of Pu-240 and Pu-242, which also help spoil the plutonium mix as potential weapon material. Thus, current H/HM value (~3.4), or slightly wetter lattices generate the most proliferation-resistant spent fuel from PWRs.

9.7 Economic Considerations

Nuclear fuel cycle cost has a very broad optimum for current practice. Although a wetter lattice has a better fuel cycle cost compared to the reference case, the optimum range of burnup is still within 50 to 70 MWd/kg. In general, the principal benefits of high burnup appear to be ex-core, such as reduced spent fuel generation per MWe-yr, less plutonium per MWe-yr, higher decay heat & more fertile contents in the plutonium mixture (less suitable for weapons), and longer duration of "self protection." These high burnup characteristics have a positive impact on the back-end fuel cycle. However, these credits

are not reflected properly in the economics. If high burnup is really deemed as important by the government, steps should be taken to increase the utilities incentives, such as:

- A waste fee based on the spent fuel mass/volume instead of that based on electricity production
- Measures to reduce carrying charges such as changes in tax rates, depreciation schedules and financing modes

A case study of power uprating showed that an increase of burnup up to 60 MWd/kg (from 50 MWd/kg) for existing PWRs is profitable. Future PWR cores might have a much larger power density, hence a much higher burnup. The economic viability actually comes from the savings in the capital cost and the O&M cost instead of the fuel cycle cost. Although the product generation (electricity) increases by 10%, the cost items do not increase linearly with the energy. Hence, a busbar cost reduction is achieved.

9.8 Recommendations for Future Work

Detailed designs are needed for various high burnup cores, which account for the presence of control and burnable materials. The following tasks are suggested for future development:

9.8.1 MCODE Development

The current version of MCODE is limited to do depletion calculations in which only actinides and fission products are considered. In the future activation products should also be included, especially B-10. Correspondingly the (n, α) reaction needs to be tallied. ORIGEN2 libraries also need to be updated. Fission yield data need to be revised according to recent ENDF/B-VI data. Other data, such as half lives and the branching ratios, also need to be reviewed. In the future, MCODE should be documented and released for wider use in the nuclear community.

9.8.2 Detailed Core Design

Overall the IXAF fuel is very promising for high burnup. Therefore a whole-core design based on IXAF fuel should be modeled over at least several cycles. Note that at present,

burnup codes, such as CASMO-4, do not properly treat this category of fuel, whereas MCODE allows good simulation of these codes.

9.8.3 High Burnup Fuel Performance Studies

It appears that the current limiting factor is the allowable fuel burnup from a material's point of view. Further experiments are needed to obtain necessary data to facilitate understanding of mechanisms of fission gas release and swelling behavior, and help guide the fuel performance modeling. Advanced fuel cladding is also needed for LWRs to achieve higher burnup than 70 MWd/kg.

9.8.4 Policy Studies

Nuclear fuel financing methods and waste fee structure should be evaluated to determine how high burnup incentives can best be introduced. First, however, actual back end costs should be studied as a function of spent fuel burnup, including storage, transportation and disposal to quantify the benefit to society of higher burnup which would justify such incentives.

9.8.5 Proliferation Study

An assessment of the potential for proliferation resistance improvements requires development of indices for this resistance, a task that has been begun but not yet completed at DOE.

9.8.6 Recycling Issue

The focus was on US conditions, i.e., once-through fuel cycle, but recycling is allowed in other countries and an evaluation of the impact of high burnup under that condition is needed.

References

[1] NEA/OECD (Nuclear Energy Agency/Organisation for Economic Co-operation and Development), "Nuclear Energy and the Kyoto Protocol," Paris, France, 2002. (also refer to http://unfccc.int for more details on the Kyoto Protocol)

[2] M. Torjman, H. Shaaban, "Nuclear Energy as a Primary Source for a Clean Hydrogen Energy System," *Energy Conversion & Management*, **39**, No. 1/2, 27-32, 1998.

[3] C. W. Forsberg, "Hydrogen, Electricity, and Nuclear Power," *Nuclear News*, 30-31, September 2002.

[4] M. F. Lyons, R. F. Boyle, J. H. Davies, V. E. Hazel, T. C. Towland, "UO_2 Properties Affecting Performance," *Nuclear Engineering & Design*, **21**, 167-199, 1972.

[5] B. Estève, R. Güldner, R. Hoffman, M. Watteau, "Framatome-ANP Extended Burnup Experience and Views on LWR Fuels," *Nuclear Energy*, **41**, No. 3, 209-217, June 2002.

[6] International Atomic Energy Agency (IAEA), "The Physical Protection of Nuclear Material," INFCIRC/225/Rev.2, December 1989.

[7] F. J. Frank, L. R. Scherpereel, "Fuel Cycle Cost Reduction Through Westinghouse Fuel Design and Core Management," *Transactions of American Nuclear Society*, **50**, 101-102, San Francisco, California, November 10-14, 1985.

[8] M. V. McMahon, M. J. Driscoll, E. E. Pilat, N. E. Todreas, "Reload Light Water Reactor Core Designs for An Ultra Long Operating Cycle," *Nuclear Technology*, **126**, 32-47, April 1999.

[9] C. S. Handwerk, M. J. Driscoll, N. E. Todreas, M. V. McHahon, "Economic Analysis of Extended Operating Cycles in Existing LWRs," MIT-NFC-TR-007, Massachusetts Institute of Technology, January 1998.

[10] M. J. Driscoll, C. S. Handwerk, M. V. McMahon, "Selection of LWR Cycle Length and Fuel Reload Fraction," *Transactions of American Nuclear Society*, **76**, 349-350, Orlando, Florida, June 1-5, 1997.

[11] C. S. Handwerk, M. J. Driscoll, M. V. McMahon, "Cost Optimization of Long-Cycle LWR Operation," *Transactions of American Nuclear Society*, **76**, 351, Orlando, Florida, June 1-5, 1997.

[12] L. Garcia-Delgado, M. J. Driscoll, J. E. Meyer, N. E. Todreas, "An Economically Optimum PWR Reload Core for A 36-Month Cycle," *Annals of Nuclear Energy*, **26**, 659-677, 1999.

[13] J. Secker, et. al., "Optimum Cycle Length and Discharge Burnup for Nuclear Fuel, A Comprehensive Study for BWRs and PWRs," EPRI-TR-1003133, Electric Power Research Institute (EPRI), November 2001.

[14] W. Wiesenack, T. Tverberg, "The OECD Halden Reactor Project Fuels Testing Programme: Methods, Selected Results and Plans," *Nuclear Engineering & Design*, **207**, 189-197, 2001.

[15] A. Strasser, D. O'Boyle, K Otoha, T. Kishida, S. Sandklef, "Outlook for Nuclear Fuel," *Power*, 11-22, October 1991.

[16] J. A. Lake, "Foundations for the Fourth Generation of Nuclear Power," *Nuclear Energy*, **40**, No. 3, 153-157, June 2001. (also refer to http://gen-iv.ne.doe.gov/)

[17] S. M. Oggianu, "High Burnup Fuels for Advanced Nuclear Reactors," Master Thesis, Nuclear Engineering Department, MIT, December 2000.

[18] Y. Long, "Modeling the Performance of High Burnup Thoria and Urania PWR Fuel," Ph.D. Thesis, Nuclear Engineering Department, MIT, May 2002.

[19] J. T. Cronin, K. S. Smith, D. M. Ver Planck, "SIMULATE-3 Methodology, Advanced Three-Dimensional Two-Group Reactor Analysis Code," Studsvik/SOA-95/18, Studsvik of America, Inc., 1995.

[20] M. Edenius, K. Ekberg, B. H. Forssen, D. Knott, "CASMO-4, A Fuel Assembly Burnup Program, User's Manual," Studsvik/SOA-95/1, Studsvik of America, Inc., 1995.

[21] D. M. Ver Planck, "TABLES-3 User's Manual," Studsvik/SOA-95/16, Studsvik of America, Inc., 1995.

[22] A. S. DiGiovine, J. D. Rhodes, III, "SIMULATE-3 User's Manual," Studsvik/SOA-95/15, Studsvik of America, Inc., 1995.

[23] D. Knott, B. H. Forssen, M. Edenius, "CASMO-4, A Fuel Assembly Burnup Program, Methodology," Studsvik/SOA-95/2, Studsvik of America, Inc., 1995.

[24] J. F. Briesmeister (editor), "MCNP™ — A General Monte Carlo N-Particle Transport Code, Version 4C," LA-13709M, Los Alamos National Laboratory, April 2000.

[25] A. G. Croff, "A User's Manual for the ORIGEN2 Computer Code," ORNL/TM-7175, Oak Ridge National Laboratory, July 1980.

[26] J. M. Cuta, A. S. Koontz, C. W. Stewart, S. D. Montgomery, K. K. Nomura, "VIPRE-01: A Thermal-Hydraulic Code for Reactor Cores, Volume-2, User's Manual (Revision 2)," EPRI-NP-2511-CCM, Electric Power Research Institute (EPRI), July 1985.

[27] G. A. Berna, C. E. Beyer, K. L. Davis, D. D. Lanning, "FRAPCON-3: A Computer Code for the Calculation of Steady-State, Thermal-Mechanical Behavior of Oxide Fuel

Rods for High Burnup," PNNL-11513, Pacific Northwest National Laboratory, December 1997.

[28] http://www.iaea.or.at/programmes/a2/ (the Power Reactor Information System on IAEA website).

[29] "Late News," *Nuclear News*, 19, July 2002.

[30] NEA/OECD, "Trends in the Nuclear Fuel Cycle, Economic, Environmental and Social Aspects," Paris, 2001.

[31] L. R. Scherpereel, F. J. Frank, "Fuel Cycle Cost Considerations of Increased Discharge Burnups," *Nuclear Technology*, **56**, 106-111, January 1982.

[32] C. K. Anderson, "Extended Cycle Length Economics," *Transaction of American Nuclear Society*, **56**, 116-117, San Diego, California, June 1988.

[33] J. Fasnacht, "Nuclear Plant Upratings — Enhancing Implementation While Reinforcing the Viability of Nuclear Power," *Nuclear News*, 44-45, April 2002.

[34] M. Gavrilas, P. Hejzlar, N. E. Todreas, Y. Shatilla, *Safety Features of Operating Light Water Reactors of Western Design*, 2nd edition, Center for Advanced Nuclear Energy Systems (CANES), MIT, 2000.

[35] Westinghouse, "Plutonium Disposition in Existing Pressurized Water Reactors," DOE/SF/19683-6, San Francisco, California, June 1994.

[36] S. Yang, B. L. Manges, D. Redden, "Braidwood Unit 1 Cycle 9 Core Operating Limits Report," NFM0000014, December 2000.

[37] NEA/OECD, "Nuclear Fuel Safety Criteria Technical Review," Paris, 2001.

[38] US NRC (Nuclear Regulatory Commission), "Standard Review Plan," NUREG-0800, Rev. 2, July 1981.

[39] Code of Federal Regulations (CFR) 10 Part 50, "Appendix A, General Design Criteria for Nuclear Power Plants," 2001. (refer also http://www.gpo.gov/nara/cfr/)

[40] M. S. Kazimi, "Class #8. Thermal Considerations in Fuel Cycle Management," class notes of 22.351, MIT, Spring 2001.

[41] L. S. Tong, *Principles of Design Improvement for Light Water Reactors*, Hemisphere Publishing Corporation, New York, 1988.

[42] J. A. Bernard, "Light Water Reactor Control Systems," *Wiley Encyclopedia of Electrical and Electronics Engineering*, John Wiley & Sons, Inc., New York, 1999.

[43] D. R. Olander, *Fundamental Aspects of Nuclear Reactor Elements*, TID-26711, Energy Research and Development Administration (ERDA), 1976.

[44] H. Bailly, D. Ménessier, C. Prunier (editors), *The Nuclear Fuel of Pressurized Water Reactors and Fast Reactors*, Intercept Ltd, Commissariat à l'Énergie Atomique (CEA), 1999.

[45] INPO (Institute of Nuclear Power Operations), "Design and Operating Considerations for Reactor Cores," SOER 96-2, November 7, 1996.

[46] A. L. Casadei, M. Y. Young, "High-Energy Cores Experience at Westinghouse," *Proceedings of 8th International Conference on Nuclear Engineering (ICONE-8)*, Baltimore, MD, April 2-6, 2000.

[47] G. M. O'Donnell, H. H. Scott, R. O. Meyer, "A New Comparative Analysis of LWR Fuel Designs," NUREG-1754, US Nuclear Regulatory Commission, December 2001.

[48] R. J. Cacciapouti, R. J. Weader, "High-Burnup Fuel and the Impact on Fuel Management," *Transactions of American Nuclear Society*, **75**, 348, Washington, D.C., November 1996.

[49] M. J. Driscoll, T. J. Downar, E. E. Pilat, "The Linear Reactivity Model for Nuclear Fuel Management," American Nuclear Society, La Grange Park, Illinois, 1990.

[50] M. A. Feltus, "An Extended Discharge Burnup Optimization Technique Using Penn State's Fuel Management Package and CASMO-3/SIMULATE-3," *Annals of Nuclear Energy*, **22**, No. 5, 267-274, 1995.

[51] R. J. Weader II, "MIT Thorium Presentation, Tutorial on Using SIMULATE-3 in Core Design," Duke Engineering & Services, November 28, 2000.

[52] H. J. MacLean, M. V. McMahon, M. J. Driscoll, "Uranium and Separative Work Utilization in Light Water Reactors," MIT-NFC-TR-009, Massachusetts Institute of Technology, January 1998.

[53] M. V. McMahon, C. S. Handwerk, H. J. MacLean, M. J. Driscoll, N. E. Todreas, "Modeling and Design of a Reload PWR Core for an Ultra-Long Operating Cycle," MIT-NFC-TR-004, Massachusetts Institute of Technology, July 1997.

[54] N. W. Brown, et. al., "The Secure, Transportable, Autonomous Reactor System," *International Conference on Future Nuclear Systems, Global'99*, Snow King Resort, Jackson, Wyoming, August 1999.

[55] D. V. Paramonov, M. D. Carelli, C. V. Lombardi, M. E. Ricotti, N. E. Todreas, E. Greenspan, K. Yamamoto, A. Nagano, H. Ninokata, J. Robertson, F. Oriolo, "IRIS Reactor Development," *Ninth International Conference on Nuclear Engineering (ICONE-9)*, Track 8 - #840, Nice, France, April 2001.

[56] M. V. McMahon, M. J. Driscoll, E. E. Pilat, "Natural Uranium and Separative Work Utilization in LWRs," *Transactions of American Nuclear Society*, **76**, 348-349, Orlando, Florida, June 1-5, 1997.

[57] R. K. Haling, "Operating Strategy for Maintaining an Optimum Power Distribution Throughout Life," GEI-92823A, TID-7672, US Atomic Energy Commission (US-AEC), 1964.

[58] K. N. Ivanov, L. Zhang, S. H. Levine, "Haling Principle — An Effective Tool for Designing PWR Reload Patterns," *Transactions of American Nuclear Society*, **70**, 347-348, New Orleans, Louisiana, June 1994.

[59] E. E. Pilat, Personal Communication, CANES, MIT, June, 2002.

[60] S. X. Sun, D. J. Kropaczek, P. J. Turinsky, "The Haling Principle — True or False?" *Transactions of American Nuclear Society*, **68**, 482-484, San Diego, California, June 20-24, 1993.

[61] R. A. Matzie, "Licensing Assessment of PWR Extended Burnup Fuel Cycles," CEND-381, Combustion Engineering Co., March 1981.

[62] Z. Xu, P. Hejzlar, M. J. Driscoll, M. S. Kazimi, "An Improved MCNP-ORIGEN Depletion Program (MCODE) and Its Verification for High-Burnup Applications," *International Conference on the New Frontiers of Nuclear Technology: Reactor Physics, Safety and High-Performance Computing (PHYSOR 2002)*, Seoul, Korea, October 7-10, 2002.

[63] P. Hejzlar, M. J. Driscoll, N. E. Todreas, "Physics Characteristics of a Large, Passive, Pressure-Tube LWR with Voided Calandria," *Nuclear Science & Engineering*, **121**, 448-460, 1995.

[64] R. L. Moore, B. G. Schnitzler, C.A. Wemple, R.S. Babcock, D.E. Wessol, "MOCUP: MCNP-ORIGEN2 Coupled Utility Program," INEL-95/0523, Idaho National Engineering Laboratory, September 1995.

[65] D. I. Poston, H. R. Trellue, "User's Manual, Version 2.0, for Monteburns, Ver. 1.0," LA-UR-99-4999, Los Alamos National Laboratory, September 1999.

[66] K. Okumura, T. Mori, M. Nakagawa, K. Kaneko, "Validation of a Continuous-Energy Monte Carlo Burn-up Code MVP-BURN and Its Application to Analysis of Post Irradiation Experiment," *Journal of Nuclear Science and Technology*, **37**, No 2, 128-138, February 2000.

[67] J. Cetnar, W. Gudowski, J. Wallenius, K. Tucek, "Simulation of Nuclide Transmutations with Monte-Carlo Continuous Energy Burnup Code (MCB1C)," *Embedded ANS Topical Meeting of Accelerator Applications/Accelerator Driven Transmutation Technology and Application (AccApp/ADTTA'01)*, Reno, NV, November 11-15, 2001.

[68] T. Horng, Personal Communication, Cambridge, MIT, August 2002.

[69] X. Zhao, P. Hejzlar, M. J. Driscoll, "Comparison of Code Results for PWR Thorium/Uranium Pin Cell Burnup," MIT-NFC-TR-027, Center for Advanced Nuclear Energy Systems (CANES), MIT, November 2000.

[70] M. D. DeHart, M. C. Brady, C. V. Parks, "OECD/NEA Burnup Credit Calculational Criticality Benchmark Phase 1-B Results," ORNL-6901, Oak Ridge National Laboratory, June 1996.

[71] A. G. Croff, "ORIGEN2: A Versatile Computer Code for Calculating the Nuclide Compositions and Characteristics of Nuclear Materials," *Nuclear Technology*, **62**, 335-352, September 1983.

[72] P. J. Finck, R. N. Blomquist, C. G. Stenberg, C. Jammes, "Evaluation of Fission Product Worth Margins in PWR Spent Nuclear Fuel Burnup Credit Calculations," ANL-FRA-1998-1, Argonne National Laboratory, 1998.

[73] K. S. Krane, *Introductory Nuclear Physics*, Wiley, 1987.

[74] J. L. Kloosterman, "New Working Libraries for Transmutation Studies," *the Global'93 Conference on Future Nuclear Systems, Emerging Fuel Cycles and Waste Disposal Options*, Seattle, Washington, September 12-17, 1993.

[75] E. L. Redmond II, "Monte Carlo Methods, Models, and Applications for the Advanced Neutron Source," Masters Thesis, Nuclear Engineering Department, MIT, 1990.

[76] P. Hejzlar, M. J. Driscoll, M. S. Kazimi, "Conceptual Reactor Physics Design of A Lead-Bismuth-Cooled Critical Actinide Burner," MIT-ANP-TR-069, Nuclear Engineering Department, MIT, February 2000.

[77] C. M. Kang, R. O. Mosteller, "Incorporation of a Predictor-Corrector Depletion Capability into the CELL-2 Code," *Transactions of American Nuclear Society*, **45**, 729-731, San Francisco, California, October 30-November 3, 1983.

[78] N. Carstens, Personal Communication, Cambridge, MIT, September 2002.

[79] Hyung-Kook Joo, Personal Communication, Korea Atomic Energy Research Institute (KAERI), August 2001.

[80] "MCNPDATA: Standard Neutron, Photon, and Electron Data Libraries for MCNP4C," DLC-200, Los Alamos National Laboratory, April 2000.

[81] M. S. Abdelrahman, N. M. Abdurrahman, "Cross Section Libraries for Studies of Plutonium Disposition in Light Water Reactors (UTXS)," ANRCP-1999-28, Amarillo National Resource Center for Plutonium, October 1999.

[82] N. Messaoudi, H. A. Abderrahim, "Use of ENDF/B-VI.5 and JEF-2.2 Evaluations for the 3-D Venus-2 Benchmark," *PHYSOR 2002*, Seoul, Korea, October 7-10, 2002.

[83] R. J. LaBauve, T. R. England, D. C. George, C. W. Maynard, "Fission Product Analytic Impulse Source Functions," *Nuclear Technology*, **56**, 322-339, February 1982.

[84] T. Takeda, N. Hirokawa, T. Noda, "Estimation of Error Propagation in Monte-Carlo Burnup Calculations," *Journal of Nuclear Science and Technology*, **36**, No. 9, 738-745, September 1999.

[85] A. G. Croff, Personal Communication, May 2002.

[86] J. E. Hoogenboom, J. L. Kloosterman, "Generation and Validation of ORIGEN-S Libraries for Depletion and Transmutation Calculations Based on JEF2.2 and EAF3 Basic Data," *Nuclear Engineering & Design*, **170**, 107-118, 1997.

[87] E. L. Redmond II, "Multigroup Cross Section Generation Via Monte Carlo Methods," PhD Thesis, Nuclear Engineering Department, MIT, June 1997.

[88] A. S. G. Mohamed, "A Transient Nodal Method Accounting for Multigroup Transport Effects," Doctor of Science Thesis, Nuclear Engineering Department, MIT, February 1994.

[89] Z. Xu, M. J. Driscoll, M. S. Kazimi, "Effect of Moderator-to-Fuel Ratio on High-Burnup Potential in UO_2-Fueled Water/Steam-Cooled Lattices," *Transactions of American Nuclear Society*, **83**, 43-44, Washington D.C., November 12-16, 2000.

[90] Z. Xu, M. J. Driscoll, M. S. Kazimi, "A Systematic Study of Moderation Effects on Neutronic Performance of UO_2 Fueled Lattices," MIT-NFC-TR-028, Center for Advanced Nuclear Energy Systems (CANES), MIT, May 2001.

[91] Z. Xu, M. J. Driscoll, M. S. Kazimi, "Neutron Spectrum Effects on Burnup, Reactivity, and Isotopics in UO_2/H_2O Lattices," *Nuclear Science & Engineering*, **141**, 175-189, 2002.

[92] J. H. Ferziger, P. F. Zweifel, "The Theory of Neutron Slowing Down in Nuclear Reactors," MIT Press, Cambridge, MA, 1966.

[93] J. Buongiorno, "The Supercritical Light-Water-Cooled Reactor and Its Potential for Improved Economics," Presentation at MIT, December 13, 2002.

[94] M. Shaw et al., "An Evaluation of Steam-Cooled Fast Breeder Reactors," WASH-1088, Division of Reactor Development and Technology, U.S. Atomic Energy Commission, April 1969.

[95] T. Okubo, T. Kugo, T. Shirakawa, S. Shimada, M. Ochiai, "Conceptual Design of Water-Cooled Reactors with Increased or Reduced Moderation," *Proc. Workshop Advanced Reactors with Innovative Fuels*, OECD, Villigen, Switzerland, October 21-23, 1998.

[96] "Fuel Review: Fuel Design Data," *Nuclear Engineering International*, **44**, No. 542, 28-30, September 1999.

[97] V. I. Pavlov, "Analysis of the Neutron-Physical Characteristics of the Fuel Lattice of the VVER-1000 Reactor," Atomic Energy, Consultants Bureau, New York, July 1993.

[98] R. W. Bain, et. al., "Steam Tables 1964, Physical Properties of Water and Steam 0-800°C, 0-1000 bars," Department of Sciences and industrial Research, National Engineering Laboratory, Edinburgh, Her Majesty's Stationery Office, 1964.

[99] S. Glasstone, M. C. Edlund, *The Elements of Nuclear Reactor Theory*, Van Nostrand, 1952.

[100] R. A. Matzie, R. S. Daleas, D. D. Miller, "Industrial Assessment of Nonbackfittable PWR Design Modifications," CEND-385, November 1980.

[101] D. Wang, M. J. Driscoll, M. S. Kazimi, "Design and Performance Assessment of A PWR Whole-Assembly Seed and Blanket Arrangement," MIT-NFC-TR-026, MIT, June 2000.

[102] P. Hejzlar, M. J. Driscoll, M. S. Kazimi, "High Performance Annular Fuel for Pressurized Water Reactors," *Transactions of American Nuclear Society*, **84**, 192, Milwaukee, WI, June 17-21, 2001.

[103] Z. Xu, P. Hejzlar, M. S. Kazimi, "On the Neutronics of Internally and Externally Cooled Annular PWR Fuel," *Transactions of American Nuclear Society*, **87**, 384-386, Washington DC, November 17-21, 2002.

[104] C. Degueldre, J. M. Paratte, "Concepts for an Inert Matrix Fuel, An Overview," *Journal of Nuclear Materials*, **274**, 1-6, 1999.

[105] K. T. Clarno, "Composition Optimization of Thorium-Uranium Pressurized Water Reactor Cores," Bachelor Thesis, Nuclear Engineering Department, MIT, June 1999.

[106] X. Zhao, M. J. Driscoll, M. S. Kazimi, "Micro-Heterogeneous Thorium Based Fuel Concepts for Pressurized Water Reactors," MIT-NFC-TR-031, Center for Advanced Nuclear Energy Systems (CANES), August 2001.

[107] P. Chodak, M. J. Driscoll, M. M. Miller, N. E. Todreas, "Destruction of Plutonium Using Non-Uranium Fuels in Pressurized Water Reactor Peripheral Assemblies," MIT-NFC-TR-001, Nuclear Engineering Department, MIT, January 1997.

[108] P. E. MacDonald (P.I.), "Advanced Proliferation Resistant, Lower Cost, Uranium-Thorium Dioxide Fuels for Light Water Reactors," Nuclear Energy Research Initiative (NERI) Project 99-0153, May 2002.

[109] A. Radkowsky, A. Galperin, "The Nonproliferative Light Water Thorium Reactor: A New Approach to Light Water Reactor Core Technology," *Nuclear Technology*, **124**, 215-222, 1998.

[110] K. Nikitin, M. Saito, M. Kawashima, V. Artisyuk, A. Shmelev, "Long-Life Water Cooled Smaller Reactor with U-Np-Pu Fuel," *Journal of Nuclear Science & Technology*, **38**, No. 7, 511-516, July 2001.

[111] S. M. Oggianu, M. S. Kazimi, H. C. No, "High Burnup Fuels for Advanced Nuclear Reactors," MIT-NFC-TR-029, Center for Advanced Nuclear Energy Systems (CANES), May 2001.

[112] D. B. Lancaster, R. L. Marsh, D. B. Bullen, H. Pfeifer, C. S. Ervin, A. E. Levin, "A Technique for the Selection of Fuel Pin Diameter for a Uranium-Zirconium Alloy-Fueled Pressurized Water Reactor," *Nuclear Technology*, **97**, 16, 1992.

[113] A. Puill, J. Bergeron, "Advanced Plutonium Fuel Assembly: An Advanced Concept for Using Plutonium in Pressurized Water Reactors," *Nuclear Technology*, **119**, 123-140, August 1997.

[114] http://www.webelements.com

[115] http://www.knovel.com/

[116] W. G. Pettus, "Void Plug for Annular Fuel Pellets," US Patent-053560, May 1987.

[117] N. E. Todreas, M. S. Kazimi, *Nuclear Systems I, Thermal Hydraulic Fundamentals*, Hemisphere Publishing Corporation, 1989.

[118] C. K. Jo, N. Z. Cho, Y. H. Kim, "Graphite-Filled Mixed-Oxide Fuel Design for Fully Loaded PWR Cores," *Annals of Nuclear Energy*, **27**, Issue 9, 819-829, June 2000.

[119] C. M. Mildrum, "Physics and Economics of Annular Fuel in PWRs," Westinghouse Nuclear Energy Systems, 1980.

[120] M. S. Kazimi (P.I.), "High Performance Fuel Design for Next Generation PWRs, 3rd Quarterly Report," MIT-NFC-PR-041, Center for Advanced Nuclear Energy Systems (CANES), MIT, May 2002.

[121] T. Bahadir, Personal Communication, Studsvik of America, Inc., June 2001.

[122] A. F. Henry, *Nuclear Reactor Analysis*, the MIT Press, Cambridge, MA, 1975.

[123] L. S. Tong, J. Weisman, *Thermal Analysis of Pressurized Water Reactors*, Third Edition, American Nuclear Society, La Grange Park, IL, 1996.

[124] R. J. Cacciapouti, R. J. Weader II, J. P. Malone, "PWR Burnable Absorber Evaluation," *NEI Fuel Cycle '95*, San Diego, California, April 1995.

[125] A. Galperin, M. Segev, A. Radkowsky, "Substitution of the Soluble Boron Reactivity Control System of A Pressurized Water Reactor by Gadolinium Burnable Poisons," *Nuclear Technology*, **75**, 127-133, November 1986.

[126] A. Galperin, "Gd Burnable Poison System for Reactivity Control of the First Cycle of A PWR," *Annals of Nuclear Energy*, **14**, No. 1, 53-57, 1987.

[127] J. R. Parrington, et. al., *Chart of Nuclides*, 15th edition, Knolls Atomic Power Laboratory, Schenectady, New York, 1996.

[128] C. W. Bagnal, R. A. Matzie, et. al., "Use of Gadolinium in PWR Extended-Burnup Fuel Cycles," CEND-391, Combustion Engineering, Inc., September 1981.

[129] A. Galperin, M. Segev, A. Radkowsky, "The Effect of Boron and Gadolinium Burnable Poisons on the Hot-to-Cold Reactivity Swing of A Pressurized Water Reactor Assembly," *Nuclear Technology*, **75**, 123-126, November 1986.

[130] M. Asou, J. Porta, "Prospects for Poisoning Reactor Cores of the Future," *Nuclear Engineering & Design*, **168**, 261-270, 1997.

[131] V. Barchevtsev, V. Artisyuk, H. Ninokata, "Concept of Erbium Doped Uranium Oxide Fuel Cycle in Light Water Reactors," *Journal of Nuclear Science and Technology*, **39**, No. 5, 506-513, May 2002.

[132] J. P. A. Renier, M. L. Grossbeck, "Development of Improved Burnable Poisons for Commercial Nuclear Power Reactors," ORNL/TM-2001/238, Oak Ridge National Laboratory (ORNL), October 2001.

[133] J. Tulenko, et. al., "Development of a Stable Polymer Burnable Poison Material with Special Attributes," seminar at the University of Cincinnati, May 28, 2002.

[134] F. Correa, M. J. Driscoll, D. D. Lanning, "An Evaluation of Tight-Pitch PWR Cores," MITNE-227, Massachusetts Institute of Technology, August 1979.

[135] E. Johansson, "Reactor Physics Calculations on Close-Packed Pressurized Water Reactor Lattices," *Nuclear Technology*, **68**, 263-268, February 1985.

[136] Y. Ronen, Y. Dali, "A High-Conversion Water Reactor Design," *Nuclear Science & Engineering*, **130**, 239-253, 1998.

[137] D. Saphier, P. Raymond, "Applying Thermal-Hydraulic Design Limits for the Highly Moderated MOX-Fueled APWRs," *Transactions of American Nuclear Society*, **71**, 529-530, November 1994.

[138] http://www.ymp.gov

[139] M. S. Kazimi, N. E. Todreas, "Nuclear Power Economic Performance: Challenges and Opportunities," *Annual Reviews in Energy and the Environment*, **24**, 139-171, 1999.

[140] Y. S. Tang, J. H. Saling, Radioactive Waste Management, Hemisphere Publishing Corporation, New York, 1990.

[141] C. W. Forsberg, "In-Repository Depleted-Uranium Isotopic Mixing with LWR SNF for Criticality Control," *International High-Level Waste Management Conference*, Las Vegas, Nevada, May 11-14, 1998.

[142] US NRC, *Nuclear Wastes: Technologies for Separations and Transmutation*, National Academy Press, 1996.

[143] C. W. Forsberg, C. M. Hopper, J. L. Richter, H. C. Vantine, "Definition of Weapons-Usable Uranium-233," ORNL/TM-13517, Oak Ridge National Laboratory, March 1998.

[144] J. C. Mark, "Explosive Properties of Reactor-Grade Plutonium," *Science & Global Security*, **4**, 111-128, 1993.

[145] B. Pellaud, "Proliferation Aspects of Plutonium Recycling," *Journal of Nuclear Materials Management*, **31**, No. 1, 30-38, Fall 2002.

[146] C. A. Bollmann, X. Zhao, M. J. Driscoll, M. S. Kazimi, "Analytical Determination of DUPIC Cycle Fuel Utilization," *Proc. 6th Int. Conf. Nuclear Engineering (ICONE6)*, San Diego, California, May 10-15, 1998.

[147] "Report of the International Workshop on Technology Opportunities for Increasing the Proliferation Resistance of Global Civilian Nuclear Power Systems (TOPS)," the Nuclear Energy Research Advisory Committee (NERAC) and the Center for Global Security Research (CGSR), Lawrence Livermore National Lab., March 2000.

[148] M. S. Kazimi, E. E. Pilat, M. J. Driscoll, Z. Xu, D. Wang, X. Zhao, "Enhancing Proliferation Resistance in Advanced Light Water Reactor Fuel Cycles," *ICONE-8*, Nice France, 2000.

[149] OECD/NEA, "The Economics of the Nuclear Fuel Cycle," Paris, France, 1994.

[150] C. A. Rusch, "Key Factors for Decisions to Extend Nuclear Plant Operating Cycles," *Transactions of American Nuclear Society*, **76**, 300-301, Orlando, Florida, June 1-5, 1997.

Appendix A. High Burnup Core Input Files for CMS Code Package

As illustrated in the code description for the CMS package in Chapter 1, three types of input files are needed for CASMO-4, TABLES-3, SIMULATE-3, respectively. Correspondingly these input files are categorized under three different directories. This appendix includes four CASMO-4 input files (fuel assembly and radial/top/bottom reflectors), one TABLES-3 input file, and one SIMULATE-3 input file. A typical Westinghouse PWR quarter core with 5 w/o enriched UO_2 fuel is modeled in these input files. Readers should refer to CMS code package manuals [10, 11, 12] in order to understand them line by line.

CASMO-4 fuel assembly input (./C4/c4.u500.inp)

```
*
*           HIGH BURNUP PWR-CORE MODEL
*
* CASMO-4 Input for segment U500
* 17X17 Westinghouse PWR Assembly
* 5.0 w/o UO2, no burnable poison
*
*  1.Base case calculation
*             BASE     BRANCHES
*       TFU 900   -> 565.8, 1200
*       TMO 583.1 -> 565.8, 600, 615
*       BOR 450   -> 0, 900, 2000
*       CRD       -> RCC
*
*  2.TFU hisotry (565.8, 1200 K)
*
*  3.TMO hisotry (565.8, 600K)
*
*  4.BOR history (0, 900, 2000 ppm)
*
*
*       by Zhiwen XU (xzw@mit.edu)
*       Massachusetts Institute of Technology

TTL * HIGH BURNUP PWR-CORE MODEL - ENR. 5.00

PDE 104.5 'KWL'            * Power density
PRE 155.1296               * Pressure (bars)
TFU 900.0                  * Average fuel temperature (K)
TMO 583.1                  * Average moderator temperature (K)
BOR 450.0                  * Average soluble boron concent.(ppm)
VOI 0.0                    * zero void fraction
SIM 'U500'                 * Segment name

***** Material compositions *****
FUE 1 10.3/5.00

***** Geometry specification *****
PWR 17 1.26 21.5           * 17X17, pin pitch 1.26cm, assm.pitch 21.5cm
PIN 1 .4096 .4178 .4750/'1' 'AIR' 'CAN'          * FUEL
PIN 2 .5690 .6147/'COO' 'BOX'                    * GUIDET
PIN 3 .5690 .6147/'COO' 'BOX'
*
```

```
* Define the control rod with the name RCC without inserting it:
PIN 3    .4331 .4369 .4839 .5690 .6147/
      'AIC' 'AIR' 'CRS' 'COO' 'BOX'//1 'RCC' 'ROD'

LPI
   2
   1  1
   1  1  1
   3  1  1  3
   1  1  1  1  1
   1  1  1  1  1  3
   3  1  1  3  1  1  1
   1  1  1  1  1  1  1  1
   1  1  1  1  1  1  1  1  1

DEP -80
NLI STA

***** Case Matrix for library *****
COE ,, 0 0.5 1 5 10 15 20 25 30 35 40 45 50 55 60 65 70 75 80
TFU 565.8 1200
TMO 565.8 600 615
BOR 0 900 2000
ROD 'RCC'

***** TFU history *****
TTL * FUEL TEMPERATURE HISOTRY
RES,,0
TFU 565.8 1200
DEP -80
NLI STA

***** TMO history *****
TTL * MODERATOR TEMPERATURE HISTORY
RES,,0
TMO 565.8 600
DEP -80
NLI STA

***** BOR history *****
TTL * BORON HISTROY
RES,,0
BOR 0 900 2000
DEP -80
NLI STA
END
```

CASMO-4 radial reflector input (./C4/REFLECTOR/c4.radref.inp)

```
*
*   CASMO-4 Input
*   Radial reflector
*
*          BASE     BRANCHES
*   BOR    450 -> 0 900 2000
*
*          by Zhiwen Xu (xzw@mit.edu)
*          Massachusetts Institute of Technology
*
TTL * PWR radial reflector

TFU 900.0               * Average fuel temperature
TMO 565.8               * equals inlet water temperature
BOR 450                 * nominal boron concentration
PRE 155.1296            * system pressure
SIM 'RADREF'            * segment name

***** Material compositions *****
FUE 1 10.3/5.0

***** Geometry specification *****
PWR 17 1.26 21.5
PIN 1 .4096 .4178 .4750/'1' 'AIR' 'CAN'    * fuel rod
PIN 2 .5690 .6147/'COO' 'BOX'              * guide tube

LPI
   2
   1  1
   1  1  1
   2  1  1  2
   1  1  1  1  1
   1  1  1  1  1  2
   2  1  1  2  1  1  1
   1  1  1  1  1  1  1  1
   1  1  1  1  1  1  1  1  1

REF 2.225 15/'CSS' 'MOD'//8     * middle row reflector calc.
NLI STA

***** BOR 0 *****
TTL * BOR 0
BOR 0
NLI STA

***** BOR 900 *****
TTL * BOR 900
BOR 900
NLI STA

***** BOR 2000 *****
TTL * BOR 2000
BOR 2000
NLI STA
END
```

CASMO-4 top reflector input (./C4/REFLECTOR/c4.topref.inp)

```
*
*   CASMO-4 Input
*   Top axial reflector
*
*         BASE     BRANCHES
*   BOR    600 -> 0 1200 1800
*
*          by Zhiwen Xu (xzw@mit.edu)
*          Massachusetts Institute of Technology
*
DIM 11 1/    * 11 by 11 full lattice, HAS TO BE PUT HERE

TTL * PWR top axial reflector

TFU 900.0               * Average fuel temperature
TMO 565.8               * equals inlet water temperature
BOR 600                 * nominal boron concentration
SIM 'TOPREF'            * segment name

***** Material compositions *****
FUE 1 10.3/5.0
SPA 13.99 18.E-6,,8.154/718=84.59 347=15.41     * Spacer composition
MOD 1.31979/302=49.419 347=0.039
            8000=44.887 1001=5.655 5000=.030    * T1
MI2 1.63107/302=39.988 347=3.455 718=17.569
            8000=34.626 1001=4.362 5000=.023    * T2

***** Geometry specification *****
PWR 11 1.26 13.94484 4*0 1
PIN 1 .4096 .4178 .4750
LPI 121*1    * full assembly
REF 8.7554 5.6893/'MOD' 'MI2'//0     * full assm. reflector calc.

NLI STA

***** LOW BORON *****
TTL * BOR LOW
BOR 0
MOD 1.31979/302=49.419 347=0.039
            8000=44.887 1001=5.655 5000=.000    * T1
MI2 1.63107/302=39.988 347=3.455 718=17.569
            8000=34.626 1001=4.362 5000=.000    * T2
NLI STA

***** HIGH BORON *****
TTL * BOR HIGH
BOR 1200.0
MOD 1.31979/302=49.419 347=0.039
            8000=44.887 1001=5.655 5000=.061    * T1
MI2 1.63107/302=39.988 347=3.455 718=17.569
            8000=34.626 1001=4.362 5000=.047    * T2
NLI STA

***** VERY HIGH BORON *****
TTL * BOR VHIGH
BOR 1800.0
MOD 1.31979/302=49.419 347=0.039
            8000=44.887 1001=5.655 5000=.091    * T1
MI2 1.63107/302=39.988 347=3.455 718=17.569
            8000=34.626 1001=4.362 5000=.070    * T2
NLI STA
END
```

CASMO-4 bottom reflector input (./C4/REFLECTOR/c4.topref.inp)

```
*
*   CASMO-4 Input
*   Bottom axial reflector
*
*         BASE     BRANCHES
*   BOR    600 -> 0 1200 1800
*
*          by Zhiwen Xu (xzw@mit.edu)
*          Massachusetts Institute of Technology
*
DIM 11 1/    * 11 by 11 full lattice, HAS TO BE PUT HERE

TTL * PWR botom axial reflector

TFU 900.0               * Average fuel temperature
TMO 565.8               * equals inlet water temperature
BOR 600                 * nominal boron concentration
SIM 'BOTREF'            * segment name

***** Material compositions *****
FUE 1 10.3/5.0
SPA 13.99 18.E-6,,8.154/718=84.59 347=15.41     * Spacer composition
MOD 2.66270/302=78.578 347=2.755
            8000=16.579 1001=2.089 5000=.011    * B1
MI2 3.22490/302=0.400 347=84.684
            8000=13.319 1001=1.678 5000=.009    * B2

***** Geometry specification *****
PWR 11 1.26 13.94484 4*0 1
PIN 1 .4096 .4178 .4750
LPI 121*1    * full assembly
REF,1.4224,8.5166/'MOD' 'MI2'//0     * full assm. reflector calc.

NLI STA

***** LOW BORON *****
TTL * BOR LOW
BOR 0
MOD 2.66270/302=78.578 347=2.755
            8000=16.579 1001=2.089 5000=.000    * B1
MI2 3.22490/302=0.400 347=84.684
            8000=13.319 1001=1.678 5000=.000    * B2
NLI STA

***** HIGH BORON *****
TTL * BOR HIGH
BOR 1200.0
MOD 2.66270/302=78.578 347=2.755
            8000=16.579 1001=2.089 5000=.022    * B1
MI2 3.22490/302=0.400 347=84.684
            8000=13.319 1001=1.678 5000=.018    * B2
NLI STA

***** VERY HIGH BORON *****
TTL * BOR VHIGH
BOR 1800.0
MOD 2.66270/302=78.578 347=2.755
            8000=16.579 1001=2.089 5000=.034    * B1
MI2 3.22490/302=0.400 347=84.684
            8000=13.319 1001=1.678 5000=.027    * B2
NLI STA
END
```

TABLES-3 input (./T3/t3.pwru500.inp)

```
'COM'  TABLES-3 input

'TIT' 'HIGH BURNUP PWR-CORE MODEL - ENR. 5.00'/

'PWR' 0 155.1296/
'LIB' 'ADD' /
'OPT' 4 1/

'COM' CASMO-4 CAX-FILES USED FOR THIS SEGMENT
'CAS' '../C4/c4.u500.cax'/

'EXP' 20 1 0 0.1 0.5 1 5 10 15 20 25 30 35 40 45 50 55 60 65 70 75 80/
'RES' 19 1 0 0.5 1 5 10 15 20 25 30 35 40 45 50 55 60 65 70 75 80/
'TFU'  3 2 565.8 900 1200/
'TMO'  4 2 565.8 583.1 600 615/
'BOR'  4 2 0 450 900 2000/
'HTFU'  3 2 565.8 900 1200/
'HTMO'  3 2 565.8 583.1 600/
'HBOR'  4 2 0 450 900 2000/
'CRD'   2 1 '   ' 'RCC'

'COM' MACROSCOPIC CROSS SECTION DEPENDENCE
'BAS.MAC' 2 'EXP' 'HTMO',,,'TMO'/
'DEL.MAC' 2 'EXP' 'TMO'/
'DEL.MAC' 2 'EXP' 'HBOR',,,'BOR'/
'DEL.MAC' 2 'EXP' 'BOR'/
'DEL.MAC' 2 'EXP' 'HTFU',,,'TFU'/
'DEL.MAC' 2 'EXP' 'TFU'/
'DEL.MAC' 2 'EXP' 'CRD'/

'SUB.MAC' 'HTMO' 'TMO' 'HTMO' 'TMO'/
'SUB.MAC' 'HBOR' 'BOR' 'HBOR' 'BOR'/
'SUB.MAC' 'HTFU' 'TFU' 'HTFU' 'TFU'/

'COM' FISSION PRODUCTS YIELDS
'BAS.FPD' 2 'EXP' 'TMO'/
'DEL.FPD' 2 'EXP' 'BOR'/
'DEL.FPD' 2 'EXP' 'TFU'/
'DEL.FPD' 2 'EXP' 'CRD'/

'COM' DISCONTINUITY FACTORS
'BAS.DFS' 2 'EXP' 'TMO'/
'DEL.DFS' 2 'EXP' 'BOR'/
'DEL.DFS' 2 'EXP' 'TFU'/
'DEL.DFS' 2 'EXP' 'CRD'/

'COM' PIN OPTION
'PIN.PIN'/

'STA'/
'END'/
'COM' -------------------- PWR RADIAL REFLECTORS --------------------

'TIT' 'PWR RADIAL REFLECTOR'
'REF' 'RADIAL' 0 155.1296/
'LIB' 'ADD'/

'CAS','../C4/REFLECTOR/c4.radref.cax' /

'COM'  VARIABLE LIST
'BOR'          4 2   0.0 450.0 900.0    2000.0/
'HBOR'         4 2   0.0 450.0 900.0  2000.0/

'COM'  MACROSCOPIC AND DFS DEPENDANCE, NO FPD
'BAS.MAC' 1,,'BOR',,,'HBOR'/
'BAS.DFS' 1,,'BOR',,,'HBOR'/

'STA'/
'END'/

'COM' --------------- PWR BOTTOM AXIAL REFLECTOR ---------------
```

```
'TIT' 'PWR BOTTOM AXIAL REFLECTOR'
'REF' 'AXIAL' 0 155.1296/
'LIB' 'ADD'/

'CAS','../C4/REFLECTOR/c4.botref.cax' /

'COM'  VARIABLE LIST
'BOR'          4 2   0.0 600.0 1200.0    1800.0/
'HBOR'         4 2   0.0 600.0 1200.0 1800.0/

'COM'  MACROSCOPIC AND DFS DEPENDANCE, NO FPD
'BAS.MAC' 1,,'BOR',,,'HBOR'/
'BAS.DFS' 1,,'BOR',,,'HBOR' /

'STA'/
'END'/

'COM' --------------- PWR TOP AXIAL REFLECTOR ---------------

'TIT' 'PWR TOP AXIAL REFLECTOR'
'REF' 'AXIAL' 0 155.1296/
'LIB' 'ADD'/

'CAS','../C4/REFLECTOR/c4.topref.cax' /

'COM'  VARIABLE LIST
'BOR'          4 2   0.0 600.0 1200.0    1800.0/
'HBOR'         4 2   0.0 600.0 1200.0 1800.0/

'COM'  MACROSCOPIC AND DFS DEPENDANCE, NO FPD
'BAS.MAC' 1,,'BOR',,,'HBOR'/
'BAS.DFS' 1,,'BOR',,,'HBOR' /

'STA'/
'END'/
```

SIMULATE-3 input (./S3/s3.u500.inp)

```
'COM'  SIMULATE-3 Input, PWR CORE DEPLETION

'COM' Dimensions of Reactor and Calculation
'DIM.PWR' 15/  PWR CORE WITH 15 ROWS OF ASSY
'DIM.CAL' 24 2 2/  QUARTER CORE, 24 AXIAL NODES, 2X2 NODES PER ASSY
'DIM.DEP' 'EXP' 'SAM' 'HTMO' 'HBOR' 'HTFU' 'PIN'/ DEPLETION ARGUMENTS
'DIM.MEM' 12*2/ ALL DATA STORED IN MEMORY

'LIB' '../T3/t3.pwru500.lib'/

'COM' Title Cards
'TIT.PRO' 'TYPICAL WESTINGHOUSE 4-LOOP PWR'/
'TIT.RUN' 'B1-CORE'/
'TIT.CAS' 'SINGLE BATCH, FREE OF POISON'/
'TIT.REF' 0 0.000E+00/

'COM' Core data
'COR.DAT' 21.50364 365.76 104.5 751.53 572.0/
'COR.SYM' 'ROT'/   CORE SYMMETRY
'PWR.OPT' 'ON'/  TURN ON PWR INLET TEMP OPTION
'PWR.CTP' 0 25 50 75 100/ CORE POWER ORDINATE
'PWR.TIN' 557 557.45 557.90 558.35 558.80/ INLET TEMP, F

'COM' Fuel segment and reflector description
'SEG.TFU' 0 0 347.38 -5.3799/ FUEL TEMP FIT VS POWER FOR ALL FUEL
'TAB.TFU' 1  0  'EXP'  10  'POW'  1
     0.   5.0   10.0   15.0   20.0   30.0   35.0   40.0   45.0   50.0
  1  0. -35.45 -52.14 -83.33 -87.25 -82.88 -83.63 -89.22 -88.07 -76.61/
'REF.LIB' 01 'RADREF'/
'REF.LIB' 02 'BOTREF'/
'REF.LIB' 03 'TOPREF'/
'SEG.LIB' 04 'U500'/  ONLY TYPE OF FUEL SEGMENT

'COM' Fuel assembly description
'FUE.GRD'  'ON'  2.82 3.36 'INC'
                64.87 3.36 'INC'
               117.07 3.36 'INC'
               169.27 3.36 'INC'
               221.46 3.36 'INC'
               273.66 3.36 'INC'
               325.86 3.36 'INC'/ Explicit spacer(grid) modeling
'FUE.ZON' 01 1 'U500NoBP' 02 0.0 04 365.76 03/ FRESH FUEL 5.0 ENR.
'FUE.ZON' 02 1 'RADREF'   02 0.0 01 365.76 03/ RADIAL REFLECTOR
'FUE.TYP' 1
 1  1  1  1  1  1  1  1  2
 1  1  1  1  1  1  1  1  2
 1  1  1  1  1  1  1  1  2
 1  1  1  1  1  1  1  1  2
 1  1  1  1  1  1  1  2  2
 1  1  1  1  1  1  1  2  0
 1  1  1  1  1  1  2  2  0
 1  1  1  1  2  2  2  0  0
 2  2  2  2  2  0  0  0  0/  LOWER RIGHT QTR CORE
'FUE.SER' 3/
01  1                 C01 C09 C17 C25 C23 C15 C07
02  1           C57 C45 C37 A01 C29 A09 C35 A03 C43 C51 C63
03  1     C61 C53 B01 A13 B09 A21 B17 A23 B15 A15 B07 C55 C59
04  1     C49 B05 B21 B25 A29 B33 A37 B39 A31 B31 B23 B03 C47
05  1 C05 C41 A17 B29 A41 B49 A45 B41 A47 B55 A43 B27 A19 C39 C03
06  1 C13 A05 B13 A33 B53 A53 B57 A57 B63 A55 B51 A35 B11 A07 C11
07  1 C21 C33 A25 B37 A49 B61 A61 B45 A63 B59 A51 B35 A27 C31 C19
08  1 C28 A12 B20 A40 B44 A60 B48 A65 B47 A59 B43 A39 B19 A11 C27
09  1 C20 C32 A28 B36 A52 B60 A64 B46 A62 B62 A50 B38 A26 C34 C22
10  1 C12 A08 B12 A36 B52 A56 B64 A58 B58 A54 B54 A34 B14 A06 C14
11  1 C04 C40 A20 B28 A44 B56 A48 B42 A46 B50 A42 B30 A18 C42 C06
12  1     C48 B04 B24 B32 A32 B40 A38 B34 A30 B26 B22 B06 C50
13  1     C60 C56 B08 A16 B16 A24 B18 A22 B10 A14 B02 C54 C62
14  1         C64 C52 C44 A04 C36 A10 C30 A02 C38 C46 C58
15  1                 C08 C16 C24 C26 C18 C10 C02
 0  0
'FUE.INI' 'CJILAB'/
```

```
'FUE.BAT' 1
  1 1 1 1 1 1 1 1
  1 1 1 1 1 1 1 1
  1 1 1 1 1 1 1 1
  1 1 1 1 1 1 1 1
  1 1 1 1 1 1 1 0
  1 1 1 1 1 1 1 0
  1 1 1 1 1 1 0 0
  1 1 1 1 0 0 0 0/
'BAT.LAB' 1 'U500NoBP'/

'COM' Hydraulics feedback
'HYD.ITE'/ Hydraulic iteration

'COM' Control rod data
'CRD.ZON' 1 1 'ARO' 0 0.0 0 365.76/ SPARE LOCATION
'CRD.ZON' 2 1 'AIC' 0 7.57 20 365.76/ AIC CONTROL ROD
'CRD.DAT' 226 1.585/
'CRD.TYP' 1
4*0           1  1  1  1  1  1  1           4*0
2*0     1 02  1 02  1 02  1 02  1 02  1     2*0
  0  1  1  1 02  1 02  1 02  1 02  1  1  1  0
  0 02  1 02  1  1  1 02  1  1  1 02  1 02  0
  1  1 02  1  1  1  1  1  1  1  1  1 02  1  1
  1 02  1  1  1 02  1 02  1 02  1  1  1 02  1
  1  1 02  1  1  1  1  1  1  1  1  1 02  1  1
  1 02  1 02  1 02  1 02  1 02  1 02  1 02  1
  1  1 02  1  1  1  1  1  1  1  1  1 02  1  1
  1 02  1  1  1 02  1 02  1 02  1  1  1 02  1
  1  1 02  1  1  1  1  1  1  1  1  1 02  1  1
  0 02  1 02  1  1  1 02  1  1  1 02  1 02  0
  0  1  1  1 02  1 02  1 02  1 02  1  1  1  0
2*0     1 02  1 02  1 02  1 02  1 02  1     2*0
4*0           1  1  1  1  1  1  1           4*0/  CONTROL ROD MAP
'CRD.SEQ' 1 000 000 000 000 115 226 226 226 226 226/ BKD
'CRD.SEQ' 2 000 000 000 115 226 226 226 226 226 226/ BKC
'CRD.SEQ' 3 000 000 115 226 226 226 226 226 226 226/ BKB
'CRD.SEQ' 4 000 115 226 226 226 226 226 226 226 226/ BKA
'CRD.SEQ' 5 226 226 226 226 226 226 226 226 226 226/ SBE
'CRD.SEQ' 6 226 226 226 226 226 226 226 226 226 226/ SBD
'CRD.SEQ' 7 226 226 226 226 226 226 226 226 226 226/ SBC
'CRD.SEQ' 8 226 226 226 226 226 226 226 226 226 226/ SBB
'CRD.SEQ' 9 226 226 226 226 226 226 226 226 226 226/ SBA
'CRD.SEQ' 10 226 226 226 226 226 226 226 226 226 226/ NO BANK REGION
'CRD.PAS' 10 6/ CONTROL ROD PASS 1
'CRD.GRP' 1
4*0           00 00 00 00 00 00 00           4*0
2*0     00  9 00  3 00  2 00  3 00  9 00     2*0
  0 00 00 00  6 00  8 00  8 00  7 00 00 00  0
  0  9 00  1 00 00 00  5 00 00 00  1 00  9  0
 00 00  7 00 00 00 00 00 00 00 00 00  6 00 00
 00  3 00 00 00  2 00  4 00  2 00 00 00  3 00
 00 00  8 00 00 00 00 00 00 00 00 00  8 00 00
 00  2 00  5 00  4 00  1 00  4 00  5 00  2 00
 00 00  8 00 00 00 00 00 00 00 00 00  8 00 00
 00  3 00 00 00  2 00  4 00  2 00 00 00  3 00
 00 00  6 00 00 00 00 00 00 00 00 00  7 00 00
  0  9 00  1 00 00 00  5 00 00 00  1 00  9  0
  0 00 00 00  7 00  8 00  8 00  6 00 00 00  0
2*0     00  9 00  3 00  2 00  3 00  9 00     2*0
4*0           00 00 00 00 00 00 00           4*0/ CRD BANK LOC.

'COM' Printing controls
'KIN.EDT' 'ON' '1-D'/
'PIN.EDT' 'ON' 'SUMM' '2PIN'/
'PRI.STA' 50*' '/
'PRI.STA' '2RPF' '2EXP' '2KIN' 'SRPF' 'SEXP' 'SKIN' '2TFU'/

'COM' Cycle depletion
'DEP.CYC' 'CYCLE 1' 0.0 01/

'ITE.KEF' 1.2/
'COM'  'ITE.BOR' 2500/
```

```
'COM'   'ERR.SUP' 'BOR'/
'DEP.STA' 'AVE' 0 0.1 0.5 1 -1 10 -2.5 45/

'STA'/
'END'/
```

Appendix B. MCODE (Ver. 1.0, February 2002) User's Manual

B.1 Introduction

MCODE (MCNP-ORIGEN DEpletion program) is a linkage program entirely written in ANSI C, which uses MCNP and ORIGEN to do burnup calculations for arbitrarily-defined MCNP regions. Any proposed lattice/assembly designs can be investigated using MCODE as long as sufficient MCNP cross section libraries are available. The code, based on MCNP, can model arbitrary three-dimensional geometry bounded by first- or second-degree surfaces and fourth-degree elliptical tori. Various combinations of fuel options can be studied, including those containing burnable poison, such as gadolinium and erbium. Besides its general applicability, MCODE has demonstrated excellent portability across various platforms. Two categories of allowed operating systems are UNIX and Windows.

B.2 Description of Required MCODE Input Files

B.2.1 File Organizations

In general, inputs to MCODE consist of two text input files (initial MCNP input and MCODE input) and an optional equilibrium MCNP source file. The initial MCNP input file models the specific problem, such as the geometry and material specifications. An MCODE input is supplemented to specify the burnup-related information, such as the depletion cells and burnup points. It should be noted that the MCODE input is the central input in MCODE which also specifies the information of MCNP/ORIGEN running environments. The current version of MCODE applications (`mcode.exe`, `mcodeout.exe`) takes only one parameter, the MCODE input, on the command line. The equilibrium MCNP source file can be specified so that each MCNP run can be more efficient (no need to do re-distribution to obtain equilibrium source neutron distribution). General relationships between these input files are shown in Fig. B.1:

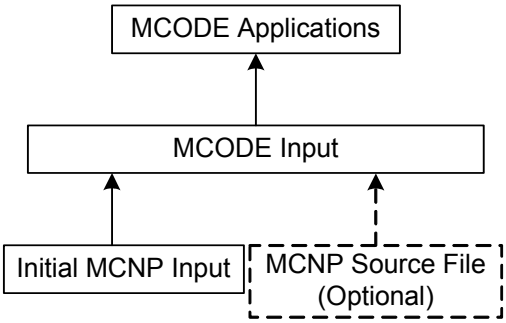

Figure B.1 Required input files for MCODE.

B.2.2 Initial MCNP Input

The initial MCNP input should first comply with the MCNP manual [14]. There are also additional constraints imposed by MCODE.

Fuel Material Specifications

Special tags are needed for the depletion material specification so that MCODE can recognize different groups of nuclides when updating them with burnup. Those special tags are

`begin_mcode_FP`	beginning of fission product isotopes;
`end_mcode_FP`	end of fission product isotopes;
`begin_mcode_ACT`	beginning of actinides;
`end_mcode_ACT`	end of actinides.

Because there is no correspondence table between MCNP nuclides and ORIGEN nuclides, an additional tag is needed to explicitly specify the ORIGEN ID for MCNP nuclide if necessary (typically used to specify excited state nuclides in ORIGEN):

`ORIGEN_ID`

and the corresponding ORIGEN ID will be followed. Note that the ORIGEN ID is defined as follows [15]:

$$\text{NUCLID} = 10000 * Z + 10 * A + \text{IS}, \tag{B.1}$$

where NUCLID = six-digit nuclide identifier,

Z = atomic number of nuclide,

A = atomic mass of nuclide,

IS = isomeric state indicator (0 = ground state, 1 = excited state).

By default MCNP IDs are transferred to ORIGEN IDs by multiplying them by 10 (ground state assumed).

One should note that: (1) all these tags are after the line comment sign ($) of MCNP; (2) the material specifications (both the material density in cell definitions and material composition definitions) in the active cell have to be in number density units, i.e., (number of atoms)/(barn·cm). Fig. B.2 gives an example of material composition definition:

```
c     9.75 wt% U-235  (10.3g/cc, 6.8967884e-2)
m1      8016.60c 4.59686e-2
        36083.50c 1.0e-24             $ begin_mcode_FP
        40091.96c 1.0e-24       40093.50c 1.0e-24       40096.62c 1.0e-24
        42095.50c 1.0e-24       42097.60c 1.0e-24       42098.50c 1.0e-24
        42100.50c 1.0e-24       43099.50c 1.0e-24       44101.50c 1.0e-24
        44102.60c 1.0e-24       45103.50c 1.0e-24       45105.50c 1.0e-24
        46104.96c 1.0e-24       46105.50c 1.0e-24       46107.96c 1.0e-24
        46108.50c 1.0e-24       47109.60c 1.0e-24       48113.60c 1.0e-24
        49115.60c 1.0e-24       53127.60c 1.0e-24       53129.60c 1.0e-24
        54131.50c 1.0e-24       54135.50c 1.0e-24       55133.60c 1.0e-24
        55134.60c 1.0e-24       55135.60c 1.0e-24       57139.60c 1.0e-24
        59141.50c 1.0e-24       60143.50c 1.0e-24       60144.96c 1.0e-24
        60145.50c 1.0e-24       60148.50c 1.0e-24       61147.50c 1.0e-24
        61148.50c 1.0e-24
        61148.60c 1.0e-24       $ ORIGEN_ID 611481
        62147.50c 1.0e-24       62148.96c 1.0e-24       62149.50c 1.0e-24
        62150.50c 1.0e-24       62151.50c 1.0e-24       62152.50c 1.0e-24
        63153.60c 1.0e-24       63154.50c 1.0e-24       63155.50c 1.0e-24
        64155.60c 1.0e-24       64156.60c 1.0e-24
        64157.60c 1.0e-24             $ end_mcode_FP
        92234.60c 1.82239e-5          $ begin_mcode_ACT
        92235.60c 2.26826e-3    92236.60c 1.0e-24       92238.60c  2.07128e-2
        93237.60c 1.0e-24       93239.60c 1.0e-24       94238.60c 1.0e-24
        94239.60c 1.0e-24       94240.60c 1.0e-24       94241.60c 1.0e-24
        94242.60c 1.0e-24       95241.60c 1.0e-24
        95242.51c 1.0e-24       $ ORIGEN_ID 952421
        95243.60c 1.0e-24       96244.60c 1.0e-24
        96245.60c 1.0e-24             $ end_mcode_ACT
```

Figure B.2 Material composition input example.

Other Constraints

There are other constraints on initial MCNP input from MCODE as well:

- In general MCNP allows an optional message block in the very beginning to change the file names and specify running options such as a continuation run. However it is not recognized by MCODE and should not be used. Since on most systems these options can be alternatively specified with an execution line command, the prohibition of message block doesn't actually limit the MCNP functionality.

- Currently only MCNP `kcode` problems (criticality calculation) are allowed in MCODE. External neutron source problems, such as accelerator-driven systems, can not be handled.

Recommendations on Choosing Number of Neutron Histories

In the MCNP `kcode` calculation, users usually need to determine how to allocate the number of neutrons per cycle and total number of cycles. The total number of neutron histories determines the accurateness of results, which depends on the available computational resources. But it is up to the user to specify number of neutrons per cycle and number of cycles.

On a single-CPU machine, one can typically specify ~2000 neutrons/cycle for a simple-geometry problem (such as a unit cell) and ~5000 neutrons/cycle for a complicated problem (such as a fuel assembly). The rule of thumb is to ensure that there are fission neutron sources in each individual fuel region. Then it is straightforward to decide the number of cycles.

On a cluster-type machine (parallel computing), one needs to select a certain number of nodes to do an MCNP calculation. Once that is determined, say 10 nodes, the user then needs to adjust the pattern of allocation of the number of neutrons per cycle and the total number of cycles. Generally speaking it is more computationally efficient to increase number of neutrons per cycle than increasing the number of cycles. Thus, it is worthwhile to increase the number of neutrons by ~50% while reducing the number of cycles by ~50% compared to cases running on a single-CPU machine.

B.2.3 MCODE Input

MCODE input is our focus in this manual, which is grouped into data cards identified by an alphabetical string of three characters. One card is allowed at most on one line except as otherwise specified. Each line may contain up to 1024 characters. Input items in a card are separated by space or tab characters (tab not recommended). Comments can start from any place starting with the special character `$`. There are currently 12 input cards for MCODE as shown in Table B.1 and all of them are required to be input explicitly. It is strongly recommended that users should not change the order of different cards, but copy

the example input and modify it according to their own needs. MCODE uses metric units as shown in Table B.2.

Table B.1 List of MCODE cards.

Card identifier	Description	Section
TTL	Case title	B.2.3.1
MCD	MCNP definition	B.2.3.2
ORG	ORIGEN definition	B.2.3.3
CEL	MCNP depletion cells	B.2.3.4
VOL	Volume of the system	B.2.3.5
PDE	Power density	B.2.3.6
NOR	Normalization option	B.2.3.7
COR	Burnup predictor-corrector option	B.2.3.8
DEP	Depletion points	B.2.3.9
NMD	Number of micro-depletion time steps	B.2.3.10
STA	Start directive	B.2.3.11
END	End directive	B.2.3.12

Table B.2 Metric units used in MCODE.

Mass	gram
Volume	cm^3
Power density	W/gU or kW/(liter-core)
Burnup	MWd/kgIHM (= GWd/MTIHM)
Time	day

B.2.3.1 TTL — Case Title

A. Function: Supplies the case title printed in MCODE output

B. Data sequences:

TTL title-string

where

TTL = command keyword

title-string = a string describing the case title

C. Remarks: None

D. Example:

```
TTL Test case
```

B.2.3.2 MCD — MCNP Definition

A. Function: Specifies MCNP running command/script, initial MCNP input, and optional MCNP source file

B. Data sequences:

MCD NMCD1 NMCD2 NMCD3 NMCD4

where

MCD = command keyword

NMCD1 = MCNP source file options

0 = none

1 = specify MCNP source file with filename in NMCD4

NMCD2 = MCNP running command/script name

NMCD3 = initial MCNP input file name

NMCD4 = MCNP source file name (optional depending on NMCD1)

C. Remarks:

MCODE works with MCNP version 4b or higher, but probably also works with earlier versions. The parameter NMCD2 is the MCNP running command/script containing additional information, e.g., `mcnp.exe`. This string is used in MCODE to issue a command such as "NMCD2 `inp=00.inp outp=00.out mct=00.mct`". Therefore it should at least be able to accept three arguments upon running. On a cluster-type machine with parallel virtual machine (PVM) running, users have the freedom of selecting the number of nodes (for example, 10) to run the MCNP problem, which is accommodated by using a script, say `mcnp.exe`, which contains only one line:

```
mcnp $1 $2 $3 tasks -10x1
```

Note that users can even increase the number of nodes by modifying this script during MCODE running as long as there are available CPUs.

The initial MCNP input file name, NMCD3, is not limited by 8 characters because MCODE will append tally descriptions to that and generate new MCNP input files.

The equilibrium source distribution file, NMCD4, is actually generated by MCNP from previous runs and it is not a text input file.

D. Example:

```
MCD  0  mcnp.exe  mcnp.inp
MCD  1  mcnp.exe  mcnp.inp  MyMcnpSrc
```

B.2.3.3 ORG — ORIGEN Definition

A. Function: Specifies ORIGEN running commands and associated ORIGEN libraries

B. Data sequence:

ORG NORG1 NORG2 NORG3 NORG4

where

ORG = command keyword

NORG1 = ORIGEN running command string (containing path)

NORG2 = directory path of ORIGEN libraries

NORG3 = decay library name

NORG4 = gamma library name

C. Remarks:

MCODE works with ORIGEN version 2.1 or 2.2. There is only one decay library in ORIGEN2.1, DECAY.LIB (NORG3). The parameter, NORG4, specifies the gamma library which supplies the number of photons per decay in an 18-energy group structure. Three available gamma libraries include:

- GXH2OBRM.LIB gamma library includes bremsstrahlung from the H_2O
- GXUO2BRM.LIB gamma library includes bremsstrahlung from the UO_2
- GXNOBREM.LIB gamma library without considering bremsstrahlung

For typical neutronic burnup calculations, the gamma library is not important since the photonuclear effect is negligible. The user is free to choose whatever gamma library he wants.

D. Example:

```
ORG  C:\ORIGEN2\ORIGEN2.EXE  C:\ORIGEN2\LIBS  DECAY.LIB  GXUO2BRM.LIB
```

B.2.3.4 CEL — MCNP Depletion Cells

A. Function: Specifies active cells for updating material compositions and their associated ORIGEN one-group cross section libraries

B. Data sequences:

```
CEL N     ID(1)  TYPE(1)  IHM(1)  VOL(1)  XSLIB(1)
          ID(2)  TYPE(2)  IHM(2)  VOL(2)  XSLIB(2)
          ……     ……      ……      ……      ……
          ID(N)  TYPE(N)  IHM(N)  VOL(N)  XSLIB(N)
```

where

CEL = command keyword

N = total number MCNP depletion cells ($N \leq 99$)

ID(i) = MCNP ID for the i^{th} cell

TYPE(i) = cell type for the i^{th} cell, currently is 1

IHM(i) = the initial heavy metal mass for the i^{th} cell (grams)

VOL(i) = the cell volume for the i^{th} cell (cm^3)

XSLIB(i) = the ORIGEN cross section library for the i^{th} cell

C. Remarks:

This card defines the MCNP cells to be depleted. In the current MCODE implementation, the maximum number of depletion cells is 99 due to the restrictions by the number of MCNP tallies. One should also be aware of the format of this data card. If multiple depletion cells exist, several lines of input will be needed.

All cell types are set to 1 right now (future use). Users need to calculate the initial heavy metal mass themselves. And usually the cell volume can be found in the MCNP output.

The ORIGEN one-group cross section library is a key issue which is being updated regularly with MCNP. One needs to be sure of using appropriate cross section libraries. Table B.3 gives the list of available ORIGEN cross section libraries.

D. Example:

```
CEL  1        10     1   19.14365  2.1083    PWRUE.LIB
```

Table B.3 List of ORIGEN one-group cross section libraries.

Name	NLIB(5)	NLIB(6)	NLIB(7)	NLIB(12)	Description
PWRU.LIB	204	205	206	1	^{235}U enriched UO_2, with a burnup of 33 MWd/kg
PWRPUU.LIB	207	208	209	2	^{235}U enriched UO_2 in a self-generated Pu recycle reactor
PWRPUPU.LIB	210	211	212	3	Pu-enriched UO_2 in a self-generated Pu recycle reactor
PWRDU3TH.LIB	213	214	215	7	ThO_2-enriched with denatured ^{233}U
PWRPUTH.LIB	216	217	218	8	Pu-enriched UO_2
PWRU50.LIB	219	220	221	9	^{235}U enriched UO_2, with a burnup of 50 MWd/kg
PWRD5D35.LIB	222	223	224	10	ThO_2-enriched with makeup, denatured ^{235}U
PWRD5D33.LIB	225	226	227	11	ThO_2-enriched with recycled, denatured ^{233}U
PWRUS.LIB	601	602	603	38	3.2 w/o ^{235}U fuel, 3-cycle PWR to achieve 33 MWd/kg
PWRUE.LIB	604	605	606	39	4.2 w/o ^{235}U fuel, 3-cycle PWR to achieve 50 MWd/kg
BWRU.LIB	251	252	253	4	^{235}U enriched UO_2
BWRPUU.LIB	254	255	256	5	^{235}U enriched UO_2 in a self-generated Pu recycle reactor
BWRPUPU.LIB	257	258	259	6	Pu-enriched fuel in a self-generated Pu recycle reactor
BWRUS.LIB	651	652	653	40	3.0 w/o ^{235}U fuel, 4-cycle BWR to achieve 27.5 MWd/kg axial varying moderator density considered
BWRUS0.LIB	654	655	656	41	3.0 w/o ^{235}U fuel, 4-cycle BWR to achieve 27.5 MWd/kg, constant axial moderator density
BWRUE.LIB	657	658	659	42	3.4 w/o ^{235}U fuel, 4-cycle BWR to achieve 40 MWd/kg
CANDUNAU.LIB	401	402	403	21	CANDU, natural uranium
CANDUSEU.LIB	404	405	406	22	CANDU, slightly enriched uranium
					LMFBR: Early oxide, LWR-Pu/U/U/U:
EMOPUUUC.LIB	301	302	303	18	Core
EMOPUUUA.LIB	304	305	306	19	Axial blanket
EMOPUUUR.LIB	307	308	309	20	Radial blanket
					LMFBR: Advanced oxide, LWR-Pu/U/U/U
AMOPUUUC.LIB	311	312	313	12	Core
AMOPUUUA.LIB	314	315	316	13	Axial blanket
AMOPUUUR.LIB	317	318	319	14	Radial blanket
					LMFBR: Advanced oxide, recycle-Pu/U/U/U
AMORUUUC.LIB	321	322	323	15	Core
AMORUUUA.LIB	324	325	326	16	Axial blanket
AMORUUUR.LIB	327	328	329	17	Radial blanket
					LMFBR: Advanced oxide, LWR-Pu/U/U/Th
AMOPUUTC.LIB	331	332	333	32	Core
AMOPUUTA.LIB	334	335	336	33	Axial blanket
AMOPUUTR.LIB	337	338	339	34	Radial blanket
					LMFBR: Advanced oxide, LWR-Pu/Th/Th/Th
AMOPTTTC.LIB	341	342	343	29	Core
AMOPTTTA.LIB	344	345	346	30	Axial blanket
AMOPTTTR.LIB	347	348	349	31	Radial blanket
					LMFBR: Advanced oxide, recycle ^{233}U/Th/Th/Th
AMO0TTTC.LIB	351	352	353	35	Core
AMO0TTTA.LIB	354	355	356	36	Axial blanket
AMO0TTTR.LIB	357	358	359	37	Radial blanket
					LMFBR: Advanced oxide, 14% denatured ^{233}U/Th/Th/Th
AMO1TTTC.LIB	361	362	363	23	Core
AMO1TTTA.LIB	364	365	366	24	Axial blanket
AMO1TTTR.LIB	367	368	369	25	Radial blanket
					LMFBR: Advanced oxide, 44% denatured ^{233}U/Th/Th/Th
AMO2TTTC.LIB	371	372	373	26	Core
AMO2TTTA.LIB	374	375	376	27	Axial blanket
AMO2TTTR.LIB	377	378	379	28	Radial blanket
FFTFC.LIB	381	382	383	0	LMFBR: Fast Flux Test Facility (FFTF) Pu/U
					Clinch River Breeder Reactor (CRBR):
CRBRC.LIB	501	502	503	0	Core
CRBRA.LIB	504	505	506	0	Axial blanket
CRBRR.LIB	507	508	509	0	Radial blanket
CRBRI.LIB	510	511	512	0	Internal blanket
THERMAL.LIB	201	202	203	0	0.0253-eV cross section library

B.2.3.5 VOL — Volume of the System

A. Function: Specifies overall volume of the entire system

B. Data sequences:

VOL Volume

where

VOL = command keyword

Volume = volume of the entire system (cm^3)

C. Remarks:

The volume here is the entire system volume, including fuel, gap, water, cladding, and structural material volumes. It is then divided by the total power to give the core average power density (kW/liter-core).

D. Example:

```
VOL  6.3504
```

B.2.3.6 PDE — Power Density

A. Function: Supplies the power density of the system

B. Data sequences:

PDE PowDen OPT

where

PDE = command keyword

PowDen = power density of the system, units given in OPT

OPT = input power density option

WGU means W/gU

KWL means kW/liter-core

C. Remarks:

In MCODE, instead of directly specifying the system power, a power density is required. Depending on the input option (WGU or KWL), the code then calculates the overall system power.

For the WGU option, the total power is the product of the PowDen and the total initial heavy metal mass (obtained from CEL card). For KWL option, the total power is calculated by multiplying the PowDen with the entire system volume (obtained from VOL card).

D. Example:

```
PDE  38.13470   WGU
```

B.2.3.7 NOR — Normalization Option

A. Function: Specifies the way of normalization in ORIGEN depletion calculations

B. Data sequences:

NOR OPT

where

NOR = command keyword

OPT = normalization option

1 = flux normalization

2 = power normalization

C. Remarks:

Power normalization is recommended because precise burnup can be achieved with this option. However, for some unusual cases, such as minor-actinide-only fuel, flux normalization is typically more stable. Users are encouraged to try both options to validate results.

D. Example:

```
NOR  2
```

B.2.3.8 COR — Burnup Predictor-Corrector Option

A. Function: Specifies whether to employ the burnup corrector

B. Data sequences:

COR OPT

where

COR = command keyword

OPT = burnup predictor-corrector option

1 = on

0 = off

C. Remarks:

It is strongly recommended that users should turn on this option. And the burnup predictor-corrector option is automatically omitted if the depletion step is ≤ 0.001 MWd/kg (too small).

D. Example:

```
COR  1
```

B.2.3.9 DEP — Depletion Points

A. Function: Defines the set of depletion points (and associated time step sizes)

B. Data sequences:

DEP OPT B(1) B(2) … B(N)

where

DEP = command keyword

OPT = units for burnup

E = exposure in MWd/kg

D = effective full power days

B(i) = the i^{th} burnup point

C. Remarks:

B(1) is always 0 because it is the start of irradiation. The maximum number of burnup points is 100. And one should use smaller time step sizes in the beginning of irradiation.

D. Example:

```
DEP  E  0 0.1 5 10 15 20 30 40 50
```

B.2.3.10 NMD — Number of Micro-Depletion Timesteps

A. Function: Specifies number of ORIGEN depletion (micro-depletion) time steps between two burnup points

B. Data sequences:

NMD M(1) M(2) …… B(N−1)

where

NMD = command keyword

M(i) = number of micro-depletion timesteps (≤ 50) between the $(i-1)^{th}$ and the i^{th} burnup points

C. Remarks:

The maximum number of ORIGEN depletion time steps is less than 50. And the number of NMD numbers should be one less than the number burnup points as in the DEP card. Results are not sensitive to the input of NMD numbers as long as a reasonable number of micro-depletion timesteps is given (~20).

D. Example:

```
NMD  10  20  20  20  20
```

B.2.3.11 STA — Start Directive

A. Function: Defines the index for the start point

B. Data sequences:

STA Point

where

STA = command keyword

Point = start point index (beginning from 0)

C. Remarks:

The burnup points are referenced according to their indices stored in the array. The first point is 0, the second is 1, and so on. If there are altogether *n* burnup points, the last point index will be *n*−1.

D. Example:

```
STA  0
```

B.2.3.12 END — End Directive

A. Function: Defines the index for the end point

B. Data sequences:

END Point

where

END = command keyword

Point = end point index

C. Remarks:

Note that the end point index should be always larger than the start point index. Also the end directive should not exceed the range of burnup points. MCODE does error checking on these parameters. The combined `start/end` directives can be used to do restart calculations, which makes MCODE very versatile and flexible.

D. Example:

```
END   9
```

B.3 Running Commands and Description of Output Files

Suppose the input files `mcode.inp`, `mcnp.inp` are correct and ready, then one can use the following commands to run MCODE:

```
mcode mcode.inp
```

Upon completion of the run, three subdirectories (`mcodeDIR`, `mcnpDIR`, `orgDIR`) and one log file (in this case, `mcode.log`) are generated.

Within the subdirectory `mcnpDIR`, numbers of MCNP running files at different burnup points exist. The file name gives the burnup point index. If the predictor-corrector option is turned on, additional MCNP prediction runs also exist with a prefix `p`.

Within the subdirectory `orgDIR`, similar ORIGEN run files are archived. But they represent the time step index, which is between two successive burnup points. Each active cell has its own ORIGEN files. For example, `03C10.PCH` means the punched material data at burnup point 3 for cell 10. With predictor-corrector on, additional burnup corrector files exist. For example, `c05C10.INP` means the ORIGEN input file for time step 5, cell 10 during burnup corrector calculation.

Within the subdirectory `mcodeDIR`, two types of data files exist. For example, `04.pow` contains the power fractions in various cells at burnup point 4. The files ending with `xs` are one-group cross section files.

Upon successful running of MCODE, a log file is generated (in this case, `mcode.log`) at the end of which there is a succinct summary of burnup results. For detailed output, one can run a supplementary data processing program, `mcodeout`. It also takes the MCODE input as the sole input:

```
mcodeout mcode.inp
```

An output file is then generated in seconds (in this case, `mcode.out`). Eight tables are included in the output file:

- TABLE 1. REACTIVITY vs TIME/BURNUP
- TABLE 2. REGION AVERAGED FLUX & CONVERSION RATIO TABLE
- TABLE 3. BURNUP/POWER MAP
- TABLE 4. ACTINIDE NUMBER DENSITY & ONE-GROUP CROSS SECTION TABLE

- TABLE 5. FISSION PRODUCT NUMBER DENSITY & ONE-GROUP CROSS SECTION TABLE
- TABLE 6. COMPOSITION TABLE (GRAMS)
- TABLE 7. NEUTRON ABSORPTION RATE TABLE (neutrons/sec)
- TABLE 8. NEUTRON IMPORTANCE ORDERING AT EOL

Appendix C. Input Files for the High Burnup Benchmark Problem

CASMO-4 Input (c4.U975Cold.inp)

```
TTL * 9.75 w/o UO2, unit cell, cold case
TFU=300 TMO=300
FUE 1 10.3/9.75
CAN ,,,,/304=100    * zircaloy-4
PIN 1  0.4096 0.4178 0.4750/'1' 'AIR' 'CAN'
PWR 2 1.26
PDE 104.5 'KWL'
FUM ,,3  * turn off fundamental mode
THE 0    * turn off thermal expansion
PRI 9*0 2
DEP -100
STA
END
```

MCODE Inputs: Central MCODE Input File (UO2.inp)

```
$ TITLE line
TTL 9.75 w/o U-235, UO2 fuel, cold condition, single region
$   CTRL command initial-inp
MCD  0    mcnp    mcnp.inp
$        ORIGEN-COMMAND            ORIGEN-LIBRARY-PATH    decay-lib   gamma-lib
ORG   C:\ORIGEN2\CODE\ORIGEN2.EXE   C:\ORIGEN2\LIBS     DECAY.LIB  GXUO2BRM.LIB
$  total#  CELL-ID TYPE   IHM(g)  VOL(cm3)  ORG-XS-LIB
CEL  1        10     1   19.14365  2.1083    PWRUE.LIB
$ TOTAL VOLUME (cm3)
VOL 6.3504
$ power density, opt: WGU=W/gIHM, KWL=kW/(liter core)
PDE 104.5 KWL
$ NORMALIZATION option, 1=FLUX, 2=POWER
NOR 2
$ Predictor-Corrector option, 1=ON, 0=OFF
COR 1
$ opt E=MWd/kg, D=EFPD
DEP E    0 0.1 0.5  1  2  3  4  5  6  7  8  9  10 11 12.5 15 17.5 20 22.5 25  &
27.5 30 32.5 35 37.5 40 42.5 45 47.5 50 52.5 55 57.5 60 62.5 65 67.5 70 72.5 75  &
77.5 80 82.5 85 87.5 90 92.5 95 97.5 100
NMD       3  10  10 20 20 20 20 20 20 20 20 20 20  20  20  20  20  20  20  20  &
20  20  20  20  20  20  20  20  20  20  20  20  20  20  20  20  20  20  20  20  &
20  20  20  20  20  20  20  20  20
STA 0   $ starting point
END 49   $ ending point
```

MCODE Inputs: Initial MCNP Input File (`mcnp.inp`)

```
EXAMPLE 1: PWR PIN-CELL (UO2 with 9.75w/o U235)
c
c     ---------------------------------------------------------------------
c     Two-dimensional unit cell model with no leakage,
c     parameters from typical Westinghouse PWR 17x17 lattices,
c     power density at 104.5 kW/(litre core), cold condition,
c     4 cm in height, single region (fuel) depletion,
c     100 fission products, 39 actinides
c     ---------------------------------------------------------------------
c
 10    1  6.8967884e-2 (-100 10 -20)               $ fuel pellet, 300K
       imp:n=1 imp:p=1 vol=2.1083 tmp=2.5851e-8
 20    2 3.76622e-5 (100 -110 10 -20)              $ gap (air)
       imp:n=1 imp:p=1 vol=8.5259e-2 tmp=2.5851e-8
 30    3 4.34418e-2 (110 -120 10 -20)              $ cladding, 300K
       imp:n=1 imp:p=1 vol=6.4174e-1 tmp=2.5851e-8
 40    4 9.99634e-2 (30 -40 50 -60 120 10 -20)     $ H2O, 300K
       imp:n=1 imp:p=1 vol=3.5151 tmp=2.5851e-8
 9999  0 (-10:20:-30:40:-50:60)                    $ external void
       imp:n=0 imp:p=0 vol=0.0000 tmp=2.53e-8
c
c      BLANK LINE MUST FOLLOW

c
c          SURFACE DEFINITIONS
c
 *10   pz  -2.00             $ bottom of unit cell
 *20   pz   2.00             $ top    of unit cell
 *30   px  -0.63             $ low-x  edge of unit cell
 *40   px   0.63             $ high-x edge of unit cell
 *50   py  -0.63             $ low-y  edge of unit cell
 *60   py   0.63             $ high-y edge of unit cell
 100   cz   0.4096           $ Fuel pellet
 110   cz   0.4178           $ Inner surface of cladding
 120   cz   0.4750           $ Outer surface of cladding

c
c        MATERIALS
c
awtab   34079  78.240500  38089  88.143700  38090  89.135400
        44105 104.007000  46107 105.987000
        47111 109.953000  48115 113.919000  50123 121.850000
        50125 123.835000  50126 124.826000  51124 122.842000
        51125 123.832000  51126 124.826000  52127 125.815000
        52129 127.800000  53130 128.791000  53131 129.781998
        54133 131.764008  58141 139.697998
        58144 142.677000  59142 140.691000
        59143 141.682999  61151 149.625000
        62153 151.608002  63156 154.585007  63157 155.577000
        96249 246.936000  97250 247.930000
c
c     9.75 wt% U-235  (10.3g/cc, 6.8967884e-2)
m1      8016.60c 4.59686e-2
        35081.55c 1.0e-24                    $ begin_mcode_FP
        36082.50c 1.0e-24      36083.50c 1.0e-24      36084.50c 1.0e-24
        37085.55c 1.0e-24      37087.55c 1.0e-24      38090.96c 1.0e-24
        39089.60c 1.0e-24      40091.96c 1.0e-24      40092.62c 1.0e-24
        40093.50c 1.0e-24      40094.62c 1.0e-24      40096.62c 1.0e-24
        41095.96c 1.0e-24      42095.50c 1.0e-24      42096.96c 1.0e-24
        42097.60c 1.0e-24      42098.50c 1.0e-24      42100.50c 1.0e-24
        43099.50c 1.0e-24      44100.96c 1.0e-24      44101.50c 1.0e-24
        44102.60c 1.0e-24      44103.50c 1.0e-24      44104.96c 1.0e-24
        45103.50c 1.0e-24      45105.50c 1.0e-24      46104.96c 1.0e-24
        46105.50c 1.0e-24      46106.96c 1.0e-24      46107.96c 1.0e-24
        46108.50c 1.0e-24      46110.96c 1.0e-24      47109.60c 1.0e-24
        48110.62c 1.0e-24      48111.62c 1.0e-24      48112.62c 1.0e-24
        48113.60c 1.0e-24      48114.62c 1.0e-24      49115.60c 1.0e-24
        51121.96c 1.0e-24      51123.96c 1.0e-24      52128.96c 1.0e-24
        53127.60c 1.0e-24      53129.60c 1.0e-24      54131.50c 1.0e-24
        54132.62c 1.0e-24      54133.60c 1.0e-24      54134.62c 1.0e-24
        54135.50c 1.0e-24      54136.62c 1.0e-24      55133.60c 1.0e-24
```

```
        55134.60c 1.0e-24      55135.60c 1.0e-24      55137.60c 1.0e-24
        56134.62c 1.0e-24      56137.62c 1.0e-24      56138.60c 1.0e-24
        57139.60c 1.0e-24      58140.96c 1.0e-24      58141.60c 1.0e-24
        58142.96c 1.0e-24      58144.96c 1.0e-24      59141.50c 1.0e-24
        59143.60c 1.0e-24      60142.96c 1.0e-24      60143.50c 1.0e-24
        60144.96c 1.0e-24      60145.50c 1.0e-24      60146.96c 1.0e-24
        60147.50c 1.0e-24      60148.50c 1.0e-24      60150.96c 1.0e-24
        61147.50c 1.0e-24      61148.50c 1.0e-24
        61148.60c 1.0e-24      $ ORIGEN_ID 611481
        61149.50c 1.0e-24      62147.50c 1.0e-24      62148.96c 1.0e-24
        62149.50c 1.0e-24      62150.50c 1.0e-24      62151.50c 1.0e-24
        62152.50c 1.0e-24      62153.60c 1.0e-24      62154.96c 1.0e-24
        63151.60c 1.0e-24      63153.60c 1.0e-24      63154.50c 1.0e-24
        63155.50c 1.0e-24      63156.60c 1.0e-24      64154.60c 1.0e-24
        64155.60c 1.0e-24      64156.60c 1.0e-24      64157.60c 1.0e-24
        64158.60c 1.0e-24      65159.96c 1.0e-24      66160.96c 1.0e-24
        66161.96c 1.0e-24      66162.96c 1.0e-24
        66163.96c 1.0e-24                     $ end_mcode_FP
        90232.60c 1.0e-24                     $ begin_mcode_ACT
        91231.60c 1.0e-24      91233.50c 1.0e-24      92232.60c 1.0e-24
        92233.60c 1.0e-24      92234.60c 1.82239e-5   92235.60c  2.26826e-3
        92236.60c 1.0e-24      92237.50c 1.0e-24      92238.60c  2.07128e-2
        93236.35c 1.0e-24      93237.60c 1.0e-24      93238.35c 1.0e-24
        93239.60c 1.0e-24      94238.60c 1.0e-24      94239.60c 1.0e-24
        94240.60c 1.0e-24      94241.60c 1.0e-24      94242.60c 1.0e-24
        94243.60c 1.0e-24      95241.60c 1.0e-24      95242.50c 1.0e-24
        95242.51c 1.0e-24      $ ORIGEN_ID 952421
        95243.60c 1.0e-24      95244.96c 1.0e-24      96242.60c 1.0e-24
        96243.60c 1.0e-24      96244.60c 1.0e-24      96245.60c 1.0e-24
        96246.60c 1.0e-24      96247.60c 1.0e-24      96248.60c 1.0e-24
        96249.96c 1.0e-24      97249.60c 1.0e-24      97250.96c 1.0e-24
        98249.60c 1.0e-24      98250.60c 1.0e-24      98251.60c 1.0e-24
        98252.60c 1.0e-24                     $ end_mcode_ACT
c
c     AIR (gap)
m2     8016.60c  3.76622e-5
c
c     Zircaloy-4  (6.550g/cc)
m3       8016.60c -0.00125    $ O
        24000.50c -0.0010     $ Cr
        26000.55c -0.0021     $ Fe
        40000.60c -0.98115    $ Zr
        50000.35c -0.00145    $ Sn
c
c     H2O (15.5MPa at 300K)  (0.997g/cc)
m4      8016.60c 3.33339e-2
        1001.60c 6.66295e-2
mt4     lwtr.01t
c
c
ksrc   0.000     0.000     -1.0
       0.000     0.000      0.0
       0.000     0.000      1.0
c
c
mode    n
kcode   1500    1.0   5   150
prdmp   150 150 150
print  -60 -85 -130 -140
```

Appendix D. Input Files for Axial Enrichment Zoning Calculation

MCODE Inputs: Central MCODE Input File (axial.inp)

```
$ TITLE line
TTL axial UO2, 6cm UO2(U8) + 6cm 19.5w/o UO2, hot
$   CTRL command initial-inp
MCD  0    mcnp    mcnp.inp
$           ORIGEN-COMMAND            ORIGEN-LIBRARY-PATH    decay-lib   gamma-
lib
ORG   C:\Codes\ORIGEN2\CODE\ORIGEN2.exe   C:\Codes\ORIGEN2\LIBS       DECAY.LIB
GXUO2BRM.LIB
$  total#  CELL-ID TYPE   IHM(g)   VOL(cm3)  ORG-XS-LIB
CEL  2        10     1   14.49684  1.581215   PWRUE.LIB
              15     1   14.49256  1.581215   PWRUE.LIB
$ TOTAL VOLUME (cm3)
VOL 9.5256
$ power density, opt: WGU=W/gIHM, KWL=kW/(liter core)
PDE 104.5 KWL
$ NORMALIZATION option, 1=FLUX, 2=POWER
NOR 2
$ Predictor-Corrector option, 1=ON, 0=OFF
COR 1
$ opt E=MWd/kg, D=EFPD
$points 0   1   2  3  4   5   6   7   8   9  10  11  12  13  14  15  16  17  18
19  20  21
DEP E   0  0.1  1  3  5  10  15  20  25  30  35  40  50  60  70  80  90 100 110
120 130 140
NMD       3   10 20 20 20  20  20  20  20  20  20  30  30  30  30  30  30  30
30  30  30
STA 0   $ starting point
END 21  $ ending point
```

MCODE Inputs: Initial MCNP Input File (mcnp.inp)

```
PWR UNIT CELL, 3cm 19.5 w/oUO2 + 3cm 0w/t UO2, HOT CONDITION
 10    1 6.95787e-2 (-100 25 -20)                $ NatU, 900K
       imp:n=1 vol=1.581215 tmp=7.7553e-8
 15    10 6.97316e-2 (-100 10 -25)               $ 19.5UO2, 900K
       imp:n=1 vol=1.581215 tmp=7.7553e-8
 20    2 3.76622e-5 (100 -110 10 -20)            $ gap (air), 583.1K
       imp:n=1 vol=8.5259e-2 tmp=5.0246e-8
 30    3 -6.550 (110 -120 10 -20)                $ cladding, 621.1K
       imp:n=1 vol=6.4174e-1 tmp=5.3520e-8
 40    4 7.06685e-2 (30 -40 50 -60 120 10 -20)   $ H2O, 583.1K
       imp:n=1 vol=3.5151 tmp=5.0246e-8
 9999  0 (-10:20:-30:40:-50:60)                  $ external void
       imp:n=0 vol=0.0000 tmp=2.53e-8
c
c      BLANK LINE MUST FOLLOW

c
c          SURFACE DEFINITIONS
c
 *10   pz  -3.00             $ bottom of unit cell
 *20   pz   3.00             $ top    of unit cell
  25   pz   0.00
 *30   px  -0.63             $ low-x  edge of unit cell
 *40   px   0.63             $ high-x edge of unit cell
 *50   py  -0.63             $ low-y  edge of unit cell
 *60   py   0.63             $ high-y edge of unit cell
 100   cz   0.4096           $ Fuel pellet
 110   cz   0.4178           $ Inner surface of cladding
 120   cz   0.4750           $ Outer surface of cladding

c
c        MATERIALS
c
awtab   34079  78.240500  38089  88.143700  38090  89.135400
        44105 104.007000  46107 105.987000  47111 109.953000
        48115 113.919000  50123 121.850000  50125 123.835000
        50126 124.826000  51124 122.842000  51125 123.832000
        51126 124.826000  52127 125.815000  52129 127.800000
        53130 128.791000  53131 129.781998  54133 131.764008
        58141 139.697998  58144 142.677000  59142 140.691000
        59143 141.682999  61151 149.625000  62153 151.608002
        63156 154.585007  63157 155.577000  96249 246.936000
        97250 247.930000
c
c     U238 in UO2  (10.4g/cc)
m1        8016.60c  4.63858e-2
        36083.50c 1.0e-24             $ begin_mcode_FP
        40091.96c 1.0e-24      40093.50c 1.0e-24      40096.62c 1.0e-24
        42095.50c 1.0e-24      42096.96c 1.0e-24      42097.60c 1.0e-24
        42098.50c 1.0e-24      42100.50c 1.0e-24      43099.50c 1.0e-24
        44100.96c 1.0e-24      44101.50c 1.0e-24      44102.60c 1.0e-24
        45103.50c 1.0e-24      44104.96c 1.0e-24      45105.50c 1.0e-24
        46104.96c 1.0e-24      46105.50c 1.0e-24      46106.96c 1.0e-24
        46107.96c 1.0e-24      46108.50c 1.0e-24      47109.60c 1.0e-24
        48111.62c 1.0e-24      48110.62c 1.0e-24      48113.60c 1.0e-24
        49115.60c 1.0e-24      53127.60c 1.0e-24      53129.60c 1.0e-24
        54131.50c 1.0e-24      54132.62c 1.0e-24      54135.50c 1.0e-24
        55133.60c 1.0e-24      55134.60c 1.0e-24      55135.60c 1.0e-24
        56134.62c 1.0e-24      57139.60c 1.0e-24      59141.50c 1.0e-24
        60142.96c 1.0e-24      60143.50c 1.0e-24      60144.96c 1.0e-24
        60145.50c 1.0e-24      60146.96c 1.0e-24      60148.50c 1.0e-24
        61147.50c 1.0e-24      61148.50c 1.0e-24
        61148.60c 1.0e-24      $ ORIGEN_ID 611481
        62147.50c 1.0e-24      62148.96c 1.0e-24      62149.50c 1.0e-24
        62150.50c 1.0e-24      62151.50c 1.0e-24      62152.50c 1.0e-24
        63153.60c 1.0e-24      63154.50c 1.0e-24      63155.50c 1.0e-24
        63156.60c 1.0e-24      64154.50c 1.0e-24      64155.60c 1.0e-24
        64156.60c 1.0e-24
        64157.60c 1.0e-24             $ end_mcode_FP
        92234.86c 1.0e-24          $ begin_mcode_ACT
        92235.54c 1.0e-24      92236.86c 1.0e-24      92238.54c 2.31929e-2
```

```
        93237.82c 1.0e-24       93238.35c 1.0e-24       93239.60c 1.0e-24
        94238.86c 1.0e-24       94239.86c 1.0e-24       94240.86c 1.0e-24
        94241.86c 1.0e-24       94242.86c 1.0e-24       95241.82c 1.0e-24
        95242.82c 1.0e-24       $ ORIGEN_ID 952421
        95243.98c 1.0e-24       96244.98c 1.0e-24
        96245.98c 1.0e-24               $ end_mcode_ACT
c
c     19.5 w/o UO2  (10.4g/cc)
m10       8016.60c  4.64878e-2
        36083.50c 1.0e-24               $ begin_mcode_FP
        40091.96c 1.0e-24       40093.50c 1.0e-24       40096.62c 1.0e-24
        42095.50c 1.0e-24       42096.96c 1.0e-24       42097.60c 1.0e-24
        42098.50c 1.0e-24       42100.50c 1.0e-24       43099.50c 1.0e-24
        44100.96c 1.0e-24       44101.50c 1.0e-24       44102.60c 1.0e-24
        45103.50c 1.0e-24       44104.96c 1.0e-24       45105.50c 1.0e-24
        46104.96c 1.0e-24       46105.50c 1.0e-24       46106.96c 1.0e-24
        46107.96c 1.0e-24       46108.50c 1.0e-24       47109.60c 1.0e-24
        48111.62c 1.0e-24       48110.62c 1.0e-24       48113.60c 1.0e-24
        49115.60c 1.0e-24       53127.60c 1.0e-24       53129.60c 1.0e-24
        54131.50c 1.0e-24       54132.62c 1.0e-24       54135.50c 1.0e-24
        55133.60c 1.0e-24       55134.60c 1.0e-24       55135.60c 1.0e-24
        56134.62c 1.0e-24       57139.60c 1.0e-24       59141.50c 1.0e-24
        60142.96c 1.0e-24       60143.50c 1.0e-24       60144.96c 1.0e-24
        60145.50c 1.0e-24       60146.96c 1.0e-24       60148.50c 1.0e-24
        61147.50c 1.0e-24       61148.50c 1.0e-24
        61148.60c 1.0e-24       $ ORIGEN_ID 611481
        62147.50c 1.0e-24       62148.96c 1.0e-24       62149.50c 1.0e-24
        62150.50c 1.0e-24       62151.50c 1.0e-24       62152.50c 1.0e-24
        63153.60c 1.0e-24       63154.50c 1.0e-24       63155.50c 1.0e-24
        63156.60c 1.0e-24       64154.50c 1.0e-24       64155.60c 1.0e-24
        64156.60c 1.0e-24
        64157.60c 1.0e-24               $ end_mcode_FP
        92234.86c 1.0e-24           $ begin_mcode_ACT
        92235.54c 4.57912e-3    92236.86c 1.0e-24       92238.54c 1.86648e-2
        93237.82c 1.0e-24       93238.35c 1.0e-24       93239.60c 1.0e-24
        94238.86c 1.0e-24       94239.86c 1.0e-24       94240.86c 1.0e-24
        94241.86c 1.0e-24       94242.86c 1.0e-24       95241.82c 1.0e-24
        95242.82c 1.0e-24       $ ORIGEN_ID 952421
        95243.98c 1.0e-24       96244.98c 1.0e-24
        96245.98c 1.0e-24               $ end_mcode_ACT
c
c     AIR (gap)
m2     8016.60c  3.76622e-5
c
c     Zircaloy-4  (6.550g/cc)
m3       8016.60c -0.00125
         24000.50c -0.00100
         26000.55c -0.00210
         40000.60c -0.98115
         50000.35c -0.01450
c
c     H2O (15.5MPa at 583.1K)  (0.705g/cc)
m4       8016.60c 1
         1001.60c 2
mt4      lwtr.04t
c
c
ksrc   0.000     0.000     -1.0
       0.000     0.000      0.0
       0.000     0.000      1.0
mode    n
kcode   1500    1.0   5   150
prdmp   150 150 150
print  -60 -85 -130 -140
```

Appendix E. VIPRE Input Files

Reference PWR lattice input (REF.INP)

```
*********************************************************
*                                                       *
*          solid PWR fuel rod---one isolated channel    *
*                                                       *
*********************************************************
1,0,0                                                    *vipre.1
solid feul rod-----one isolated channel                  *vipre.2
geom,1,1,48,0,0,0      *normal geometry input            *geom.1
144.0,0.0,0.5                                            *geom.2
1, 0.136210887, 1.175005126, 1.175005126, 0,0,0.0,0.0    *geom.4
prop,0,0,2,1   *internal EPRI functions                  *prop.1
rods,1,1,1,1,0,0,0,0,0,0,0                               *rods.1
0.0,0.0,0,0                                              *rods.2
-1       * chopped cosine power shape                    *rods.3
1.55     * peak-to-average ratio                         *rods.5
1,1,1.0,1,1,1.0                                          *rods.9
0
1,nucl, 0.374015748, 0.322519685, 6,0.0,0.022519685      *rods.62
0,0,0,0,0,1056.66,0.94,0.0                               *rods.63
oper,1,1,0,1,0,1,0,0,0                                   *oper.1
-1.0,1.3,0.0,0.005,                                      *oper.2
0                                                        *oper.3
2250,558.86, 0.722375639, 110.4588, 0.0                  *oper.5
0                  *no forcing functions                 *oper.12
corr,1,1,                                                *corr.1
epri,epri,epri,none                                      *corr.2
0.2                                                      *corr.3
ditb,thsp,thsp,w-3l,cond,g5.7                            *corr.6
w-3l               *dnb analysis by w-3l                 *corr.9
0.042,0.066,1.00  *w-3l input data                       *corr.11
cont                                                     *cont.1
0.0,0,750,50,3,0,   *iterative solution                  *cont.2
0.0,0.0,0.001,0.0,0.0,0.9,1.5,1.0                        *cont.3
5,0,0,0,0,0,1,1,0,0,0,1,0,0                              *cont.6
1000.,0.0,0.0,0.0,0.0,0.0                                *cont.7
endd
*
*end of data input
0
```

IXAF VIPRE Input (ANN.INP)

```
*************************************************************
*                                                           *
*                  annular fuel---one isolated channel      *
*                                                           *
*************************************************************
1,0,0                                                        *vipre.1
annular fule-----one isolated channel                        *vipre.2
geom,2,2,24,0,0,0      *normal geometry input                *geom.1
144.0945,0.0,0.5                                               *geom.2
1,0.0907289,1.0677695,1.0677695,0,0,0.0,0.0                  *geom.4
2,0.1350249,1.9006620,1.9006620,0,0,0.0,0.0                  *geom.4
prop,0,0,2,1   *internal EPRI functions                      *prop.1
rods,1,2,1,1,4,0,0,0,0,0,0                                   *rods.1
0.0,0.0,0,0                                                  *rods.2
-1                                                           *rods.3
1.55                                                         *rods.5
1,1,1.0,1,2,1.0                                              *rods.9
-1,1,1.0,1,1,1.0                                             *rods.9
0
1,tube,0.605,0.339882,5                                      *rods.68
2,1,0.0224921,0.0,?   *inner cladding                        *rods.69
2,2,0.0024488,0.0,?   *inner gap                              *rods.69
8,3,0.0826772,1.0,?    *fuel ring                             *rods.69
2,4,0.0024409,0.0      *outer gap                            *rods.69
2,1,0.0225000,0.0       *outer cladding                        *rods.69
1,17,409.0,clad                                                *rods.70
0.0,0.0671,7.3304509,?
25,0.0671,7.3304509
50,0.0671,7.33045093,?
65,0.0671,7.33045093
80.33,0.0671,7.33045093,?
260.33,0.07212,8.11585329
692.33,0.07904,9.80167423,?
1502.33,0.08955,13.2923001
1507.73,0.11988,13.3211893,?
1543.73,0.14089,13.5166505
1579.73,0.14686,13.717249,?
1615.73,0.1717,13.9231981
1651.73,0.1949,14.1347101,?
1687.73,0.18388,14.3519980
1723.73,0.1478,14.5752746,?
1759.73,0.112,14.804753
1786.73,0.085,14.9810589
*2240.33,0.085,18.5665964
2,1,0.025,igap                                                 *rods.70
1,1.240834,0.2156263    *Cp=5195J/kg-K *gap=6000               *rods.71
3,23,650.617,FUO2                                            *rods.70
86,0.05677357,4.73275874,?
176,0.06078589,4.29917259
266,0.06366347,3.93877428,?
356,0.06581210,3.63454049
446,0.06747631,3.37435643,?
536,0.06880819,3.1493668
626,0.06990545,2.95294976,?
716,0.07083283,2.78005572
806,0.07163441,2.62676801,?
896,0.07234099,2.49000319
986,0.07297458,2.36730189,?
1076,0.07355124,2.25667975
1166,0.07408294,2.1565193,?
1256,0.07457886,2.06549023
1346,0.07504628,1.98248979,?
1436,0.07549123,1.90659753
1526,0.0759191,1.83704065,?
1616,0.07633503,1.77316713
1706,0.0767443,1.7144247,?
1796,0.07715268,1.66034425
1886,0.07756663,1.61052668,?
1976,0.07799351,1.5646323                                     *rods.71
2500,0.07799351,1.5646323
4,1,0.025,ogap                                               *rods.70
1,1.240834,0.2149314    *Cp=5195J/kg-K *gap=6000               *rods.71
```

```
oper,1,1,0,1,0,1,0,0,0                                          *oper.1
-1.0,1.3,0.0,0.005,                                             *oper.2
0                                                               *oper.3
2248.12,562.46,1.79,195.5,0.0                                    *oper.5
0                 *no forcing functions                             *oper.12
corr,2,2,0                                                         *corr.1
epri,epri,epri,none                                              *corr.2
0.2                                                              *corr.3
ditb,thsp,thsp,w-3l,cond,g5.7     *correlation for boiling curve   *corr.6
w-3s,w-3l                    *dnb analysis by w-3l                *corr.9
0.0               *w-3s input data                                *corr.10
0.042,0.066,1.00   *w-3l input data                              *corr.11
grid,0,3                                                         *grid.1
0.6,0.4,1.0                                                      *grid.2
1,2
1
0.0,2,144.0,3
1,9                                                              *grid.4
2                                                                *grid.5
0.0,2,12.007874,1,32.007874,1,52.007874,1,?
72.007874,1,92.007874,1,112.007874,1,132.007874,1,
144.0,3,                              *grid loc.                 *grid.6
0
cont                                                             *cont.1
0.0,0,750,50,3,0,   *iterative solution                          *cont.2
0.0,0.0,0.001,0.0,0.0,0.9,1.5,1.0                                *cont.3
5,0,0,0,0,0,1,1,0,0,0,1,0,0                                      *cont.6
1000.,0.0,0.0,0.0,0.0,0.0                                        *cont.7
endd
*
*end of data input
0
```